

Western Australian School of Mines

Static Testing of Large Scale Ground Support Panels

Ellen C Morton

**This thesis is presented for the Degree of
Master of Science (Mining Engineering)
of
Curtin University of Technology**

January 2009

Declaration

To the best of my knowledge and belief this thesis contains no material previously published by any other person except where due acknowledgment has been made.

This thesis contains no material which has been accepted for the award of any other degree or diploma in any university.

Signature:

Date:.....23/10/2009.....

Acknowledgements

The author is indebted to many people who have assisted this research project over the last three years.

Firstly I would like to thank Professor Ernesto Villaescusa for having complete faith in my abilities to undertake this research and for his continued encouragement, guidance and support throughout the project.

Secondly I would like to thank my supervisor Alan Thompson for being able to simplify apparently complex problems into simple mechanics and for his patience throughout the sometimes tiring process of creating this document.

Thirdly I would like to thank John Player who started the construction of the test facility and provided assistance throughout the project.

I would like to thank the rest of the WASM Rock Mechanics team for all their assistance with manual labour and lateral thinking when I was completely stumped.

I would like to thank all the companies that provided materials and personnel to enable testing to be undertaken. I would especially like to thank Richard Varden who made this process seamless.

I would finally like my family and, in particular, my husband Peter, and my sister Louise, for their unwavering faith during the times when the path was not clear.

Table of Contents

CHAPTER 1	INTRODUCTION	1
CHAPTER 2	SURFACE SUPPORT FUNCTION.....	4
CHAPTER 3	WASM TEST FACILITY	7
3.1	INTRODUCTION.....	7
3.2	TEST FRAME DESIGN.....	7
3.3	BOUNDARY CONDITIONS	8
3.4	TEST PROCEDURE AND INSTRUMENTATION.....	9
CHAPTER 4	MESH	10
4.1	INTRODUCTION.....	10
4.2	THEORY OF MESH SUPPORT	12
4.3	PREVIOUS TESTING	13
4.3.1	<i>Ortlepp and others</i>	15
4.3.2	<i>Kuijpers et al.</i>	18
4.3.3	<i>Pakalnis and Ames</i>	20
4.3.4	<i>Tannant and others</i>	24
4.3.5	<i>Thompson et al.</i>	28
4.3.6	<i>Potvin and Giles</i>	35
4.3.7	<i>Other testing</i>	37
4.3.8	<i>Discussion of previous testing</i>	38
4.4	MESH TEST METHODOLOGY	40
4.5	MATERIALS	41
4.6	MESH CONFIGURATIONS	44
4.6.1	<i>Cross wires up</i>	45
4.6.2	<i>Cross wires down</i>	45
4.6.3	<i>Small-scale testing</i>	46
4.6.4	<i>Overlap testing</i>	46
4.7	BOUNDARY CONDITIONS	48
4.7.1	<i>Clamping</i>	48
4.7.2	<i>Lacing</i>	49
4.7.3	<i>Fixed boundary</i>	51
4.8	LOADING METHOD	52
4.9	WELD MESH RESULTS	54
4.9.1	<i>Clamping boundary restraint method test results</i>	55
4.9.2	<i>Lacing boundary restraint method test results</i>	56
4.9.3	<i>Assessment of the Lacing restraint</i>	63
4.9.4	<i>Fixed boundary restraint method test results</i>	64
4.9.5	<i>Results from varied configuration</i>	69
4.9.6	<i>Discussion of weld mesh results</i>	76
4.10	CHAIN LINK TEST RESULTS.....	80
4.10.1	<i>Lacing boundary restraint method test results</i>	80
4.10.2	<i>Fixed boundary restraint method test results</i>	85
4.10.3	<i>Discussion chain link test results</i>	98
4.11	COMPARISON OF MESH PRODUCTS	103

4.12	ANALYSIS TECHNIQUES	107
4.12.1	<i>Pakalnis and Ames methods</i>	107
4.12.2	<i>Tannant's method</i>	108
4.12.3	<i>Thompson's method</i>	110
4.12.4	<i>The WASM analysis technique</i>	111
4.12.5	<i>Discussion of analysis techniques</i>	122
4.13	DISCUSSION	124
CHAPTER 5 SHOTCRETE.....		125
5.1	INTRODUCTION.....	125
5.2	THEORY OF SHOTCRETE SUPPORT	126
5.3	SHOTCRETE PROPERTIES	129
5.4	COMPONENTS OF SHOTCRETE.....	132
5.5	SHOTCRETE DESIGN	134
5.5.1	<i>Mix design</i>	134
5.5.2	<i>Layer thickness and reinforcing</i>	136
5.6	SHOTCRETE PLACEMENT	139
5.7	PREVIOUS SHOTCRETE TESTING.....	140
5.7.1	<i>Early strength</i>	140
5.7.2	<i>Quality control and assessment</i>	144
5.7.3	<i>Large-scale testing</i>	155
5.7.4	<i>Other test methods</i>	164
5.8	SHOTCRETE TEST METHODOLOGY	165
5.8.1	<i>Substrate preparation</i>	165
5.8.2	<i>Sample procurement</i>	167
5.8.3	<i>Curing</i>	168
5.8.4	<i>Test methodology</i>	168
5.9	MATERIALS	170
5.10	RESULTS.....	171
5.10.1	<i>Site 1 and 2 - polypropylene fibres</i>	171
5.10.2	<i>Site 3 - steel fibres</i>	180
5.10.3	<i>Site 3 - mesh reinforcing</i>	182
5.10.4	<i>Comparison of results</i>	184
5.11	DISCUSSION	187
CHAPTER 6 MEMBRANES		189
6.1	INTRODUCTION.....	189
6.2	PRODUCT TYPES	192
6.3	THEORY OF MEMBRANE SUPPORT.....	193
6.4	MEMBRANE FAILURE MECHANISMS.....	195
6.5	PREVIOUS TESTING	197
6.5.1	<i>Small-scale testing</i>	198
6.5.2	<i>Large-scale testing</i>	206
6.6	ANALYSIS METHODS	211
6.7	WASM MEMBRANE TESTING	212
6.7.1	<i>Paver test - beam model</i>	213
6.7.2	<i>Punch test - membrane model</i>	217
6.8	RESULTS	219
6.8.1	<i>Paver test results</i>	219
6.8.2	<i>Punch test results</i>	223
6.8.3	<i>Comparison of the test methods</i>	227
6.9	DISCUSSION.....	228

CHAPTER 7	COMPARISON OF MATERIALS	229
CHAPTER 8	CONCLUDING REMARKS	233
CHAPTER 9	REFERENCES	235
CHAPTER 10	FURTHER READING	245
10.1	MESH.....	245
10.2	SHOTCRETE	245
10.3	MEMBRANES	248

APPENDIX 1: GROUND SUPPORT DESIGN TABLES PROVIDED BY ORTLEPP ET AL. (1975).

APPENDIX 2: SUMMARY OF WELD MESH TESTING RESULTS.

APPENDIX 3: INDIVIDUAL MESH TEST REPORT SHEETS – WELD MESH

APPENDIX 4: SUMMARY OF CHAIN LINK TEST RESULTS

APPENDIX 5: INDIVIDUAL MESH TEST REPORT SHEETS – HIGH TENSILE CHAIN LINK MESH

APPENDIX 6: COMPARISON OF THE WASM TEST DATA WITH THE PREDICTED RUPTURE FORCE USING TANNANT’S FORMULAS.

APPENDIX 7: SHOTCRETE MIX DESIGNS.

APPENDIX 8: INDIVIDUAL SHOTCRETE TEST REPORT SHEETS

APPENDIX 9: INDIVIDUAL MEMBRANE TEST REPORT SHEETS.

List of Figures

Figure 1: Ground support scheme	5
Figure 2: WASM Static Test facility.....	7
Figure 3: Schematic of Ortlepp's drop test facility.....	17
Figure 4: Ortlepp's drop test facility (Stacey and Ortlepp, 1997)	17
Figure 5: Concrete and steel blocks are used to simulate a rock mass under the test arrangement (Kuijpers et al., 2002).	18
Figure 6: Kuijpers et al. (2002) final test arrangement.....	19
Figure 7: Pakalnis and Ames test arrangement.....	20
Figure 8: Tannant (1995, 1997 and 2001a) test facility.	25
Figure 9: Tannant (1995) bolting patterns (a) 1.2m x 1.2m diamond pattern (b) 1.2m x 1.5m diamond pattern and (c) 1.2m x 1.2m square pattern.....	25
Figure 10: Chart showing the principle of stiffness as described by Tannant.	27
Figure 11: Schematic of the Thompson et al. (1999) mesh test facility.	29
Figure 12: Test variations used by Thompson et al. 1999.	30
Figure 13: Force transfer concept using a diamond or oblique bolting pattern.	31
Figure 14: Force transfer concept using a square bolting pattern.	32
Figure 15: Gross deformation of the mesh observed using the square bolting pattern (Thompson et al. 1999).	32
Figure 16: Stiffening of the wires at the weld locations.....	33
Figure 17: Theoretical representation of mesh wire tension (Thompson et al. 1999).	33
Figure 18: Potvin and Giles (2008) test setup.....	35
Figure 19: Potvin mesh layout with test setup.	36
Figure 20: "Crinkling" of the mesh (Potvin and Giles 2008).....	36
Figure 21: Crinkled mesh configuration tested by Ortlepp and Erasmus 2002.	37
Figure 22: Typical weld mesh sheet layout.	42
Figure 23: High tensile chain link mesh layout (G65/4).	43
Figure 24: Diamond Configuration for (a) S95, (b) G65 and (c) G80.	44
Figure 25: Cross wires up were adopted as the standard test procedure.	45
Figure 26: The sample orientation was altered to determine the effect of orientation on the force - displacement characteristics of the mesh.....	45
Figure 27: Setup of small - scale tests.	46
Figure 28: Mesh being pushed apart at the overlap between sheets.	47
Figure 29: Test layout where two sheets have been overlapped.	47
Figure 30: Clamping test arrangement.	48
Figure 31: Lacing boundary setup with wire rope grips in foreground.....	49
Figure 32: Two layers of bricks were used to raise the position of the sample.	50
Figure 33: Fixed boundary system adopted as standard test arrangement.	51
Figure 34: Square loading plate setup square to the mesh grid.	52
Figure 35: Square loading plate setup diagonal to the mesh grid.	52
Figure 36: Point loading of the wires caused by the flat base of the plate.	53
Figure 37: Curved loading plate setup square to the mesh grid.....	53
Figure 38: Slippage of mesh from under the clamping frame.....	55
Figure 39: Weld mesh force - displacement results using lacing boundary condition.	56
Figure 40: Typical force - displacement result using the lacing boundary method.....	57
Figure 41: Dissection of a typical force - displacement curve resulting from the lacing boundary method.	57
Figure 42: Load transfer concept for weld mesh.....	58
Figure 43: Terminology related to force - displacement results of mesh testing.	60
Figure 44: An example of failure propagation starting with the directly loaded wires.....	61
Figure 45: Initial peak at rupture followed by a steady decline in force.....	61
Figure 46: Some tests exhibited a decrease in force followed by an increase.....	62
Figure 47: Rupture force - displacement results for all lacing tests.	63
Figure 48: Force - displacement results for fixed boundary conditions.	64
Figure 49: Dissection of a typical force - displacement curve using the fixed boundary method.	65
Figure 50: Load transfer concept for weld mesh.....	66
Figure 51: Rupture force - displacement results for fixed weld mesh tests.	66

Figure 52: Welded wire mesh failure mechanisms; L – R weld failure and failure of the wire through the HAZ and tensile wire failure.	67
Figure 53: Rupture force – displacement results with failure modes.	68
Figure 54: Force – displacement results for different sample orientations.	69
Figure 55: Force - displacement results from the small-scale test program.	70
Figure 56: Rupture results for small-scale tests.	71
Figure 57: Force - displacement results for overlap tests.	72
Figure 58: Load transfer only occurs in one direction during the early stages of the test.	73
Figure 59: The plate simply pushes apart the overlap.	73
Figure 60: Lacing of the overlap to enable better load transfer.	74
Figure 61: Force - displacement comparison of the laced test with the standard overlap results and a typical standard full size sample results.	74
Figure 62: The lacing allows forces to be transferred along two wires on the outer edge rather than one wire as indicated in Figure 58.	75
Figure 63: Force - displacement response of weld mesh using various boundary restraint systems.	76
Figure 64: Comparison of rupture force – displacement for the lacing and fixed boundary methods.	78
Figure 65: Welds may be in compression or tension depending upon the orientation of the wires (Thompson et al., 1999).	79
Figure 66: Force - displacement results for chain link mesh using the laced boundary method.	81
Figure 67: Dissection of the force – displacement reaction of chain link mesh.	81
Figure 68: Tension in the sample is dependent upon the amount of connection between the wires.	82
Figure 69: Force transfer around the chain link Product S95/4.	83
Figure 70: Due to high displacements stress is concentrated on the edge of the loading plate.	84
Figure 71: (a) Shear failure of the wires either as a result of the plate or the mesh “cutting” itself or (b) tensile wire failure.	84
Figure 72: Hole in the mesh after rupture.	85
Figure 73: Force –displacement results for Product S95/4 mesh using the fixed boundary method.	86
Figure 74: Rupture force – displacement chart for Product S95/4 using the fixed boundary system.	87
Figure 75: The flat based plate (a) causes point loading even at low displacements whilst curved plate (b) reduces the effect.	88
Figure 76: Force – displacement result for Product G65/4.	89
Figure 77: Triple plate configuration used to increase displacement capacity.	89
Figure 78: Force transfer around Product G65/4.	90
Figure 79: Force transfer concept of Product G65/4.	90
Figure 80: Rupture results for Product G65/4.	91
Figure 81: Rebound of mesh due to the release of stored elastic energy.	92
Figure 82: Force transfer concept of Product G80/4.	92
Figure 83: Rupture force – displacement results for Product G80/4.	93
Figure 84: Necking of the wire at a link away from the edge of the plate.	94
Figure 85: Unravelling of chain link.	94
Figure 86: Force – displacement results for Product G65/3.	95
Figure 87: Rupture force – displacement chart for Product G65/3.	96
Figure 88: Force – displacement results for Product G80/2.	97
Figure 89: Rupture force – displacement chart for Product G80/2.	97
Figure 90: Comparison of the lacing boundary and fixed boundary results.	99
Figure 91: Diamond configurations of (a) S95/4 and (b) G65/4.	100
Figure 92: Rupture force and displacement results for S95/4 and G65/4.	100
Figure 93: Force transfer mechanisms for (a) S95/4 and (b) G65/4.	101
Figure 94: Evaluation of the effect of wire diameter using (a) Product G65 and (b) Product G80.	103
Figure 95: Comparison of the various mesh types using the fixed boundary system.	104
Figure 96: Comparison of results of various mesh types.	105
Figure 97: Weld mesh and chain link mesh after failure.	106

Figure 98: Difference in force transfer mechanism between (a) weld mesh and (b) chain link mesh.	106
Figure 99: Small load cell used to collect data at particular restraining points.	108
Figure 100: Force - displacement curve where peak load is equal to rupture load.	109
Figure 101: Force-Displacement curve where peak load is not equal to the rupture load.....	109
Figure 102: Standardised test results show little variation in the force – displacement reaction.....	112
Figure 103: The force - displacement results for the lacing and fixed boundary condition (a) and the overlay of the force – displacement curve showing vary little variation (b).	112
Figure 104: Curve matching (a) Linear (b) Quadratic (c) Exponential (d) Power (e) Polynomial – 3 rd Order and (f) Polynomial – 4 th Order.	114
Figure 105: Standardised force – displacement reaction for (a) S95/4 (b) G65/4 (c) G80/4 (d) G65/3 and (e) G80/2.	118
Figure 106: Comparison of the force – displacement reaction of the various mesh types.....	119
Figure 107: Comparison of the force – displacement reaction of the G80 products.	119
Figure 108: Curve matching (a) Linear (b) Quadratic (c) Power (d) Exponential (e) Polynomial – 3 rd Order and (f) Polynomial – 4 th Order.	121
Figure 109: Failure mechanism of shotcrete (Barrett and McCreath 1995).	128
Figure 110: Updated shotcrete failure mechanisms.	128
Figure 111: Particle size distribution for shotcrete aggregates (EFNARC 1996).	133
Figure 112: Grimstad and Barton Q chart (1993).	137
Figure 113: Papworth (2002) shotcrete design chart incorporating shotcrete toughness.....	138
Figure 114: Soil Penetrometer (Bernard 2005).	142
Figure 115: Needle Penetrometer (Bernard 2007).	142
Figure 116: Beam test.	143
Figure 117: UCS test setup in the WASM test lab.	145
Figure 118: Position of the rollers in the third point loading test setup (ASTM C 07 08).	148
Figure 119: Third point loading test setup (ASTM C 1609 07)	148
Figure 120: Force displacement parameters calculated for the third point loading test (ASTM C 1609 07).	149
Figure 121: Round Determinate Panel (RDP) test setup (Bernard 2005).	152
Figure 122: Specification for sample supports used in RDP tests (ASTM C 1550 08).	154
Figure 123: Spherical loading point used in the RDP test (ASTM C 1550 08).	154
Figure 124: Plan of (a) Setup 1 flat profiles (b) Setup 2 arched profiles and (c) Setup 3 irregular profiles.	156
Figure 125: Failure modes described by Fernandez Delgado et al. (1976).	157
Figure 126: Test Setup 2 failure modes (confined) – Fernandez Delgado et al., 1976.	158
Figure 127: Test Setup 3 failure modes (confined) – Fernandez Delgado et al., 1976.	159
Figure 128: Holmgren (1976) test facility with hinged base for spraying.	160
Figure 129: Sandstone substrate prepared for spraying.	166
Figure 130: Diamond drill assembly for drilling punch plate in the substrate.	166
Figure 131: Gap filler is used to fill between the punch plate and the main substrate.	167
Figure 132: Upright substrate ready for spraying.	167
Figure 133: The formwork is removed and the centre of the sample is marked.....	169
Figure 134: Rotation of the sample.....	169
Figure 135: Sample on the test frame ready for the final test setup.	169
Figure 136: Shotcrete test setup.	170
Figure 137: Site 1 force – displacement results.....	172
Figure 138: Site 2 force – displacement results.....	172
Figure 139: Comparison of Site 1 and Site 2 test results using the same thickness and curing time.....	173
Figure 140: Shotcrete test phases.	174
Figure 141: An example indicating how the LVDT results can be used to determine the behaviour of the substrate.....	176
Figure 142: The LVDT results from ST001 indicated where adhesion loss began.	177
Figure 143: Poly fibres with two different failure modes.	177

Figure 144: Typical force – displacement curve with energy shown as the shaded area. .	178
Figure 145: Site 1 cumulative energy results.....	179
Figure 146: Site 2 cumulative energy results.....	179
Figure 147: Site 3 force – displacement results.....	180
Figure 148: Steel fibres showed no signs of tensile yield.....	181
Figure 149: Cumulative energy results for Site 3.....	181
Figure 150: Mesh and fibre reinforced shotcrete force – displacement results alongside fibre reinforced shotcrete results.....	182
Figure 151: Mesh and fibre reinforced shotcrete energy results alongside fibre reinforced shotcrete results.....	183
Figure 152: Mesh reinforcing within the cracked shotcrete sample.....	183
Figure 153: Rupture force – displacement results for all sites.....	185
Figure 154: Rupture force – thickness results for all sites.....	186
Figure 155: Rupture energy / thickness relationship.....	187
Figure 156: Membrane support model.....	194
Figure 157: Beam support model.....	194
Figure 158: Failure mechanism of membranes.....	195
Figure 159: Membrane failure modes; (a) direct shear, (b) direct tension and (c) adhesion loss (after Espley and Kaiser 2002).....	196
Figure 160: Tensile test sample (dog bone shape).....	199
Figure 161: Tensile testing of “dog bone” sample (Tannant et al., 1999b).....	200
Figure 162: Two variations of the glued dolly adhesion test.....	201
Figure 163: Coated and uncoated cores under compression (Espley et al., 1999).....	202
Figure 164: Pull plate test (Archibald 2001a).....	206
Figure 165: Large-scale pull test (Finn 2001).....	207
Figure 166: Punch test concept.....	208
Figure 167: Coated panel test (Kuijpers 2001).....	209
Figure 168: Coated paver test setup (Espley et al., 1999).....	209
Figure 169: Box of rocks test set-up (Tarr et al., 2006).....	211
Figure 170: Force diagram explaining failure mechanism of membranes (Tannant 2001b).....	211
Figure 171: Pavers setup ready to be used as a base for the membrane.....	213
Figure 172: Spraying of the pavers.....	214
Figure 173: Face plate and planks on top of sample ready for rotation.....	214
Figure 174: Sample rotation in progress.....	215
Figure 175: Sample after pallet has been removed.....	215
Figure 176: Sample setup with LVDT’s and clamping frame in place.....	216
Figure 177: Membrane spraying.....	217
Figure 178: Measurement of sample thickness.....	218
Figure 179: Sprayed samples in curing chamber.....	218
Figure 180: The gaps in the membrane measured up to 7mm.....	219
Figure 181: Force – displacement results for the paver test method.....	220
Figure 182: Shear failure of the sample.....	221
Figure 183: Deformation of the sample results in the pavers going into compression and tension.....	221
Figure 184: Cracking in pavers.....	221
Figure 185: Flipping of paver pallet.....	222
Figure 186: Failure of uncoated pavers once face plate had been removed.....	222
Figure 187: Force - displacement results.....	224
Figure 188: Peak force and thickness relationship for punch test method.....	225
Figure 189: Test TT008 at the completion of the test.....	226
Figure 190: The punch disc after failure.....	226
Figure 191: Comparison of Paver test results and Punch test results.....	227
Figure 192: Comparison of surface support elements.....	229
Figure 193: Typical force – displacement curve with energy shown as the shaded area. .	230
Figure 194: Energy absorption capacities of various mesh types at rupture and shotcrete.....	231

List of Tables

Table 1: Material types with data acquisition sample recording rate	9
Table 2: Test results (Ortlepp 1983).	16
Table 3: Test results (Pakalnis and Ames, 1983).	21
Table 4: Predicted and actual peak forces provided by Pakalnis and Ames (1983).	24
Table 5: Tannant et al. (1997) test results using a 1.2m bolting pattern.	27
Table 6: Test parameters used by Thompson et al 1999.	30
Table 7: High tensile chain link sample configurations.	44
Table 8: Summary of number of tests.	54
Table 9: Mesh quality assessment for 100 x 100mm grid, 5.6mm diameter welded wire mesh.	68
Table 10: Chain link mesh products and the boundary conditions used to test the samples.	80
Table 11: Average statistical fit results from the analysis of the shape of the weld mesh curves using Curve Expert TM	115
Table 12: Average polynomial coefficients describing the shape of the weld mesh curve.	116
Table 13: Average statistical fit results from the analysis of the shape of the chain link mesh curves using Curve Expert TM	120
Table 14: Average polynomial coefficients describing the shape of the weld mesh curve.	122
Table 15: Basic Mix design Jolin and Beaupre (2003)	135
Table 16: Number of tests conducted on each configuration.	161
Table 17: Number of tests conducted on each configuration.	162
Table 18: Test results excluded from analysis.	171
Table 19: Summary of test results for Sites 1 and 2.	173
Table 20: Summary of Site 3 test results.	181
Table 21: Available membrane products with primary polymer base.	193
Table 22: Sample dimensions for various thicknesses. Adapted from ASTM D 638.	199
Table 23: Toxicity rating of various polymers (after Schwendeman 1972).	203
Table 24: Flammability rating of polymer components (after Schwendeman et al., 1972).	204
Table 25: Average thickness of each membrane test.	223
Table 26: Summary of Punch Test results.	224
Table 27: Average energy absorption capacity of chain link mesh at rupture.	232

Executive Summary

The Western Australian School of Mines (WASM) developed a large area static test facility to enable the evaluation of three forms of surface support; namely, mesh, shotcrete and membranes. The purpose of this thesis is to document the test conditions and procedures under which these tests were conducted and to document the outcomes from testing.

A review of previous mesh testing established that the most common method used for the evaluation of mesh types was two-dimensional linear elastic analyses, often using catenary principles. These analysis techniques have been used to estimate the tension in the wires of mesh and the strength characteristics of the mesh. These methods assume that forces are only transferred along directly loaded wires and that failure of the mesh is only related to the tensile strength of the wire.

The force – displacement response from fully restrained mesh tests conducted at the WASM test facility have been characterised into distinct phases, clearly demonstrating the non-linear behaviour of mesh. The initial force response to displacement is slow; however the force response increases dramatically with further displacement. This behaviour has been shown to follow a cubic relationship.

The force – displacement results have also been used to develop load transfer concepts for both weld mesh and chain link mesh. These concepts suggest that forces are transferred away from the directly loaded wires through adjoining wires, distributing forces over a greater area of the mesh. The force capacity of the weld mesh is not only dependent on the tensile strength of the wire but also the quality of the welding process. Likewise, the force capacity of chain link mesh is not only dependent on the tensile strength of the wire but also diamond configuration which allows load to be shared across a greater area of mesh.

Several other test conditions were evaluated as part of the test program, including mesh sheet overlaps and wire orientation. The results have demonstrated that the boundary conditions and mesh orientation alters the force – displacement response of mesh.

Most current shotcrete testing techniques focus on quality assurance and quality control. Shotcrete support mechanism and failure mechanisms are complex and not well understood. The WASM punch test method was developed to evaluate shotcrete using realistic shotcrete failure mechanisms such as shear and flexural failure and adhesion loss.

The behaviour of shotcrete is characterised by an initial stiff reaction followed by rupture of the cement matrix. Rupture generally occurs at displacements of less than 5mm. The rupture force of fibre reinforced shotcrete is dependent only on the cement content of the shotcrete mix and the thickness of the layer, and not on the fibre type. The post rupture reaction of shotcrete is dependent on the reinforcing material; namely fibres or mesh. Mesh reinforced shotcrete had much greater force and displacement capacity compared with fibre reinforced shotcrete.

Membranes have two theoretical support models (Norcroft, 2006); namely, the membrane support model and the beam support model. A total of 6 tests were undertaken to investigate the behaviour of a particular membrane product under the two theoretical support models. These tests were aimed at determining a suitable test method that could determine the capacity of the membrane and the behaviour of the membrane under realistic loading conditions.

The results from both test programs demonstrated that the membrane has limited force and displacement capacity and cannot be compared with conventional mesh and shotcrete as suggested in the product data sheet. The failure mechanism was shear failure with minimal adhesion loss observed.

The development of the WASM test facility has enabled the evaluation and comparison of various surface support elements. The results of this testing have provide a valuable insight into the performance of each of the individual products.

CHAPTER 1 INTRODUCTION

The demand for mineral resources is ever-increasing and with fewer mineral resources being discovered close to the earth's surface, many mines have had to extract ore from greater depths in order to supply this demand. Recently, high volume production methods, such as block caving, have been developed to capitalise on low grade resources. These methods, combined with greater depths below the surface, increase the need for adequate ground support schemes to minimise the risk of rock falls in development excavations.

Typically, modern day ground support schemes consist of rock reinforcement systems and surface support systems.

A rock reinforcement system consists of one or more elements fixed within a bore hole, drilled into the rock mass, and an exterior face plate. A pattern of reinforcement systems is often used to stabilise large blocks and prevent large-scale ground deterioration. The type of element, and the spacing of each system, depends on the materials available locally and the prevailing geological conditions; namely, the geometry of the potentially unstable blocks and the loading conditions.

Surface support elements are used between reinforcement systems to prevent smaller scale instability and unravelling of the rock mass. The surface support elements are restrained by the face plates used with the rock reinforcement systems to form an integrated scheme. Surface support elements are the focus of this thesis.

Surface support elements include simple rolls or sheets of steel wire mesh, or sprayed layers such as shotcrete and membranes that harden and apply a reactive force to the rock face.

Shotcrete is defined as pneumatically applied concrete. In the early 1900s the “Cement Gun Company” developed a machine for spraying fine cement mortar using compressed air. In the 1950s the processes were improved to enable the spraying of coarse concrete called shotcrete. The early forms of shotcrete were often reinforced with small diameter steel wire mesh to improve the shear strength and flexural strength of the material. In the 1980s the mesh was replaced by short steel fibres. In the 1990s, fibres manufactured from polymers were introduced. Chemical admixtures have also evolved over the last few decades; the emergence of more effective plasticizers, accelerators and curing agents have resulted in improved consistency of the product.

The evolution of mesh from a shotcrete reinforcing element to a stand-alone surface support element is not well documented. In the 1950s, small diameter woven mesh was applied and restrained with plates attached to reinforcement elements. As excavation sizes increased and the demand on the surface support systems increased, several mesh configurations were developed including welded wire mesh and chain link mesh. Over time the wire diameter increased and the mesh manufacturing processes improved.

In the 1980s, mining processes were revolutionised with the development of large-scale mechanised rock drills. Chain link mesh was too flexible for use with the large-scale equipment and welded wire mesh (weld mesh) gained popularity. The weld mesh adopted by the mining community was the same product commonly used as concrete slab reinforcement by the civil construction industry.

There has been little change in the type of weld mesh product used in mining applications over the last 20 years. However, improvements to manufacturing processes have resulted in better quality products.

Increasing depths within the Western Australian mines have created higher force – displacement demands on surface support elements. Recently, mines have been considering varying grid sizes and wire diameters of weld mesh to meet specific needs. These changing demands have also led to a resurgence of the use of chain link mesh. High tensile chain link mesh has been developed to meet the higher force – displacement demands.

Membranes are polymer based spray-on liners. They are designed to be relatively thin (3 – 10mm) in thickness. They were first developed in the 1950s and since then a number of concerted research efforts have been made to establish membranes as a replacement for conventional support elements such as mesh and shotcrete. To date membranes have not been accepted for wide scale use within the mining industry.

The Western Australian School of Mines (WASM) developed a static test facility in 2005 with the aim of developing methods to test three forms of surface support; namely, mesh, shotcrete and membranes. It is envisaged that the test methods will provide a better understanding of the static force – displacement behaviours of each surface support element

The primary purposes of the investigations reported in this thesis are to document the test conditions and procedures under which the large area static tests were conducted and to document the outcomes from testing. A brief overview of the theoretical behaviour of surface support elements is followed by individual chapters relating to mesh, shotcrete and membranes.

Each chapter provides an introduction to the element, a description of the theoretical principles of how the element provides support to an excavation, an outline of the design methods commonly used for the product and a literature review of previous testing conducted both in Australia and internationally. The test results for each element are presented and common analysis techniques are applied and discussed. Finally the force – displacement characteristics of the three surface support elements are compared.

CHAPTER 2 SURFACE SUPPORT FUNCTION

In order to understand the role of surface support in preventing rock mass deterioration, it is necessary to first understand the loading conditions that will be imparted on the system.

Research into the behaviour of the rock mass surrounding an excavation (and hence the loading conditions) is extensive and in many cases inconclusive. It is not the purpose of this thesis to discuss the loading concepts in detail but rather to provide the basic concepts that are the background to testing any ground support element

In simple terms a rock mass consists of intact rock that may or may not be broken by fractures called discontinuities. There are many papers which concentrate on categorising the rock mass according to the type and number of discontinuities that are present within the rock mass.

Windsor (2007) provides the most concise summary of the rock mass categories by suggesting there are only three basic categories; massive rock, stratified rock and jointed rock. Massive rock has few, if any, discontinuities. Failure is most likely to occur as *“tensile or compressive failure through intact rock”*. Stratified rock is generally rock that is broken into platelets by continuous discontinuities that are oriented parallel to the underlying strata. Failure is most likely to be caused by *“slip and separation on bedding planes and cross joints”* with some *“compressive and tensile failure through intact rock”*. Jointed rock can be described as rock which has a number of discontinuity sets oriented obliquely to the overall strata. Windsor further subdivides jointed rock into sparsely jointed, closely jointed and arbitrarily jointed rock. Failure is characterised by *“slip and separation on pre-existing discontinuities”* with minimal failure through intact rock.

The basic concept of a ground support scheme is to stabilise the near surface rock of an excavation by limiting the slip and separation of pre-existing or newly formed discontinuities within the rock mass.

The rate at which failure propagates through the rock mass defines whether loading on the ground support scheme is static or dynamic. Static loading occurs when the rock mass separates along existing and newly formed discontinuities, causing blocks to impart a force onto the ground support scheme. The force will either remain constant over long periods of time or increase in small increments.

Dynamic loading occurs when failure occurs rapidly and is combined with a release of energy. Generally, new fractures are formed during dynamic failures. Dynamic loading of ground support schemes is often followed by static loading conditions. Only static loading conditions have been considered as part of this thesis.

Reinforcement systems such as cable bolts or friction stabilisers are used internally to minimise movement within the rock mass.

Surface support elements, which are the focus of this thesis, are used as areal support between the reinforcement systems in closely jointed rock masses. They are used to complement the reinforcement systems by retaining rock fragments and maintaining the overall integrity of the rock mass at the excavation surface.

Integration of the reinforcement systems and the surface support elements, to form a ground support scheme, is usually provided through plates attached to the reinforcement element. A typical ground support scheme is illustrated in Figure 1.

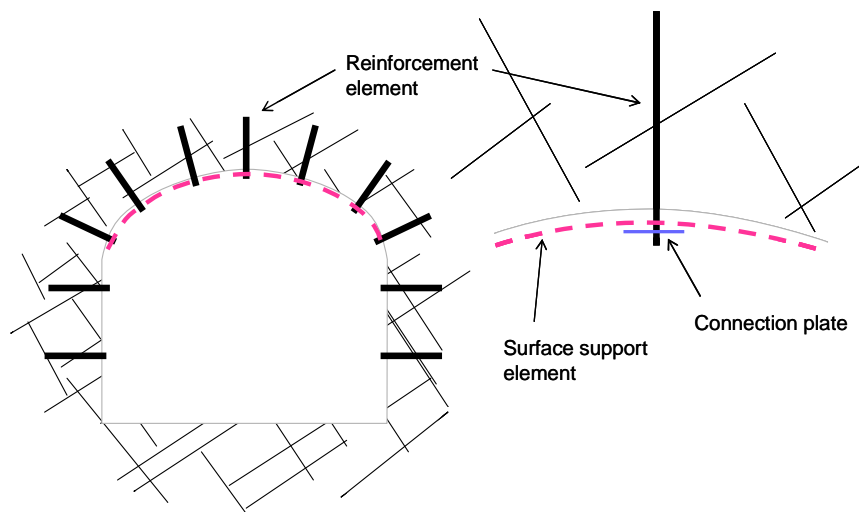


Figure 1: Ground support scheme.

Schwendeman et al. (1971) suggest that surface support elements are required to “provide a measure of support over the entire roof and wall surface”. For the element to be effective they suggest that the following benefits must be realised:

- *Uniformly support the roof and walls*
- *Prevent detached portions of the roof or wall from falling out.*
- *Help seal cracks already present and prevent their propagation.*
- *Seal the rock and coal against the adverse effects of the mine environment*
- *Warn the miner in the vicinity of the danger of a collapse if the liner yields slowly under breaking loads.*

Surface support systems include various mesh products, shotcrete and membranes.

Detailed discussion of each type of individual surface support element is provided in the respective chapters on mesh, shotcrete and membranes.

CHAPTER 3 WASM TEST FACILITY

3.1 INTRODUCTION

The Western Australian School of Mines (WASM) Static Test Facility was designed and built by the WASM Rock Mechanics Department in 2004 to complement the WASM Dynamic Test Facility built in 2002. Commissioning of the static facility took place in early 2005 with formal testing beginning in April 2005.

3.2 TEST FRAME DESIGN

The static test facility (Figure 2) consists of a load bearing upper steel beam with a mechanical screw feed jack mounted on top. The mechanical jack drives a loading shaft that passes through the beam. A 50 tonne capacity load cell is mounted between the shaft and a spherical ended cylinder. A 300mm square, 35mm thick hardened steel plate with a spherical seat, is used to load the sample.

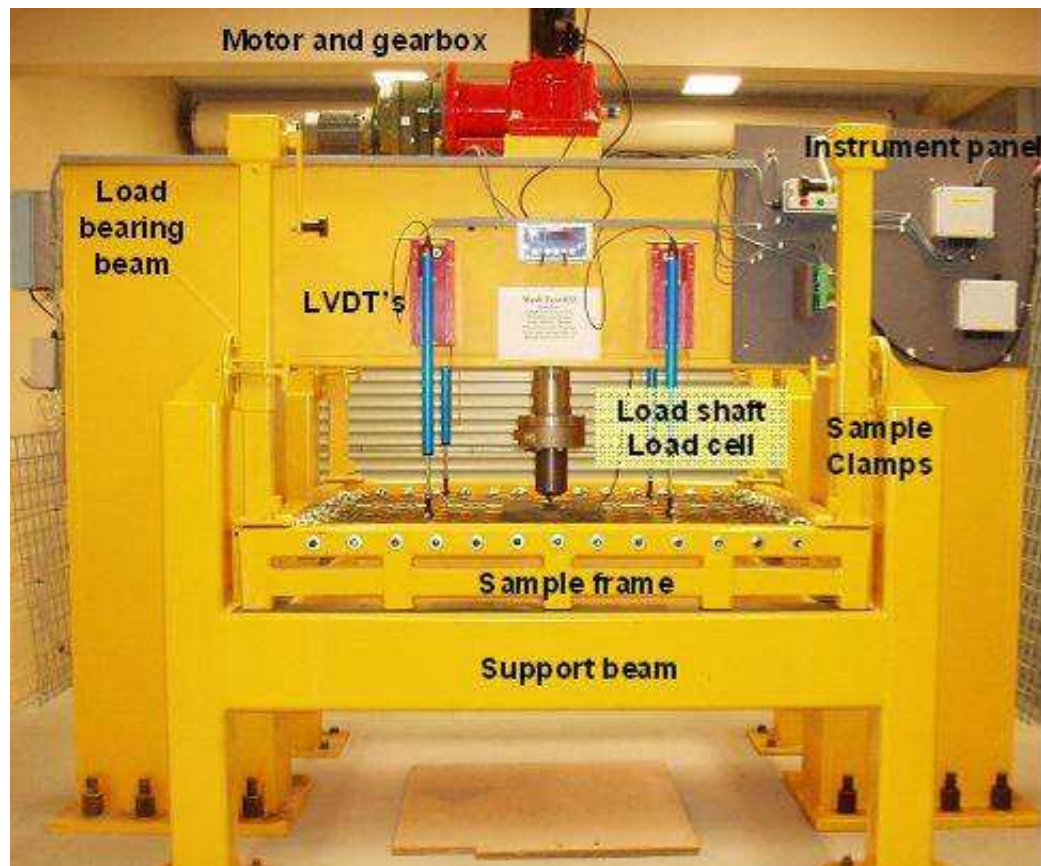


Figure 2: WASM Static Test facility

The motor has an encoder mounted on the tail shaft. This connects to a frequency control unit which allows the motor speed, and thus the displacement rate, to be set. The maximum displacement rate is 8mm per minute with testing undertaken at approximately 4mm per minute to simulate static loading conditions.

An inner support frame forms the base for the sample. Different test setups were used depending on the materials being tested and the boundary restraint conditions. The sample preparation, boundary conditions and test setup were fundamental aspects of the investigation reported in this thesis. A general test method is provided below.

3.3 BOUNDARY CONDITIONS

The application of boundary conditions is the most important aspect of any laboratory testing of ground support panels. The boundary conditions can either try to replicate actual loading conditions or they can attempt to simulate the continuation of the material beyond the sample boundary. Either way, the boundary restraint conditions applied to the sample can have a considerable impact on the force - displacement reactions of the sample.

Boundary conditions used within the WASM test arrangement have been selected on the basis of the reaction mechanism for each surface support type. A detailed description of each boundary condition used has been provided in the relevant sections.

3.4 TEST PROCEDURE AND INSTRUMENTATION

The preparation of the different surface support types has been described in the relevant sections.

Once the sample has been prepared and placed within the testing machine, the loading plate is placed on the sample and the jack positioned to be in contact with the plate. The data acquisition system is activated and testing is started. The following instrumentation is used during testing:

- Linear voltage displacement transducers (LVDTs) are used to record the overall deformation of the sample. One LVDT is positioned in the centre of each quadrant of the sample to measure the displacement at that point.
- A laser is positioned on the load bearing beam next to the load shaft and records the distance from the laser position to the plate. Each measurement is subtracted from the first measurement to determine a relative displacement. This relative displacement is recorded as the plate displacement.
- The displacement rate of the jack is determined by measuring a voltage output from the motor. The voltage output ranges from 0V to 10 volts. At 10V the jack is at its maximum displacement rate of 8mm per minute. The displacement rate was calibrated using the laser measurement.
- A load cell is mounted behind the loading point to determine the reaction force from the sample caused by the displacement. The maximum capacity of the load cell is 50 tonnes.

Table 1 indicates the different sampling rates used during testing of the various surface support elements.

Table 1: Material types with data acquisition sample recording rate

Material Type	Sampling Rate (samples /sec)
Mesh	2
Shotcrete	5
Membranes	2

CHAPTER 4 MESH

4.1 INTRODUCTION

Wire mesh has been used as a component of ground support in mining since the 1950s. Today it is used in one form or another in almost every mining operation in Australia and elsewhere in the world.

The most common type of mesh used within the Australian mining industry is welded wire mesh (or weld mesh). Weld mesh was originally developed for the building and construction industry as internal reinforcement for concrete. It was adapted to a surface support element by the mining industry in the 1950s and became more popular in the Australian mining industry in the 1980s with the emergence of mechanised mining techniques. Weld mesh is constructed using longitudinal (long) wires and transverse (cross) wires arranged in a grid like pattern and welded at each intersection. Typically the grid pattern is 100mm x 100mm with the wires being 5.6mm in diameter. More recently manufacturers and mining companies have investigated altering grid patterns and wires diameters to better suit expected ground conditions.

Chain link mesh consists of preformed zigzag wires interwoven and joined at the ends. The gauge of the mesh and the quality of the mesh varies, depending on the available manufacturing resources of suppliers in the various regions. With increasing depths and high stresses the need for chain link mesh in the Australian mining industry is becoming more apparent. It is used primarily in dynamic loading environments where high displacement capacities are required. Until recently, chain link mesh was predominantly installed manually with operators having to work close to the rock face. This practice is particularly hazardous and has limited the use of chain link mesh in the Australian mining industry. Recent trials have been undertaken to install chain link mesh mechanically, increasing the likelihood of higher usage within Australia.

Other mesh types such as expanded metal mesh are also used but are less common.

Despite the popularity of mesh, limited research has been conducted on the force and displacement properties of the various mesh types. There are no universal standard requirements for mesh products used within the mining industry.

No published records of mesh research can be found prior to 1983. In 1983, mesh research was published in South Africa by Rand Mines Limited (Ortlepp, 1983) and by the Ontario Ministry of Labour in Canada (Pakalnis and Ames, 1983).

Ortlepp (1983) developed a fully restrained laboratory test that has formed the basis of several other testing programs undertaken more recently.

Pakalnis and Ames (1983) designed a field test method to evaluate meshing systems in-situ. The method involved the fixing of a large plate behind the installed mesh. The plate was pulled using a block and chain assembly and the force and displacement were measured.

In the 1990s, Ortlepp and Stacey (1996 and 1997) in conjunction with the Safety in Mines Research Committee (SIMRAC South Africa) conducted further tests using quasi – static and dynamic loading conditions. Tannant (1995) and Thompson et al. (1999) both conducted large-scale mesh tests to determine the force and displacement properties of various mesh types. Tannant used two-dimensional catenary principles to develop an equation to predict the peak force of the mesh at a given displacement. Tannant also developed a numerical value for the stiffness of mesh based on Hooke's Law.

Thompson et al. (1999) conducted testing to enable the development and calibration of a mesh modelling program. The original program used the catenary principles developed by Tannant to simulate the mesh behaviour. Thompson (2003) recognised that there was limited value in the two-dimensional catenary approach and altered the package to enable three-dimensional analysis of the mesh reaction.

Villaescusa (1999) conducted small-scale shear tests in accordance with the current Australian standards on weld shear strength (AS1304). He identified three failure modes; weld failure, failure through the heat affected zone (HAZ) and wire failure. He suggests that in order to achieve a good quality mesh, the product must have weld strengths equal to, or greater than, the wire strength.

Numerous papers have been written since 2001 including Roth et al. (2004), Van Sint Jan and Cavieres (2004), Dolinar (2006), Potvin and Giles (2008). These papers generally report results from limited test programs evaluating specific products.

4.2 THEORY OF MESH SUPPORT

The primary function of mesh, restrained by reinforcement systems, is to improve the safety of the mining environment by retaining detached blocks between the reinforcing elements, preventing them from falling.

The expected size of the blocks, formed by discontinuities in the rock mass, is used to decide whether or not mesh is used. Previously, rather than a particular engineered design approach, the type of mesh, the grid aperture and the wire diameters were generic, based on what products were commonly available and whether suitable installation methods were practical to the site application. Ortlepp et al. (1975) provide design tables for a general ground support scheme that includes mesh. These tables are provided in Appendix 1.

Mesh is clamped to the rock surface with plates that are connected to the reinforcement elements. Methods of installing mesh vary from manual installation to mechanical installation depending on the available resources, equipment and mesh type. The type of plate and pressure applied to the plate can have a significant effect on the performance of the mesh.

The stiffness and capacity of the mesh must also be matched to the capacity of the reinforcement element.

Recently, many mines have been examining alternative grid configurations and wire diameters that may be more appropriate to specific applications.

A number of attempts have been made to characterise the force – displacement properties of mesh and allow for the comparison of various mesh types with varying grid sizes and wire diameters. These attempts are discussed in the following sections.

4.3 PREVIOUS TESTING

Despite the extent of use of mesh both in Australia and overseas, there is relatively little test data published on mesh compared with data available for shotcrete or membranes. This may be due to the perception that mesh is a simple retaining system and does not have the same level of complexity in the interaction with the rock mass as shotcrete or membranes. In reality, it is important to understand the properties of each individual component used in a ground support scheme and this includes mesh.

In Australia there is only one recognised small-scale test. This is called the weld shear test and is prescribed in AS1304 – 1991 “*Welded wire reinforcing fabric for concrete*”. The test involves taking a small t-bar section from a larger sheet of mesh and clamping the cross wire using a specifically designed apparatus. The longitudinal wire is then pulled and the forces measured.

Most manufacturers conduct these tests routinely as a quality assessment tool. Villaescusa (1999) conducted independent tests using this method. The testing identified three failure modes, namely “*shear failure at the weld points, failure on the heat affected zone (HAZ) and tensile failure of the wire*”. Villaescusa suggests that the failure mode provides an indication of the quality of the manufacturing process. Weld failure can suggest poor manufacturing processes with dirty electrodes or dirty wires preventing the formation of a good weld. He suggests that HAZ failure is caused by a “*weakening of the wire during the welding process due to excessive weld head pressure and temperature*”.

The AS1304 standard was originally designed to apply to mesh being used for concrete reinforcing. The standard recommends that the “*minimum average shear value in Newtons (N) shall not be less than 250 multiplied by the nominal area or the longitudinal wire in square millimetres (mm²)*”. Villaescusa (1999) suggests that mesh for mining applications requires a much higher standard and recommends that “*the weld strength must be designed to have a strength equal to that of the line wire strength*”. He suggests applying a factor of 500 to the nominal wire area instead of the recommended factor of 250.

More recently AS1304 has been superseded by AS4671 – 2001 “*Steel reinforcing materials*”. This specifies that “*the welded connection at the intersection of bars in a mesh shall be capable of resisting a direct shear force of not less than that determined by the following equation:*”

$$0.5 \times R_{ek.L} A_s \quad (4.1)$$

where:

- $R_{ek.L}$ is the specified lower characteristic yield stress (MPa)
- A_s is the nominal cross-sectional area of the largest bar at the joint (mm²)

The yield stress is determined from the test method prescribed in ISO15630-2:2001 “*Steel for the reinforcement and pre-stressing of concrete – Test methods – Part 2 - Welded fabric*”. The methodology of the ISO is very similar to that of AS1304 although the ISO clamping mechanism design is less prescriptive. Three different clamping options are provided with the following descriptions:

- a) *The cross wire or bar is simply supported by a smooth steel plate, with a slot for the pulling wire or bar. Neither the deflection of the pulling wire or bar nor the rotation of the cross wire or bar is prevented.*
- b) *In addition to the provisions applicable to type a holders, the deflection of the tail of the pulling wire or bar is prevented, but not the rotation of the cross wire or bar. The tail of the pulling wire or bar is supported at a distance of 50 mm from the support surface. The tail support shall allow small movements in the direction of the side movement of the cross wire or bar due to the reaction from the tail support is prevented by a stopper, adjustable according to the size of the test piece. No initial compression of the joint is allowed.*
- c) *In addition to the provisions applicable to type b holders, the rotation of the cross wire or bar is prevented. The cross wire or bar is firmly tightened between jaws with suitable surface structure. The jaws will also prevent any side movement of the cross wire or bar.*

ISO15630 suggests a loading rate of between 6 N/mm²/s and 60 N/mm²/s should be used. ASTM A 497/A-07 “*Standard Specification for Steel Welded Wire Reinforcement, Deformed, for Concrete*” also suggests a similar method for weld shear testing.

No further published work can be found on the small-scale testing of weld mesh for mining applications.

Large-scale mesh testing for mining applications has been conducted all over the world. Test facilities have been built in South Africa (Ortlepp 1983; Ortlepp and Stacey 1996 and 1997; Stacey and Ortlepp 2001; Kuijpers et al. 2002), North America (Pakalnis and Ames 1983; Tannant 1995 and 2001a; Tannant et al. 1997; Dolinar 2006) and Australia (Thompson et al. 1999; Thompson 2001; Roth et al. 2004; Potvin and Giles, 2008). The following sections provide a summary of the test facilities and the test methodologies.

4.3.1 ORTLEPP AND OTHERS

Ortlepp (1983) provides a limited description of static mesh testing undertaken in South Africa. A steel frame with *“a peripheral clamping arrangement”* was used to restrain the mesh. A sample size of 1.1m was used. Loading was undertaken using *“an articulated arrangement of four steel plates”* covering an area of 0.4m x 0.5m. Seven different mesh types were tested. The mesh types and failure loads are provided in Table 2. No definitions are provided for failure load so it is unclear whether the mesh was tested to, or beyond, the first break. Ortlepp notes that *“failure of the strands invariably occurred at a mesh intersection or cross over”*.

Ortlepp also suggests that the mesh results may not be directly comparable as, even though the same area of mesh was used, the differing grid patterns resulted in a varying number of wires being loaded. The differences in the wire diameters may also cause the results to be non-comparable. He used three methods of normalising the data for comparison. These were:

1. Normalising with respect to the nominal cross - sectional area of the wire
2. Normalising with respect to the loaded cross - sectional area of the wire
3. Normalising with respect to the tensile strength of the wire.

The results suggest that *“the interlinking construction of the diamond mesh causes the least impairment of the potential strength of the wire”*. In other words, the full strength of the wire is utilised as a result of the configuration of the diamond mesh.

Table 2: Test results (Ortlepp 1983).

Mesh type	Grid pattern (mm)	Wire diameter (mm)	Failure load (kN)
Diamond stainless	55 x 55	2.5	71.3
Diamond stainless	65 x 65	2.5	66.8
Diamond stainless	65 x 65	2.5	64.1
Diamond galvanised	55 x 55	3.2	60.0
Diamond galvanised	50 x 50	3.2	58.8
Diamond galvanised	50 x 50	3.2	57.7
Diamond galvanised	105 x 105	4.0	51.0
Diamond galvanised	105 x 105	4.0	44.5
Diamond galvanised	100 x 100	4.0	50.0
Square woven stainless	60 x 60	2.3	51.8
Square woven stainless	60 x 60	2.3	50.0
Stranded wire weave	125 x 110	3.2 and 2.2	38.0
Stranded wire weave	110 x 120	3.2 and 2.5	30.0
Stranded wire weave	100 x 75	3.2 and 2.0	23.0
Stranded wire weave	125 x 110	3.2 and 2.5	16.0
Hexagonal twisted	120 x 120	3.0	28.0
Hexagonal twisted	100 x 100	2.7	25.0
Hexagonal twisted	120 x 120	2.7	20.0
Weld mesh	100 x 100	3.2	20.0
Weld mesh	100 x 100	3.2	19.0
Polyethylene rope net	100 x 100	10	60.6
Polyethylene rope net	150 x 150	8	14.0

Further static tests by Ortlepp have not been reported. In the 1990s, Stacey and Ortlepp (1997) constructed a drop test facility to enable the testing of support systems subject to dynamic loading conditions. The test facility consists of a 2m x 2m mesh sample pre-loaded with tiered layers of concrete and steel blocks to simulate a rock mass. The sample is attached to a flexible steel frame which is restrained using tensioned wire guy ropes in each corner. Rock bolts are installed on a 1m by 1m pattern through the mesh. The setup is displayed in Figure 3 and Figure 4. Dynamic loading conditions are not the subject of this thesis and so the results of this testing will not be discussed further.

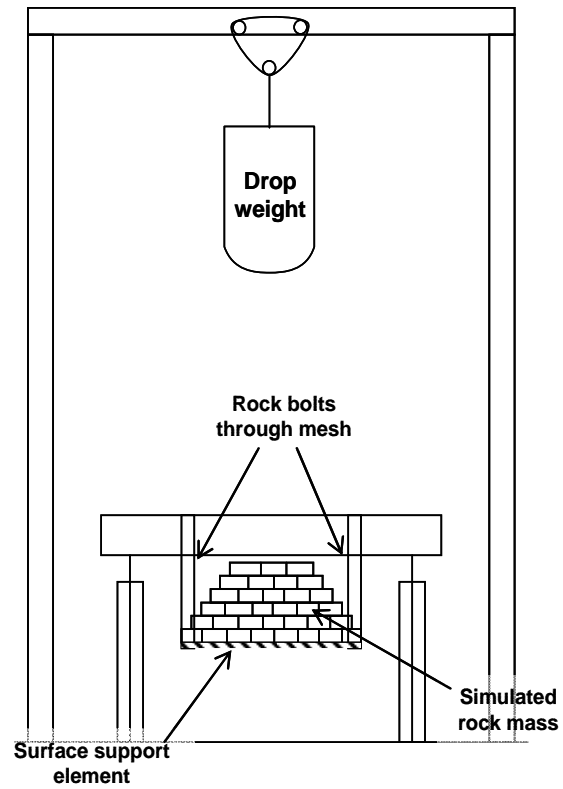


Figure 3: Schematic of Ortlepp's drop test facility

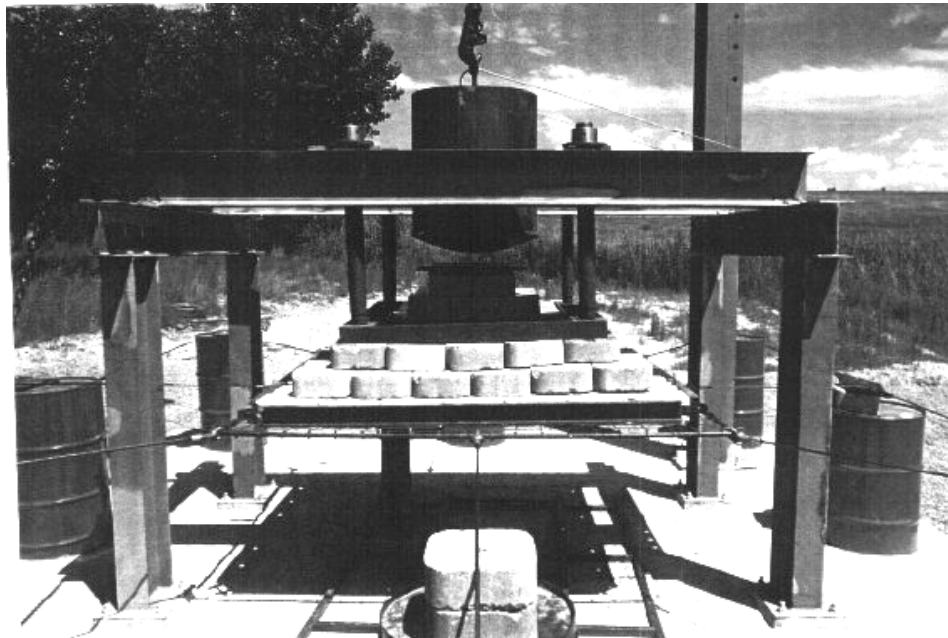


Figure 4: Ortlepp's drop test facility (Stacey and Ortlepp, 1997)

4.3.2 KUIJPERS ET AL.

Kuijpers et al. (2002) modified Ortlepp's drop test facility (Figure 3) to enable the quasi-static and dynamic testing of full-sized surface support elements. The term quasi-static was not defined but implies that the load was applied at a rapid, consistent rate rather than the instantaneous loading caused in the drop test method.

The majority of the tests were carried out on chain link mesh (diamond mesh) with an aperture of 100mm and a wire diameter of 4.2mm. Weld mesh with a 100mm x 100mm grid and a wire diameter of 3.15mm was also tested along with a "Brunswick" system consisting of "heavy welded mesh plus additional straps of extra heavy welded mesh". Tests were conducted with and without lacing.

The test arrangement was altered over the course of the program. The first test arrangement used the same configuration as Ortlepp's drop test facility. The sample was pre-loaded with concrete and steel blocks, in order to simulate a rock mass (Figure 5). It was determined that the concrete and steel blocks interfered with the test arrangement and consequently it was *"impossible to determine the actual capacity and function of the mesh"*.

Various configurations using the concrete and steel blocks were attempted but it was still found that the blocks had some influence over the result. The final test arrangement is shown in Figure 6.



Figure 5: Concrete and steel blocks are used to simulate a rock mass under the test arrangement (Kuijpers et al., 2002).



Figure 6: Kuijpers et al. (2002) final test arrangement

The results demonstrated that the boundary conditions can have a substantial impact on the results of a test. The span can also affect the stiffness of the mesh but *“no obvious difference in stiffness between welded wire mesh and chain link mesh could be found”*. In some cases the chain link mesh was observed to provide a stiffer response than weld mesh. This is in contrast to observations made by other authors such as Pakalnis and Ames (1983) and Haile (1999). The reason for the discrepancy between the test results and observations could not be determined. However it is suggested that the discrepancy may be a function of the geometries or the wire thicknesses of the mesh being tested.

Kuijpers et al. (2002) also undertook dynamic testing, the results of which are not discussed here.

4.3.3 PAKALNIS AND AMES

Pakalnis and Ames (1983) conducted a series of tests on various types of mesh to “determine the load – displacement characteristics of installed mine mesh”.

The test method involved the placement of a 305mm square loading plate behind the centre of an installed mesh sheet. The sheet was installed using a bolting pattern of 1.2m x 1.2m representing the most common practice in the Ontario mines district. A five tonne capacity dynamometer was attached to the centre of the load plate which, in turn, was attached to a chain block pulling apparatus. The pulling apparatus was attached to the opposite wall of the drive and incremental loads were applied. A schematic of the test configuration is given in Figure 7.

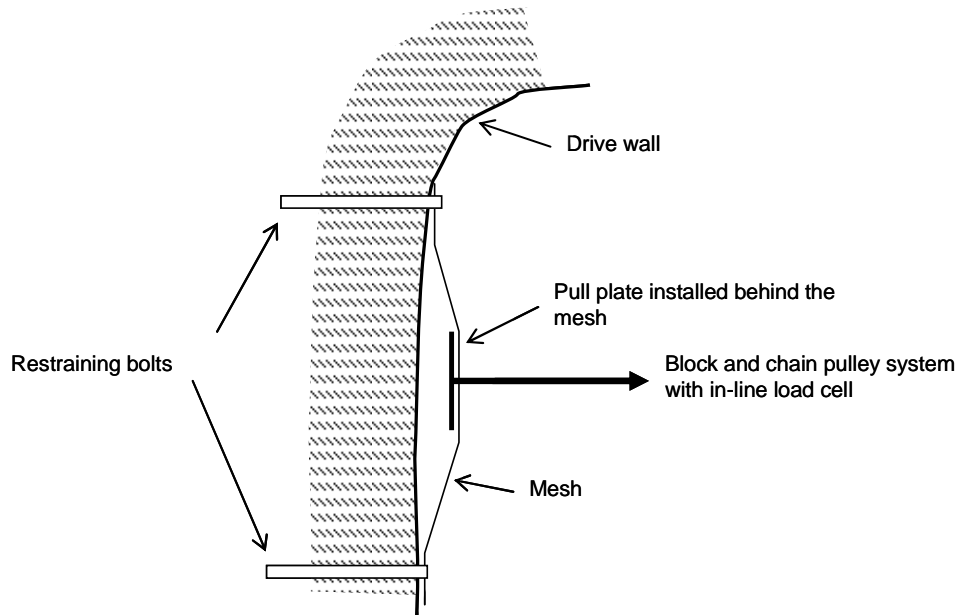


Figure 7: Pakalnis and Ames test arrangement

The test results indicated that “the amount of displacement is more dependent on the type of screening rather than the wire thickness”. Weld mesh was capable of displacements between 250 and 300mm whereas chain link mesh was capable of displacements of between 350 and 450mm. The forces were more dependent upon the wire diameter with thicker wires having a higher capacity. Table 3 provides a summary of the test results.

Table 3: Test results (Pakalnis and Ames, 1983).

Mesh type	Grid Pattern (mm)	Wire Diameter (mm)	Test peak load (kN)	Central displacement (mm)
Weld Mesh	100 x 100	5.7	36.0	292
Weld Mesh	100 x 100	4.9	32.9	286
Weld Mesh	100 x 100	3.8	18.7	273
Weld Mesh	100 x 50	2.7	13.8	311
Chain link	50	3.0	28.9	413
Chain link*	50	3.0	17.3	349
Chain link**	50	3.8	15.6	400
Chain link	50	3.8	36.5	425
Chain link*	50	3.8	32.0	438

Note: * Samples were galvanised post welding
 ** Samples were constructed from galvanised wire

Pakalnis and Ames discussed two techniques for estimating the forces within the wires of the mesh; one by Coates (1965) and one by McFarlane (1978).

The first technique was developed by Coates (1965) to estimate the force applied to mesh and then to estimate the tension applied to each wire. The equations, developed from catenary principles, assume a uniform loading distribution over the entire area of mesh and that the dominant failure mechanism is tensile failure of the wires.

Coates proposed that loading between the bolts can be characterised by principles of arching more commonly applied in caving theory. Using these principles it is determined that the vertical pressure on a membrane can be represented by equation 4.2. This equation has been applied to mesh using the assumption that uniform loading occurs over the entire area of the mesh.

$$p_v = b\gamma \frac{(1-e)^{k \tan \phi^2 z/b}}{2k \tan \phi} \quad (4.2)$$

where:

- p_v = vertical pressure (kN/m²)
- b = width of the arch (m)
- γ = unit weight of the rock (kN/m³)
- z = height of caving ground (m)
- ϕ = internal friction angle of the rock
- k = is the ratio of the horizontal stress to the vertical stress

The equation is simplified to Equation 4.3 by assuming the following values:

- The spacing of the bolts in metres (s) is equal to width of the arch (b).
- The depth of failure (z) is less than the bolt spacing (s). This assumes that there is no loss of support capacity by the bolts
- The internal friction angle (ϕ) is assumed to be greater than 45 degrees making the ratio of the horizontal stress to the vertical stress (k) less than 0.33. This assumption is based on the caving theory.

This results in the following equation:

$$p_v \leq 0.727\gamma s \quad (4.3)$$

This new equation is a function of only the unit weight of the rock and the bolt spacing. By using the sum of moments, the tension of each wire can be calculated using the following equation:

$$T = \frac{p_v s^2}{8h} \quad (4.4)$$

where:

- T = the tensile force per linear metre (kN/m)
- s = bolt spacing (m)
- h = displacement (m)

This equation assumes uniform loading over the entire area of the mesh and that *“the section is representative of a sufficient length to make two-dimensional analysis valid”*.

The second technique is based on works conducted by MacFarlane (1978) that consider the shearing of welds as the main failure mechanism. MacFarlane’s works are published in internal company reports and are not available for review, but Pakalnis and Ames indicate that the technique is based on catenary principles. Catenary principles suggest that a cable under uniform load forms a curve of a specific shape. As such, tensile force of the wires can be calculated using the understanding of the changing nature of the curve. The following formulae are provided by Pakalnis and Ames:

$$\left(\frac{p_v}{4}\right)\left(\frac{l}{2}\right) - dH = 0 \quad (4.5)$$

$$T_a = \sqrt{\left(\frac{p_v}{4}\right)^2 + H^2} \quad (4.6)$$

where:

- p_v is the screen load (kN).
- l is the catenary length (mm).
- d equals the centre point sag (or displacement) (mm).
- H is the horizontal component of the end reaction.
- T_a is equivalent to the axial force in the catenary (kN).

Pakalnis and Ames applied both these techniques to predict the peak forces for the mesh used in the test program and then compared these peak forces with the test program results. The results of the predictions are provided in Table 4.

Table 4: Predicted and actual peak forces provided by Pakalnis and Ames (1983).

Mesh type	Grid Pattern (mm)	Wire Diameter (mm)	Test peak load (kN)	Coates peak load prediction (kN)	McFarlane peak load prediction (kN)
Weld Mesh	100 x 50	2.7	13.8	74	3.6
Weld Mesh	100 x 100	3.8	18.7	122	6.2
Weld Mesh	100 x 100	4.9	32.9	218	11.0
Weld Mesh	100 x 100	5.7	36.0	307	15.4
Chain link	50	3.0	28.9	239	NA
Chain link	50	3.8	36.5	380	NA

Pakalnis and Ames suggest that Coates' analysis technique "*over-estimates the load capabilities of the installed screen*". They suggest that one reason for the over-estimation is that the mesh is not fully restrained and therefore cannot be treated in the same manner as a membrane. They also suggest that the loading area will also affect the results. The results also indicate that the McFarlane analysis technique grossly underestimates the actual peak forces.

4.3.4 TANNANT AND OTHERS

In the 1990s Tannant and colleagues undertook extensive testing to attempt to simulate the reaction of mesh under realistic loading conditions.

The test facility consisted of a base frame with an overhead winching system. The mesh was bolted to the base frame using 19mm bolts and 127mm steel plates. The standard test arrangement used a bolting pattern of 1.2m x 1.2m with the bolts positioned on the directly loaded wires (forming a diamond pattern).

A 300mm square plate is pulled up through the mesh using an electric winch at a loading rate of between 15 and 24mm per second. The force is measured using an in-line 10 tonne load cell. A diagram of the test facility is given in Figure 8.

In 1995 Tannant published the results of welded wire mesh testing using different bolting configurations. Eighty one tests were conducted using three configurations as illustrated in Figure 9. The results indicated that the failure mode was dependent on the bolting pattern. The diamond pattern caused failure of the mesh through tensile failure of the wires, usually near the edge of the rock bolt plate or the pulling plate. More deformation was observed in the square bolting pattern tests and resulted in the mesh squares distorting into "rhomboidal shapes".

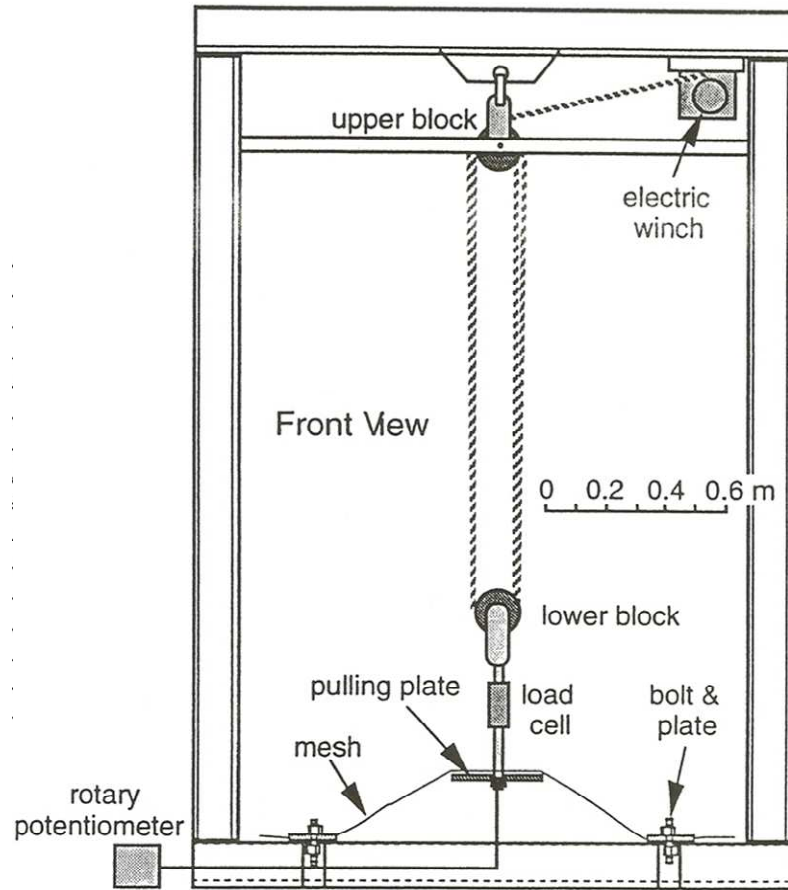


Figure 8: Tannant (1995, 1997 and 2001a) test facility.

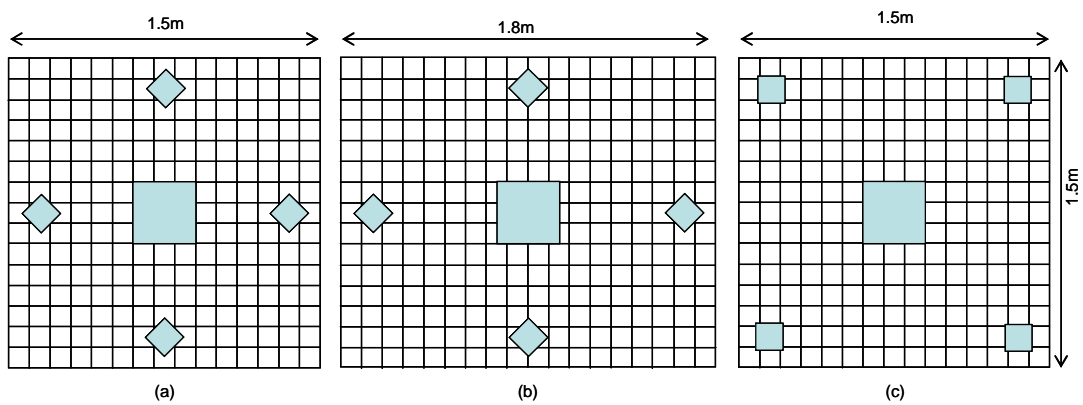


Figure 9: Tannant (1995) bolting patterns (a) 1.2m x 1.2m diamond pattern (b) 1.2m x 1.5m diamond pattern and (c) 1.2m x 1.2m square pattern.

Tannant et al. (1997) also compared the force – displacement responses of welded wire mesh, chain link mesh and expanded metal mesh. The results indicate that *“welded wire mesh clearly has a much stiffer initial loading response whereas chain link and expanded metal have larger displacement capacities and exhibit significant post peak ductility”*. The results also indicate that *“welded wire mesh with larger diameter wires displays higher peak load capacities as well as greater displacements at peak load”*. Tannant suggests that *“the load capacities of the mesh are roughly proportional to the tensile capacity of the wire”*.

Tannant used material property principles, such as Hooke's Law, to determine a numeric value for the mesh stiffness and to predict the maximum load capacity for each mesh type based on the tensile strength of the wire. The stiffness is used to *“quantify how quickly load increases after the mesh has been loaded half way to its peak”*. Peak load is defined as the first major peak prior to a drop in force. The equation is given by:

$$K = \frac{L_p - L_{50}}{d_p - d_{50}} \quad (4.7)$$

where:

- K = stiffness (kN/mm)
- L_p = Peak load (first major peak) (kN)
- L_{50} = 50% of peak load (kN)
- d_p = Displacement at peak load (mm)
- d_{50} = displacement at 50% of peak load (mm)

A straight line is determined by the points (d_p, L_p) and (d_{50}, L_{50}) as indicated in Figure 10. The numerical value where this line intersects the x axis (d_o) is described as *“the displacement needed to activate the load carrying capacity of the mesh”*.

The results of this analysis are provided in Table 5.

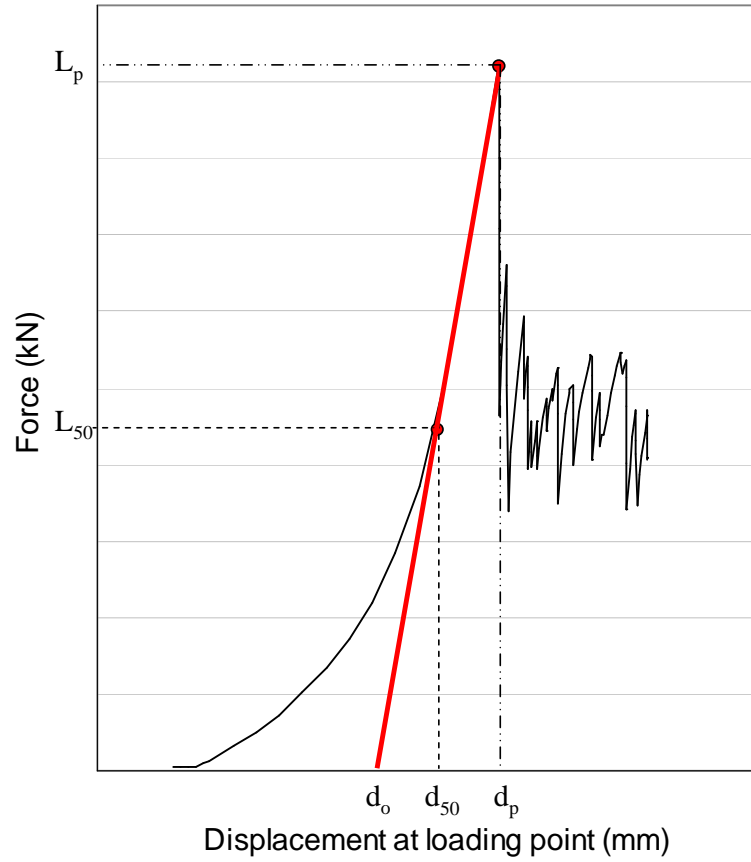


Figure 10: Chart showing the principle of stiffness as described by Tannant.

Table 5: Tannant et al. (1997) test results using a 1.2m bolting pattern.

Mesh type	Wire diameter (mm)	No of tests	Stiffness k (kN/mm)	Displacement offset d_o (mm)	Displacement at peak d_p (mm)	Peak Load L_p (kN)
Weld Mesh	3.7	5	0.15	5	105	14.8
Weld Mesh	4.9	6	0.27	23	114	24.3
Weld Mesh	5.8	4	0.38	33	152	38.2
Chain link mesh	3.7	4	0.24	273	417	34.4
Expanded metal mesh	NA	5	0.06	129	595	24.6

Tannant (1995) suggests the peak load can be predicted using analysis based on catenary principles. He assumes that point loading occurs at the centre of a single wire and that the forces are transferred uniformly along the wire. Using these assumptions the following equation is used to predict peak load:

$$L_p = \frac{2NT}{\sqrt{1 + (s/4d_p)^2}} \quad (4.8)$$

where:

- N = Number of wires carrying load
- T = Tensile load capacity of the wires (kN)
- s = spacing of bolts (mm)
- d_p = displacement at peak force (mm)

The application of this analysis was published in an internal report (Tannant 1994) and is not available for review.

Tannant et al. (1997) also compares the displacement capacity of each mesh type. The displacement at peak load for welded wire mesh was between 100 and 250mm. Comparatively chain link mesh and expanded metal mesh were capable of much higher displacements of between 400 and 600mm.

Tannant states that *“the displacement capacity at the peak load is related to the drift convergence that can be tolerated before support rehabilitation is required”*. He suggests that *“400 – 600 millimetres of relative displacement between rock bolts constitutes excessive displacement and probably infers poor stability conditions within a drift”* and that *“welded wire mesh showing more than 100 – 250mm of bagging (depending on the mesh gauge) has likely reached or exceeded its peak strength”* and should be rehabilitated.

4.3.5 THOMPSON ET AL.

Thompson et al. (1999) suggests that *“theoretical investigations (into mesh force - displacement reactions) are required since it is not feasible to mechanically test for the large number of possible combinations of bolting and loading conditions with various mesh considerations”*. Full – scale testing was undertaken to provide results for the calibration of a modelling program developed to simulate the force - displacement reaction for welded wire mesh.

The test facility used to evaluate the mesh was developed in conjunction with an Australian mine site and is displayed in Figure 11. The mesh was connected to the floor of a concrete pit using 20mm anchor bolts and 200mm x 200mm square plates. A square loading frame was placed under the sample and fixed to a cross head using four bolts. The cross head and loading frame were attached to a threaded bar which passed through an overhead beam supporting a rotating capstan. Displacement was controlled manually by rotating the capstan. One rotation equalled 10mm of vertical displacement. An electronic load cell was used to measure the force applied to the mesh.

The plate size, plate orientation, bolt spacing and bolt orientation were all varied. Figure 12 and Table 6 provide descriptions of the twelve configurations.

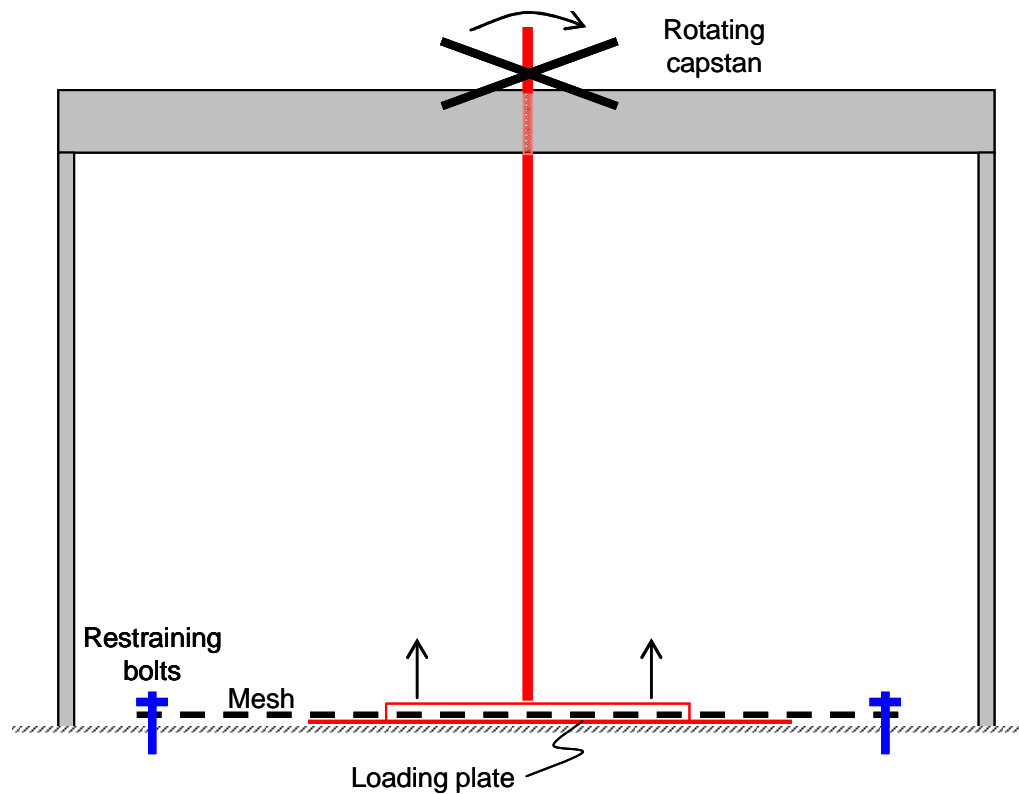


Figure 11: Schematic of the Thompson et al. (1999) mesh test facility.

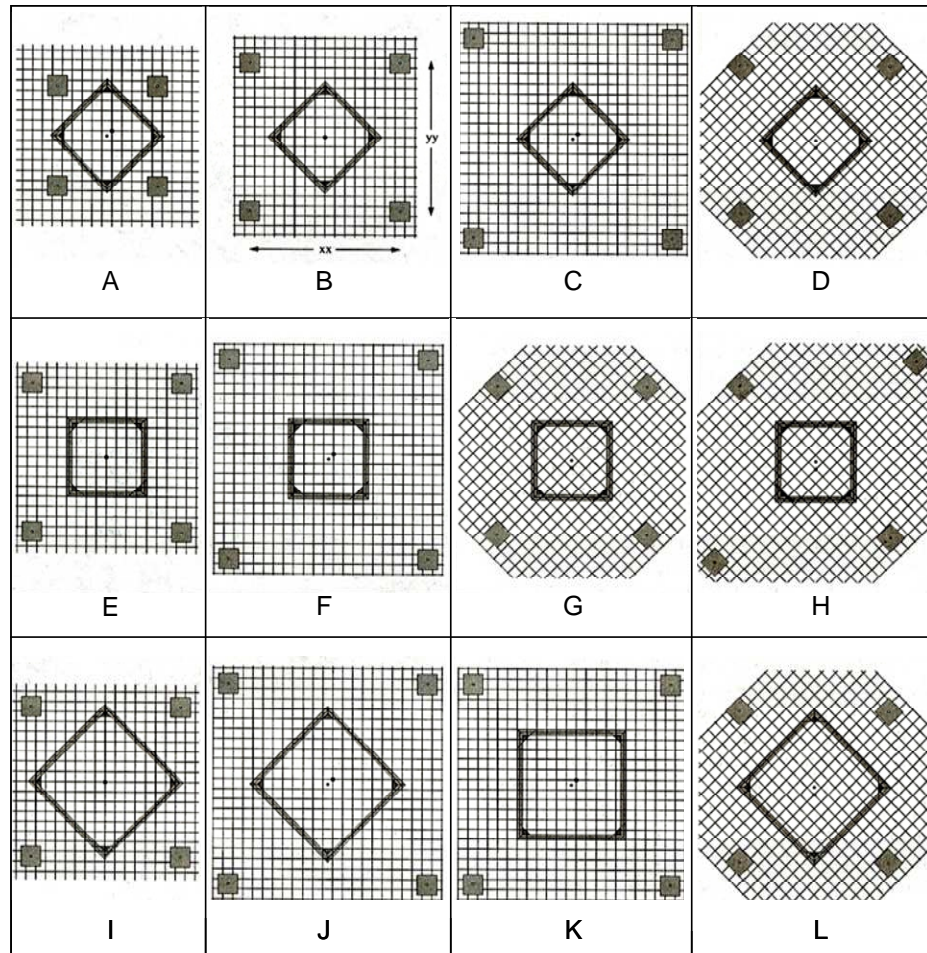


Figure 12: Test variations used by Thompson et al. 1999.

Table 6: Test parameters used by Thompson et al 1999.

Test Arrangement	Bolt configuration	Bolt Spacing (m)		Plate Orientation	Plate size (mm)
		a	b		
A	Square	1.0	1.0	Oblique	750
B	Square	1.5	1.5	Oblique	750
C	Square	2.0	2.0	Oblique	750
D	Oblique	1.5	1.5	Oblique	750
E	Square	1.5	1.5	Square	750
F	Square	2.0	2.0	Square	750
G	Oblique	1.5	1.5	Square	750
H	Oblique	1.5	2.0	Square	750
I	Square	1.5	1.5	Oblique	1050
D	Square	2.0	2.0	Oblique	1050
K	Square	2.0	2.0	Square	1050
L	Oblique	1.5	1.5	Oblique	1050

Most tests displayed some signs of slippage as a result of the wires sliding under the bolt plate and aligning against the restraining bolt. In a few of the tests the wires hooked over the plate to prevent slippage.

There was a marked difference in the deformation of the samples with respect to the bolting pattern irrespective of the loading frame orientation. Observations from the oblique bolt configuration indicated that forces were transferred directly to the bolts from the loading plate. Some forces were transferred away from the bolts in the latter stages of the test although the primary loaded wires transmitted the bulk of the forces. This concept is illustrated in Figure 13.

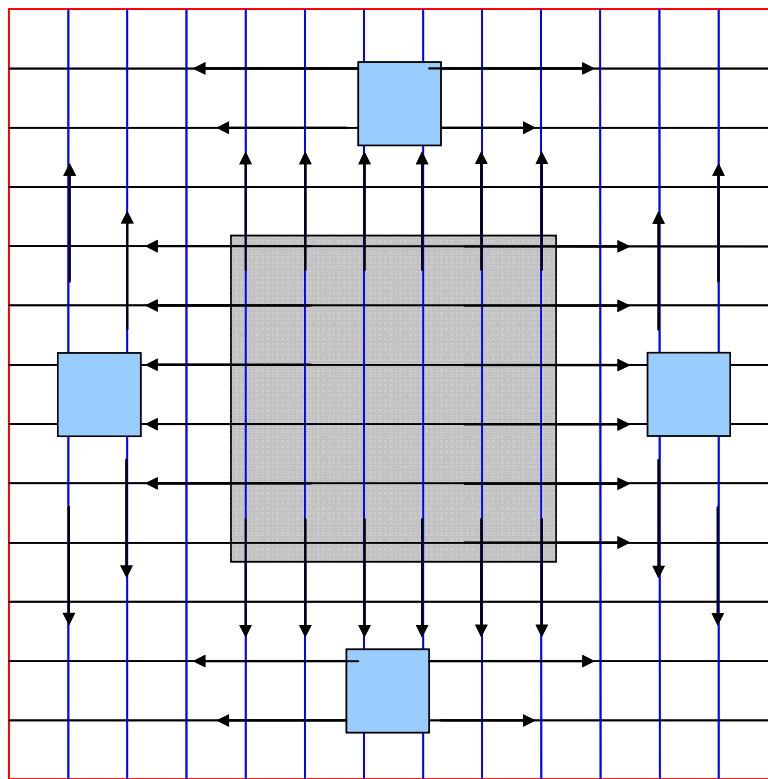


Figure 13: Force transfer concept using a diamond or oblique bolting pattern.

The square bolt arrangement did not restrain the directly loaded wires and consequently the mesh deformed considerably as the forces were transferred through in-direct paths to the bolts as shown in Figure 14. The arrows in Figure 14(a) indicate the direction of the force transfer around the mesh. Figure 14(b) and Figure 15 illustrates the distortion of the grid that occurs in the intermediate zone (indicated in pink).

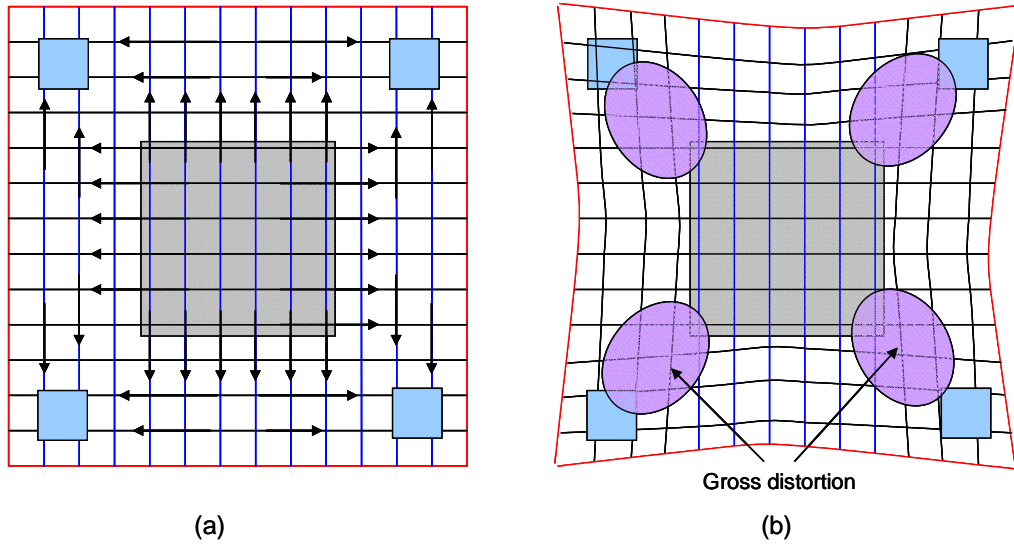


Figure 14: Force transfer concept using a square bolting pattern.

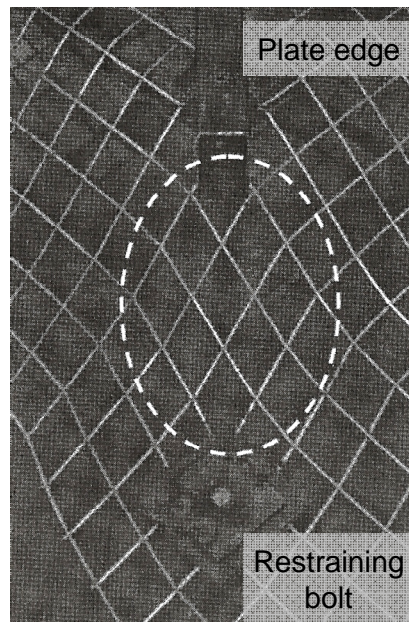


Figure 15: Gross deformation of the mesh observed using the square bolting pattern (Thompson et al. 1999).

In all tests where considerable distortion occurred, it was observed that the welds caused some local increase in the bending stiffness of the wire. This was indicated by the wires at the welds remaining perpendicular to each other, whereas in the centre of the mesh grid away from the welds the wires become oblique to each other. This concept is provided in Figure 16.

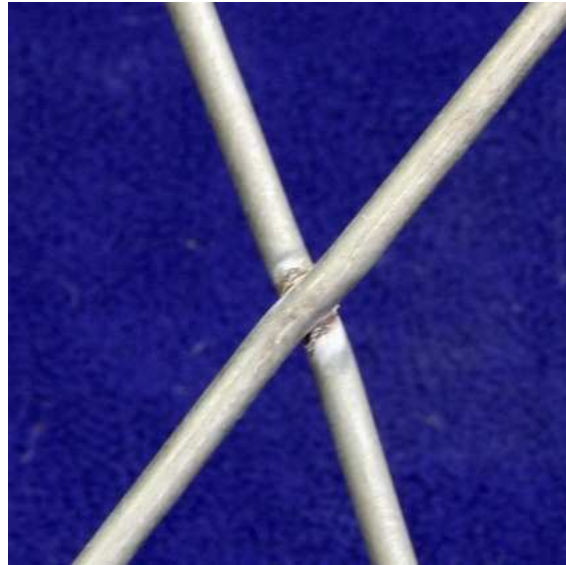


Figure 16: Stiffening of the wires at the weld locations.

Thompson et al. (1999) used Tannant's analysis techniques, described in Section 4.3.4, as the basis for the development of a theoretical modelling program to replicate mesh behaviour. The model assumes that all the forces are absorbed by the directly loaded wires. Thompson's theoretical force transfer diagram for one directly loaded wire is given in Figure 17.

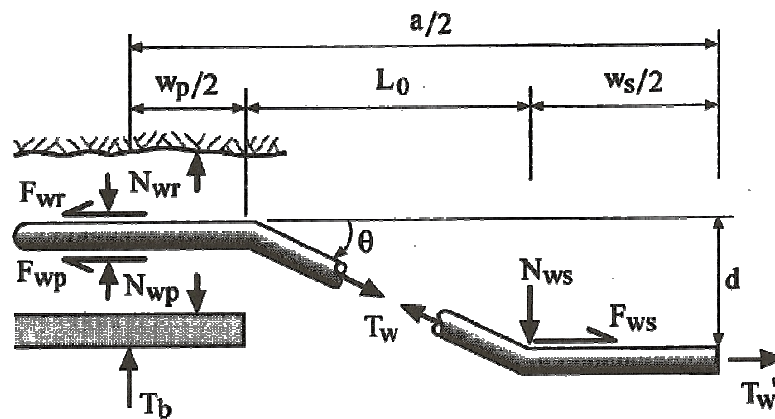


Figure 17: Theoretical representation of mesh wire tension (Thompson et al. 1999).

The force - displacement results from the test program were used to calibrate the model. Slip at the plate interface was accounted for in the modelling program.

The modelling found that in all cases the wire forces were predicted to remain lower than the wire yield strength due to slip at the plates and bolts. This was consistent with the observations from the field tests. In some cases a good correlation between the model and the field trials was established but in most cases the predicted force was less than the measured force. The differences could be related to the number of wires assumed to be acting and also to the discounting of the bending stiffness in the wires. Better predictions were achieved if it was assumed that the secondary loaded wires were transmitting some of the load

Thompson (2001a) reviewed the previous modelling results (1999) and determined that *“extending the empirical approach would be of little value in attempting to quantify the performance of alternative mesh configurations”*.

The modelling program was extended to incorporate the ability to assess the following changes in configuration:

- Variable wire diameters
- Variable wire spacing
- Non-linear stress strain properties for the wire
- Weld strength
- Slip of the mesh at the plates and bolts
- Variable bolt tension
- Variable bolt spacing
- Variable mesh orientation relative to the bolting pattern
- Mesh lay relative to the wire loading (cross wires up or down)
- Variable load types and areas
- Large mesh displacements causing changes in mesh geometry.

The program employs “nodes” at each individual wire cross over point (weld location). At each node the displacements and rotations must be replicated and consequently the forces and moments need to be in equilibrium. Matrix transformations are used to translate the applied forces and displacements at a particular node, into resultant displacements and forces which in turn become the applied force and displacement for that node. The number of analysis steps and the force and displacement increments are specified depending upon the required output. The program was not completed prior to the paper being published and as such no modelling results are presented.

4.3.6 POTVIN AND GILES

More recently Potvin and Giles (2008) have designed and constructed a test frame at the University of Western Australia. The rudimentary test frame consists of a steel frame with bolts mounted in the corners and the centres of each side as indicated in Figure 18. The mesh is held in place using plates attached to the bolts.

A central loading plate is attached to a block and tackle arrangement with an in-line load cell mounted just above the plate to record force. An LVDT is used under the sample to measure the displacement.



Figure 18: Potvin and Giles (2008) test setup.

The test facility has been used to evaluate a specially designed mesh element. Potvin and Giles (2008) combine the concept of cable lacing commonly used for support in South Africa and weld mesh. The concept is illustrated in Figure 19. The results indicate that it is possible to achieve up to 17 tonnes and 700mm of displacement but the configuration of the sample and the test setup suggests it is likely that only the boundary cables were being tested rather than the combined configuration.

No results are provided for the force-displacement properties of the mesh alone.

Further improvements to the combined design are suggested by incorporating a “crinkled mesh” design as shown in Figure 20. The design of the crinkled mesh was originally proposed by Kuijpers et al. (2002) and developed and tested by Ortlepp and Erasmus (2002). The original design is displayed in Figure 21. Testing of this product in South Africa proved inconclusive.

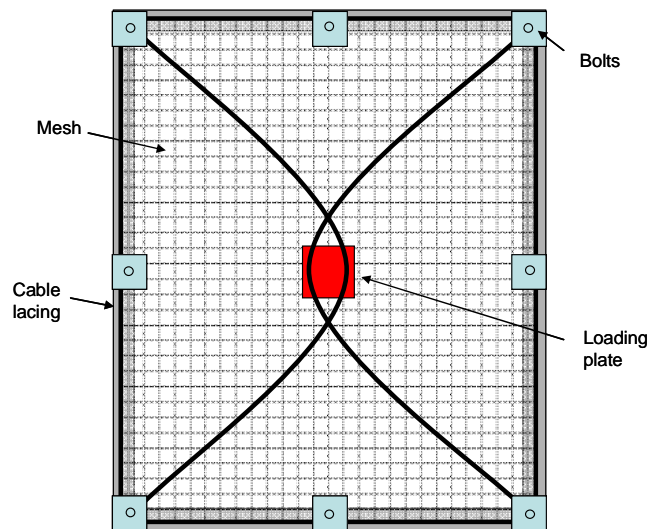


Figure 19: Potvin mesh layout with test setup.

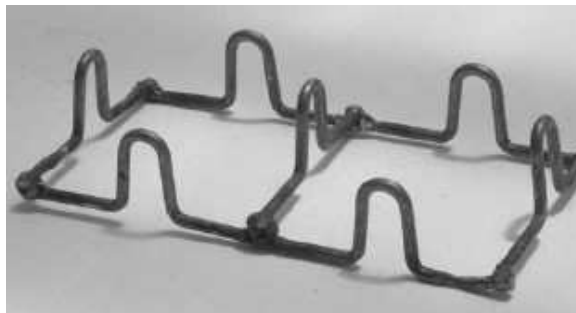


Figure 20: “Crinkling” of the mesh (Potvin and Giles 2008)

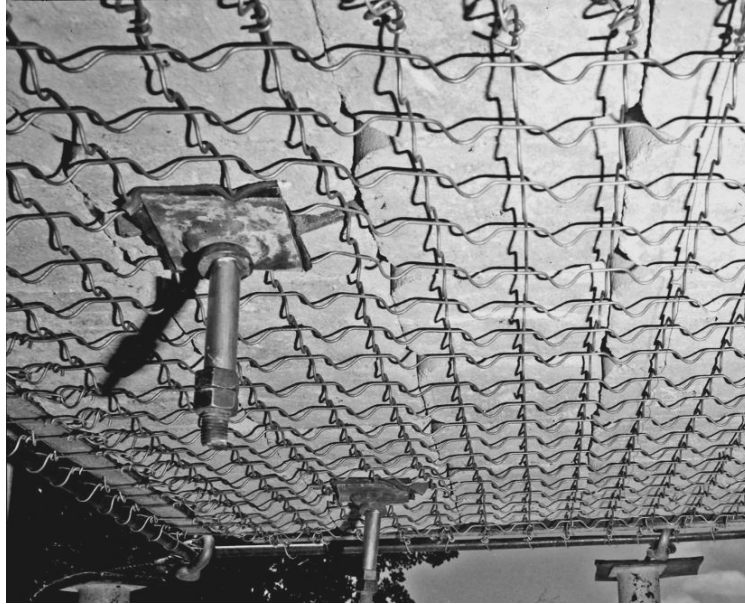


Figure 21: Crinkled mesh configuration tested by Ortlepp and Erasmus 2002.

4.3.7 OTHER TESTING

Further testing has been conducted by Roth et al. (2004), Van Sint Jan et al. (2004), and Dolinar (2006). Van Sint Jan et al. (2004) developed a test facility based on the drop test facility constructed by Ortlepp (1983). Chain link mesh was tested and the results were used to compare the performance to that of mesh reinforced shotcrete and fibre reinforced shotcrete. The testing found that chain link mesh tended to unravel after the first wire failure and that the wire strands tend to break more easily when used as reinforcing compared to when the mesh is acting alone.

Roth et al. (2004) used the same test facility as Thompson et al. (1999) to evaluate the performance of the Geobruigg high tensile chain link mesh. Both 3mm and 4mm diameter wire meshes were tested. The results from this test program were compared with the results presented by Thompson et al. (1999). The results demonstrated that the high tensile chain link mesh developed by Geobruigg had much higher force and displacement capacities than that of weld mesh. More recently Roth et al. (2007) attempted to simulate the test results using numerical modelling. Further work is still required in calibrating the model.

Dolinar (2006) developed a test facility in the USA similar to that of Tannant (1995). Tannant's analysis methods were used to compare the test results from this program with the previous programs conducted by Tannant.

4.3.8 DISCUSSION OF PREVIOUS TESTING

The different test methods described above each have their advantages and disadvantages. The description of Ortlepp's test facility is brief and not enough information is provided about the facility and the loading mechanisms for critical review. Tannant's loading rate of 18 – 22 mm/s appears to be relatively fast compared with true static loading conditions. The effect of the loading rate on mesh has not previously been investigated. Pakalnis and Ames provide the only true in-situ test results.

Mesh is a relatively simple retention system compared with other passive resistance support systems such as shotcrete or membranes. It does not have the same level of complexity in the interaction with the rock mass as shotcrete or membranes. Two-dimensional analysis, often using catenary principles, is the most common method. This method assumes that forces are only transferred along directly loaded wires. It does not account for forces being transferred away from the loaded area by adjoining wires.

Pakalnis and Ames's (1983) attempts to predict the tension in each individual wire assumes that only the directly loaded wires are withstanding the applied forces. In fact, the mesh geometry allows for forces to be transferred away from the directly loaded area and involves many more wires; consequently the capacity of the mesh is increased. It is this primary property that enables mesh to be effective as a ground support element.

Tannant's definition of the d_0 parameter is also an over simplification, ignoring the non linearity of mesh products. The characterisation of the stiffness of the mesh should reflect the nature of the mesh. This will be tested using the WASM test data.

The techniques used by both Pakalnis and Ames and Tannant concentrate primarily on the force capacity of the mesh. The analysis techniques do not consider the displacement capacity of the mesh although in many circumstances it may be displacement that is the critical design parameter rather than force.

Thompson's modelling of the force - displacement characteristics is the best attempt at determining a design criterion for mesh. It encompasses three-dimensional deformation of each node on the mesh. So far no outputs from the program have been published. The program has been designed specifically for weld mesh. Further modifications are required to simulate the deformation and force transfer properties of chain link mesh.

The WASM mesh test program has been undertaken to determine the force – displacement characteristics of different mesh systems to enable the further development of a three-dimensional assessment to be used in mesh design. The test program has also been designed to enable the comparison of the force – displacement characteristics of mesh with those of shotcrete and membranes.

4.4 MESH TEST METHODOLOGY

The testing facility has been described in Chapter 3. Mesh tests are setup using the following process:

1. The sample is placed in the test frame according to the specified sample configuration. The different configurations are described in Section 4.6.
2. The sample is restrained according to the specified boundary conditions given in Section 4.7.
3. Initial measurements are recorded to determine the position of the mesh.
4. The loading plate is positioned in line with the loading point, on the sample.
5. The initial measurements are repeated to determine the displacement as a result of the plate placement.
6. The jack is lowered to be in contact with the plate.
7. Measurements are taken for the third time to ensure no displacement has occurred as a result of the positioning of the jack.
8. The data acquisition system and the jack are activated to begin testing.
9. Testing is continued until the mesh is deemed to have exceeded its serviceable limit or there is a risk of damage to any of the test frame components.

4.5 MATERIALS

Two basic types of mesh are used as surface support in underground mining. The most common type of steel wire mesh is welded wire mesh (weld mesh). Less common, though increasingly necessary, is the application of steel wire chain link mesh in high ground deformation environments.

Testing was undertaken on three different mesh types; weld mesh, plastic geogrid and chain link mesh. Weld mesh was predominantly tested with the samples sourced from a number of different mine sites and manufacturing locations.

The welded wire mesh is constructed by laying out wires (that form the long wires) and placing cross wires over the top to form a grid pattern. The wires are then mechanically welded together by placing electrodes at each intersection and passing a current or voltage through the wires. This creates heat which in turn melts the wires to form the weld. The sheets are then cut to size. Only one weld mesh geometry was tested consisting of 100mm x 100mm grids. The most common wire is 5.6mm in diameter used on both the cross wire and long wires. Other wire diameters were tested but these results are confidential and consequently have not been discussed in this thesis. The mesh sheets provided from site were typically 3m long by 2.4m wide. Two samples were cut from each sheet. The typical sheet configuration is provided in Figure 22. Off-cuts from the sheet were retained for further testing as required. If the sheets size varied from the standard dimensions, the manufacturer was requested to mark long wires and cross wires to ensure the consistency in the test setup.

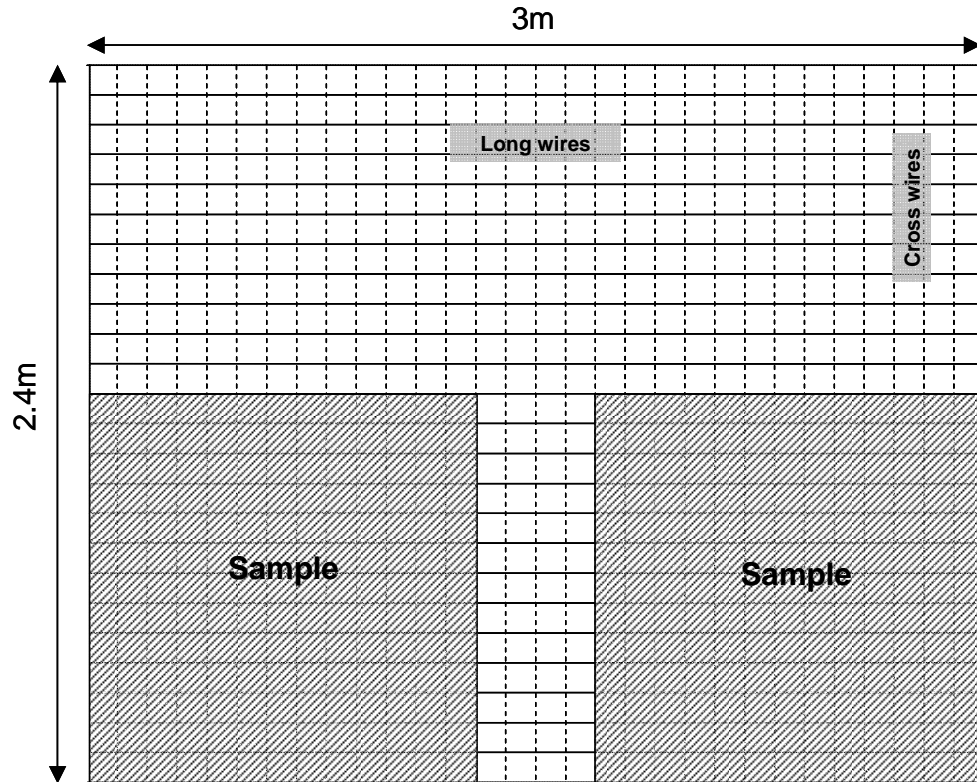


Figure 22: Typical weld mesh sheet layout.

One test was conducted on a plastic grid mesh which has a similar pattern to weld mesh. The grid spacing is 50mm x 50mm. The result has not been discussed in this thesis.

Twenty three tests were conducted on high tensile chain link mesh specially designed by Geobruigg Pty Ltd. Different wire diameters and different diamond geometries were tested. Two tests were also conducted on a generic 3mm chain link mesh which consists of interwoven wires with looped ends. The samples were poor quality and may not have been truly representative of the product. Consequently, the results from these tests have not been presented in this thesis.

Chain link mesh consists of a series of long wires bent into a zigzag pattern and then interwoven to form a sheet. The Geobruug mesh consists of high tensile wires which are joined at the edges using specially designed and patented “knots” to prevent unravelling of the wires. The samples were custom made to the WASM size specifications to enable a proper fit on the test frame. An example of the sample layout is provided in Figure 23. Three different wire dimensions and three different diamond configurations were tested. The configurations are provided in Table 7 and Figure 24.

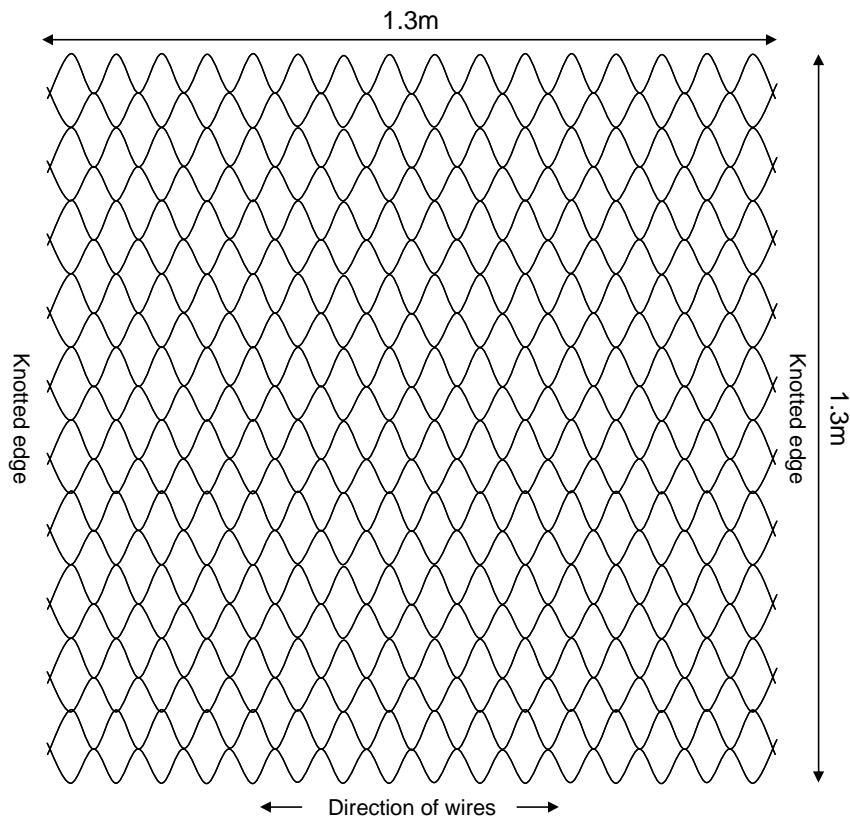
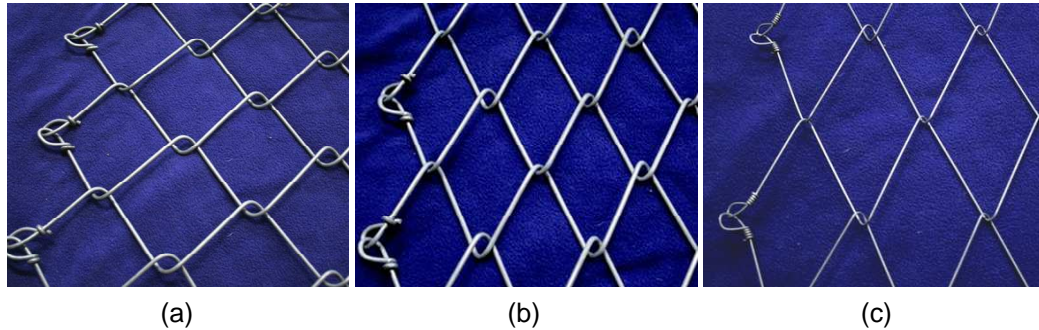


Figure 23: High tensile chain link mesh layout (G65/4).

Table 7: High tensile chain link sample configurations.

Mesh Product	Wire Diameter	Diamond Size	No of wires	No of diamonds
S95/4	4mm	150mm x 150mm	20	9
G65/4	4mm	80mm x 140mm	20	16
G80/4	4mm	100mm x 180mm	14	13
G65/3	3mm	80mm x 140mm	20	16
G80/2	2mm	100mm x 175mm	14	13

**Figure 24: Diamond Configuration for (a) S95, (b) G65 and (c) G80.**

4.6 MESH CONFIGURATIONS

The wire configuration for weld mesh results in only one direction of wire being in direct contact with the loading mechanism. This allows for the number of alternative test configurations that are described in the following sections.

No alternative test configurations were tested for chain link mesh due to the single configuration of the mesh and the availability of samples from the manufacturer.

4.6.1 CROSS WIRES UP

Samples were placed in the frame with the cross wires up and across the frame as indicated in Figure 25. This was used as the standard test arrangement.

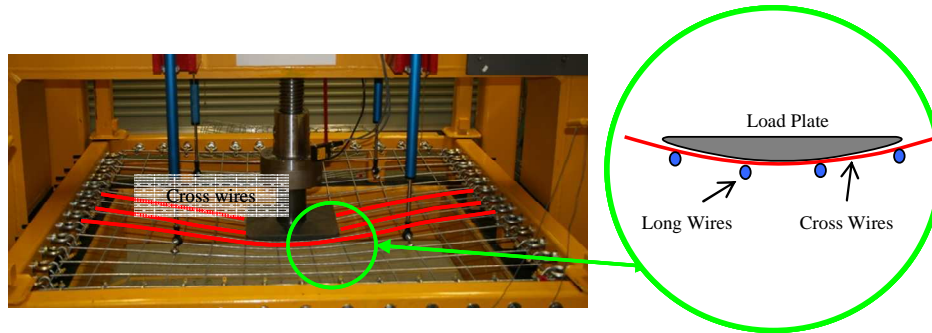


Figure 25: Cross wires up were adopted as the standard test procedure.

4.6.2 CROSS WIRES DOWN

Samples were placed in the frame with cross wires down and across the frame. The wire orientation in these tests reflects the “recommended” way of installing mesh underground as illustrated in Figure 26. This was used to evaluate the effects of the wire direction in comparison with the standard test arrangement.

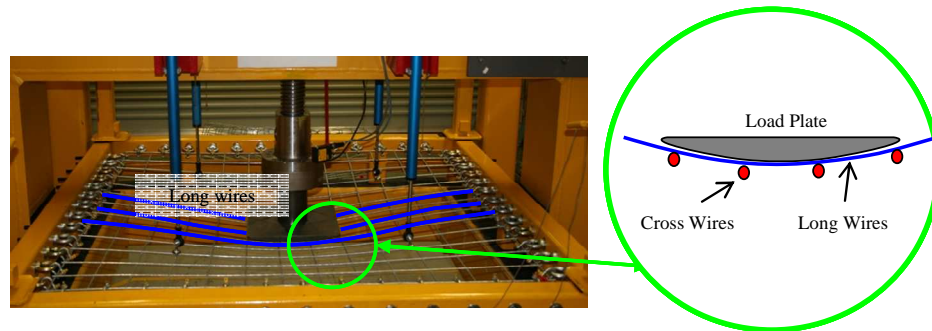


Figure 26: The sample orientation was altered to determine the effect of orientation on the force - displacement characteristics of the mesh.

4.6.3 SMALL-SCALE TESTING

The full scale testing of different orientations indicated slight differences between the “cross wires up” and “cross wires down” test configurations. In order to maximise the use of the test materials available, and to confirm the results of the large scale testing, samples of 1300mm x 400mm were cut and tested with cross wires up and cross wires down. The results from these tests were analysed in isolation from the large scale tests.



Figure 27: Setup of small – scale tests.

4.6.4 OVERLAP TESTING

Continuous coverage of the roof of a mine is achieved by overlapping adjoining sheets by 200mm – 300mm. Observations of mesh in underground conditions indicate that, where loading occurs on the overlap, the mesh tends to peel apart rather than transfer the load to other parts of the mesh (Figure 28).



Figure 28: Mesh being pushed apart at the overlap between sheets.

In order to simulate this condition, one 1300mm x 700mm weld mesh sample and another of dimensions 1300mm x 800mm were cut from the same sheet in the same orientation. The samples were overlapped in the centre as indicated in Figure 29. On the overlaps, both sheets were held using one shackle at each restraint point. The rest of the sheet was restrained according to the standard test.

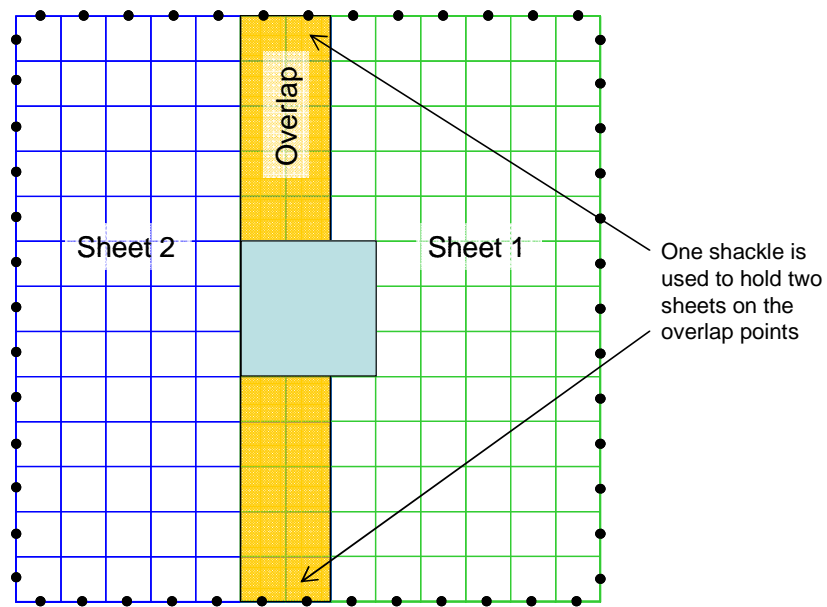


Figure 29: Test layout where two sheets have been overlapped.

4.7 BOUNDARY CONDITIONS

The boundary conditions of any laboratory test setup can have a large impact on the results derived. Several different boundary conditions were trialed at WASM prior to developing the final test arrangement.

4.7.1 CLAMPING

The first setup to be trialed involved clamping the sample to the sample support frame. A 1600mm square mesh sample was placed on the sample support frame and a boundary restraint frame was placed over the sample. Clamping posts were wound down on each corner of the frame to hold the boundary restraint frame in place. The full test setup is given in Figure 30. Only three tests were conducted using this method.

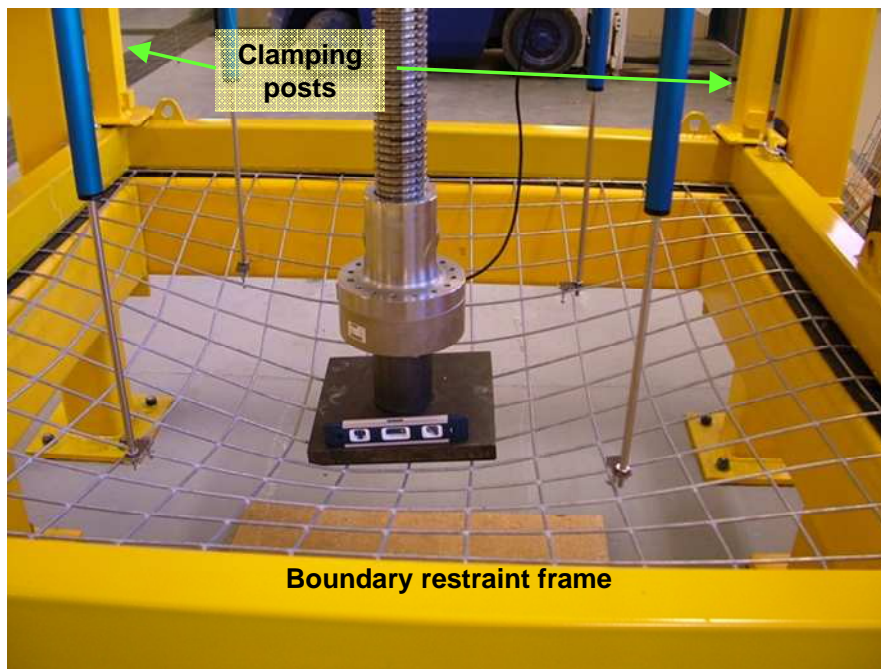


Figure 30: Clamping test arrangement.

4.7.2 LACING

Observations of the force - displacement reaction of the mesh using the clamping method indicated that the normal force provided by the clamping frame between the corner posts was not great enough to prevent slippage of the mesh from underneath the frame. It was decided that the mesh edges had to be more securely restrained in order to adequately test the mesh samples.

Wires ropes are commonly used to join sections of high tensile mesh in catch fence applications.

The sample size was reduced to 1300mm x 1300mm to fit inside the 1600mm x 1580mm clamping frame. Six millimetre stainless steel wire rope was used to lace the sample to the frame. Each side was laced individually and secured at each end using 2 wire rope grips (Figure 31).

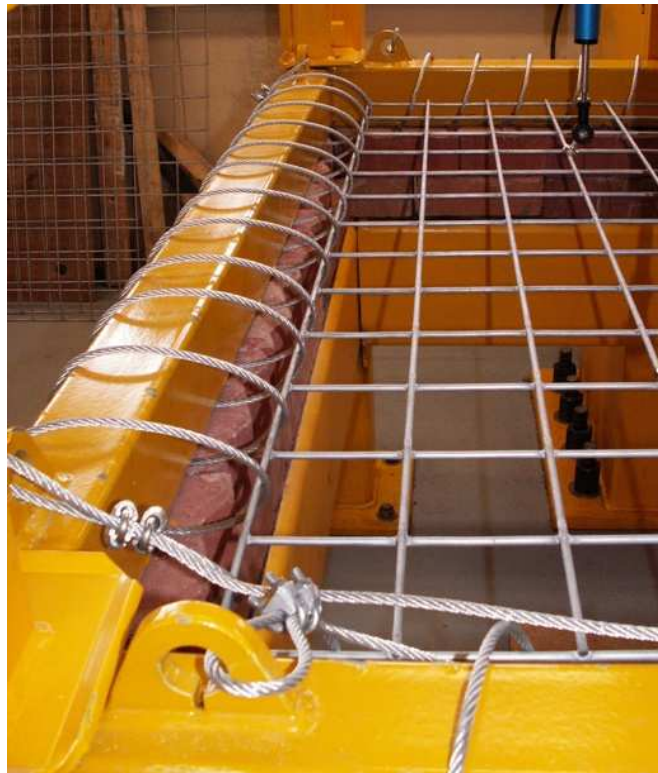


Figure 31: Lacing boundary setup with wire rope grips in foreground.

Tension was applied to the mesh manually and was dependent on the type of mesh and the number of people assisting in the sample setup. Generally 2 people were required to setup a test.

In order to increase the displacement capacity of the test facility, two layers of bricks were placed on the sample support frame as indicated in Figure 32. These bricks were used to raise the height of the sample, bringing it closer to the load bearing beam thus resulting in more displacement capacity in the system.

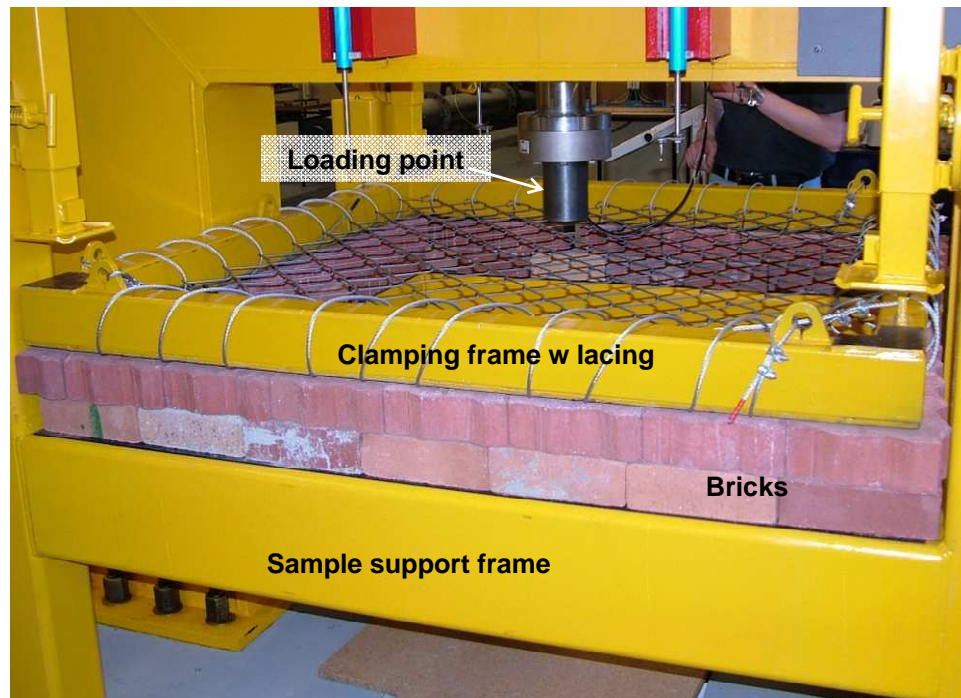


Figure 32: Two layers of bricks were used to raise the position of the sample.

The sample and clamping frame assembly were positioned on the sample support frame and the corner clamps were wound down to secure the clamping frame in place. The test setup was then continued using the steps described in Section 4.4.

Ten tests were completed using this method.

4.7.3 FIXED BOUNDARY

Although the lacing boundary resulted in adequate force - displacement curves, it was deemed that the lacing was having a considerable impact on the displacement characteristics of the mesh. Further discussions of these influences are undertaken in later sections. Lengthy test setup times and high resource usage limited the amount of testing that could be undertaken. As a result of the limitations of the lacing method, a new boundary restraint method was devised to improve the test method.

A new frame was designed to allow a solid hooking fixture to pass through the frame and secure the mesh. The frame was constructed using 6mm thick steel tubing to prevent deformation of the frame at high forces. The frame incorporated legs to replace the bricks used in the lacing method. Commercially available threaded hooks were initially trialled as a restraint method but were found to be too soft and had too high a bending moment applied and subsequently were deemed unsuitable.

The attachment fixture had to be mounted firmly against the frame to reduce the bending moments on the restraints. A system involving high tensile threaded bar, eye nuts and “D” shackles was devised and is illustrated in Figure 33. Sixty two tests were conducted using this test method; some of these results are confidential and are not presented or discussed.



Figure 33: Fixed boundary system adopted as standard test arrangement.

4.8 LOADING METHOD

Several different loading methods were trialled. Initially a 300mm x 300mm flat hardened steel plate was used to load the sample. The plate was oriented square to the mesh grid in the initial tests (Figure 34). As the plate is a similar dimension to the mesh grid, the plate tended to slip off the wires during the test; this resulted in non - symmetrical loading. The plate was rotated 45 degrees to be diagonal to the mesh grid to prevent this slippage (Figure 35). The flat base was observed to cause point loading of the wires around the edges of the plate, particularly at large displacements (Figure 36).



Figure 34: Square loading plate setup square to the mesh grid.



Figure 35: Square loading plate setup diagonal to the mesh grid.

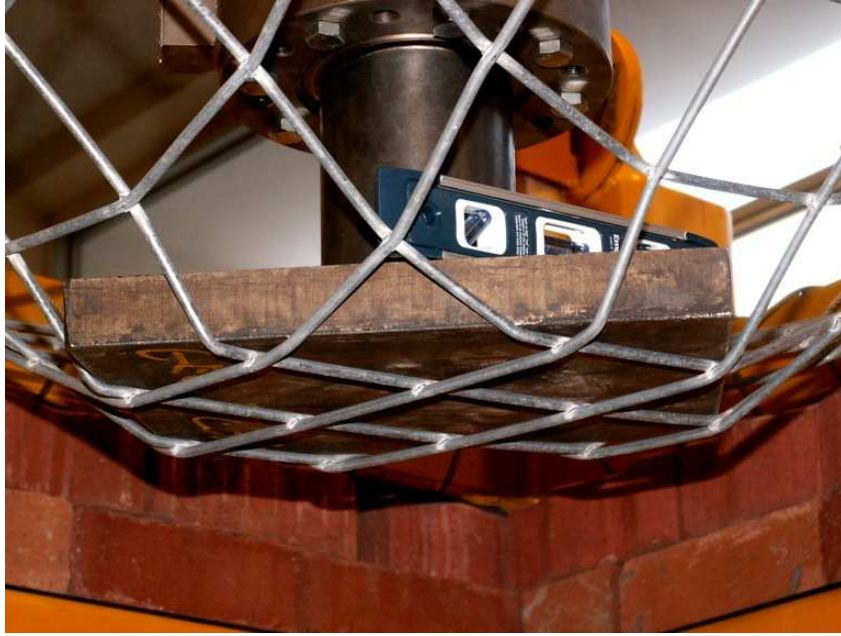


Figure 36: Point loading of the wires caused by the flat base of the plate.

A 500mm x 500mm steel reinforced rubber mat was placed between the steel plate and the mesh in an attempt to alleviate the point loading; this proved unsuccessful.

A second 300mm x 300mm hardened steel plate was manufactured with a curved base to allow for more uniform loading conditions. The base of the plate is shown in Figure 37. The plate was used for the majority of testing.



Figure 37: Curved loading plate setup square to the mesh grid.

4.9 WELD MESH RESULTS

A total of 75 weld mesh tests were conducted using various test configurations that are summarised in Table 8.

Appendix 2 presents a summary of the test results and the individual test report sheets are provided within Appendix 3.

Table 8: Summary of number of tests.

Boundary condition	Test arrangement	No of tests
Clamping	Standard	1
Clamping	0.6m x 1.6m sample size	1
Lacing	Standard	9
Fixed	Standard	47
Fixed	Orientation change from standard	2
Fixed	Small-scale tests	7
Fixed	Hole cut in mesh	1
Fixed	Standard test with dynamic loading mechanism	2
Fixed	Overlap tests	3
Fixed 5 per side	Standard	1
Hook	Standard	1

The results from several of these test arrangements have not been presented in detail but some comments are made in the following paragraphs.

Two tests (test numbers MT056 and MT057) were conducted using the dynamic loading mechanism to enable a comparison of results between mesh tests conducted at the WASM dynamic test facility and the WASM static test facility. The comparison of results has been published in Player et al. (2008). The test report sheets are given in Appendix 3.

One test (MT027) was conducted whereby a hole was cut in the mesh under the test plate to simulate a common industry practice of cutting holes to facilitate cable bolt installation. The result was inconclusive and no further tests were conducted. The report sheet is also given in Appendix 3.

The “hook” test (MT015) and the “fixed 5 per side” test (MT016) are described in the individual test report sheets given in Appendix 3. These tests were conducted as trials to determine a suitable boundary condition after the lacing boundary was deemed unsuitable. The boundary condition with hooks was unsuccessful as the hooks bent during testing; no further tests were conducted. The fixed 5 per side test indicated promising results and a further 47 fully restrained standard tests were conducted using this method.

Some of the 47 fixed boundary test results are confidential and are not included in Appendix 3.

4.9.1 CLAMPING BOUNDARY RESTRAINT METHOD TEST RESULTS

The first weld mesh test conducted using the clamped boundary condition slipped during testing (Figure 38) resulting in the wires not effectively transmitting forces. The displacement capacity of the mechanical jack was exceeded prior to any obvious plastic deformation of the wires. Slight modifications were made to the clamping frame and a second test using a sample size of 0.6m x 1.6m was conducted after the initial lacing tests to determine if the slippage could be reduced or quantified. The changes did not prevent the slippage from occurring and the method was abandoned in favour of the lacing test which allowed for restraint at discrete points. A comparison of the force – displacement results from application of the various boundary conditions is provided in Section 4.9.6.

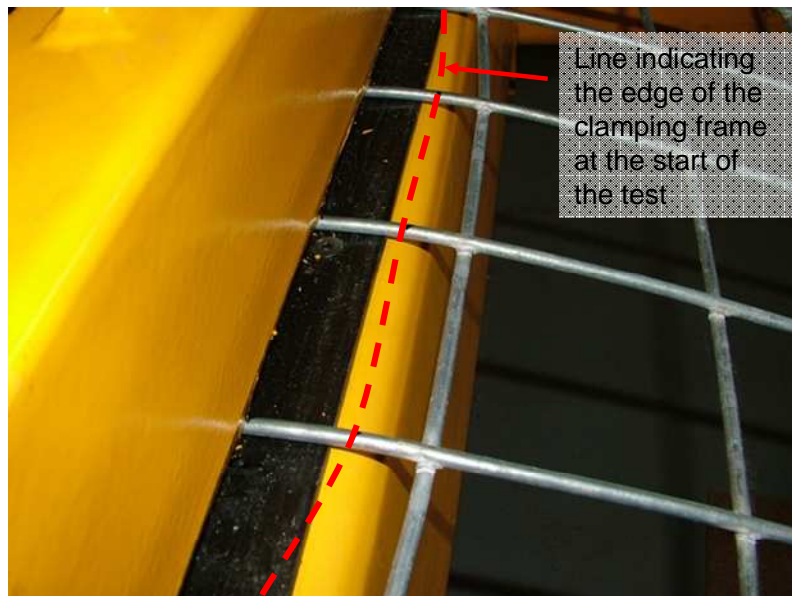


Figure 38: Slippage of mesh from under the clamping frame.

4.9.2 LACING BOUNDARY RESTRAINT METHOD TEST RESULTS

The lacing boundary condition (Section 4.7.2) was developed to enable the restraint of the mesh sample at discrete points. A 3mm diameter mild steel rope was used in the first lacing test (MT002). The wire rope failed prior to the mesh but the methodology provided much greater restraint to the mesh than the clamping restraints. The rope was upgraded to a 6mm high tensile wire rope and a further seven weld mesh tests were conducted using this boundary condition. The results are provided in Figure 39. A typical force - displacement result is given in Figure 40.

The typical force - displacement curve cannot be approximated by a straight line as suggested by Tannant (1995). However, the curve can be used to describe various phases during the test as defined in Figure 41.

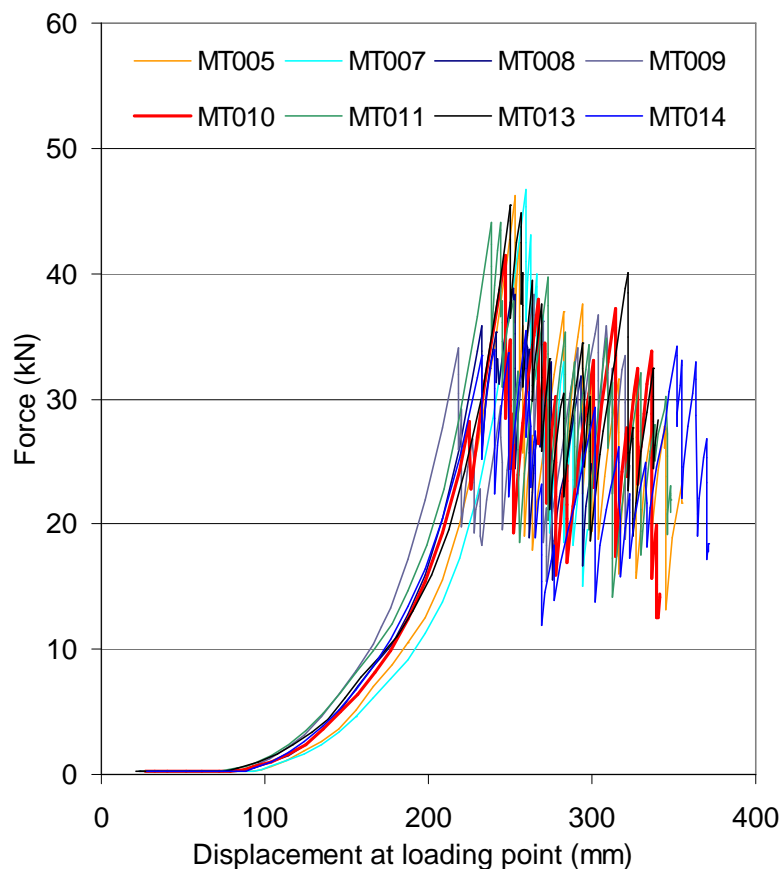


Figure 39: Weld mesh force – displacement results using lacing boundary condition.

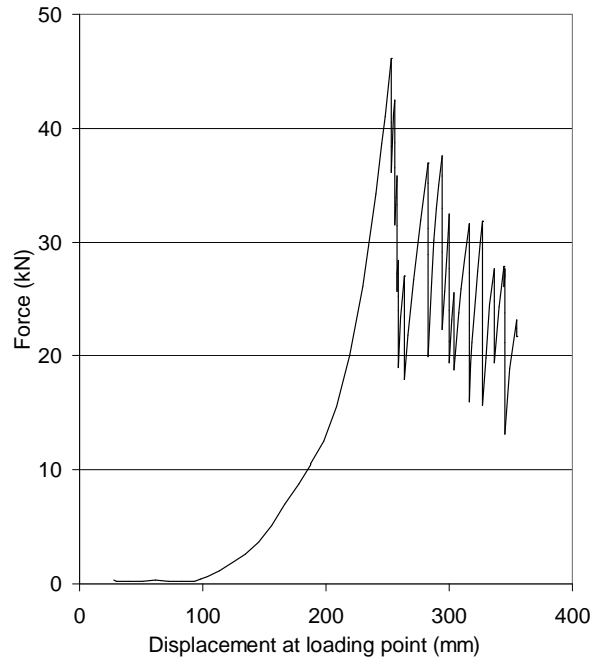


Figure 40: Typical force - displacement result using the lacing boundary method.

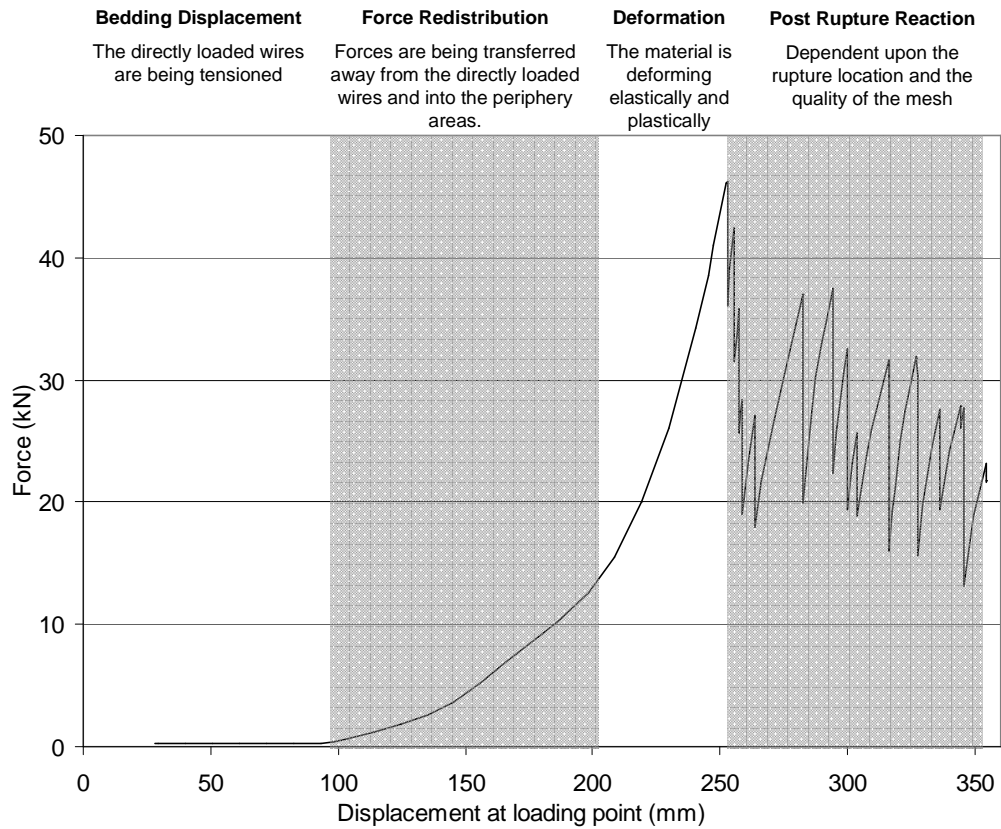


Figure 41: Dissection of a typical force – displacement curve resulting from the lacing boundary method.

The first phase relates directly to tension in the mesh at the start of the test and the effectiveness of the boundary restraint method. The wire rope lacing was difficult to tension manually resulting in very little tension in the mesh at the start of the test. This lack of tension in the wire ropes increased the displacement component of the test results, particularly at low forces. Between 75mm and 100mm of displacement occurred before the slack in the boundary restraint system and the directly loaded wires was absorbed and forces began to increase. This has been called the bedding displacement.

Other contributing factors to the bedding displacement are the rotation of the mesh about the restraint points and slight variations in the mesh geometry resulting in differences in the initial tension in the mesh.

The reaction forces begin to increase once the directly loaded wires are tensioned. As displacement continues, forces begin to be transferred away from the directly loaded wires. This force transfer concept is illustrated in Figure 42. Initially the load transfer is gradual with forces increasing slowly compared with the rate of displacement. When the forces reach 10kN, on average, 73% of the rupture displacement has already been consumed.

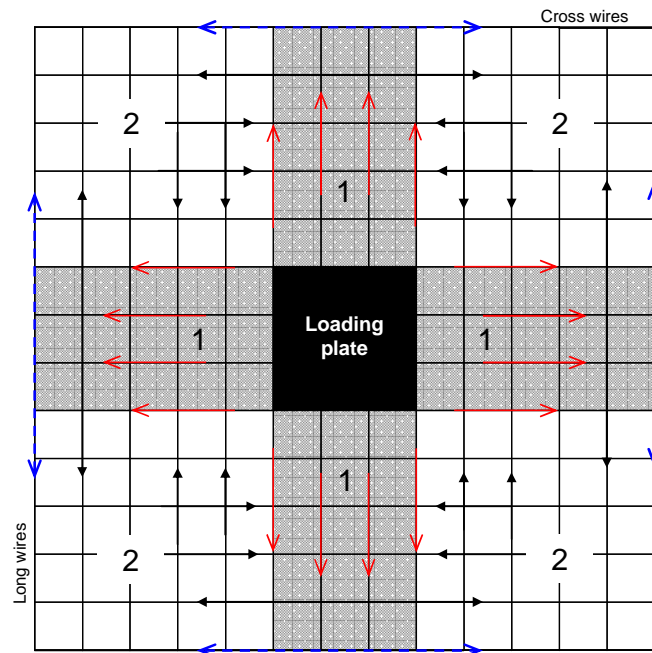


Figure 42: Load transfer concept for weld mesh.

As more wires become tensioned, the rate of reaction force increase accelerates, resulting in greater force changes over small displacement increments. At 20kN, on average 86% of the rupture displacement has been consumed. Most analysis techniques described in the previous sections focus on the deformation phase of the test. The deformation portion of the force – displacement curve can be loosely approximated by a straight line.

The curve typically comes to a peak, at which point an element of the mesh system breaks resulting in a dramatic drop in force. This peak may or may not be the maximum force that is measured during the test. In three of the tests the maximum force occurred at the initial failure. In the other five tests the peak force occurred some time after the initial failure.

Tannant (1995) defines peak load as the “*first major peak in load*” which is usually followed by a substantial drop in load. The assumption of this definition is that the first major peak is the maximum that occurs throughout the test. The WASM tests demonstrated that the peak may or may not occur at the first failure. For clarity in presenting the results of the test program it is essential to differentiate between the initial failure, the peak force and complete failure. To achieve clarity the following terminology is proposed.

In keeping with scientific terminology, the peak force will remain the maximum force occurring during the test.

The term “rupture” has been used to define the point at which a component of the system first breaks. “Rupture force” and “rupture displacement” have been used to describe the force and displacement at the point of first rupture.

The concepts of rupture, peak and post rupture performance are defined in Figure 43.

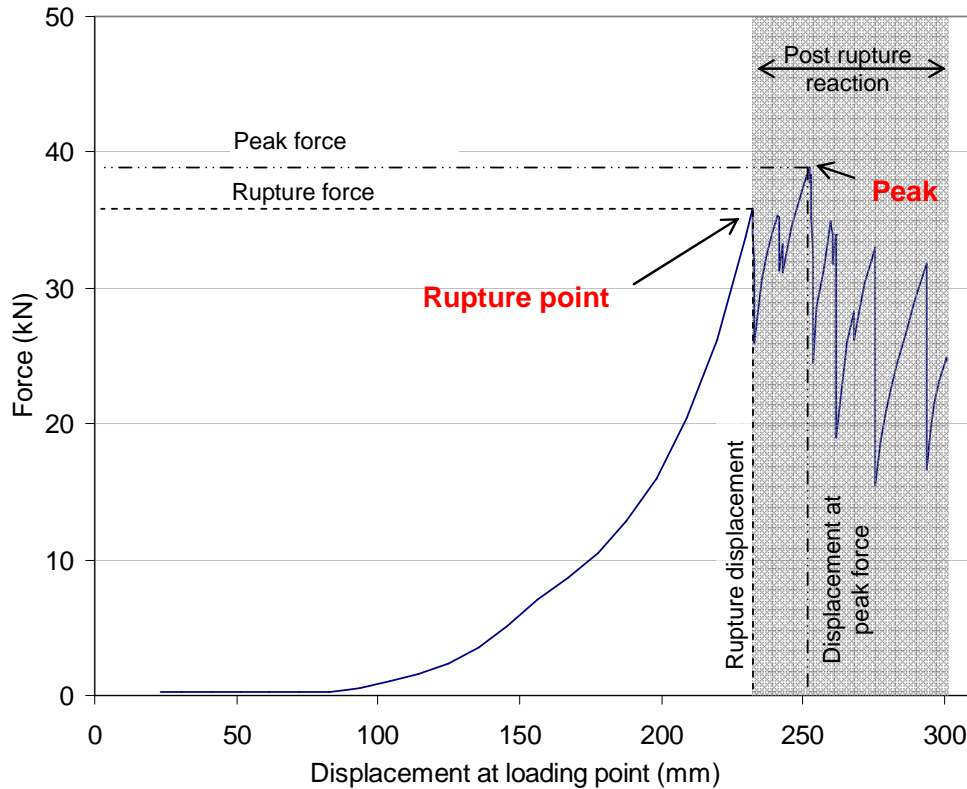


Figure 43: Terminology related to force – displacement results of mesh testing.

All tests (except Test MT008) exhibited weld failure as the rupture mode. Test MT008 exhibited wire failure through the heat affected zone adjacent to the weld. The samples were always observed to rupture at the boundary on one of the four directly loaded wires; but the side on which the initial failure occurred was variable.

After rupture the forces build up to a second peak and the next failure occurs accompanied by another sharp reduction in force. Peaks and troughs continue as failure progresses. The second rupture typically occurs on a directly loaded wire on an edge, perpendicular to the edge of the sample that initially failed. Failure of the wires (or welds) then propagated preferentially only along two sides at right angles to each other starting with the directly loaded wires. Failure progresses to periphery wires only after the directly loaded wires had broken. This concept is provided in Figure 44. The preferential failure along two sides resulted in plate rotation and caused the loading shaft to push against the edge of the test frame. In the early tests, the tests were continued until a drop in force was observed over a successive number of failures. This feature (indicated in Figure 45) was initially used to describe complete failure of the sample.

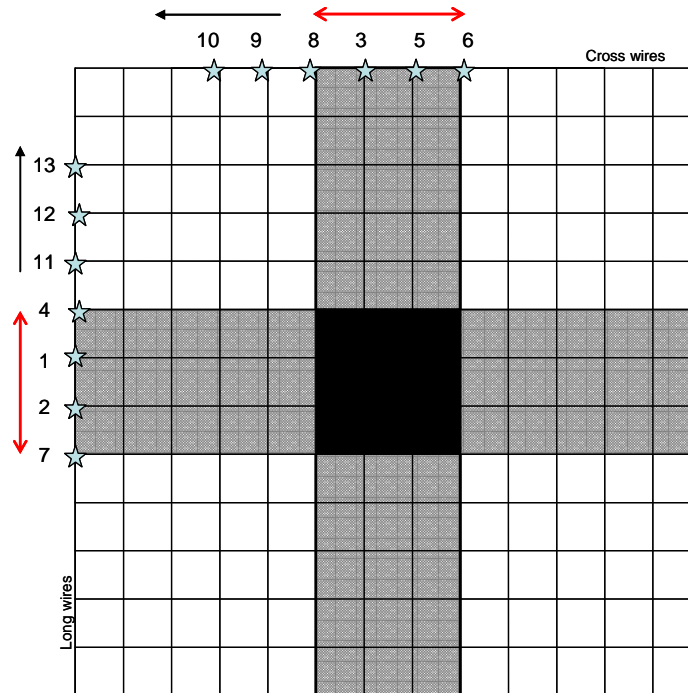


Figure 44: An example of failure propagation starting with the directly loaded wires.

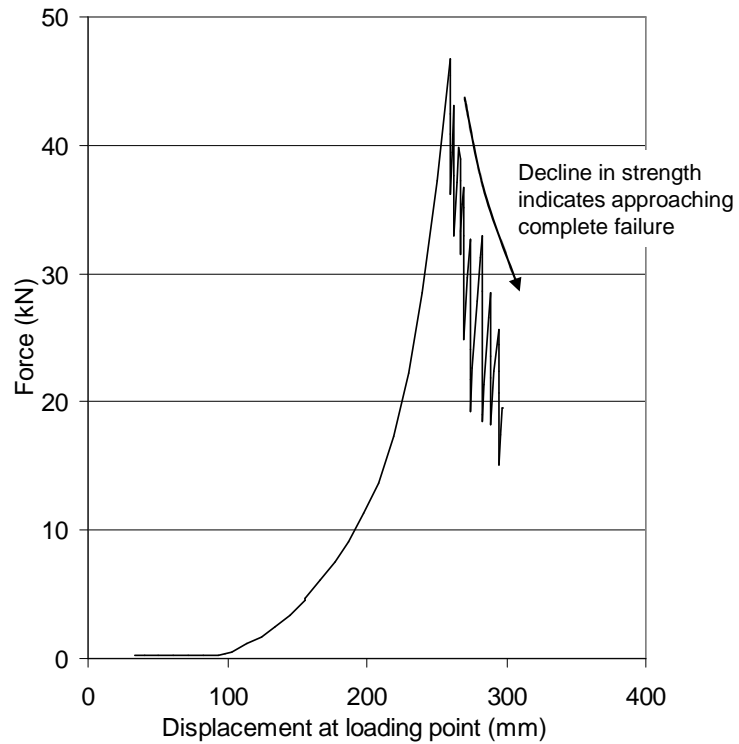


Figure 45: Initial peak at rupture followed by a steady decline in force.

Later tests were extended to cause more failures. The same decrease was observed but was followed by an increase in the forces as illustrated in Figure 46.

Further investigation of what constitutes failure suggests that the term failure is very subjective. Leslie and Potter (2004) define failure as the “*inability of a material to perform within previously specified limits*” or a “*condition at which a structure ceases to fulfil its functional purpose or reaches a limit state*”.

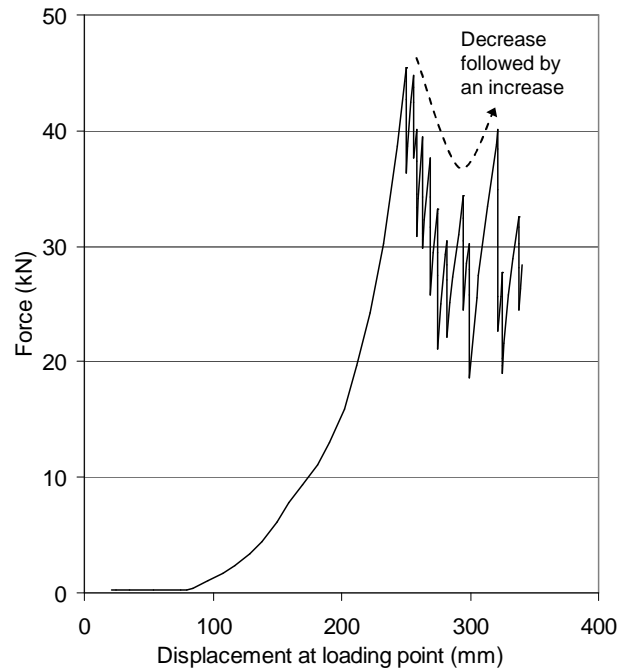


Figure 46: Some tests exhibited a decrease in force followed by an increase.

One rupture cannot be considered “failure” as the mesh is still capable of sustaining load after the first break. The limit state or the point at which the mesh ceases to fulfil its functional purpose is site dependent and a matter of conjecture. One site may have high force requirements, whilst another may require high or low displacement capacity.

The actual duration of the test was dependent upon the number of failures and plate rotation and the test program. Consequently, the final deformation in a particular test is not representative of the total displacement capacity of the mesh.

Due to potential damage to the shaft due to plate rotation, all later tests were limited to 5 – 6 ruptures; consequently, complete failure may not have been achieved.

The post rupture response depends on the position of the first rupture and the forces at which this occurs. The variability and the subjectivity of the post rupture response means that little analysis can be undertaken on this phase without sophisticated computer modelling.

The rupture point is well defined and therefore can be used to compare various mesh products. A summary of the rupture force – displacement results for all weld mesh tests using the lacing boundary condition is provided in Figure 47. The average rupture force is 39.2kN and the average rupture displacement is 239mm.

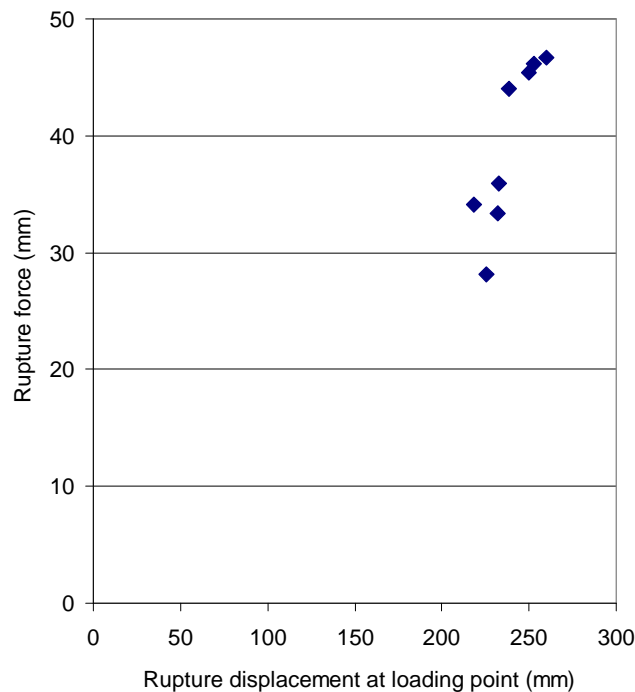


Figure 47: Rupture force – displacement results for all lacing tests.

4.9.3 ASSESSMENT OF THE LACING RESTRAINT

The setup time for each test using this configuration was 3 hours and required two people. The brick layers used to raise the frame were slightly uneven and interfered with the wire rope lacing. This had a minor effect on the test results but limited the practical application of the test.

A less complex, more rigid boundary restraint system was devised to simplify the setup, and to minimise the influence of the test arrangement on the results.

4.9.4 FIXED BOUNDARY RESTRAINT METHOD TEST RESULTS

A system comprising of D shackles, eye nuts and 8mm high tensile, threaded bar passing through a fixed frame was developed; this has been described previously in Section 4.7.3. The force - displacement results are given in Figure 48.

The typical force - displacement curve from the fixed boundary systems exhibited the same phases as the lacing boundary system. These phases are illustrated in Figure 49.

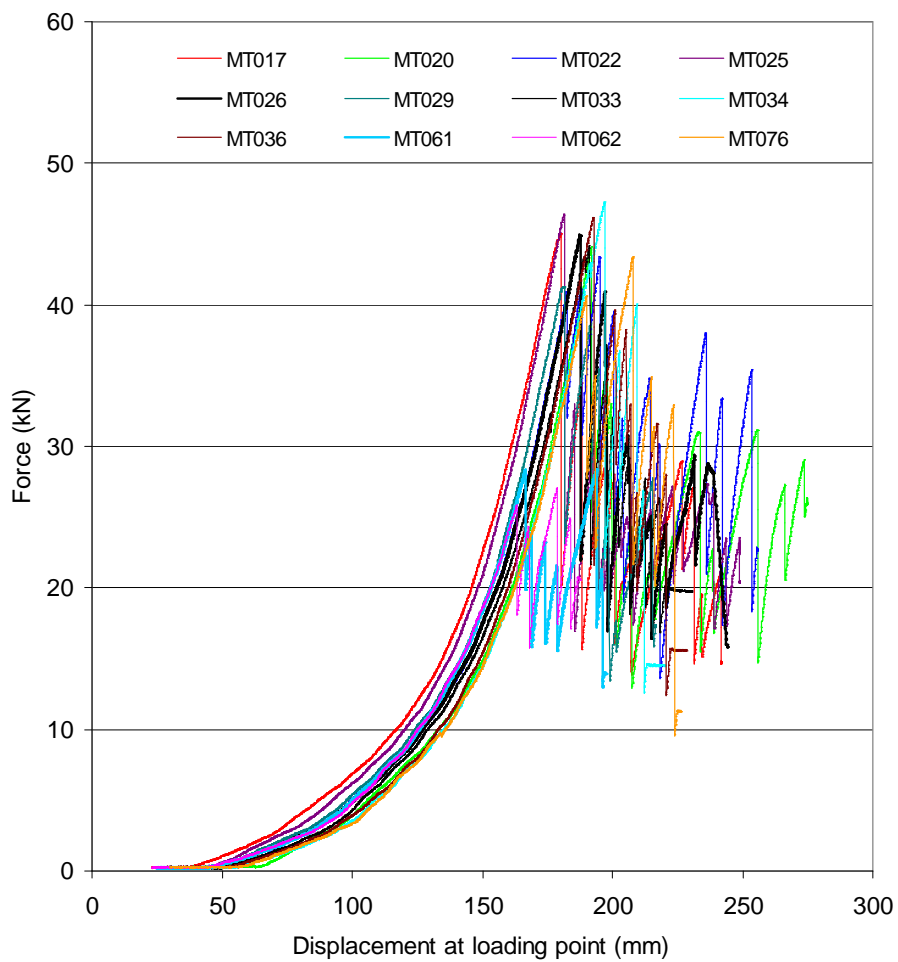


Figure 48: Force – displacement results for fixed boundary conditions.

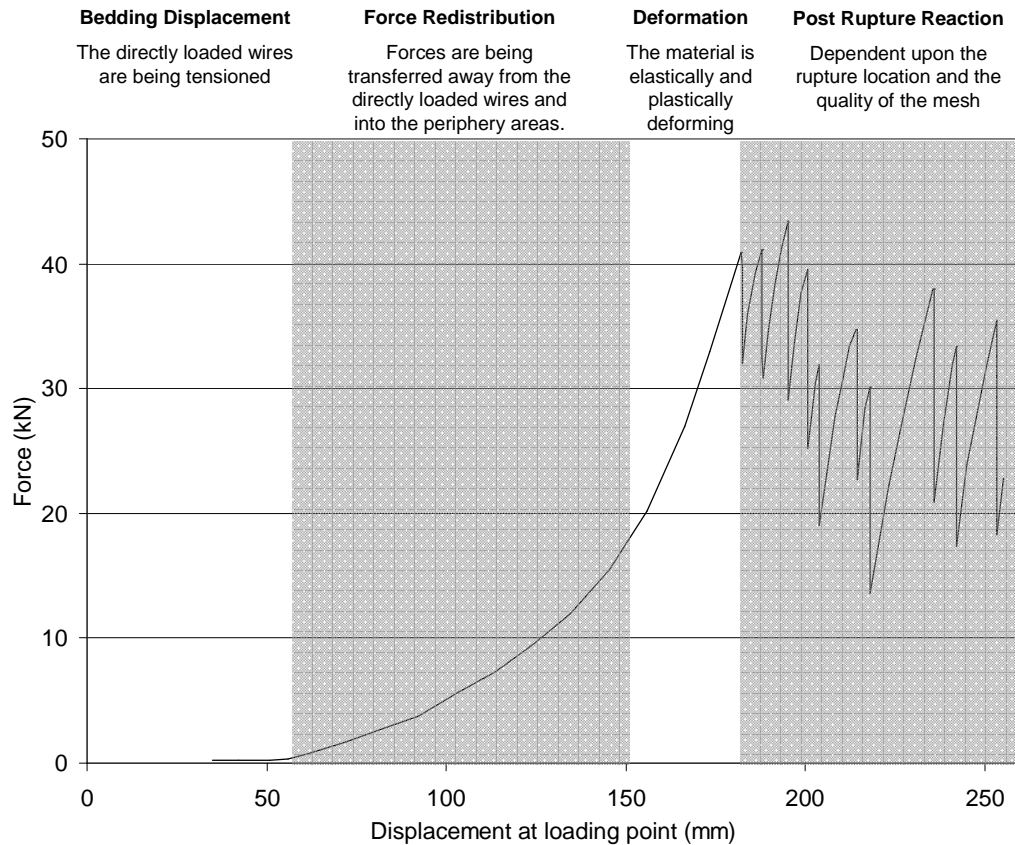


Figure 49: Dissection of a typical force – displacement curve using the fixed boundary method.

Typically the bedding displacement is between 40mm and 60mm and includes the displacement due to the placement of the loading plate. Due to the shape of the test frame, at the beginning of the test the mesh is tensioned in the long wire direction but is loose in the cross wire direction. As with the lacing test method, forces only begin to increase once the directly loaded wires develop tension in both directions.

The same force transfer concept was observed in the fixed boundary method as in the lacing boundary method and is illustrated in Figure 50.

The boundary system was devised to be as rigid as possible, whilst still enabling the mesh to be installed in the test frame. Although it would be ideal to simulate a perfect boundary condition with the mesh perfectly taut at the beginning of the test, it was infeasible and impractical given the variations in the different mesh types that were tested.

Rupture (as defined in Section 4.9.2 and Figure 43) has been used to analyse the test results. Figure 51 provides a summary of the force - displacement results at rupture.

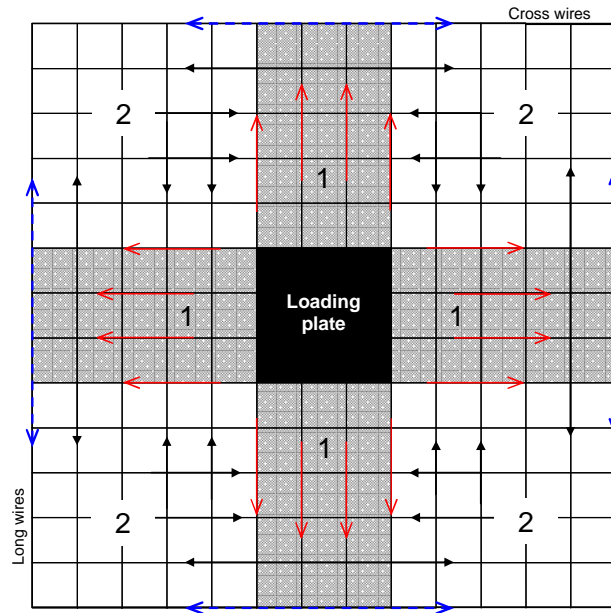


Figure 50: Load transfer concept for weld mesh.

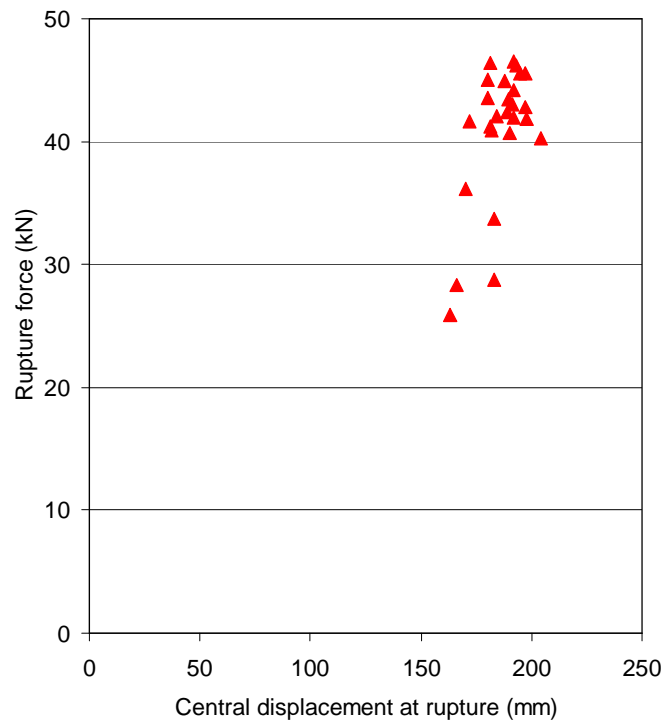


Figure 51: Rupture force – displacement results for fixed weld mesh tests.

A large scatter can be seen in these results. Further analyses were undertaken based on the failure mechanisms.

Three different welded wire mesh failure mechanisms were observed; weld failure, failure of the wire through the heat affected zone (HAZ) and tensile wire failure. Wires exhibiting each of these failure modes are shown in Figure 52.

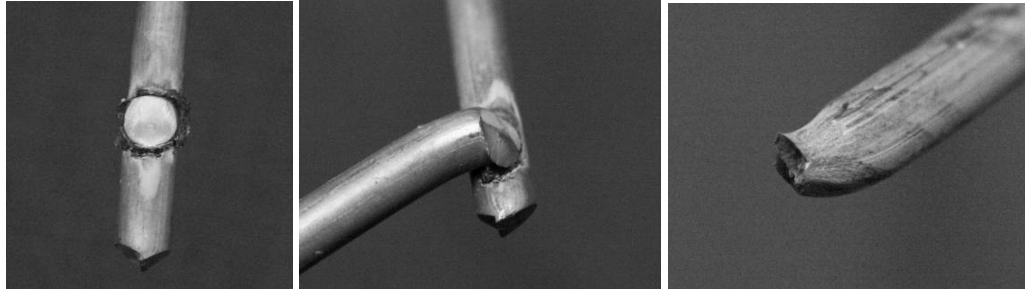


Figure 52: Welded wire mesh failure mechanisms; L – R weld failure and failure of the wire through the HAZ and tensile wire failure.

Tensile failure of the wire occurs when the weld strength is greater than the strength of the wire. Typically this failure is located at the centre restraining point but could occur on any side of the mesh. Weld failure is characterised by shear failure of the weld itself. The wires generally remain intact. Failure through the heat affected zone is distinct from weld failure as the wire itself is broken at the weld location, the weld material remains intact. Failure through the heat affected zone is often caused by a reduction in the cross sectional area of the wire due to the application of too much heat during the welding process.

Figure 51 has been reproduced to indicate failure modes (Figure 53). The failure mode alone does not indicate quality of the mesh as weld failure can occur at any level. However, the rupture force, in combination with the failure mode, can be used to determine the quality of the mesh (Table 9).

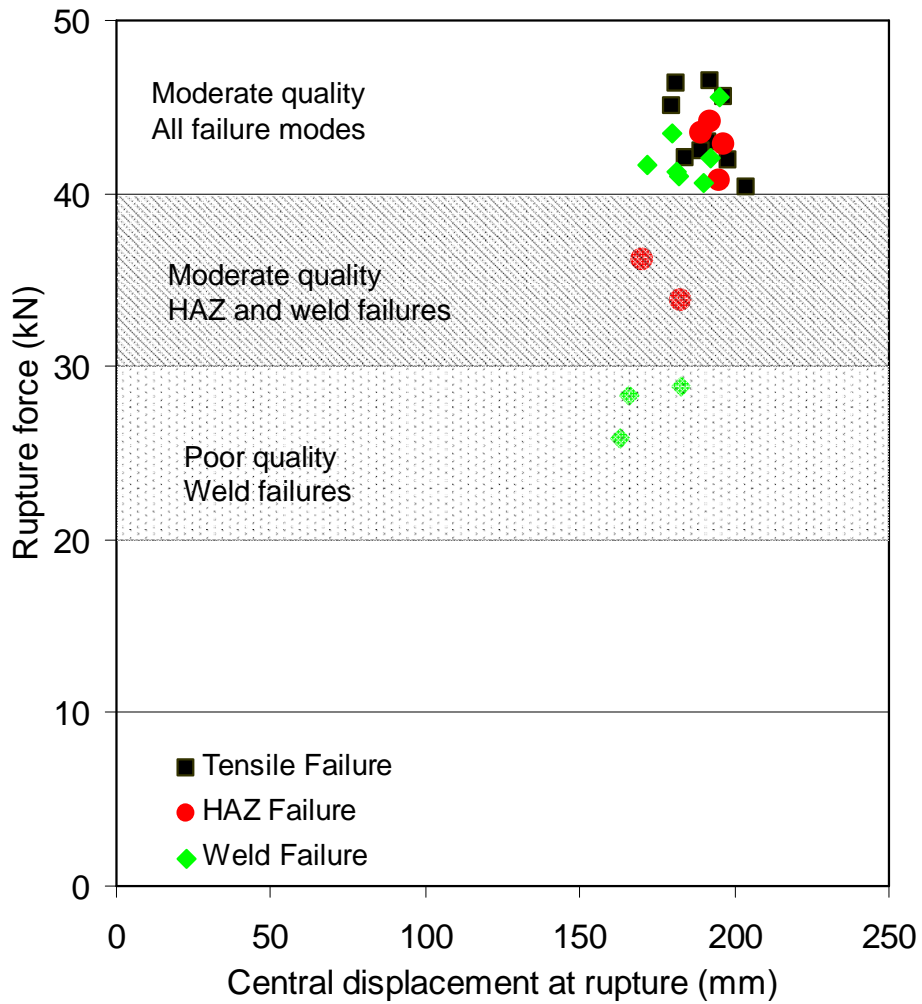


Figure 53: Rupture force – displacement results with failure modes.

Table 9: Mesh quality assessment for 100 x 100mm grid, 5.6mm diameter welded wire mesh.

Rating	Failure mode	Rupture force range (kN)
Poor	Weld	<30
Satisfactory	Weld or HAZ	30-40
Good	Weld, HAZ or Tensile	>40

4.9.5 RESULTS FROM VARIED CONFIGURATION

4.9.5.1 Sample orientation

The standard test configuration was undertaken with the cross wires in contact with the loading plate (cross wires up). Two tests (MT021 and MT024) were undertaken whereby the samples were flipped so that the long wires were in contact with the loading plate (cross wires down). This aimed to determine if there was any effect on the force – displacement results due to wire orientation. Both MT021 and MT024 had corresponding samples from the same sheet that were tested using the standard test arrangement (MT022 and MT025, respectively). The results of these four tests are provided in Figure 54.

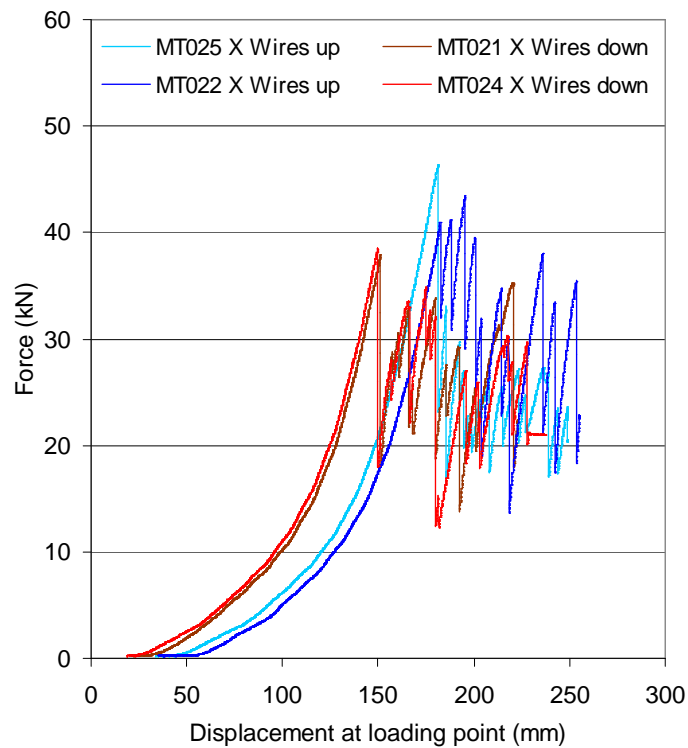


Figure 54: Force – displacement results for different sample orientations.

The rupture results indicate that sample orientation may have an effect on both the force and displacement performance of the mesh. The test conducted in the cross wires down orientation had a smaller bedding displacement than that of the test conducted for the cross wires up orientation. The difference was approximately 20mm. There was also an apparent decrease in the rupture force by approximately 10% for the cross wires down orientation.

The difference in result cannot be directly attributed to the failure mechanism. Both the cross wires down tests exhibited failure through the heat affected zone whilst tests MT022 and MT025 exhibited weld failure and tensile failure respectively.

4.9.5.2 *Small-scale tests*

In order to confirm the relationship between wire orientations and rupture force, seven small-scale tests were undertaken. All samples came from the same sheet of mesh to reduce the potential variation in quality. The force – displacement results are given in Figure 55. The modified test setup results are shown in red colours whereas the standard test arrangement results are displayed in green and blue colours.

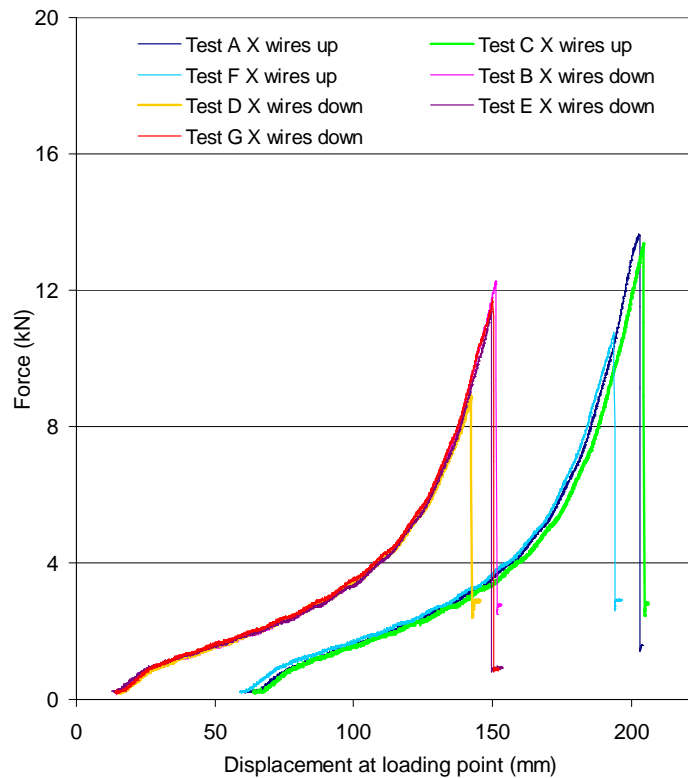


Figure 55: Force - displacement results from the small-scale test program.

The small-scale tests displayed similar relationships to those exhibited in the large-scale tests. The rupture forces for the tests where the long wires were above and in contact with the loading plate were 12% less than those undertaken under the standard test conditions. The rupture displacement for the modified test setup was 25% lower than the standard test setup. This is illustrated in Figure 56.

All tests exhibited either weld failure or failure through the heat affected zone. The failure mode was not related to the sample orientation and did not appear to contribute to the difference in results.

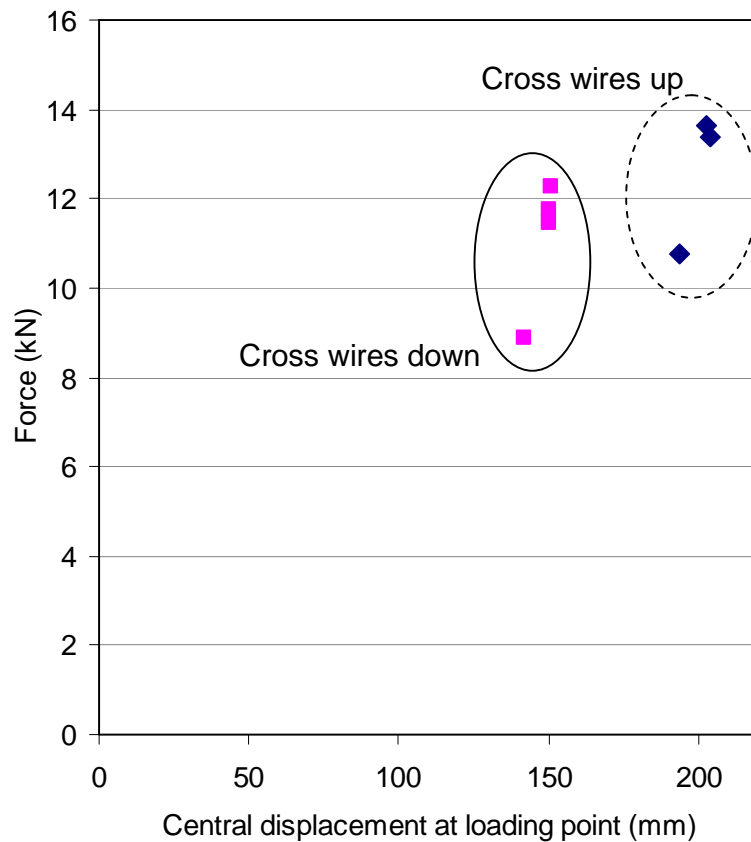


Figure 56: Rupture results for small-scale tests.

4.9.5.3 Overlap

The sample configuration has been described in Section 4.6.3. The force - displacement results are presented in Figure 57.

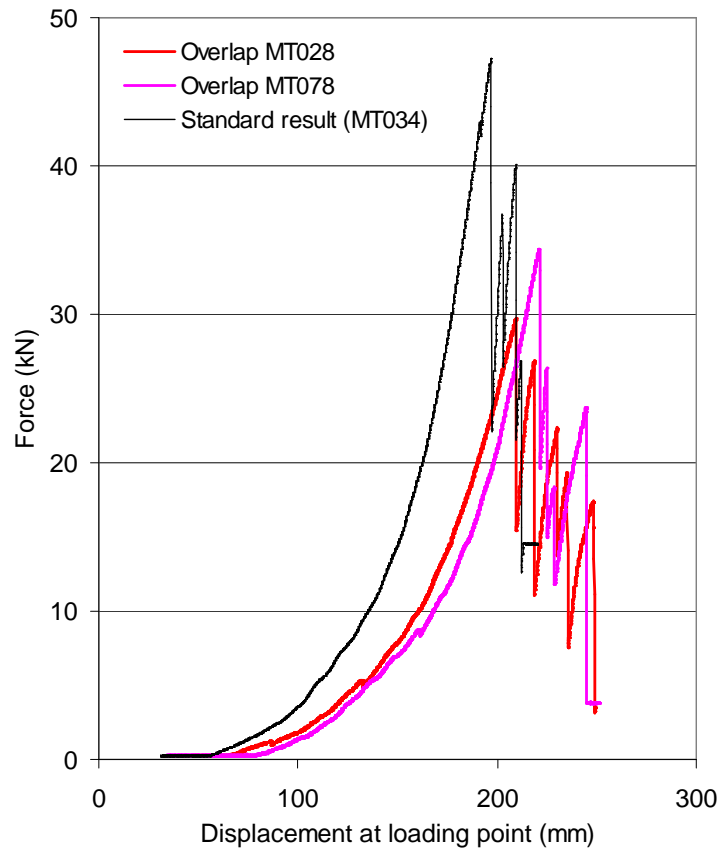


Figure 57: Force - displacement results for overlap tests.

The bedding displacement increased from an average of 51mm recorded for the standard sample tests to approximately 75mm for the overlap tests. The force redistribution rate was also significantly slower. Observations indicate that forces were only transferred in the direction of the cross wires and were not transferred in the long wire direction (Figure 58). This was because the plate simply pushed the overlap apart as indicated in Figure 59.

A third test was conducted where the overlap was laced using high tensile 6mm wire rope (Figure 60). The lacing was terminated on the second wire in from the edge to prevent stress concentrations at the boundary restraint and to allow for better load

transfer around the mesh. The force - displacement results from this test are provided in Figure 61.

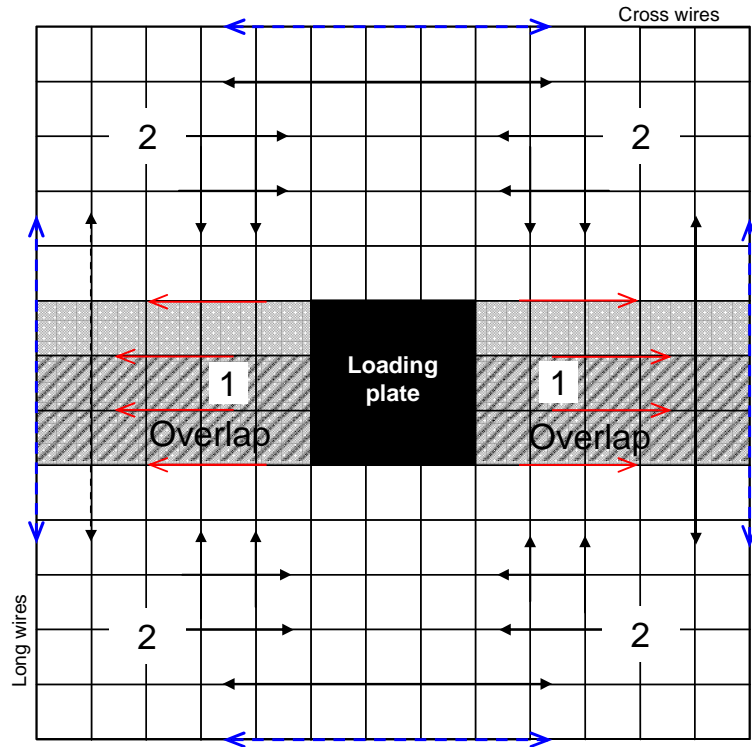


Figure 58: Load transfer only occurs in one direction during the early stages of the test.

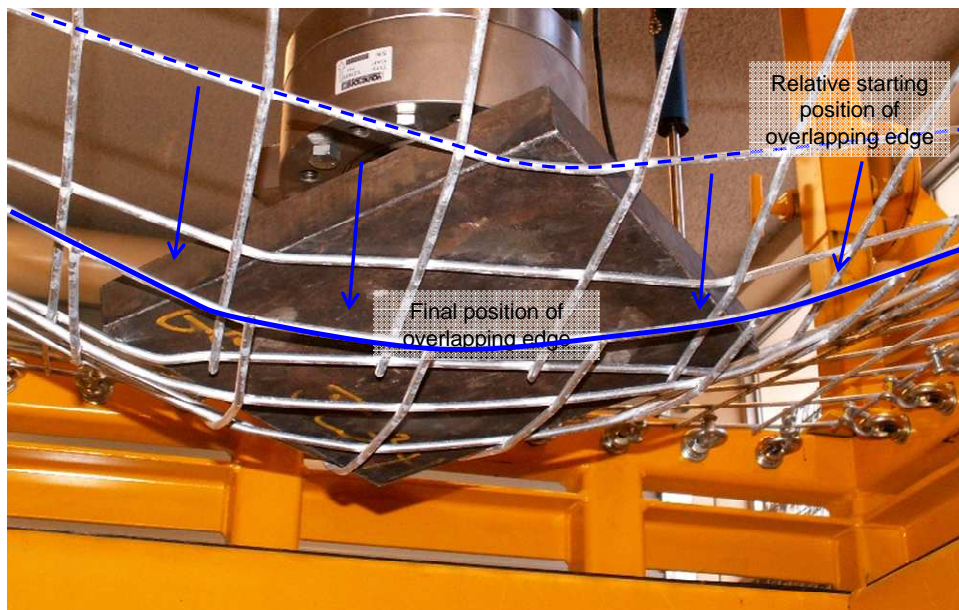


Figure 59: The plate simply pushes apart the overlap.



Figure 60: Lacing of the overlap to enable better load transfer.

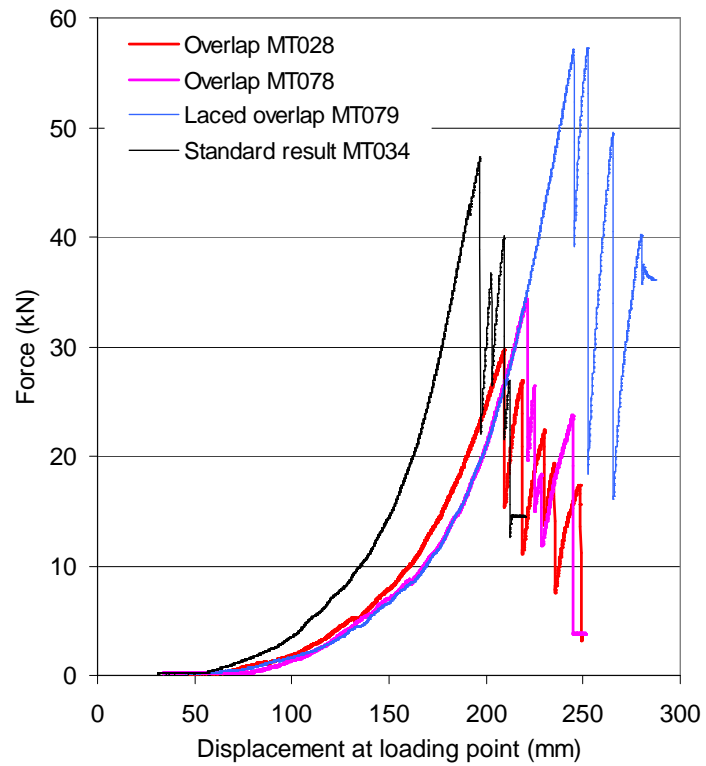


Figure 61: Force - displacement comparison of the laced test with the standard overlap results and a typical standard full size sample results.

The results demonstrate that the force transfer rate during the force redistribution phase did not improve with the addition of the lacing. This is likely to be due to the difficulty encountered in achieving adequate tension on the lacing. The lacing impeded the mesh separation observed in the standard overlap tests. A large increase in the rupture force was observed with the lacing test. The increase was also almost 50% greater than rupture force of the standard test arrangement. There are two possible explanations for this; firstly, that two sets of wires were acting along the overlap, effectively doubling the strength in that direction; or, secondly, that by fixing the lacing on the second wire to prevent stress concentrations on the boundary wire, more wires were engaged in the force transfer in the later stages of the test. The altered force transfer concept is illustrated in Figure 62. Further scope exists for testing overlap restraint devices, such as smaller diameter wire ropes or D shackles, to improve the performance of overlaps in the field.

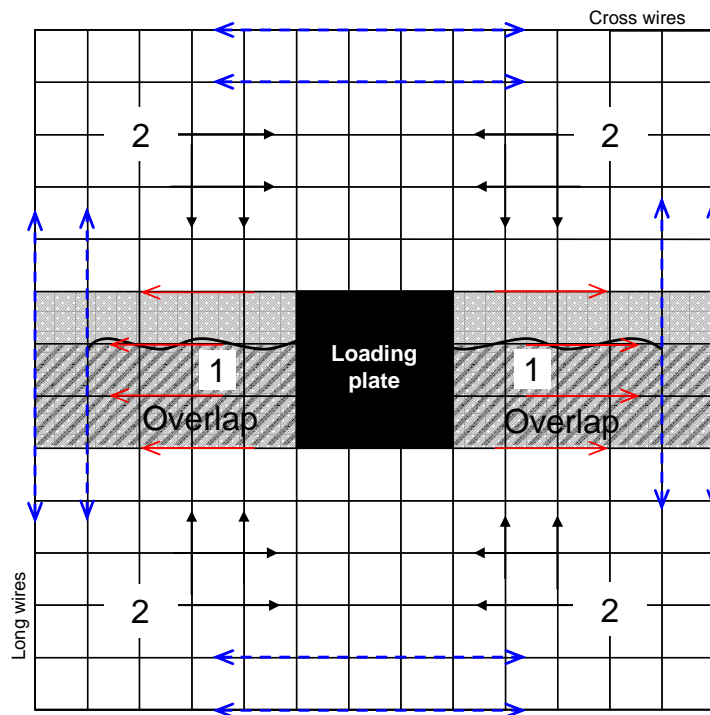


Figure 62: The lacing allows forces to be transferred along two wires on the outer edge rather than one wire as indicated in Figure 58.

4.9.6 DISCUSSION OF WELD MESH RESULTS

Figure 63 provides a comparison of the three boundary restraint methods.

The amount of measured displacement is affected primarily by the initial tension in the mesh, the boundary system stiffness, the mesh stiffness and the nominal force capacity of the mesh. The initial tension in the mesh is a function of the mesh type and the boundary conditions. The greater the tension in the mesh and the stiffer the boundary condition, the quicker the mesh will effectively transfer load.

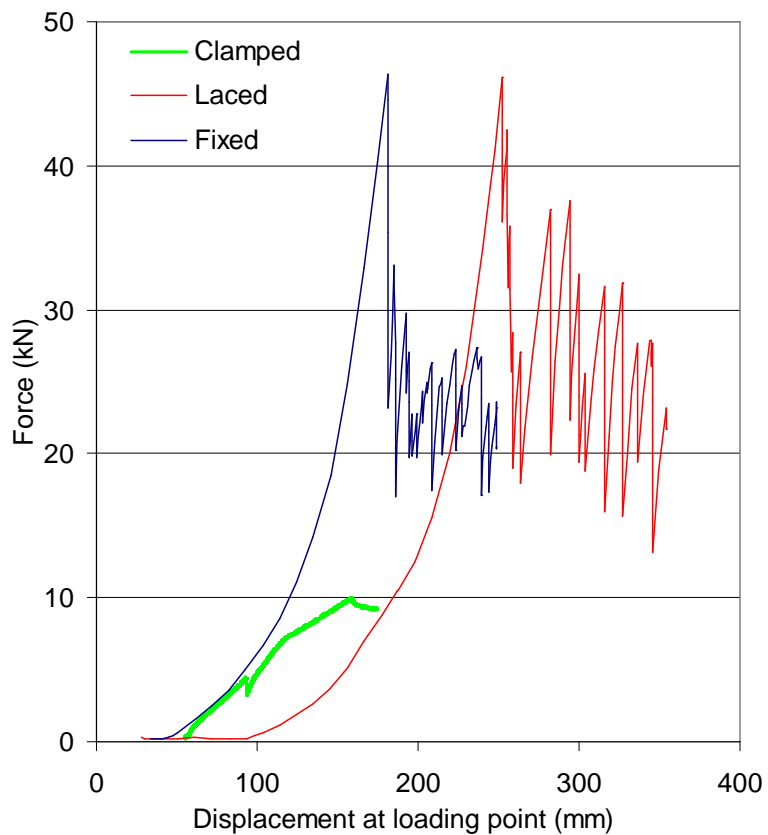


Figure 63: Force - displacement response of weld mesh using various boundary restraint systems.

The clamping method was proven to be inadequate and could not effectively restrain the mesh; this resulted in significant displacements without substantial increases in force.

Full tension of the wire rope used in the lacing boundary configuration was almost impossible to achieve manually. This created a considerable amount of variability in the magnitudes of displacement prior the system taking load. The fixed boundary system reduced (but did not eliminate) the amount of bedding displacement and resulted in a more realistic force – displacement reaction. This is indicated by the reduction in the bedding displacement from an average of 88mm using the lacing restraint method to an average of 50mm using the fixed boundary restraint method.

The percentage of rupture displacement consumed at 10kN changed from 74% for the lacing boundary condition to 70% for the fixed boundary condition. This indicates that the majority of this difference in the rupture displacement is caused by the boundary restraint system. Once tensioned, the behaviour of the mesh was not affected by the boundary restraint system given that the same sample area and the same loading area were used with both restraint methods.

The lacing boundary system and the fixed boundary system behaved similarly in the later phases of the test. This supports the similarities in rupture forces as indicated in Figure 64. The differences in the rupture displacements are primarily due to differences in the bedding displacement.

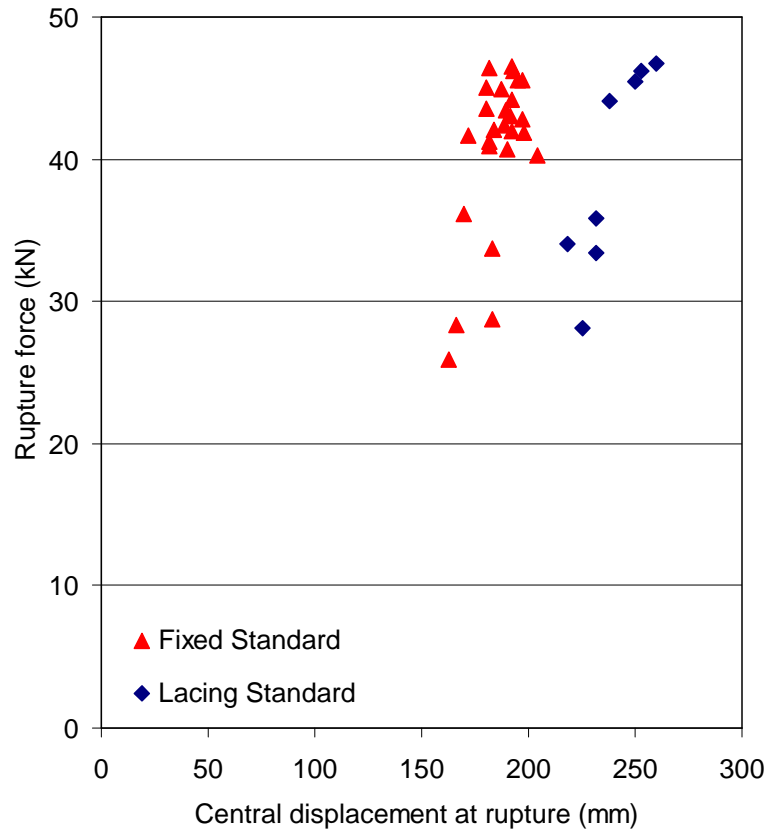


Figure 64: Comparison of rupture force – displacement for the lacing and fixed boundary methods.

The overlap tests demonstrate that the amount of restraint imposed upon the mesh is critical to the mesh capacity. The mesh was unable to transfer forces across the overlap boundary and accordingly higher displacements were observed due to pushing apart of the mesh. The force capacity was also limited as all the forces were transferred axially in one direction rather in two directions. These reactions have also been observed in the underground mining environment. It is considered that this may be rectified by binding sheets together at the overlaps using a simple restraining device.

The force – displacement capacity of the mesh may also be affected by the orientation of the mesh sheet. The test results displayed a considerable difference in test results, depending on which wires were in contact with the loading plate. Thompson et al., (1999) implied that the wire orientation may be of some importance, suggesting that there may be a difference in force capacity if the welds at the intersections of the wires are in compression or tension.

In the weld mesh manufacturing process the long wires are laid out and the cross wires are placed over the long wires. The electrodes are then applied to the cross wires. This process means that if the cross wires are in contact with the load then the weld is in compression. If the long wires are in contact with the load then the weld is in tension. This concept is explained in Figure 65.

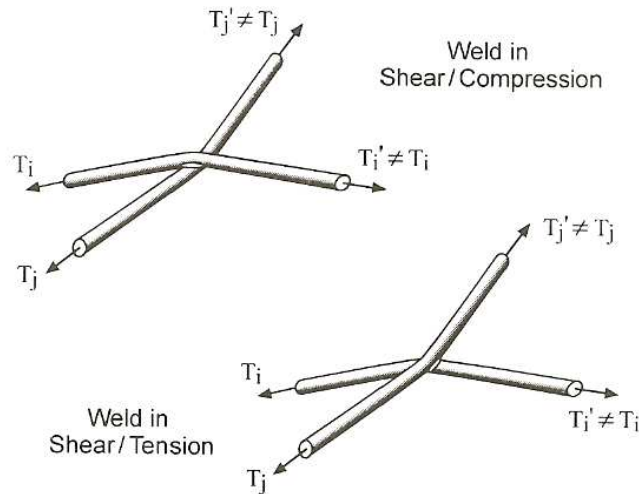


Figure 65: Welds may be in compression or tension depending upon the orientation of the wires (Thompson et al., 1999).

It is inconclusive as to whether the boundary method had an effect on the failure mechanism. The lacing method resulted only in weld failures whereas the more rigid boundary system caused all three failure modes. In all likelihood this is a function of the quality of the mesh rather than an influence of the boundary system. A second set of samples was sourced just prior to changing from the lacing system to the fixed system. Although these samples came from the same mine site they were not from the same manufactured batch. There was approximately six months between batches and no samples from the first batch have been tested using the fixed boundary system.

The WASM test results demonstrate that it is possible to produce simplified repeatable results that enable the comparison of various mesh configurations.

Further analysis of the test results are presented in Section 4.12.

4.10 CHAIN LINK TEST RESULTS

A total of twenty three tests were conducted on chain link mesh. The boundary conditions and mesh products are listed in Table 10.

Table 10: Chain link mesh products and the boundary conditions used to test the samples.

Mesh Product	Boundary condition	Sample size	No. of tests
S95/4	Clamping	1.6m x 1.6m	1
S95/4	Lacing	1.3m x 1.3m	2
S95/4	Fixed	1.3m x 1.3m	6
G65/4	Fixed	1.3m x 1.3m	3
G80/4	Fixed	1.3m x 1.3m	3
G65/3	Fixed	1.3m x 1.3m	3
G80/2	Fixed	1.3m x 1.3m	3

One test was conducted using the clamping boundary condition. As with the weld mesh tests, considerable slippage of the mesh occurred during the testing and the displacement capacity of the test facility was exceeded prior to initiation of rupture of the mesh. The maximum force during this test was less than 10kN after 148mm of displacement. A further two tests were conducted using the lacing boundary system. These results are presented in the Section 4.10.1. The remaining tests were conducted using the fixed boundary method. A summary of the chain link test results is provided in Appendix 4. Individual test report sheets are contained with Appendix 5.

4.10.1 LACING BOUNDARY RESTRAINT METHOD TEST RESULTS

Only two tests were conducted on chain link mesh (product S95/4) using the lacing boundary restraint method. The force – displacement results for the two tests conducted using this boundary condition are given in Figure 66. As with weld mesh test, the force - displacement curve can be broken into components representing the different deformation phases that occur during the test (Figure 67).

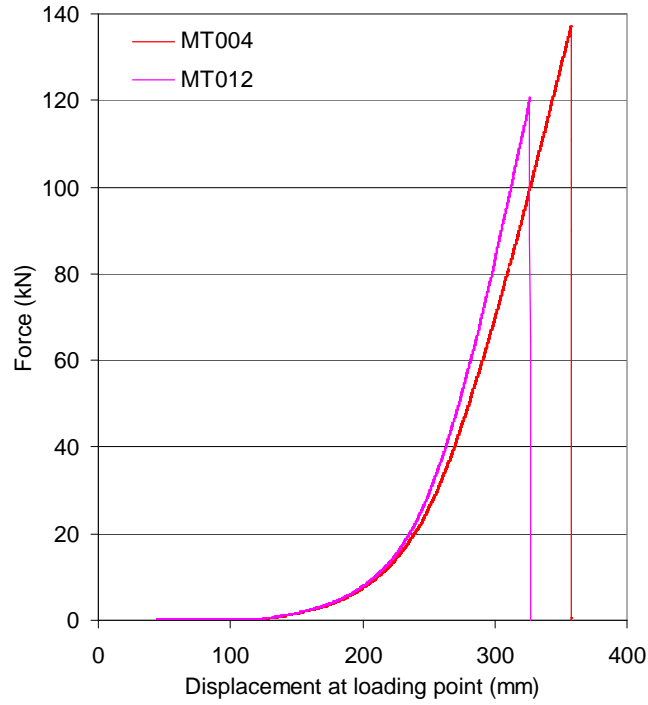


Figure 66: Force - displacement results for chain link mesh using the laced boundary method.

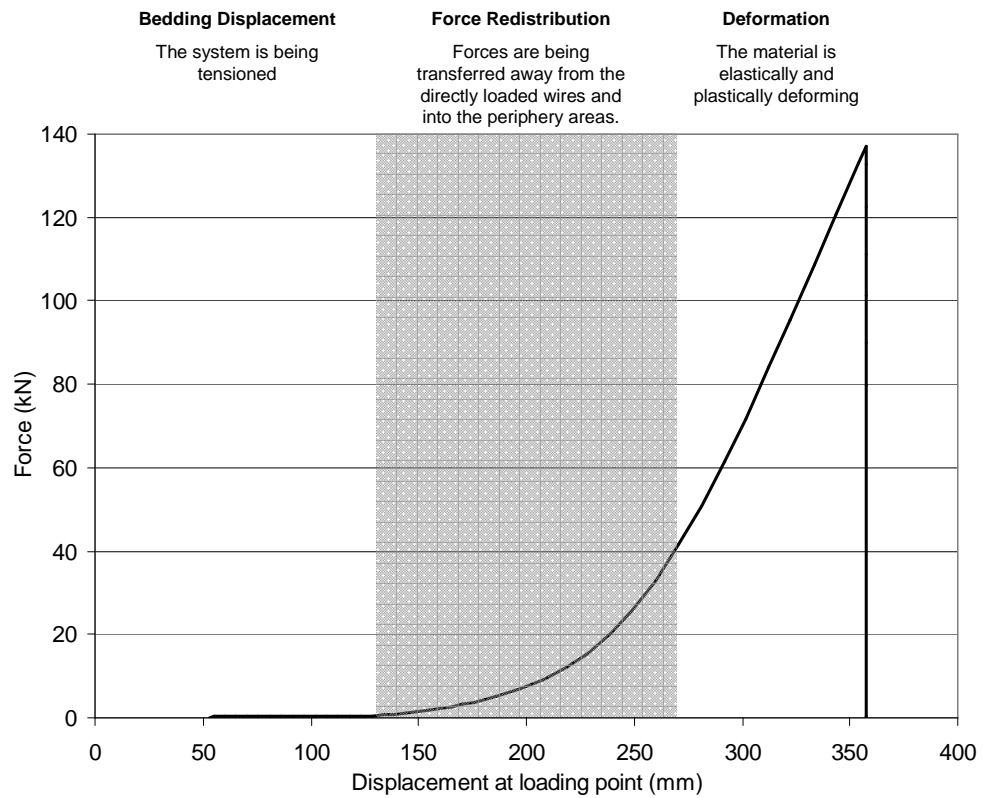


Figure 67: Dissection of the force – displacement reaction of chain link mesh.

The bedding component is affected by the stiffness of the boundary restraint system and the initial tension in the mesh. The chain link mesh configuration is stiff in the direction of the wires but very flexible in the link direction as illustrated in Figure 68. Chain link mesh has a much higher displacement capacity when compared to weld mesh. Much of this displacement occurs at low forces due to the tensioning of the links between the wires. The initial tensions in the mesh samples for these tests were observed to be similar and this is confirmed by the bedding displacements which were 124mm and 122mm for MT004 and MT012, respectively.

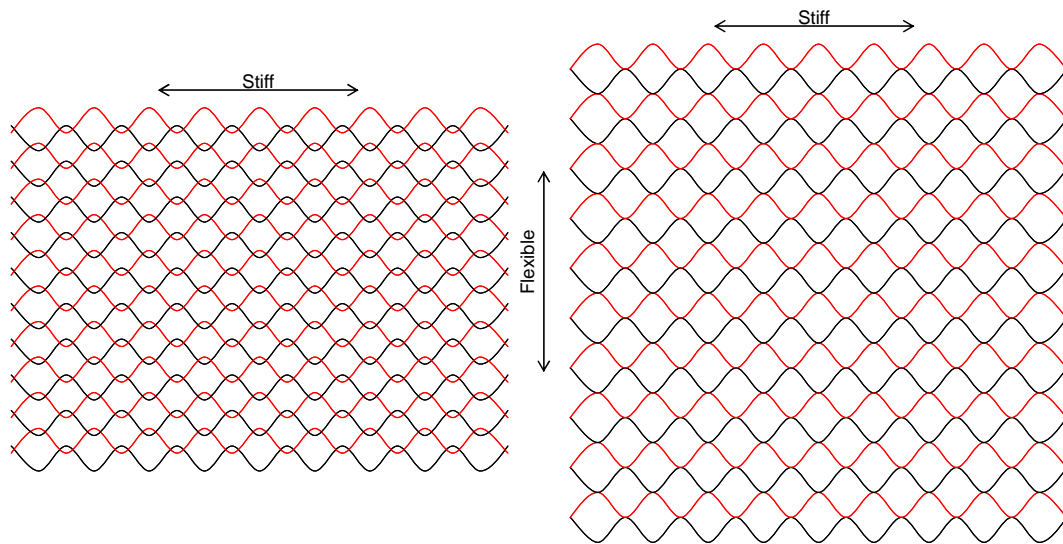


Figure 68: Tension in the sample is dependent upon the amount of connection between the wires.

Load transfer around the mesh sample was observed to be very different from that of the weld mesh. Forces were transferred diagonally between the wires rather than laterally along the wires (Figure 69). This allows wires beyond the directly loaded wires to be more actively engaged in redistributing the forces applied to the mesh.

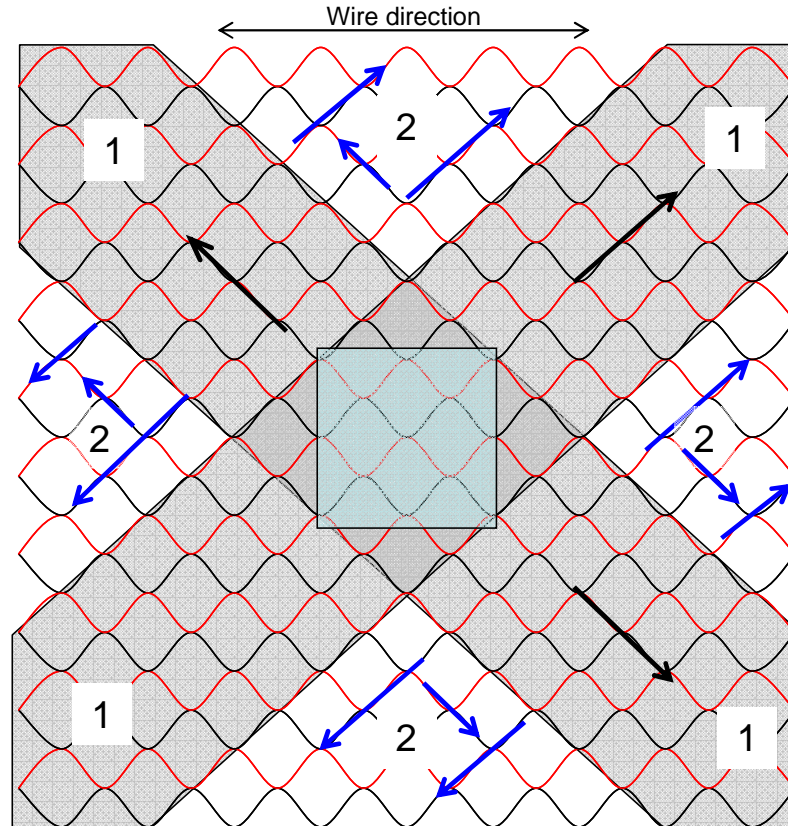


Figure 69: Force transfer around the chain link Product S95/4.

At high displacements the flexibility of the chain link mesh system caused the mesh to wrap around the plate. Consequently the greatest stress concentrations occurred on the wires at the plate edges rather than at the boundary restraint points as indicated in Figure 70.

Rupture occurred underneath the plate in both tests either as a result of the plate shearing through the wire, the mesh shearing through itself at a “link” (Figure 71a) or tensile failure of the wire (Figure 71b). The actual mechanism was difficult to determine, although it is likely that the use of the flat steel plate with sharp edges contributed to the failure of the sample. Safety considerations limited access to the sample once the forces reached 100kN and as such the mesh reaction around the plate could not be closely monitored. At rupture, a hole developed in the mesh as a result of the wire failure (Figure 72). This caused the force to drop to zero and, in one case, the plate fell through the mesh completely to end the test.

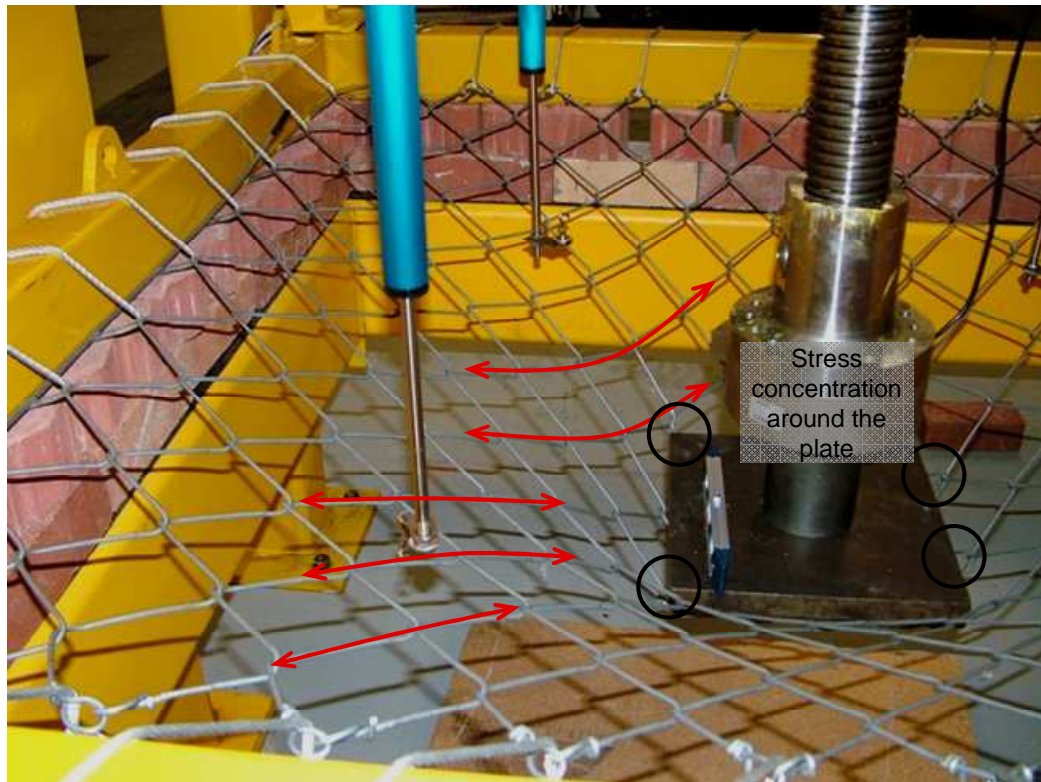


Figure 70: Due to high displacements stress is concentrated on the edge of the loading plate.



(a)

(b)

Figure 71: (a) Shear failure of the wires either as a result of the plate or the mesh "cutting" itself or (b) tensile wire failure.



Figure 72: Hole in the mesh after rupture.

4.10.2 FIXED BOUNDARY RESTRAINT METHOD TEST RESULTS

As outlined in Section 4.9.2 the lacing boundary had many limitations and consequently the fixed boundary system was developed.

A further six tests were conducted on Product S95/4 using this test method. The force - displacement results are provided in Figure 73.

The response of the mesh is very similar to that recorded in the lacing tests. The typical curve can be characterised by the same terms; bedding displacement, force redistribution and deformation of the mesh.

Due to the shape of the test frame and the mesh configuration, the mesh is tensioned in the wire direction but still loose in the diamond direction. Consequently, considerable differences in the tension of mesh were noted prior to the start of the test and accordingly the bedding displacement varied by over 100mm. The variations in tension were further exacerbated by slight variations in the dimensions of the sample created during the manufacturing process.

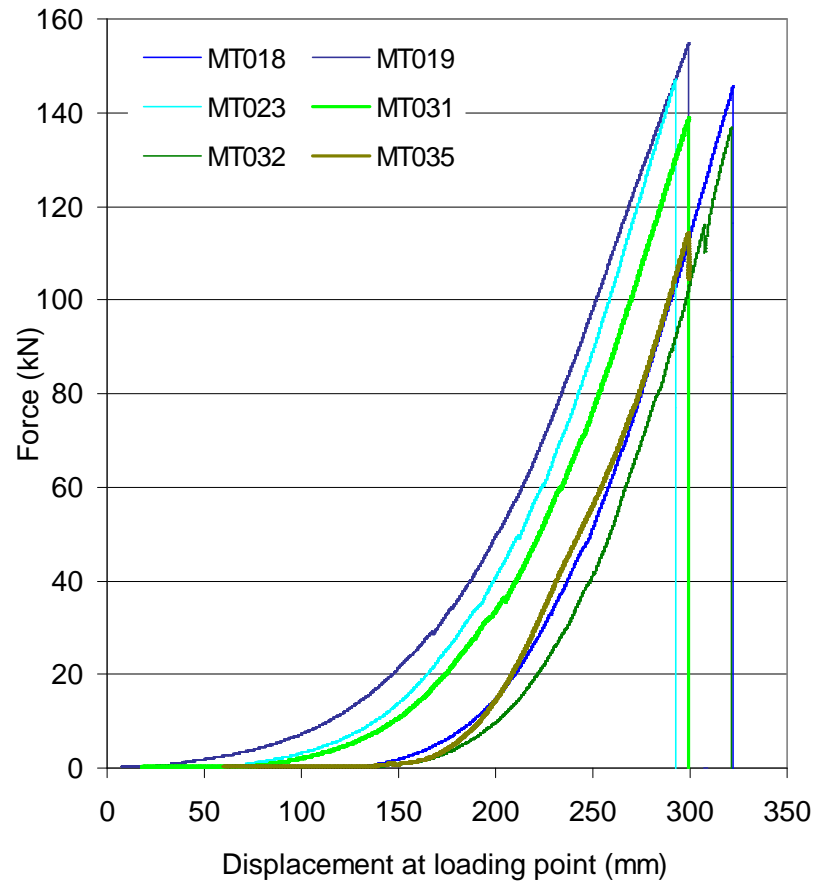


Figure 73: Force –displacement results for Product S95/4 mesh using the fixed boundary method.

Once the mesh developed tension, the force transfer around the sample was similar to the tests conducted on the lacing boundary system. This concept has been discussed in Section 4.10.1.

As defined in Section 4.9.2, rupture is the point at which a component of the system first breaks. “Rupture force” and “rupture displacement” are used to describe the force and displacement at the point of first rupture. The force – displacement results at rupture are provided in Figure 74. The average rupture force was 145kN at 307mm of displacement.

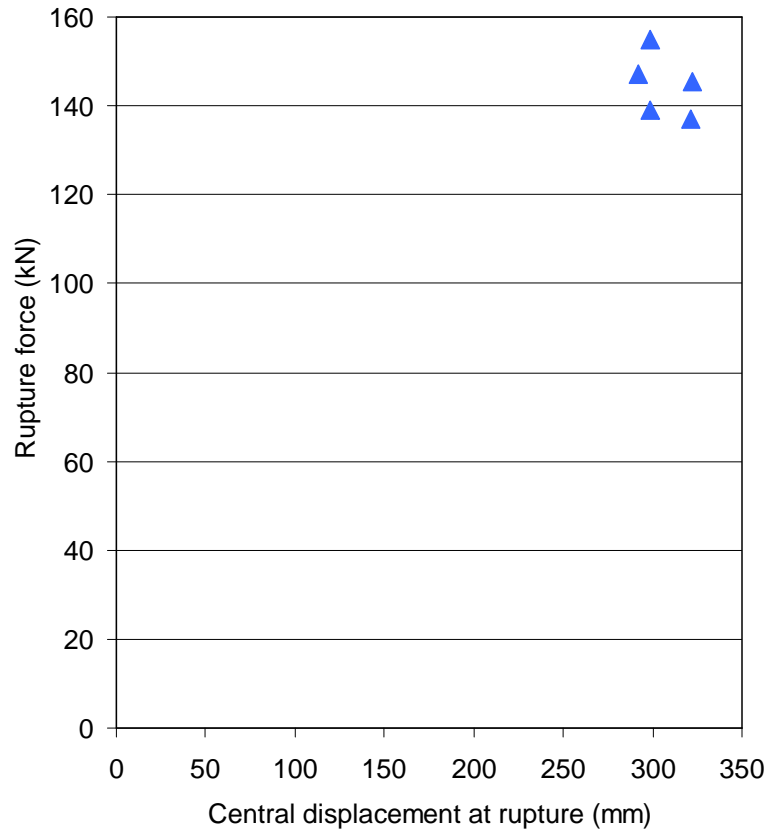


Figure 74: Rupture force – displacement chart for Product S95/4 using the fixed boundary system.

The same failure mechanisms were observed as in the lacing tests. This was despite the curved loading plate being used in Tests MT031 and MT032. The curved loading plate (Figure 75b) was manufactured to minimise the point loading that developed around the edges of the flat steel plate (Figure 75a). The curved base still had some sharp edges after manufacturing. Small modifications were made to the plate after these tests and test MT035 was conducted to determine whether any benefit had been achieved. The sample was very loose in the test frame; consequently, the displacement capacity of the jack was exceeded prior to failure of the sample being achieved. The maximum force of this test was 114.3kN at the maximum displacement of 299mm. The shape of the base of the plate appeared to have no effect on the force - displacement reaction of the mesh.

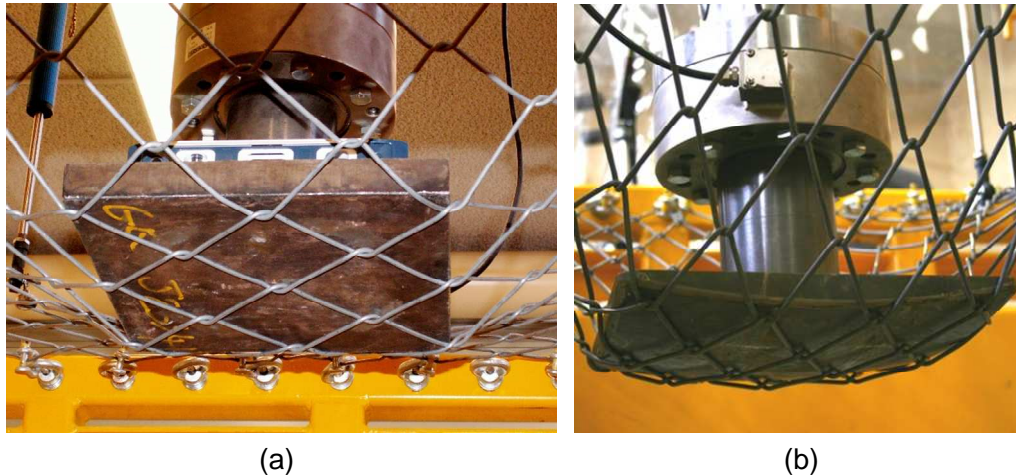


Figure 75: The flat based plate (a) causes point loading even at low displacements whilst curved plate (b) reduces the effect.

Samples of four more products (G65/4, G80/4, G65/3 and G80/2) were provided by the company to enable comparison with S95/4. Three tests were completed for each product.

4.10.2.1 Product G65/4

The results for Product G65/4 are provided in Figure 76. The response of the mesh is very similar to that recorded for S95/4. The typical curve can be characterised by the same terms; bedding displacement, force redistribution and deformation of the mesh.

Test MT085 reached the displacement capacity of the jack without rupture. The maximum force was 166.7kN at 309mm of displacement. The sample was unloaded 6mm and the jack was adjusted to increase the displacement capacity by approximately 15mm. The sample was then re-loaded and failure was achieved. In order to ensure that complete failure was obtained, a triple plate configuration was used in Tests MT092 and MT093 to increase the displacement capacity by approximately 70mm (Figure 77). The curved base plate was on the bottom of the configuration to ensure the same loading conditions were applied.

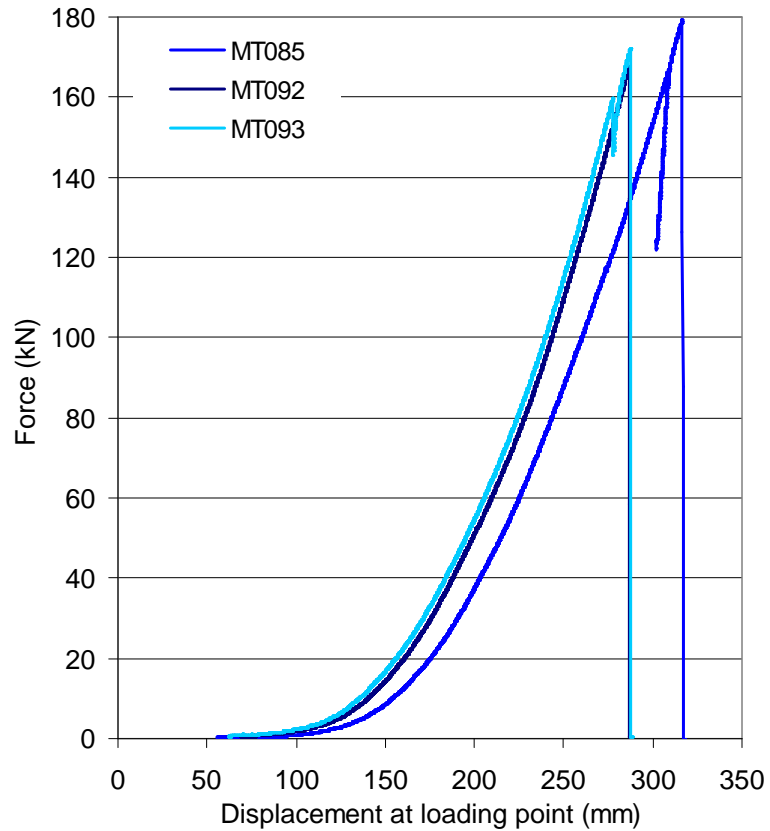


Figure 76: Force – displacement result for Product G65/4.



Figure 77: Triple plate configuration used to increase displacement capacity.

For this product, the forces were primarily transferred in the direction of the diamonds as indicated in Figure 78. Only a small proportion of the forces were transferred in the direction of the wires (indicated in pink in Figure 78). This force transfer concept can be seen in the photograph shown in Figure 79 taken during testing. The load in kilograms is shown at the top of the picture.

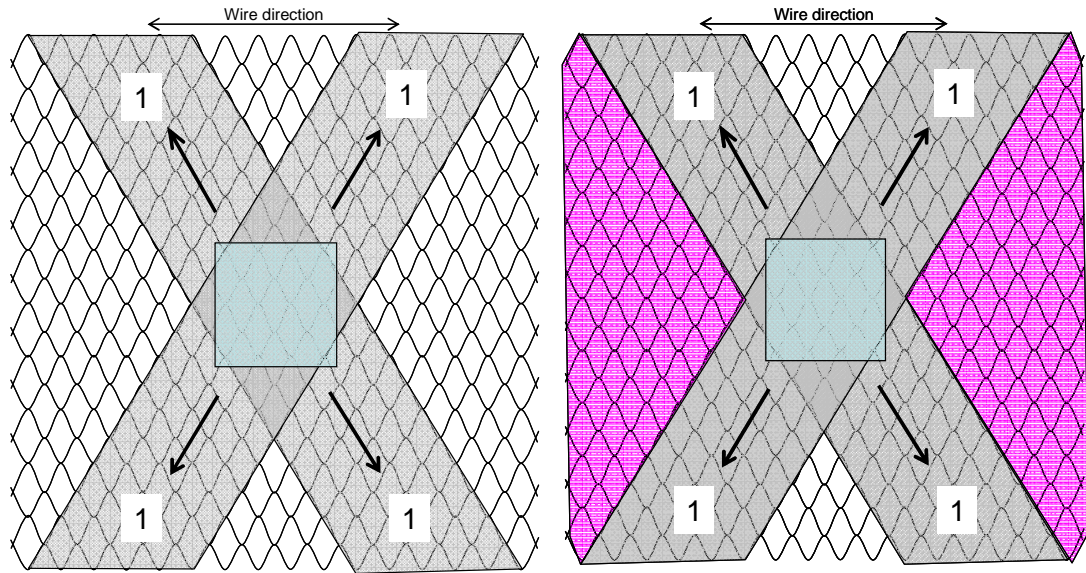


Figure 78: Force transfer around Product G65/4.

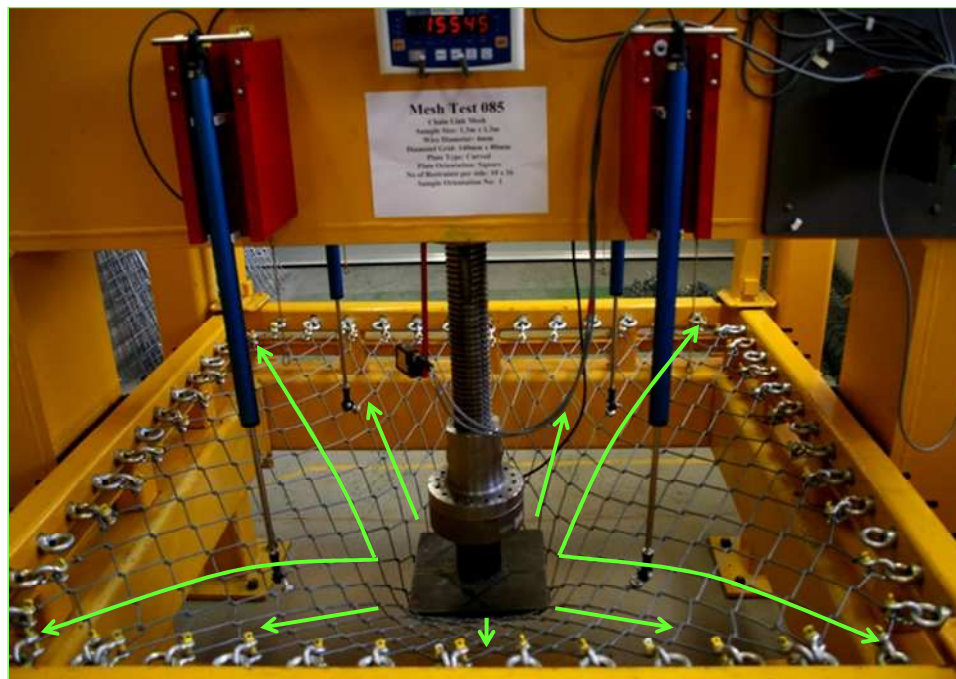


Figure 79: Force transfer concept of Product G65/4.

Due to the high forces on the mesh during the later stages of the test, some deformation of the test frame was observed. After the completion of the first test some plastic deformation of the frame was noted. Markers were put on the test frame to enable the measurement of the deformation in the following tests. The inwards movement of the frame was between 5 and 10mm but the test frame returned to its original position once the forces were released, indicating elastic deformation rather than plastic deformation. This bending was only observed during the testing of product G65/4 samples. The drop in force of test MT093 at approximately 160kN was caused by a slip of the test frame on the sample support frame and not a rupture. This slip had a minor effect on the force – displacement results.

The rupture force – displacement results are provided in Figure 80. The average rupture force was 174kN at an average of 302mm of displacement.

Although the failure mechanism was same as that of S95/4, at rupture the sample released its elastic energy and a rebound of the sample was observed (Figure 81). There appeared to be very little plastic deformation of the wires around the plate.

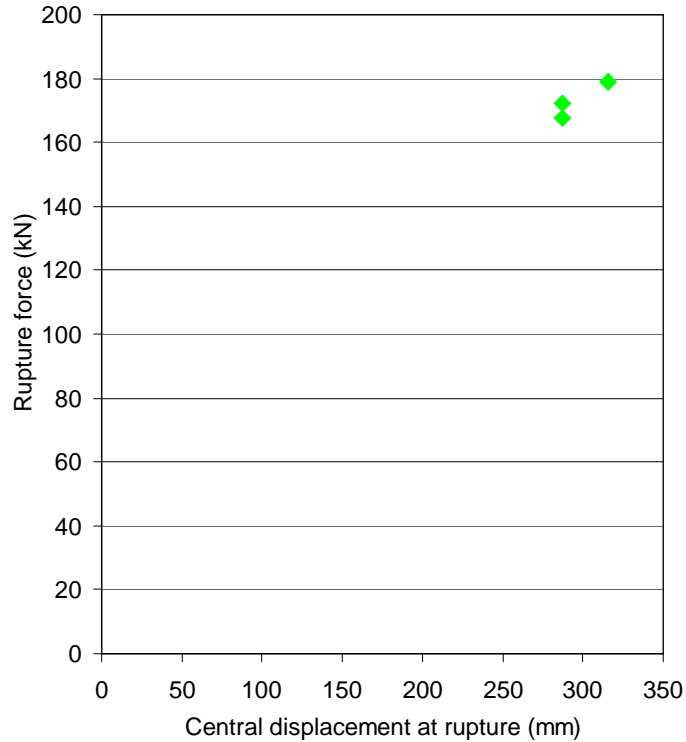


Figure 80: Rupture results for Product G65/4.



Figure 81: Rebound of mesh due to the release of stored elastic energy.

4.10.2.2 Product G80/4

The results for Product G80/4 are provided in Figure 82. All samples were extremely tight on the test frame and consequently the bedding displacement for all three tests was zero. The force transfer around the mesh was similar to G65/4.

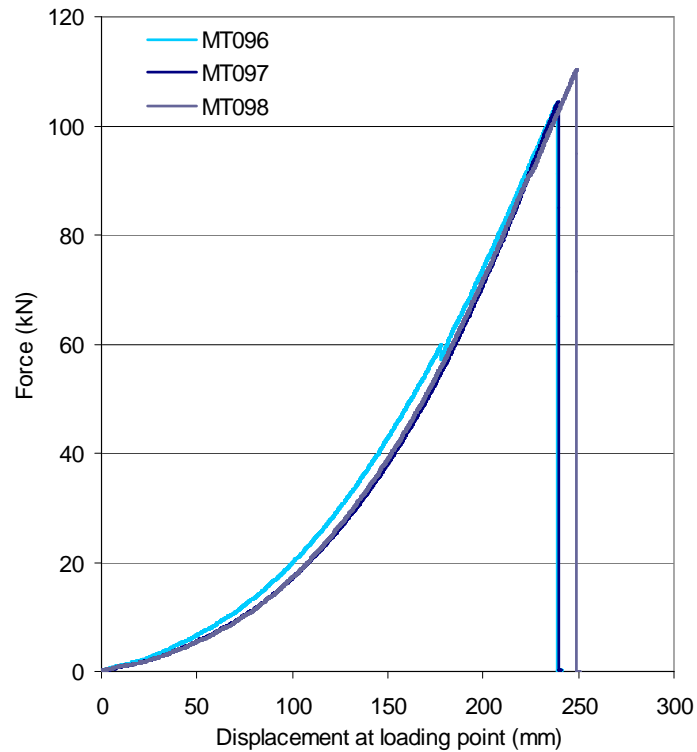


Figure 82: Force transfer concept of Product G80/4.

The rupture results are provided in Figure 83. The average rupture force was 106kN at 243mm of displacement.

The failure mechanism of this product was much more apparent than with the previous tests. Significant necking of the wires could be identified at the “links” (Figure 84) but was not observed around the edges of the plate. This suggests that rupture was caused by the wires shearing through each other rather than the plate cutting through the wires.

As illustrated in Figure 85, the wires that broke unravelled from each other creating a much larger hole in the mesh than was observed with the previous products. This is likely to be a function of the high tension in the mesh.

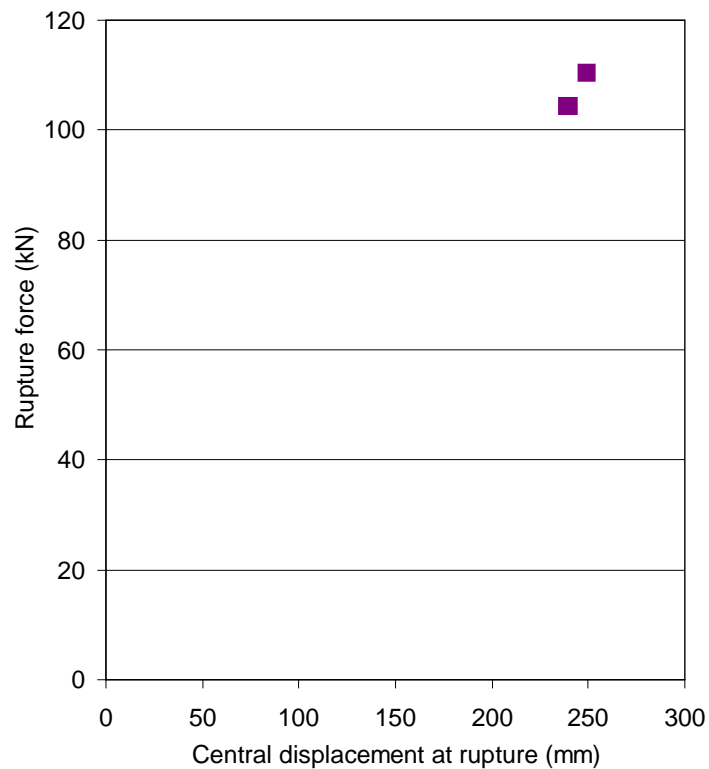


Figure 83: Rupture force – displacement results for Product G80/4.

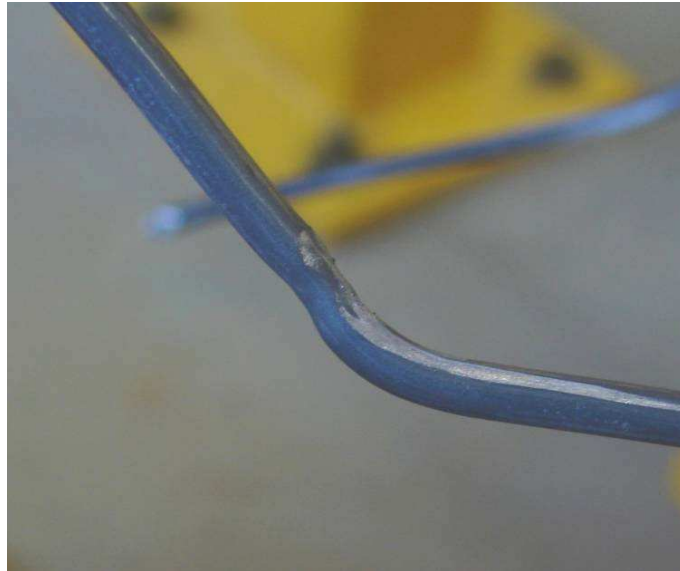


Figure 84: Necking of the wire at a link away from the edge of the plate.

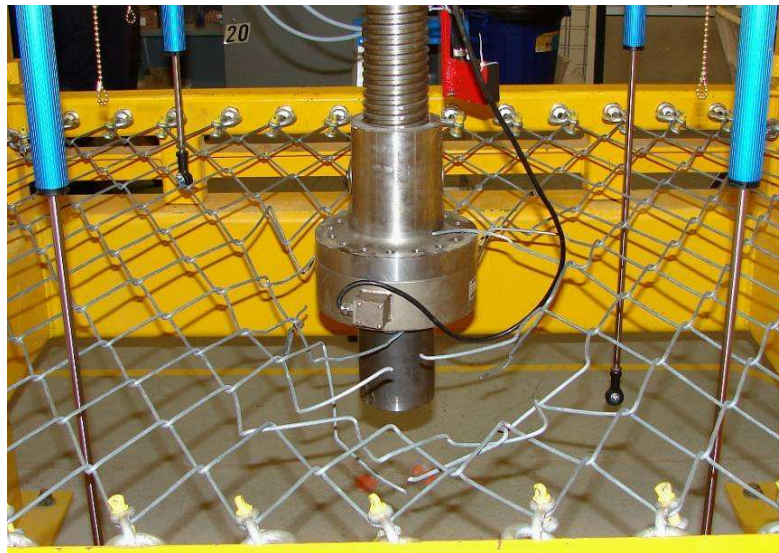


Figure 85: Unravelling of chain link.

4.10.2.3 Product G65/3

The results for Product G65/3 are provided in Figure 86. All samples were initially very loose on the test frame. The lack of tension caused high bedding displacements (between 95mm and 160mm).

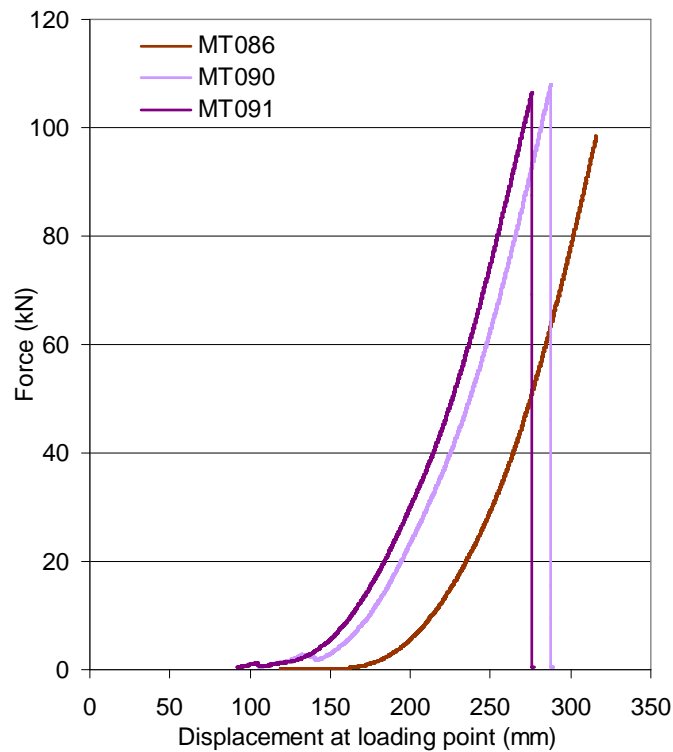


Figure 86: Force – displacement results for Product G65/3.

Despite changes to the jack, test MT086 also reached the displacement capacity without failure. The triple plate configuration was used in tests MT090 and MT091 to ensure failure was achieved. No differences were observed in the load transfer around the mesh or the failure mechanism between G65/4 and G65/3 due to the identical diamond configurations.

The rupture force – displacement results are provided in Figure 87. The average rupture force was 107kN at an average of 281mm of displacement.

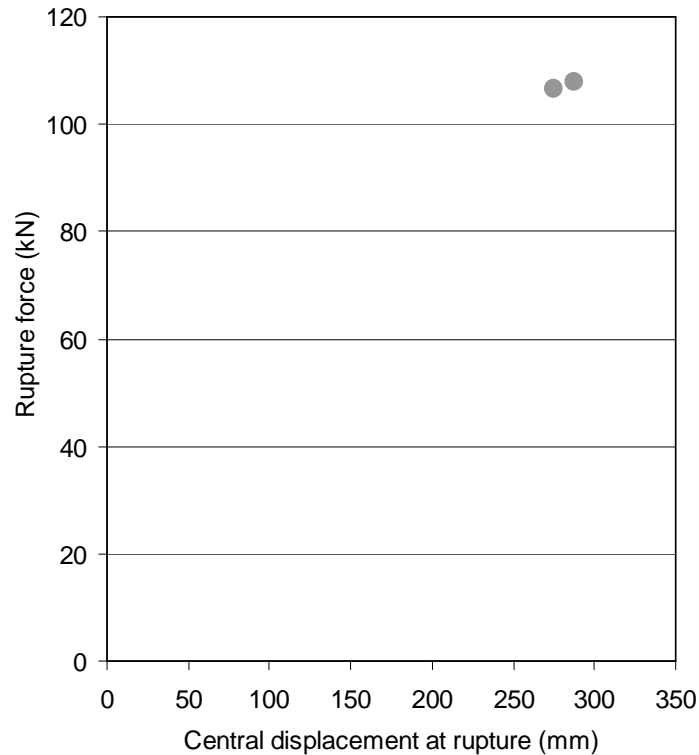


Figure 87: Rupture force – displacement chart for Product G65/3.

4.10.2.4 Product G80/2

The results for Product G80/2 are provided in Figure 88. Test MT087 was observed to only have medium tension once installed on the test frame whilst MT088 and MT089 were both observed to be extremely tight. The difference in tension does not appear to have affected the bedding displacement with MT087 recording 71mm whilst MT088 and MT089 recorded 75mm and 78mm respectively.

The response of the mesh is less stiff than S95/4, G65/4 and G65/3, with force transfer occurring at a much slower rate. The rupture force is also significantly lower than the other products. This is likely to be due to the difference in the diamond configuration and the number of wires. These differences are discussed in Section 4.10.3.1. The force - displacement results at rupture are shown in Figure 89. The average rupture force was 26kN at 206mm of displacement.

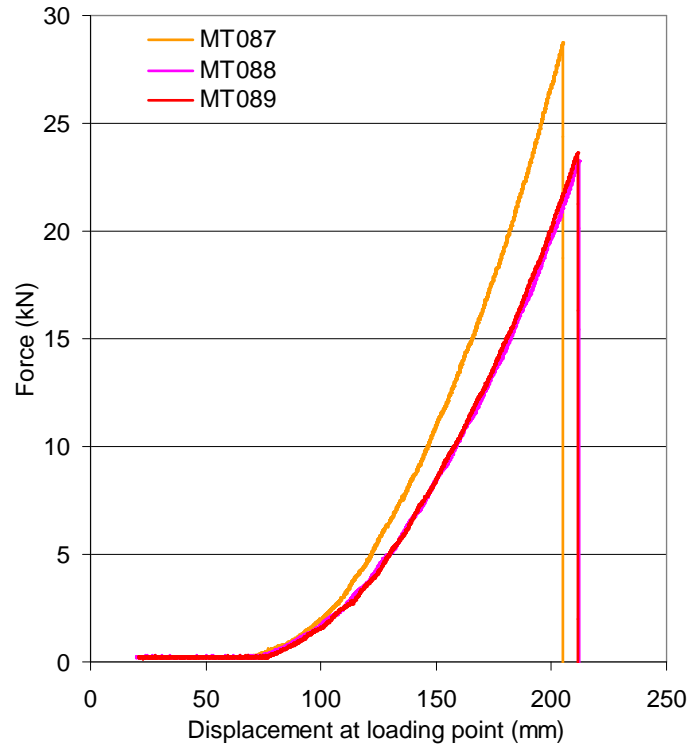


Figure 88: Force – displacement results for Product G80/2.

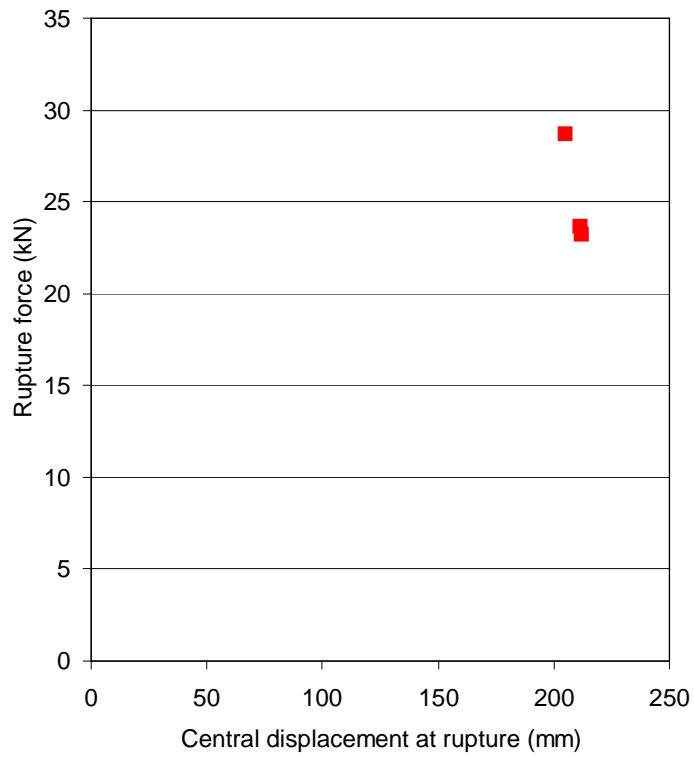


Figure 89: Rupture force – displacement chart for Product G80/2.

4.10.3 DISCUSSION CHAIN LINK TEST RESULTS

The configuration of the chain link samples have resulted in a number of variables affecting the force – displacement results. These are:

- Boundary condition
- Number of wires in the sample
- Wire diameter
- Diamond configuration

Comparisons between tests can only be made where one variable is changed. For example:

- Boundary systems can only be compared if the same mesh product is used in both setups.
- Wire diameters can only be compared if the boundary condition, diamond configuration and number of wires are consistent.
- Diamond configurations can only be compared if the boundary condition, wire diameter and number of wires are equivalent.

A comparison of the effect of the number of wires on the force - displacement results is not possible with the samples provided. Product G80 had fewer wires and also a diamond configuration different from Product S95 and G65; consequently, it is difficult to determine whether any differences in the test results were caused by the variation in the number of wires or the change in diamond configuration.

The boundary conditions appeared to have a limited effect on the force - displacement response of the chain link mesh. Product S95/4 was the only product tested using both the lacing and the fixed boundary conditions. As discussed in Section 4.10.2, significant variations were observed in the tension of the samples at the start of the test. As shown in Figure 90, the low tensioned samples tested with the fixed boundary condition produced similar force – displacement response to the samples tested with the laced boundary configuration.

There appears to be slight differences in the behaviour of the systems, indicated by the shapes of the curves, but these are likely to be due to the differences in stiffness between the shackles and the wire ropes rather than differences in the mesh product.

Further analysis and discussion of the shape of the force – displacement curve is undertaken in Section 4.12.4.2.

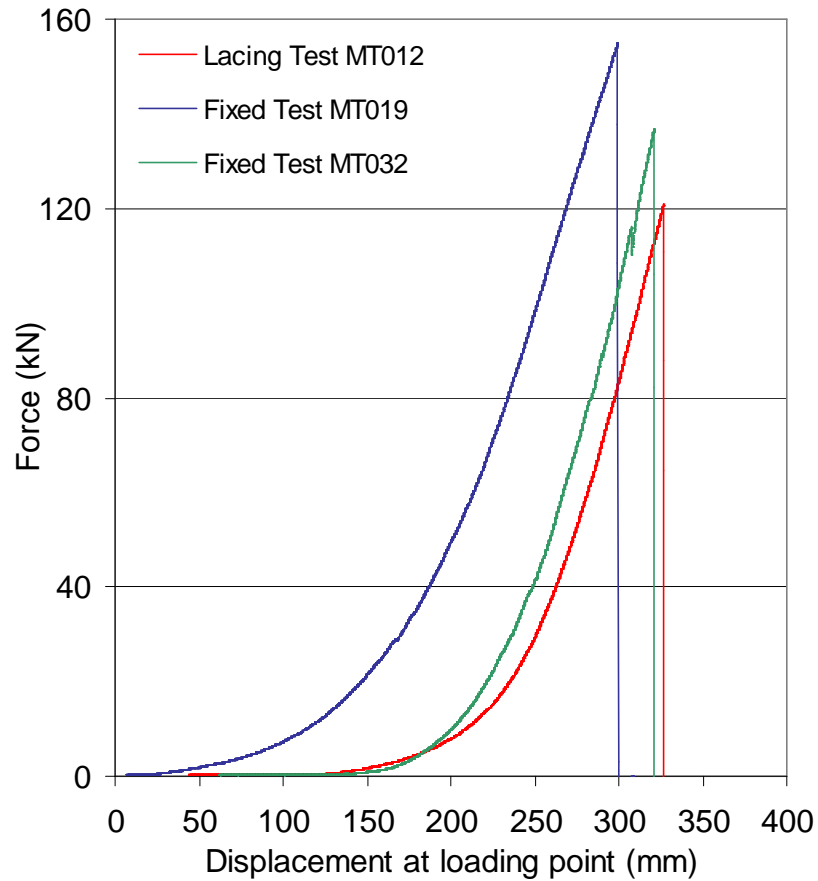


Figure 90: Comparison of the lacing boundary and fixed boundary results.

4.10.3.1 Comparison of mesh diamond configurations

The results from Products S95/4 and G65/4 can be used to determine the effect of the diamond configuration on the force – displacement response. Both products contain 20 wires with 4mm diameter. The diamond configurations are shown in Figure 91. A summary of the rupture force and associated displacements is provided in Figure 92.

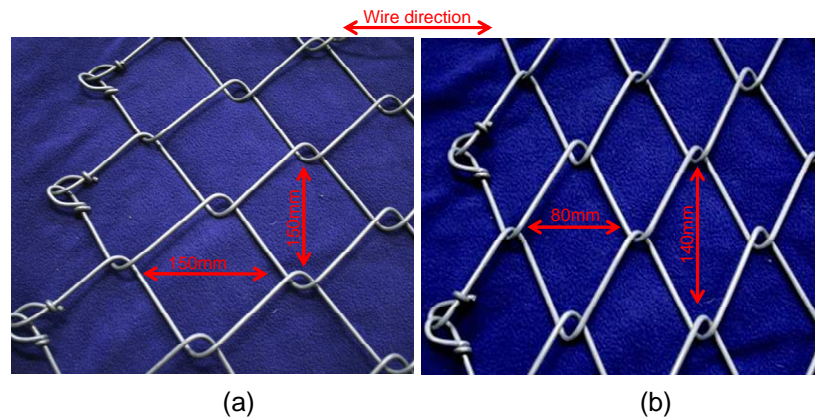


Figure 91: Diamond configurations of (a) S95/4 and (b) G65/4.

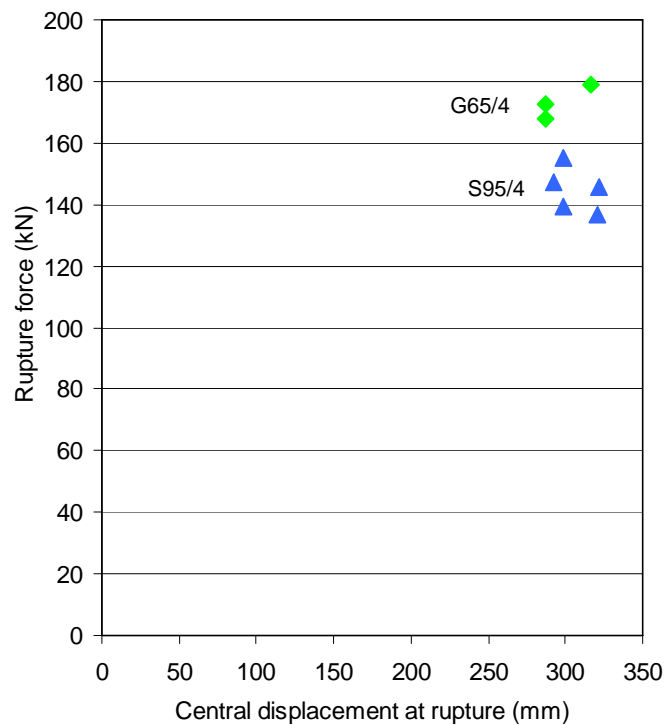


Figure 92: Rupture force and displacement results for S95/4 and G65/4.

There was very little difference in the rupture displacement between the two diamond configurations. The rupture force of Product S95/4 (144kN) was slightly lower than that of G65/4 (173kN). The lower forces of Product S95/4 may be related to the variation in the product discussed in Section 4.10.2 or to the effects of the flat steel plate used to load the samples in most of the tests.

The two mesh products also displayed different force transfer mechanisms (Figure 93). The symmetrical diamond shape of Product S95/4 resulted in the force being transferred uniformly around the mesh. The asymmetrical shape of Product G65/4 resulted in most of the forces being transferred in the long direction of the diamonds. In field applications most bolting applications assume the mesh transfers load uniformly in both directions and, consequently, the bolting pattern used to restrain the mesh are square or diamond in shape. Force transfer in a single direction may be beneficial in certain circumstances providing that the bolting pattern is designed to account for this property, particularly at the overlap between mesh sheets.

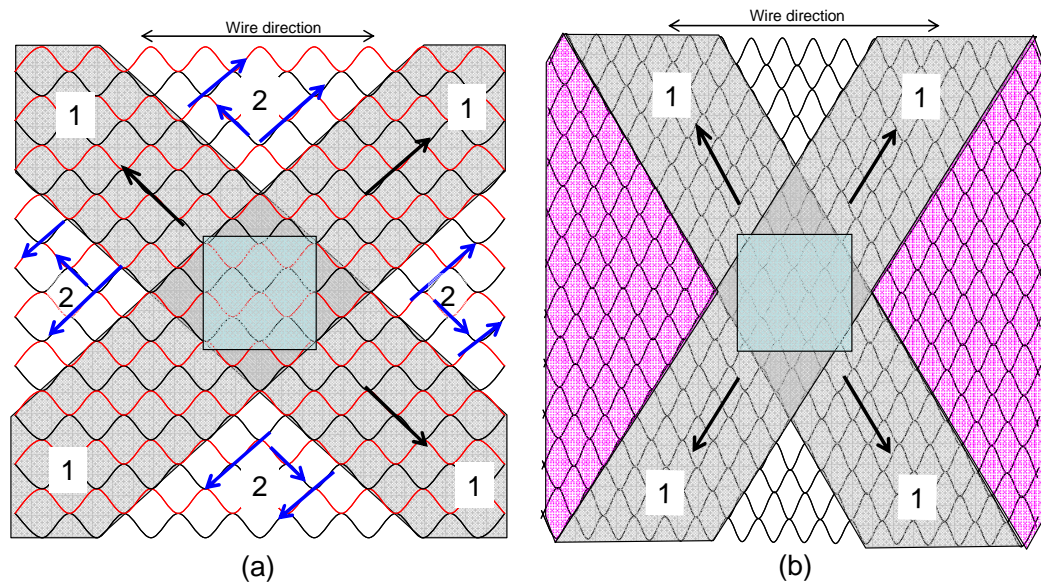


Figure 93: Force transfer mechanisms for (a) S95/4 and (b) G65/4.

4.10.3.2 Comparison of wire diameters

Products G65 and G80 can be analysed separately to determine the effect of the wire diameter on the force - displacement results. A summary of the rupture force - displacement results for each product is provided in Figure 94. The average rupture force of Products G65/4 was 179kN compared with G65/3 which was 108kN, a reduction of 40%. The decrease in force capacity corresponds directly with the reduction of cross-sectional area of the wire.

This same trend is observed in Product G80. There is a 75% difference in cross-sectional area between G80/4 and G80/2. The results show that the average rupture force of Product G80/2 (29kN) is 25% of G80/4 (110kN).

Determining the effect of the wire diameter on the rupture displacement was difficult due to variations in the tension of the mesh at the start of the test. The difference in the rupture displacement between G65/4 and G65/3 was only 1%. However, Product G65/3 had very low tension at the start of the tests; this resulted in high bedding displacements which have affected the results.

The average rupture displacements for G80/4 and G80/2 are 243mm and 209mm, respectively. Again there was a significant difference in the bedding displacements between the two products; G80/4 was highly tensioned and consequently there was only 2mm of bedding displacement; G80/2 also appeared to be highly tensioned but the average bedding displacement was 75mm.

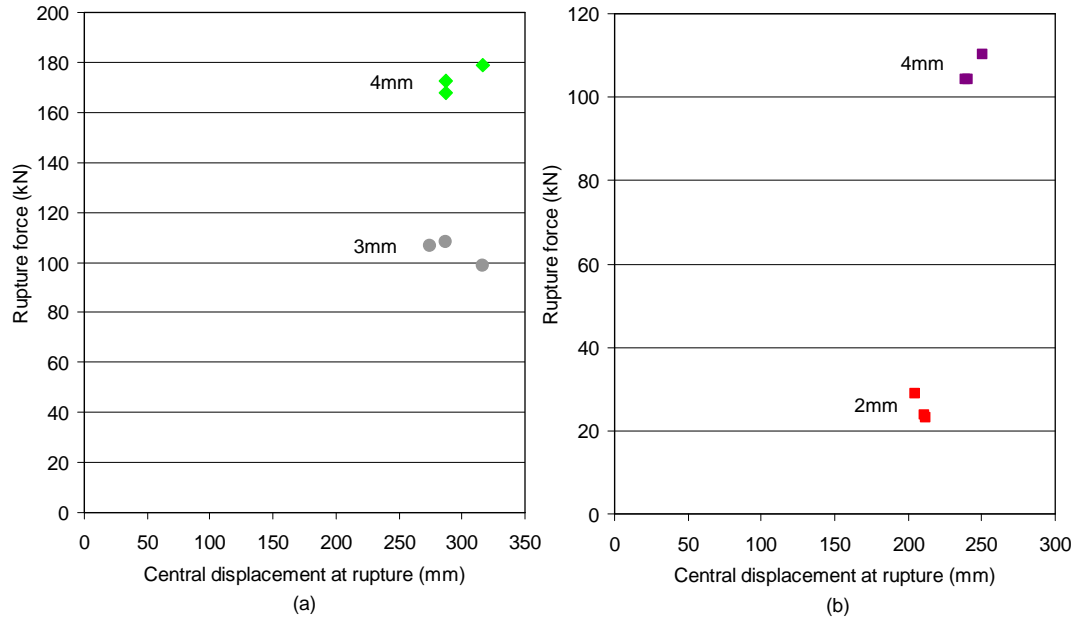


Figure 94: Evaluation of the effect of wire diameter using (a) Product G65 and (b) Product G80.

4.11 COMPARISON OF MESH PRODUCTS

Figure 95 provides a comparison of the force - displacement responses for weld mesh and chain link mesh. Both mesh types had a tensioning phase which is quantified by the bedding displacement. This phase was followed by a force redistribution phase whereby forces were transferred away from the primary wires and along the secondary wires.

Slight variations were observed in the tension of the chain link mesh samples prior to the beginning of each test. This was taken into account by measuring the displacement of the mesh due to the placement of the loading plate before the commencement of a test. Highly tensioned sheets had minimal displacement whereas loose sheets displaced considerably as a result of the placement of the loading plate. The initial tension did not appear to have a substantial effect on the overall force - displacement response of the mesh.

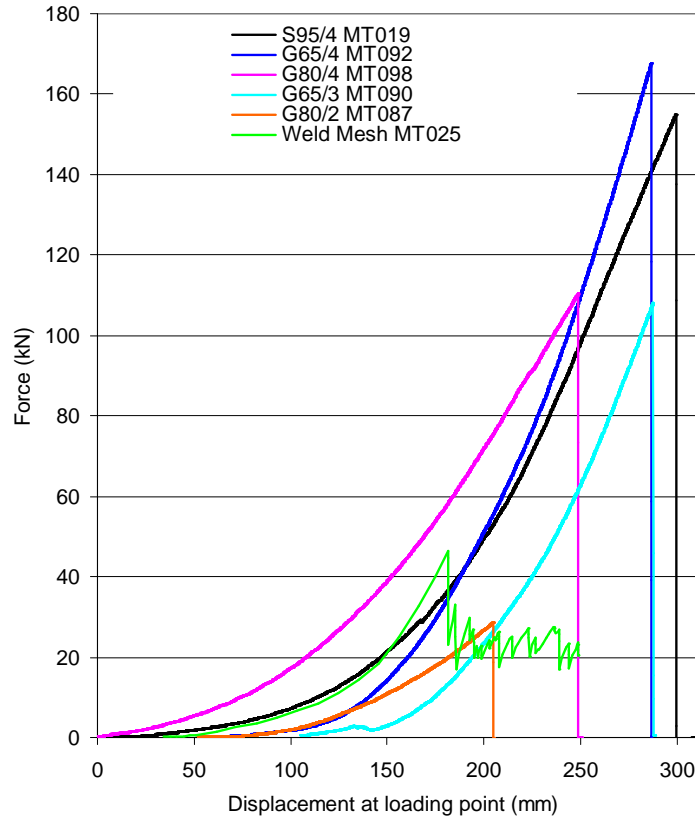


Figure 95: Comparison of the various mesh types using the fixed boundary system.

Once the entire mesh sample was tensioned due to plate displacement, the wires began to deform and eventually culminated in rupture.

The rupture force and displacement results are provided in Figure 96. The different mesh types contain a different number of wires and typically this would not enable a direct comparison of the results. The weld mesh samples contained 28 wires with a diameter of 5.6mm. The chain link samples contained fewer wires (14 or 20) with smaller diameters (2 – 4mm). Notwithstanding this, the rupture force of weld mesh was significantly less than most of the chain link mesh products despite the weld mesh containing a greater number of wires. The higher capacity of the chain link mesh is related to the tensile strength of the wire. The tensile strength of the Geobrug wire is 1770MPa whilst the tensile strength of the weld mesh wire is estimated at 450MPa.

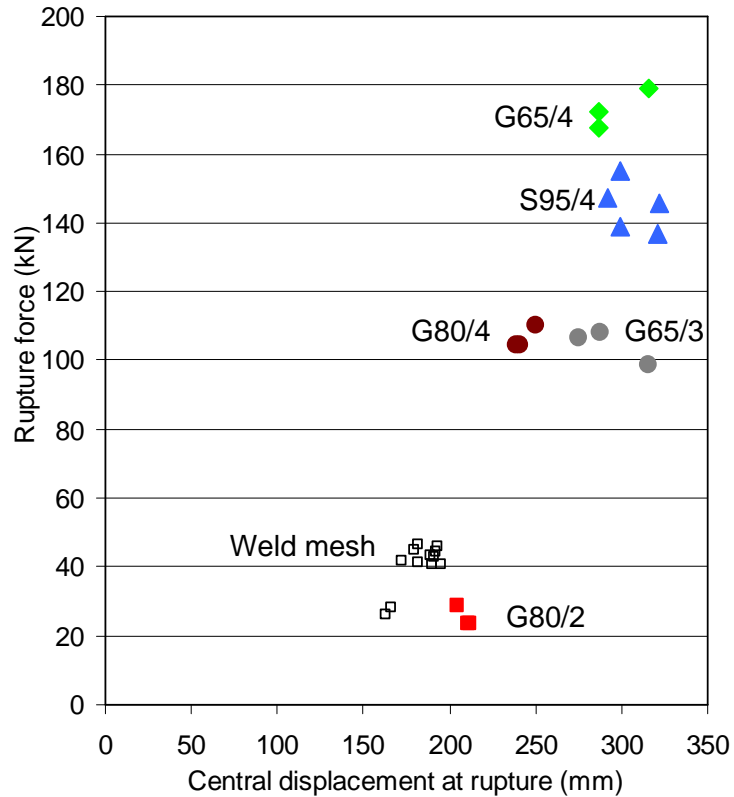


Figure 96: Comparison of results of various mesh types.

Significant differences in the failure mechanisms and the location of those failures were observed between weld mesh and chain link mesh. The rupture of weld mesh always occurred at the boundary on a directly loaded wire. The failure mechanism of welded wire mesh is a measure of the mesh quality. Three different welded wire mesh failure mechanisms were observed; namely, tensile wire failure, failure of the wire through the heat affected zone (HAZ), and weld failure.

Only one failure mechanism was observed for chain link mesh. The chain link mesh failed on the edge of the plate, either as a result of the plate cutting through the wires or as a result of the wires cutting each other at a “link”. This failure mechanism limits the direct applicability of the test and causes some variability in the results. Generally only one or two wires broke. The load dropped completely after the first rupture as a result of plate movement effectively ending the test.

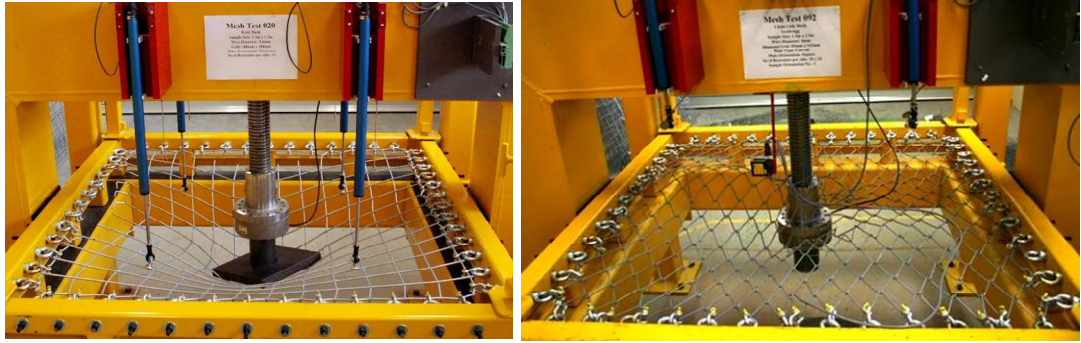


Figure 97: Weld mesh and chain link mesh after failure.

The wire configurations of the different mesh types resulted in very different force transfer behaviour. The proposed force transfer mechanisms are provided in Figure 97. Weld mesh primarily transfers forces along the directly loaded wires with the secondary loaded wires not tensioning until a large amount of displacement has occurred. The chain link mesh transfers the forces diagonally; this involves engaging a much greater portion of the sample. This latter mechanism is highly dependent upon the initial tension in the sample and the configuration of the diamonds.

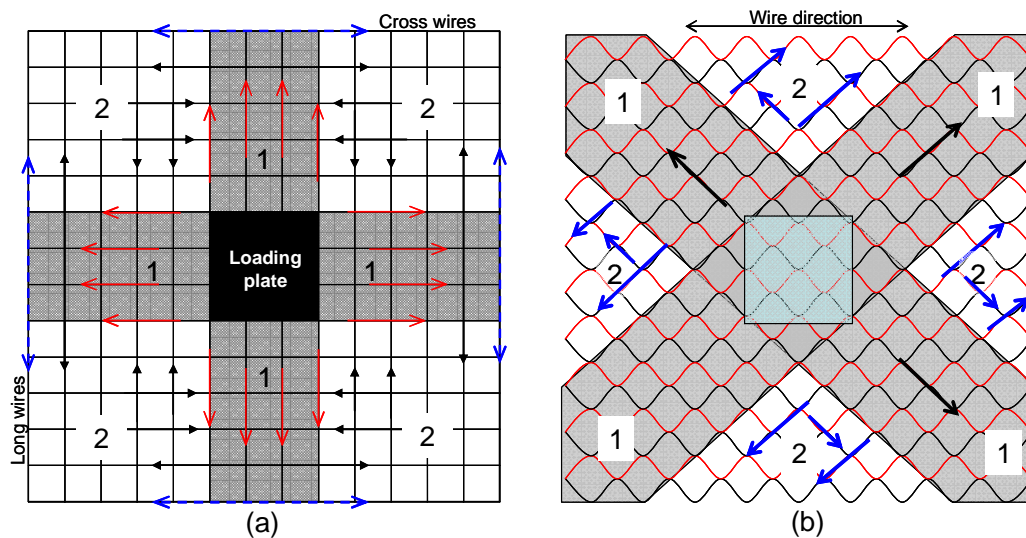


Figure 98: Difference in force transfer mechanism between (a) weld mesh and (b) chain link mesh.

Overall it can be stated that the Geobrug high tensile chain link mesh has much greater force and displacement capacities compared with weld mesh; although better installation methods must be devised before it will become widely accepted by the Australian mining industry.

4.12 ANALYSIS TECHNIQUES

The various analysis techniques proposed by other authors and discussed in Section 4.3 have been applied to the WASM test data to determine the validity of the techniques.

4.12.1 PAKALNIS AND AMES METHODS

Testing has shown that the mechanisms of force transfer from the loading area to the boundary are complex. The tension in the wires varies across the sheet of mesh, depending on whether or not the wire is under direct load.

Coates' assumption that uniform loading occurs over the entire sheet is incorrect. Likewise, McFarlane's assumption that all forces are transferred along the directly loaded wires is also incorrect.

Furthermore the concept of tension within the wires cannot be applied to chain link mesh where the load is transferred along the links, diagonal to the wire direction.

Attempts were made to determine the forces within the directly loaded wires by measuring the loads acting at restraint points. Small capacity load cells (90kN) were placed behind two of the restraining bolts used in the fixed boundary method (Figure 99). These load cells were assumed to measure the forces acting along the two wires perpendicular to the boundary.

Attempts to correlate the load cell data with the predictions of tension derived from both Coates and McFarlane's formulae proved unsuccessful and no further analysis was carried out.

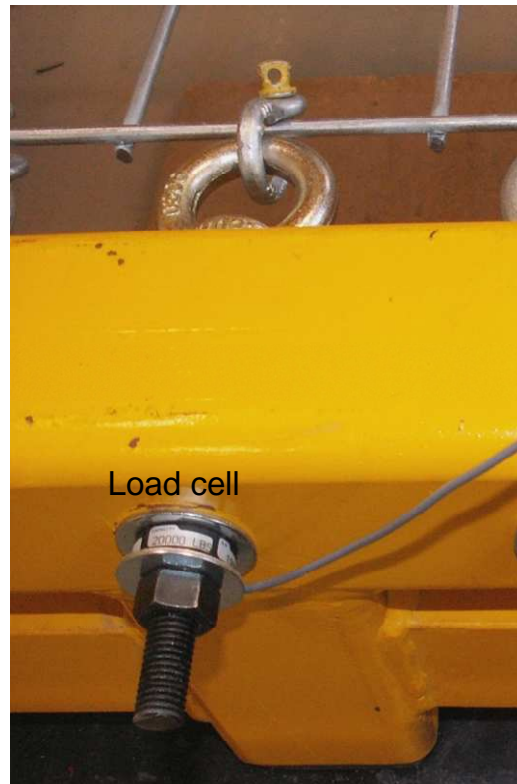


Figure 99: Small load cell used to collect data at particular restraining points.

4.12.2 TANNANT'S METHOD

Tannant's analysis (1995) encompasses three principles; stiffness, displacement offset and force capacity predictions.

The stiffness value presented by Tannant is directly influenced by the definition of the peak load. Where peak load corresponds to the rupture load (as in Figure 100), a linear relationship can provide an approximate representation of the force - displacement curve, after the sample is fully tensioned and prior to rupture. Where peak load is not concurrent with the rupture load (Figure 101) a linear relationship does not represent the force - displacement reaction and thus the stiffness equation cannot be applied in accordance with Tannant's definitions.

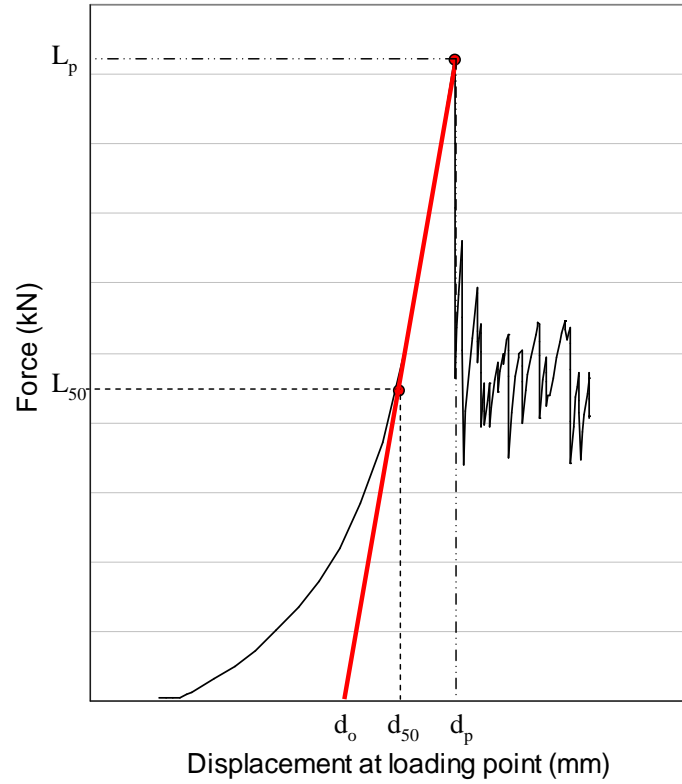


Figure 100: Force - displacement curve where peak load is equal to rupture load.

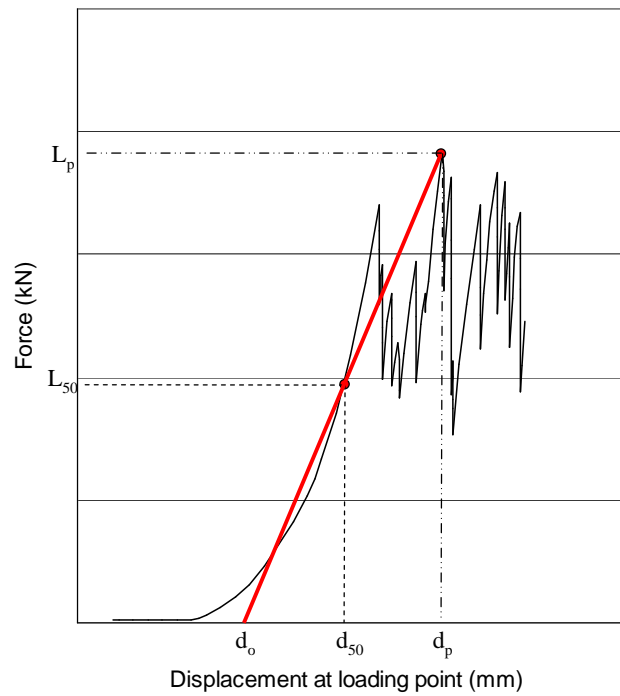


Figure 101: Force-Displacement curve where peak load is not equal to the rupture load.

The stiffness equation was also used by Tannant to determine the point at which the load carrying capacity of the mesh is activated (d_o). The language used by Tannant in describing this parameter is misleading. The displacement offset is simply a measure of when the forces are being transferred across the entire sample as described in Section 4.9.4. "Load carrying" does not start at this point. Forces are already being transmitted by the mesh but the rate of the increase in force compared with the displacement increase is low.

Tannant's formula for the theoretical load capacity (L_p) of mesh (Equation 4.8) was applied to the WASM weld mesh data to determine if it was possible to predict the rupture force of the mesh. Again this formula requires some knowledge of the force – displacement properties of the mesh to obtain a result. It is assumed that "N" is equal to 8 given that the plate is in contact with 4 wires in each direction.

The results are provided in Appendix 6. The results demonstrate that in most cases the rupture force of the mesh was greatly overestimated. Even if it is assumed that only 4 wires are in contact with the plate (i.e. that the forces are only being transferred in one direction) the estimations still do not correlate with the test results.

The results were not applied to chain link mesh as it is difficult to determine the number of wires that are carrying load given that the forces are transferred diagonally around the mesh.

4.12.3 THOMPSON'S METHOD

Thompson's (1999) analysis techniques are also based on catenary principles and as with Tannant's analysis method assumes that the entire load is being conducted only along the primary loaded wires. Thompson (2001) realised the limitations of Tannant's analysis method and sought to develop a mesh simulation program to replicate the three dimensional non-linear reaction of the mesh. Initial attempts to use Thompson's model to simulate the tests from WASM have proven inconclusive to date.

4.12.4 THE WASM ANALYSIS TECHNIQUE

Most previous analysis techniques have assumed two-dimensional linear behaviour of the mesh. The results from the WASM test program clearly demonstrate that the behaviour of the mesh is not two-dimensional and that linear elastic principles cannot be applied. The WASM analysis technique starts by determining the actual shape of the force - displacement reaction curve. This will enable the development of better modelling codes to be used as design tools for surface support systems.

4.12.4.1 *Weld mesh*

The force – displacement results were standardised to a common scale to allow the comparison of the curve shape. This was achieved by adjusting the displacement for each test such that at 20kN of force the displacement was equal to 210mm using the following formula:

$$d_a = d_o - (210 - d_{20}) \quad (4.9)$$

where:

- d_a is the adjusted displacement
- d_o is the original measured displacement
- d_{20} is the displacement measured at 20kN

This formula is applied to all displacements for each test and the results re-plotted (Figure 102). The shape of the force-displacement curve for weld mesh proved to be very consistent. Changes in the boundary restraint method and the plate orientation had very little effect on the shape of the curve as can be seen in Figure 103.

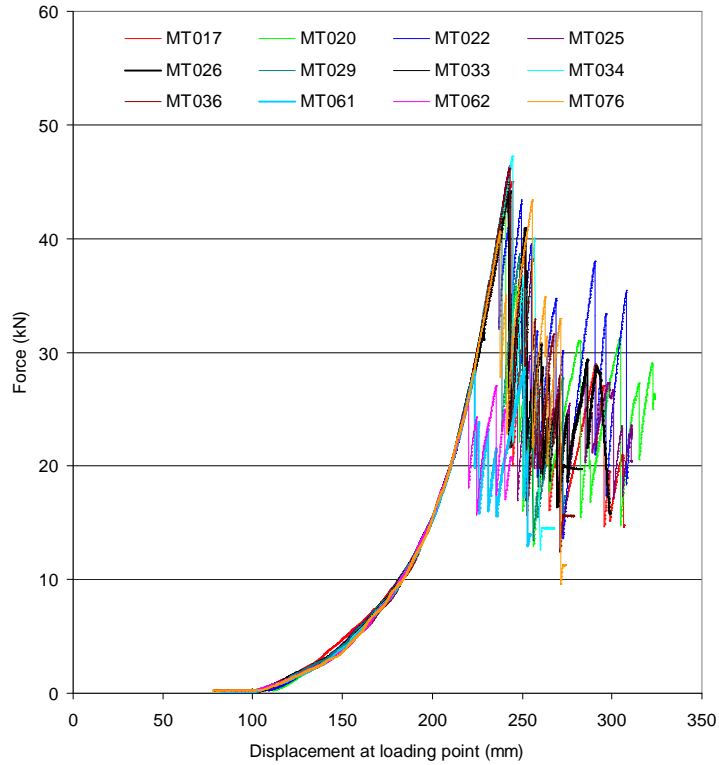


Figure 102: Standardised test results show little variation in the force – displacement reaction.

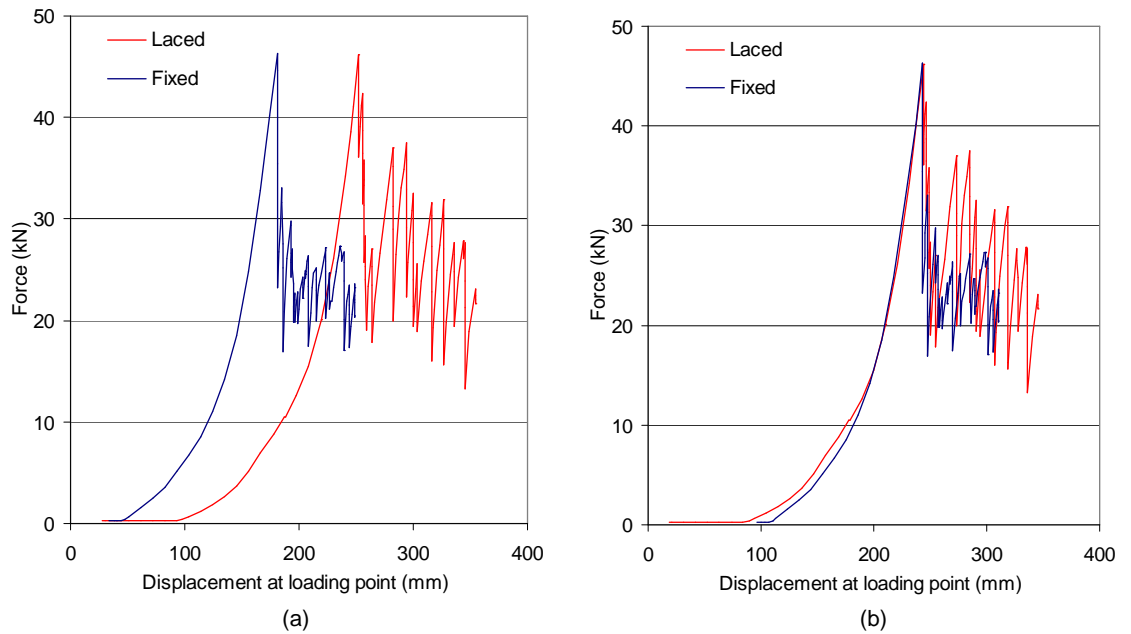


Figure 103: The force - displacement results for the lacing and fixed boundary condition (a) and the overlay of the force – displacement curve showing vary little variation (b).

The force – displacement data (not standardised) for each test was imported into a curve modelling computer program called Curve Expert™ to enable analysis of the shape of the curve. The program was used to compare the pre-rupture segment of the force - displacement curve with the statistical representations of the following curves:

- Linear ($y = a + bx$)
- Quadratic ($y = a + bx + cx^2$)
- Exponential ($y = ae^{bx}$)
- Power ($y = ax^b$)
- Polynomial ($y = a + bx + cx^2 + dx^3 + \dots$)

Figure 104 shows comparisons between each of the curves and the actual data from one of the tests. A summary of the average R squared values for each of the different curve types is provided in Table 11.

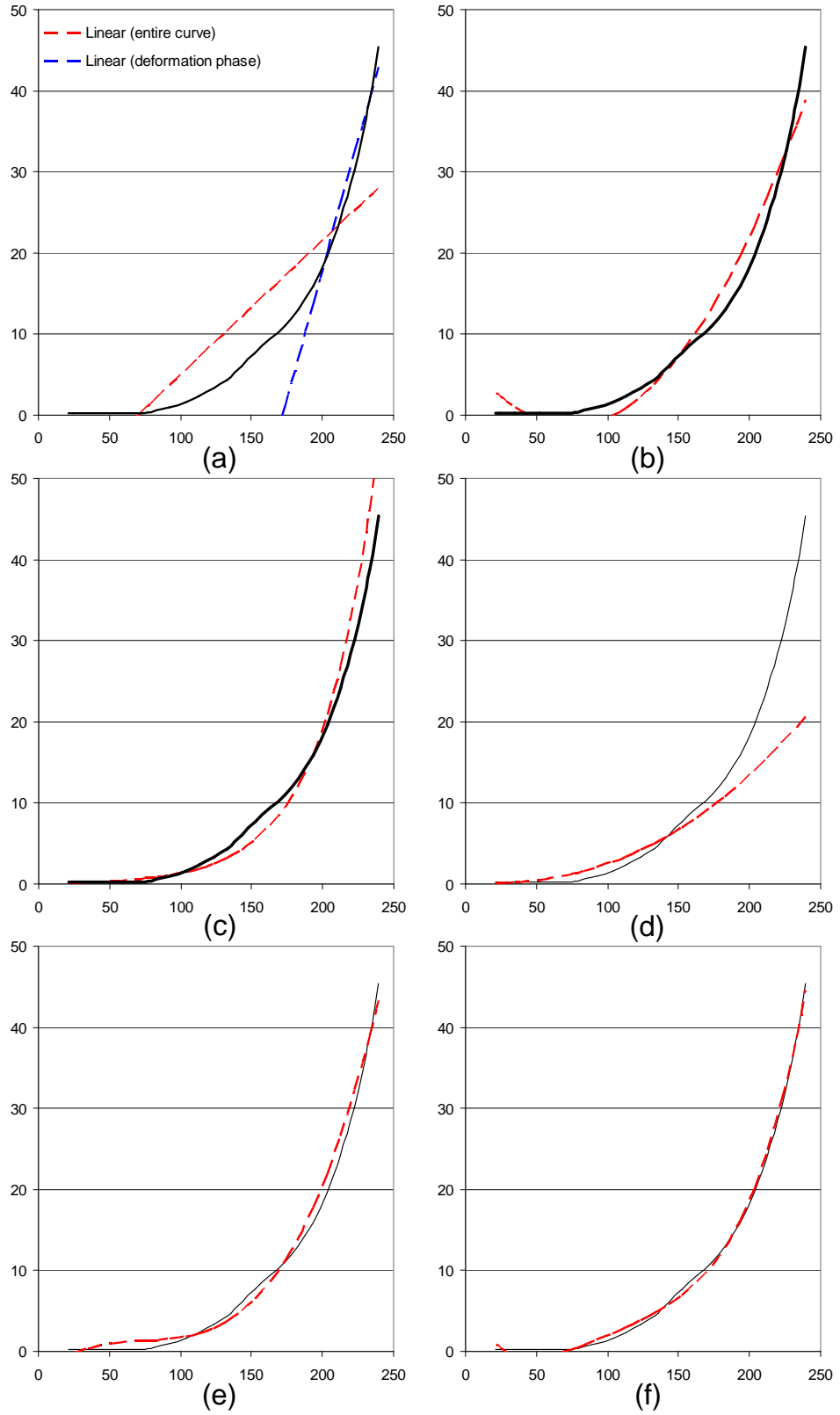


Figure 104: Curve matching (a) Linear (b) Quadratic (c) Exponential (d) Power (e) Polynomial – 3rd Order and (f) Polynomial – 4th Order.

Table 11: Average statistical fit results from the analysis of the shape of the weld mesh curves using Curve Expert™.

Curve type	Laced Boundary	Fixed Boundary
	Mean R squared value	Mean R squared value
4th order Polynomial	0.9992	0.9998
Exponential	0.9985	0.9989
3rd order Polynomial	0.9973	0.9990
Power	0.9961	0.9976
Quadratic	0.9871	0.9760
Linear	0.8747	0.9116

These average values were determined by taking the R squared value of each curve type as determined by Curve Expert™ for each weld mesh test and calculating the average. The results indicate that a linear relationship is not representative of the total pre-rupture force - displacement curve. The deformation phase of the test can be represented by a linear relationship; however, analysis has not been undertaken on that portion of the curve as the purpose of this investigation is to characterise the entire pre-rupture force – displacement response.

The quadratic and the power relationships provide a reasonable match during the early stages of the test but diverge in the later stages. The exponential relationship provides an excellent match in most cases but also greatly over-estimated the forces in the later stages of the test. An exponential curve could not be fitted to some of the test curves by the Curve Expert program due to the regression analysis not converging.

The best representation for the full pre rupture force - displacement response is a 4th order polynomial although there is minimal difference between the 4th order polynomial and the 3rd order polynomial.

A 3rd order (cubic) relationship was used for further analysis in order to reduce the complexity of the equation. The equation is given by:

$$y = dx^3 + cx^2 + bx + a \quad (4.10)$$

where:

- y is the predicted force.
- x is the measured displacement.
- a, b, c and d are constant coefficients.

Curve Expert TM was used to determine the constants a, b, c and d for each curve. The averages of the coefficients for each boundary condition are provided in Table 12. Despite the similar curves shapes achieved with the two boundary restraint methods, the constants derived by the analysis were different due to the differences in the displacements between the two boundary conditions at the start of the test.

Table 12: Average polynomial coefficients describing the shape of the weld mesh curve.

Coefficient	Laced Boundary	Fixed Boundary
	Average value	Average value
a	-3.24	-7.49
b	0.136	0.307
c	-0.0017	-0.0038
d	0.0000075	0.0000193

4.12.4.2 Chain link mesh

Analysis of the curve shape was also undertaken on the chain link mesh results. As chain link has a much higher force capacity than weld mesh, standardising the results at 20kN (as in the weld mesh example) was not applicable. The results were instead standardised to 60kN of force at 210mm of displacement using the following formula.

$$d_a = d_o - (210 - d_{60}) \quad (4.11)$$

where:

- d_a is the adjusted displacement
- d_o is the original measured displacement
- d_{60} is the displacement measured at 60kN

The analysis has only been applied to the tests conducted using the fixed boundary condition. The standardised results for each mesh type are provided in Figure 105. S95/4 showed some variations in the shapes of the curves; this indicated differences in the stiffness of the mesh between samples. The variations are likely to be related to slight disparities in the samples due to the manufacturing process. All the other mesh types generated very consistent results with little variation in the shapes of the curves. The curve shapes for each of the mesh types is given in Figure 105. A comparison of the curve shapes between the different types of mesh is provided in Figure 106. The S95/4, G65/4 and G65/3 products all have similar curve shapes. Both the G80 products (G80/4 and G80/2) also had similar curve shapes although this shape was different from the other three products. The change in curve shape is related to a change in the stiffness of the product. The rate of force transfer around the sheet was less for the G80 products than that of the S95 and G65 products. It is difficult to determine the cause of change in stiffness as the G80 products had less wires than the S95 and S65 products as well as different diamond configuration.

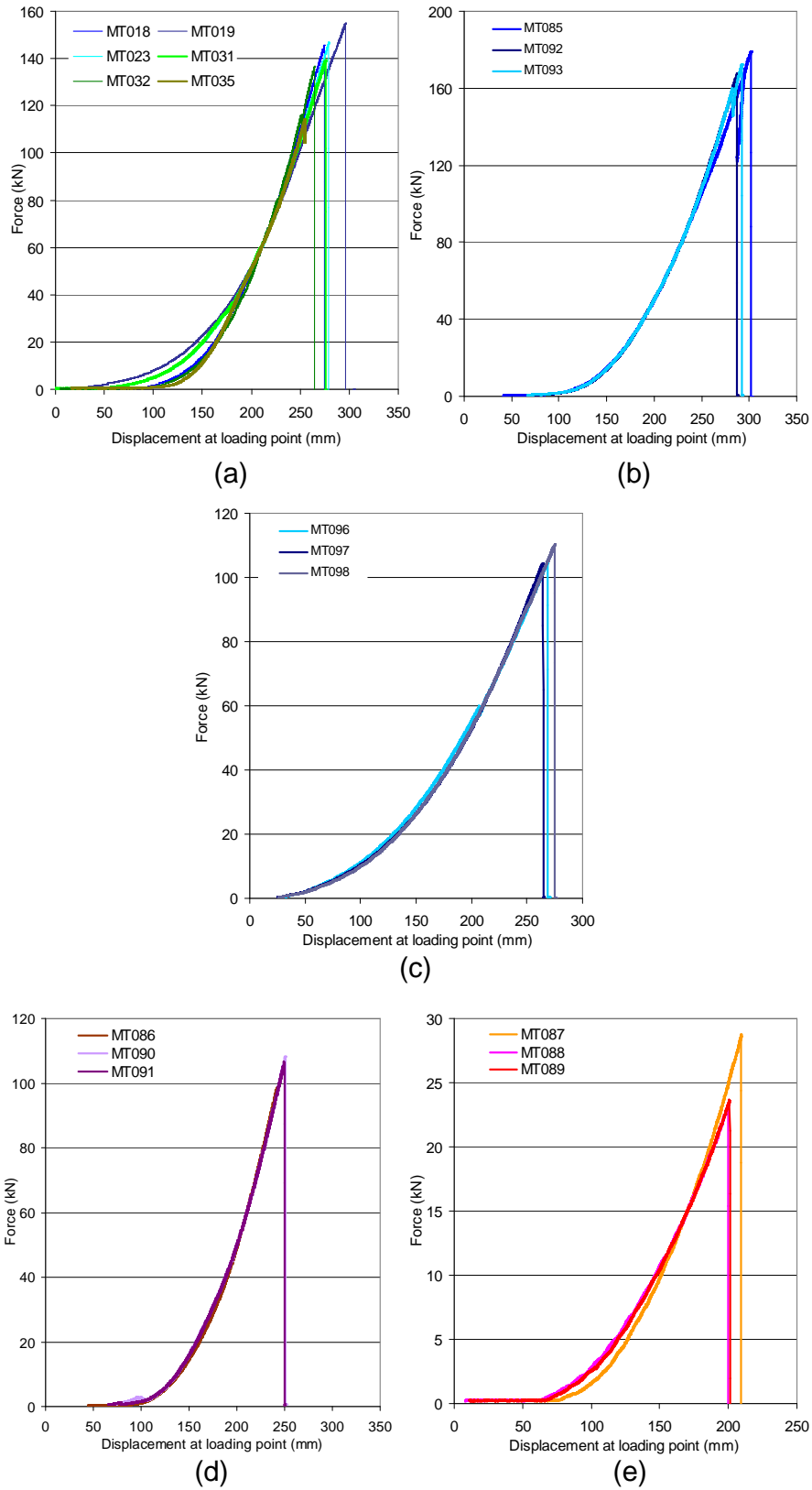


Figure 105: Standardised force – displacement reaction for (a) S95/4 (b) G65/4 (c) G80/4 (d) G65/3 and (e) G80/2.

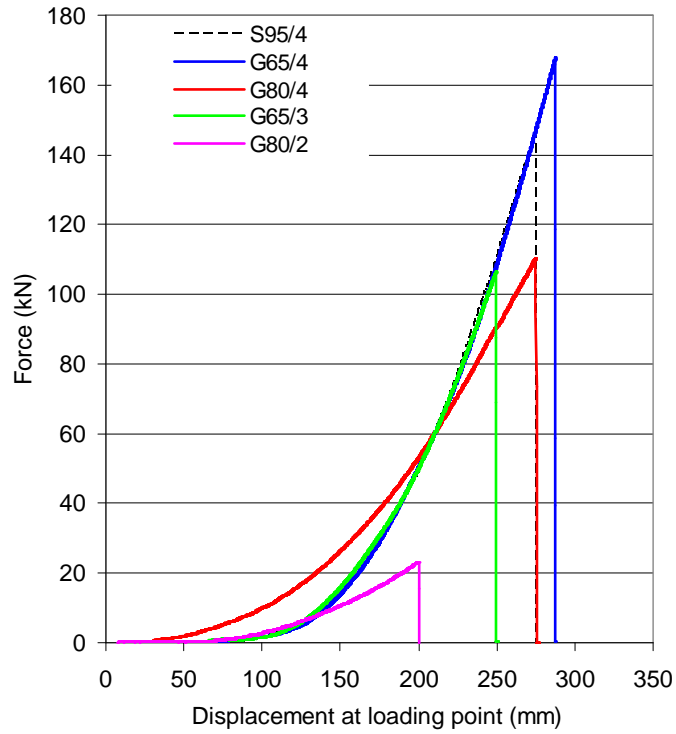


Figure 106: Comparison of the force – displacement reaction of the various mesh types.

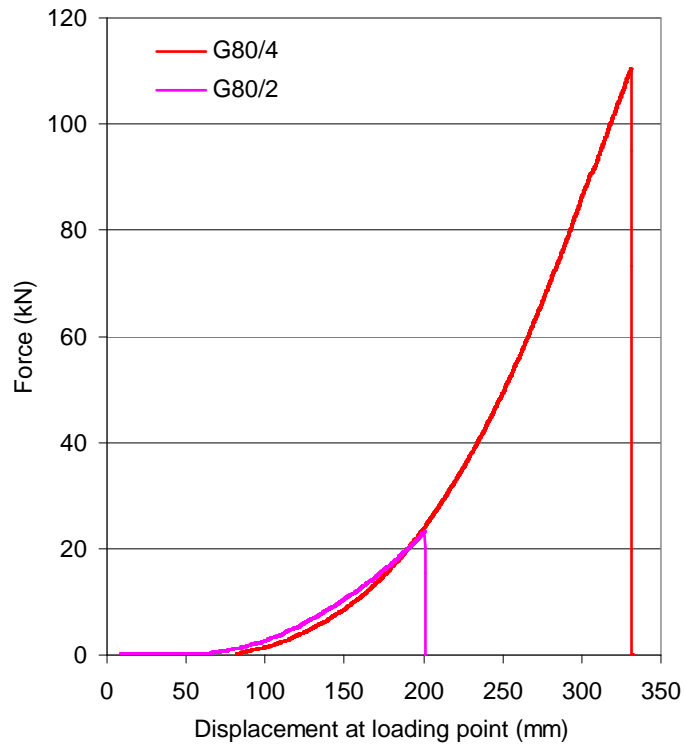


Figure 107: Comparison of the force – displacement reaction of the G80 products.

As with the weld mesh data, regression analyses were undertaken using the Curve Expert™ program. The results of the analyses are provided in Table 13. These results are very similar to the weld mesh results. Figure 108 shows the fit of each curve type to Product G65/4.

Table 13: Average statistical fit results from the analysis of the shape of the chin link mesh curves using Curve Expert™.

Curve type	Mean R squared value				
	A	B	C	D	E
4th order Polynomial	0.9998	0.9999	1.0000	0.9999	0.9999
3rd order Polynomial	0.9995	0.9998	0.9999	0.9999	0.9998
Quadratic	0.9966	0.9998	0.9998	0.9994	0.9997
Power	0.9981	0.9967	DNC	0.9932	0.9982
Exponential	0.9916	0.9889	DNC	DNC	DNC
Linear	0.8975	0.9432	0.9643	0.9353	0.9359

Note: DNC – did not converge

The best fit curve was a 4th order polynomial, followed by the 3rd order polynomial. The program was unable match an exponential curve to twelve of the fifteen test results. Power, quadratic and linear fits all provided poor matches to the data although as with weld mesh, the deformation phase of the test may be approximated by a straight line.

Even though the G80 products appear to have a force – displacement response different from the other mesh products, there is no apparent change to the type of best fit curve. The best fit curve is still a 3rd order polynomial, however, it is expected that the coefficients of the equation for the G80 products will vary significantly from the other chain link mesh types.

The coefficients used for each mesh type are provided in Table 14. Despite the similar curve shapes shown in Figure 106, coefficient “a” of Product S95/4 is very different from the corresponding coefficient for the G65 products. Following closer examination of the data, a high degree of variability was observed in the coefficients of S95/4, which corresponds with the variability in the test data. As expected, Product G80/4 also has very different coefficients from the other mesh types due to the high tension in the mesh at the start of the test and the lower stiffness at the end of the test.

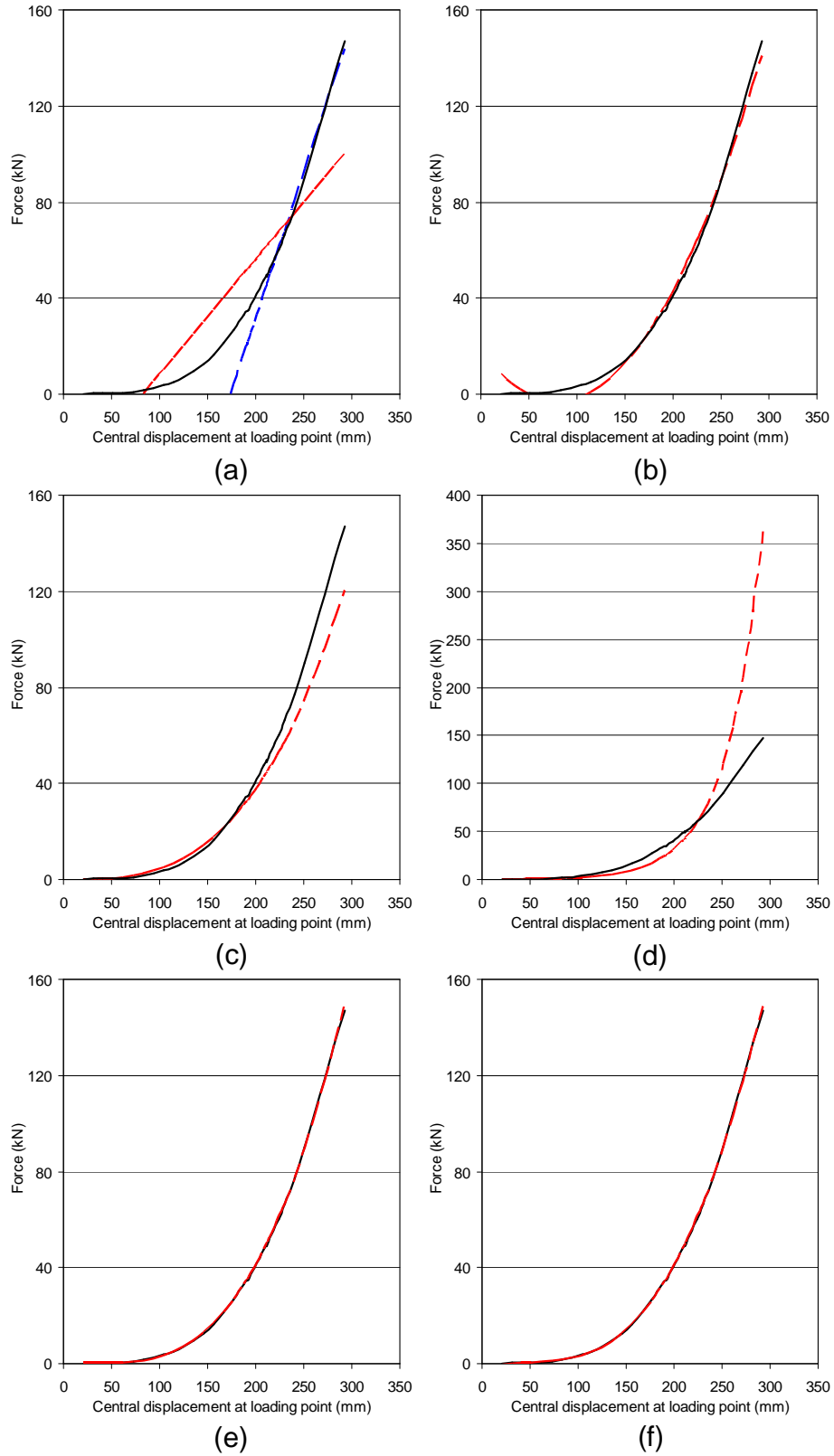


Figure 108: Curve matching (a) Linear (b) Quadratic (c) Power (d) Exponential (e) Polynomial – 3rd Order and (f) Polynomial – 4th Order.

Table 14: Average polynomial coefficients describing the shape of the weld mesh curve.

Coefficient	S95/4	G65/4	G80/4	G65/3	G80/2
	Average value				
a	2.49	29.66	0.80	29.68	3.51
b	0.024	-0.645	0.020	-0.384	-0.117
c	-0.0012	0.0033	0.0014	0.0005	0.0010
d	0.0000085	0.0000017	0.0000013	0.0000058	0.0000004

4.12.5 DISCUSSION OF ANALYSIS TECHNIQUES

The aim of Coates' (1965) analysis technique was to determine the tension in the wires to evaluate whether they were nearing their ultimate tensile strength. As discussed in Section 4.12.1, attempts to compare the predicted values with the actual forces acting on the wires measured using small load cells, were unsuccessful.

Tannant's analysis technique (1995) assumes uniform loading in one direction and attempts to simulate the reaction between rock bolts and the mesh. Using Tannant's equations, the stiffness of the mesh can only be estimated when peak load and rupture load are equal. A better approximation of the stiffness would require the use of the rupture load as the principal reference. The stiffness should be consistent for all samples of the same mesh type.

Tannant (1995) suggests that *"welded wire mesh showing more than about 250mm of relative displacement should be rehabilitated"*. Tannant et al. (1997) amends this statement, claiming that *"welded wire mesh showing more than about 100 to 150mm of relative displacement should be rehabilitated"*. The amount of displacement that occurs during a test is entirely dependent on the test arrangement and the initial tension imposed upon the mesh during the test setup. In a practical situation the displacement of the mesh is dependent upon how tightly the mesh has been stretched across the excavation during installation, and the amount of force applied by the restraining plates. Thompson et al. (1999) found that *"large wire forces were developed, and these were sufficient to cause the slip of the mesh relative to the plates at relatively low applied loadings"*. It should be apparent then, that the support characteristics of mesh cannot be numerically represented solely by the amount of displacement to which the mesh has been subjected.

Tannant's method for predicting peak load was not successful as this method assumes that all the forces are transferred along the directly loaded wires; however, as discussed in the previous sections this is not the case. The force transfer mechanisms for both weld mesh and chain link mesh show that all wires are involved in the transfer of forces, but to differing levels. Consequently simple two-dimensional analysis cannot be used to determine the peak forces in mesh. Furthermore, the method is dependent upon a known value of rupture displacement. As discussed throughout this chapter, displacement is a highly variable characteristic that is greatly influenced by many external factors.

There is also very little benefit in determining the peak load of the mesh based on the tensile strength of the wire. Weld mesh in particular can be highly affected by the quality of the manufacturing process. Some knowledge of the quality of the product and the effect of the quality on the force – displacement properties of the mesh are required to be able to predict the rupture forces and displacements.

The WASM analysis method has been successful in determining the shape of the curve; however this method still cannot be used to predict the point of rupture. The point of rupture depends on the quality of the manufacturing process and consequently some form of testing is still required to assess the product. This assessment may be indirectly undertaken using the weld shear test method; however, it is recommended that the industry adopts the change in standards proposed by Villaescusa (1999) as this testing has demonstrated that it is possible to create weld strengths that are equal to or better than the tensile strength of the wire.

The WASM analysis technique cannot be used as a design tool at this stage, although a basic understanding of the force – displacement characteristics may be used in comparison with field data to determine if mesh applied in-situ is nearing capacity. If field data indicates significant displacement with small increments of loading then the mesh is still transferring forces to peripheral areas of the mesh and rehabilitation is likely to be unnecessary. If the field data suggest that the rate of displacement is reducing, this indicates that the mesh is in the deformation phase of the force - displacement reaction and rehabilitation may be necessary.

4.13 DISCUSSION

The testing completed as part of this investigation was conducted with the purpose of developing a method that could provide consistent results and enable the comparison of the performance of different mesh products. The results generated from the test facility are indeed consistent and enable a true comparison of the force – displacement response of various mesh products. Furthermore, the test facility has enabled the force – displacement response of mesh to be characterised.

The primary purpose of most of the current analysis techniques is to determine the tension within individual wires rather than understanding the mesh reaction as a complete system. In order to determine the tension of the mesh, important assumptions are required. In particular it is assumed that only the directly loaded wires are transmitting the forces. Although this is the case for a part of the test duration it is certainly not the case as rupture approaches. Mesh is an effective ground support system because it is not reliant on a small number of wires but rather on all the wires in the sheet. Consequently mesh has the ability to transfer forces away from the directly loaded wires, thereby increasing the overall force capacity.

Design guidelines for mesh can only be developed with the aid of non-linear modelling. The model must be capable of determining the force - displacement response of the mesh under varied boundary conditions. The WASM test results may be used initially to calibrate the model, especially given the consistency of the force – displacement responses. The model must be able to incorporate the tension of the mesh after installation and the effects of plate slippage. Future modelling must be calibrated against field measurements. Field data is required for the following parameters:

- The initial tension in the mesh
- The amount of force applied by the plates
- The quality of the mesh

Further research is required to develop a specific small-scale field test that can more accurately quantify the quality of the mesh. The weld shear tests currently conducted by suppliers are used as a qualitative assessment rather than a quantitative assessment.

CHAPTER 5 SHOTCRETE

5.1 INTRODUCTION

The principle of a sprayed concrete was developed in the early 1900s for civil engineering construction applications. The “Cement Gun Company” developed a machine to pneumatically apply fine cement mortar. The mortar was called “Gunitite”. In the mid 1950s the spraying machine was adapted to enable the application of coarse aggregate concrete. The sprayed concrete was called shotcrete and used specifically in civil tunnelling construction. Today, shotcrete is used in most civil engineering works.

Shotcrete was first used in mining in the 1920s, mainly in specialist applications and in areas where the rock mass was particularly poor. Shotcrete utilisation in mining applications has increased significantly in recent years. Shotcrete can be placed rapidly and offers immediate confinement to the rock mass. Longer term, shotcrete provides a strong, continuous areal support for an excavation surface. Shotcrete also allows rock bolt patterns to be matched to the ground conditions rather than being controlled by the need to adequately restrain mesh as is the case in many mines. These benefits have resulted in improvements in production rates and lower overall ground support costs compared with the placement of mesh.

In recent years, there have been significant technological advances associated with shotcrete materials and their placement. These advances include improved mix design (e.g. the use of silica fume to improve cohesiveness), chemical admixtures (e.g. the development of alkali free accelerators), the development of steel and plastic fibres for internal reinforcement, and advances in the equipment used for placement.

A large amount of shotcrete research has been undertaken by both the civil construction and the mining industries. The research areas include:

- The force – displacement properties of shotcrete with and without reinforcing.
- The adhesive strength between shotcrete and rock surfaces.
- The failure mechanisms of shotcrete.
- Chemical additives and admixtures.

Standard protocols for shotcrete testing have been developed primarily in Europe (e.g. DIN, EN and EFNARC) and the United States (ASTM). These standards have been adopted throughout the rest of the world. Most of the standard protocols do not apply to mining situations. The most common standard test methods used in the mining industry are the UCS test, the beam third point loading test (EFNARC beam test), the EFNARC square plate test and the Round Determinate Panel (RDP) test.

With such a large amount of information available, it is difficult to summarise every aspect of shotcrete. For the purpose of this thesis, only a few selected papers, relevant to mining applications, have been reviewed in detail.

5.2 THEORY OF SHOTCRETE SUPPORT

Shotcrete has been in regular use in the mining industry since the early 1950s and over this time much debate has taken place over the support mechanisms of shotcrete. Gyenge and Coates (1972) detail three shotcrete support mechanism theories. One of these three theories, originally described by Deere et al. (1969), suggests that the *“supporting effect is due to the following factors (a) the shotcrete performs a binding function similar to that of mortar in stone in a wall (b) it prevents deterioration of the rock, otherwise caused by air and water (c) it provides considerable resistance to the fall of loose rock because of its shear strength as it adheres to the rock surface and (d) in the case of thicker shotcrete layers (150mm – 250mm), it provides structural support”*.

Another theory suggested by Keeley (1934) states that *“because the gunite air seal on the rock surface allows the ordinary absolute air pressure to hold the walls and the back of a rock excavation, it thus prevents them loosening and falling”*.

The final theory, developed by Coates (1967), proposes that the actual reaction is a combination of the two functions described above.

The basic support theory proposed by Deere et al. (1969) has gained the most recognition over the past three decades, but the complexity of the interaction between the shotcrete and the rock mass, and the difficulty in measuring this reaction, means further development of the support mechanism theory has not occurred.

Studies by Holmgren (1976, 2001) and Fernandez-Delgado et al. (1976) showed that adhesion loss and flexure are the primary modes of shotcrete failure. A further review conducted by Barrett and McCreath (1995) identified that shotcrete capacity in blocky ground, under static conditions, is governed by six mechanisms: namely, adhesion loss, direct shear, flexural failure, punching shear, compressive and tensile failure (Figure 109). Adhesion loss occurs where the bond between the shotcrete and the rock is broken, often due to poor surface preparation prior to spraying or due to shrinkage of the shotcrete during curing.

Flexural failure is bending failure of the shotcrete and can only occur after the adhesion is broken. For flexural failure to occur, the shear strength of the material must be higher than the flexural strength.

The writer disagrees with the definitions provided for “*direct shear*” and “*punching shear*”. Direct shear (or shear failure) occurs over a single planar interface, typically represented as a line. Punching shear, shown as direct shear in Figure 109, is direct shear that occurs over a complex three-dimensional surface. The punching shear failure as shown in Figure 109 is a combined mechanism of flexural failure and shear failure. The updated failure mechanisms are shown in Figure 110.

These failure mechanisms are generally not well understood and further research is required to understand the complexities of the rock / shotcrete interaction.

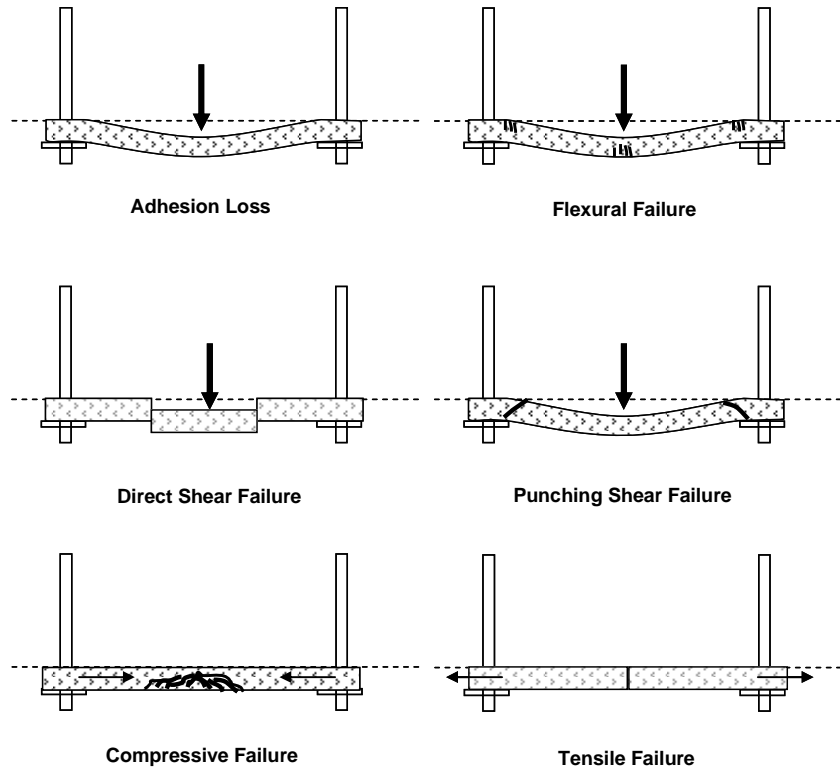


Figure 109: Failure mechanism of shotcrete (Barrett and McCreath 1995).

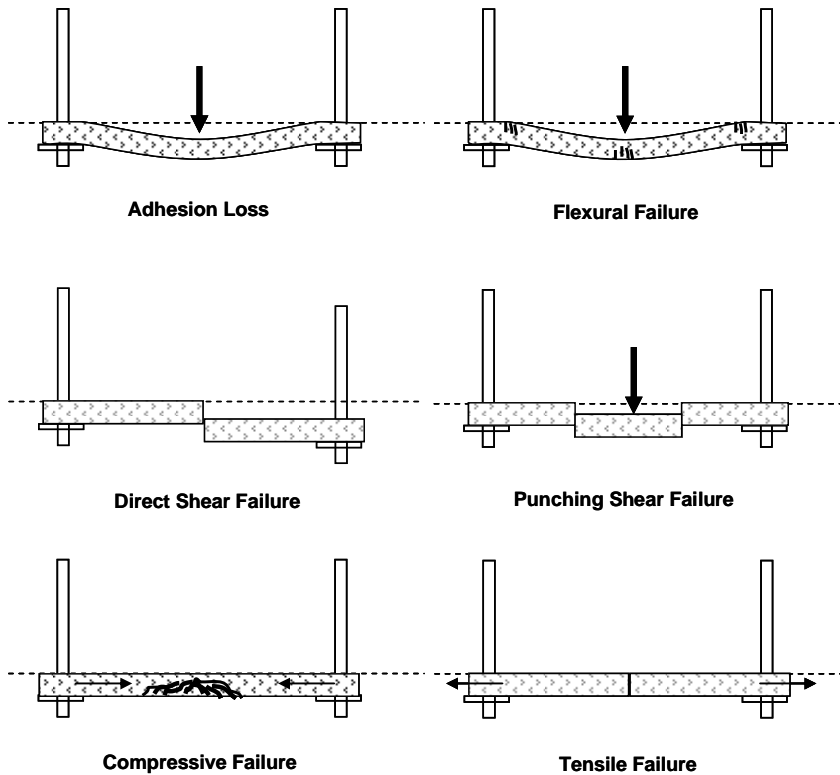


Figure 110: Updated shotcrete failure mechanisms.

5.3 SHOTCRETE PROPERTIES

There are many mechanical properties that can be associated with shotcrete. The critical properties are:

- Compressive strength
- Tensile strength
- Shear strength
- Flexural strength
- Adhesion
- Toughness

Compressive strength is often used as a quality control parameter specified in contractual agreements. It is determined using the unconfined compressive strength (UCS) test. This test method is described in Section 5.7.2.1.

Tensile strength is difficult to determine. Small-scale testing of the tensile strength is not common, though it can be undertaken using an indirect tensile test or uniaxial tensile strength (UTS) test. More frequently tensile strength is indirectly measured during a flexural strength test.

Although shear failure is a common failure mechanism in shotcrete, very little research has been undertaken on determining the shear strength.

Flexural failure is one of the most common failure mechanisms observed in shotcrete. Flexural strength may be calculated using the third point beam test, the EFNARC plate test or the round determinate panel (RDP) test. These test methods are described in Section 5.7.2.

Adhesion between the rock surface and the shotcrete is an essential parameter that usually determines the failure mechanism of shotcrete. The degree of adhesion is affected by many factors including; the type of rock surface the shotcrete is applied to, the preparation of the surface and the shotcrete mix design. Despite its importance, adhesion is difficult to quantify as an individual parameter, although attempts have been made by Kuchta (2002), Malmgren et al. (2005) and Bae et al, (2004). Often adhesion strength is measured in conjunction with flexural or shear strength.

Toughness or the energy absorbed is calculated by determining the area under the force – displacement curve. Some methodologies use this parameter to design shotcrete; however, the determination of toughness is highly dependent upon the test method and the displacement at which the toughness is measured. Johnston (1982) states that, *“at one extreme, toughness can be measured in terms of the total area under the load – deflection curve. However, by the time the load is close enough to zero for this area to be computed fully, the material has far exceeded a useful level of serviceability in terms of cracking and deflection. At the other extreme the term first crack toughness is often used to identify the area under the load - deflection curve up to the first - crack deflection, although this property is more correctly called resilience”*. In an attempt to standardise the calculation of toughness, ASTM C 1018 -94b suggested that the following toughness indices be reported:

- First crack toughness
- Toughness index I_5
- Toughness index I_{10}
- Toughness index I_{20}

The first crack toughness was defined as “the energy equivalent to the area under the load - deflection curve up to the first crack deflection”. Toughness index I_5 was defined as “the number obtained by dividing the area up to a deflection of 3.0 times the first crack deflection by the area up to first crack”. The I_{10} and I_{20} indices were measured up to a deflection of 5.5 and 10.5 times the first crack respectively. The rationale for the naming was that in a purely elastic - plastic material the displacement at I_5 would equal 5mm, at I_{10} it would equal 10mm and at I_{20} the displacement would equal 20mm. Recently, this ASTM has been superseded by ASTM C 1609-06 (and updated in 2007) and new definitions have been proposed. Toughness is now calculated specifically for the third point loading test method, using the span and depth of the sample.

In 2002, ASTM C 1550 was developed for the round determinate panel test. This test was developed by Bernard (1999). A detailed description of the test method is provided in Section 5.7.2.4. The standard specifies that toughness be calculated at 5mm, 10mm and 40mm central displacements. The measurements at 5mm and 10mm are directly related to elastic / plastic theory described in ASTM C 1018. Bernard (2002) states that, “a displacement of 40 mm is used to assess performance at high levels of deformation typical of applications such as mines where large cracks can be tolerated”.

5.4 COMPONENTS OF SHOTCRETE

The basic components of shotcrete are:

- Cement
- Aggregate
- Sand
- Water

There are two types of cement used in shotcrete; low heat cement and general purpose cement. According to Vandewalle (2005), *“one aspect that has to be considered carefully when selecting the type of cement is its compatibility with any admixtures... such as accelerators or water reducing agents”*. The most common type of cement used in mining applications is general purpose cement.

Water is arguably the most critical aspects of the shotcrete mix design although it is often the least controlled. The water quality and, in particular, the total dissolved solids (TDS) can have a detrimental effect on the cement hydration processes and the long term durability of the shotcrete. Remote mining applications must consider the access to good quality water sources during the design process.

The quantity of water will be determined by the desired water / cement ratio but will also be affected the amount of clay in sand, type and amount of additives, the water content of the primary ingredients and the environmental conditions. The water may be added during the spraying process (dry mix method) or during the batching process (wet mix method). Mining operations in Australia typically use only the wet mix application; consequently, dry mix applications and the associated mix designs will not be discussed.

Aggregates comprise the greatest percentage of the concrete mix. There are several different specifications for the aggregate size distribution. The *“European specification for sprayed concrete”* (EFNARC 1996) is the most commonly referred to specification. The size ranges are shown in Figure 111. The aggregate is made up of both coarse and fine fractions. The coarse aggregate size is limited to 12mm to avoid blockages in the pump lines, associated with the spraying equipment. A high proportion of large aggregate also causes excessive rebound and high volumes of overspray during placement.

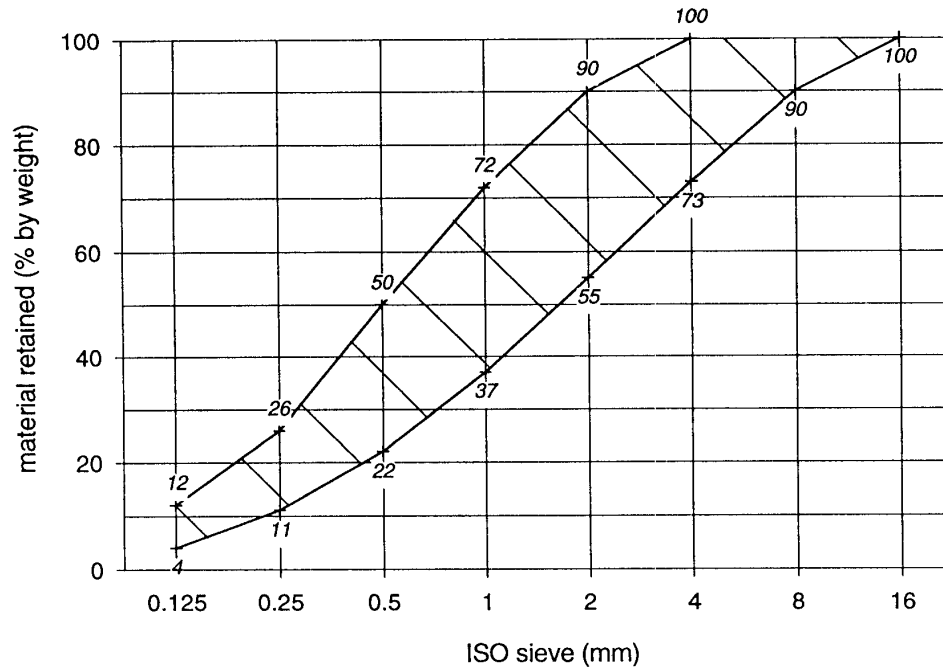


Figure 111: Particle size distribution for shotcrete aggregates (EFNARC 1996).

The type of aggregate depends on the materials available. Suitability is determined by the amount of fine particles and presence of clay minerals that may lead to the breakdown of the aggregate during the batching process.

The fine particle distribution is comprised of sand. The quality of the sand, and more specifically, the clay content, has a significant effect on the mix design. Sands with higher clay contents usually require the addition of extra water to ensure proper hydration of the cement.

Additives such as micro-silica and fly ash are also used to reduce the cement content whilst improving the compressive strength, density and the adhesion strength, of the final product (Vandewalle, 2005).

Admixtures such as plasticizers and super plasticizers are also added to ensure the consistency and workability of the mix is maintained.

Stabilisers or retardants are incorporated to prevent cement hydration (and therefore concrete setting) during transport to the spraying location, which in some cases, can take several hours. The effect of the stabilisers is counteracted by the addition of activators during the spraying process.

Set accelerators are used to reduce the setting time of the mix after application. There are two types of set accelerator used in the Australian mining industry. Alkali accelerators are typically silicate or aluminate based. They were predominantly used in the 1980s and are known to improve the early compressive strength of the concrete. However, higher dosages of these types of accelerators are known to compromise the long term compressive strength of the concrete and the caustic nature of these products can cause skin reactions with prolonged exposure.

Alkali-free accelerators were developed in the mid 1990s in response to occupational health and safety concerns with the alkali accelerators. These accelerators have less impact on the long term strength than the alkali based accelerators (Prudencio, 1998).

The flexural and shear strengths of the shotcrete are often increased by the addition of reinforcing. Traditionally, reinforcing consisted of either weld mesh or chain link mesh, constructed using small diameter wires. In the 1980s short steel fibres were developed. These fibres were added to the mix during the batching process and alleviated the need for lengthy mesh installation. These fibres have been modified over the last two decades to include various lengths, diameters and materials (e.g. polypropylene fibres).

5.5 SHOTCRETE DESIGN

The design of shotcrete can be broken into the two areas. Firstly there is the basic concrete mix design and secondly the layer thickness and reinforcing.

5.5.1 MIX DESIGN

According to Maher et al. (1975), shotcrete mix design *“is a difficult and complex process involving a certain amount of trial and error”*. There are different mix designs for placement using the dry mix method and wet mix method. Only the wet mix placement method will be discussed.

Hoek and Brown (1982) suggest the following factors are also considered in the mix design:

- *Shootability – must be able to be placed overhead with minimum rebound.*
- *Early strength – must be strong enough to provide support to the ground at ages less than 4 – 8 hours.*
- *Long-term strength – must achieve a specified 28 day strength with the dosage of accelerator needed to achieve shootability and early strength.*
- *Durability – long term resistance to the environment.*
- *Economy – low cost materials and minimum losses.*

Jolin and Beaupre (2003) provide a basic mix design (Table 15). Similar quantities are recommended by Melbey and Garshol (1994), Austin and Robins (1995) and Vandewalle (2005).

Table 15: Basic Mix design Jolin and Beaupre (2003)

Ingredient	Quantity for 1 m
Cement	400 kg
Fine aggregate	1110 kg
Coarse aggregate (max 10 mm)	460 kg
Water	180 kg
Silica fume	40 kg
Water-reducing admixture	1500 ml
Superplasticizer	5000 ml
Air-entraining admixture	2500 ml

This mix design is aimed at achieving a UCS of 32MPa at 28 days. The aggregate size distribution (Section 5.4) is aimed at providing smooth consistent mix with as little rebound as possible. The accelerator dosages provide a set time of between 4 and 8 hours.

Recently, the early strength of shotcrete has become increasingly important. Some mines are experiencing poorer rock conditions resulting in a requirement for more immediate rock support. Some mines are wishing to achieve set times of less than 1 hour. There are currently no guidelines published on how to modify the mix design to improve the performance of one or more of the mechanical properties listed above.

5.5.2 LAYER THICKNESS AND REINFORCING

Traditionally the standard thickness for shotcrete has always been specified as 75mm. Ortlepp et al. (1975) provides guidelines for surface support applications and suggests that in jointed blocky rock masses with high vertical stresses, “*shotcrete by its self, 8cm thick should be adequate*”. The engineering basis for this thickness is unclear.

More recently, mines have been specifying shotcrete thicknesses anywhere from 25mm with fibre reinforcement, to 150mm with mesh reinforcement. Proper engineering design based on the expected pressures exerted by the surrounding rock mass can be undertaken for perfectly circular tunnels but cannot be applied to standard mining profiles.

The only specification for shotcrete thickness design is provided by Grimstad and Barton’s 1993 “Q system” rock mass classification. The rock mass is classified according to the following parameters:

- RQD
- Number of joint sets (J_n)
- Joint Roughness (J_r)
- Joint Alteration (J_a)
- Water inflow (J_w)
- Stress conditions (SRF)

Numerical values are given to each of the above parameters and the following formula is used to generate a numerical rating called the “Q” value.

$$Q = \frac{RQD}{J_n} \times \frac{J_r}{J_a} \times \frac{J_w}{SRF} \quad (5.1)$$

To determine the appropriate ground support requirements a “Q” value is plotted against the ratio of the excavation height to the “*excavation support ratio (ESR)*” (Figure 112). The excavation support ratio is a numerical rating based on the expected excavation life span.

Papworth (2002) extended the use of the Q chart to include the toughness as a design parameter (Figure 113).

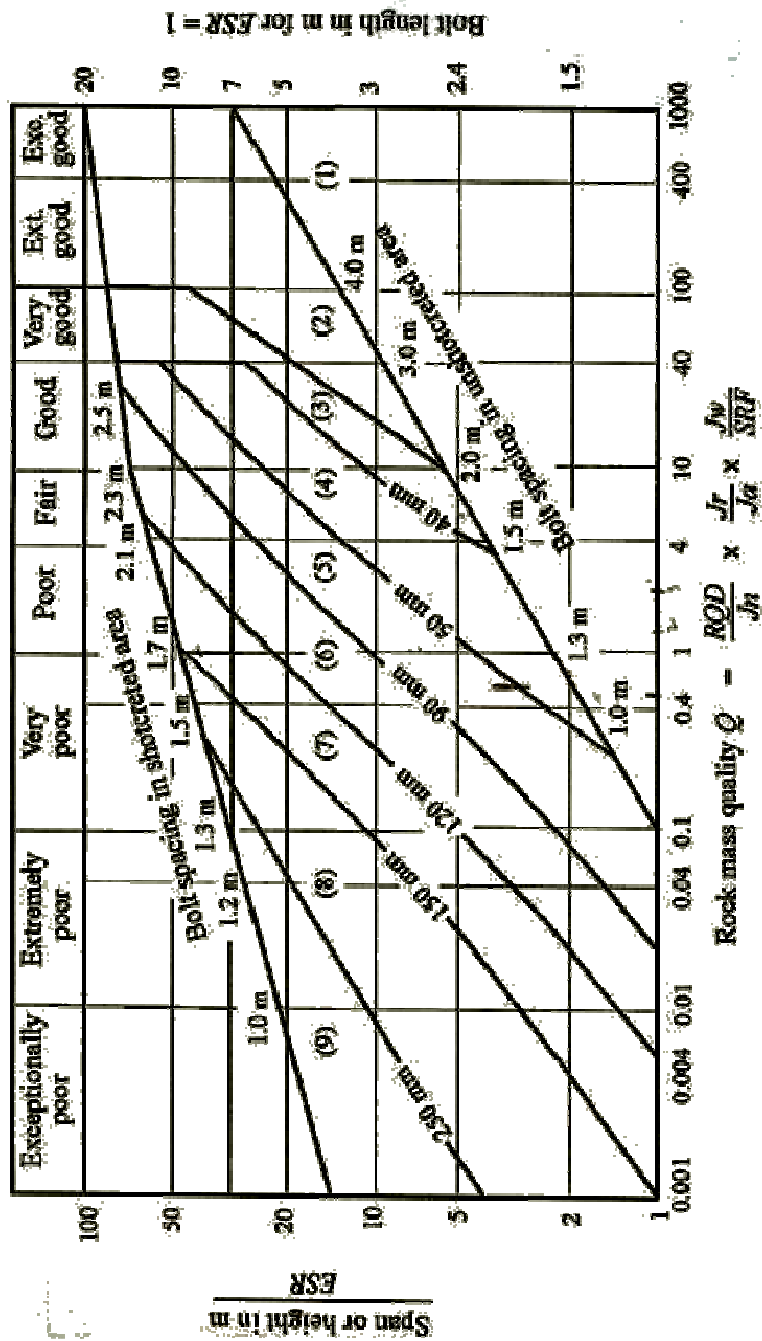


Figure 112: Grimstad and Barton Q chart (1993).

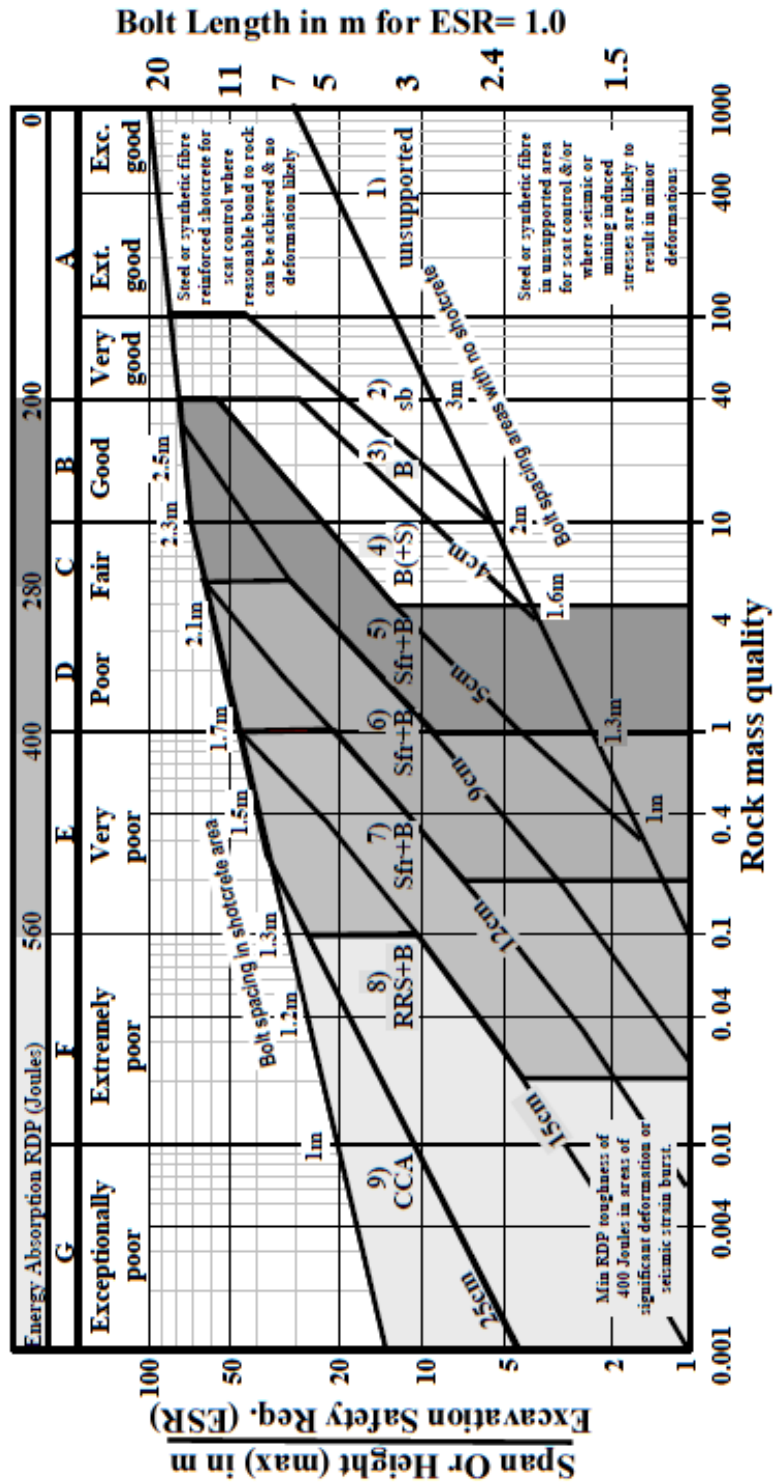


Figure 113: Papworth (2002) shotcrete design chart incorporating shotcrete toughness.

Both the original Grimstad and Barton (1993) method and the Papworth (2002) method are based on empirical case studies. The validity of the rock classification system is not the subject of this thesis. Notwithstanding, the engineering basis for the design of ground support schemes, based on classification methods alone, is questionable.

The design of the reinforcing of shotcrete is also not well developed. There have been many efforts to characterise the force – displacement properties of shotcrete with various reinforcing agents (including mesh, polypropylene fibres and steel fibres). These efforts have usually only compared two types of reinforcing using small-scale test methods which do not reflect the actual force – displacement reaction observed in field conditions.

There are no other known design methods for shotcrete.

5.6 SHOTCRETE PLACEMENT

There are two methods of placing shotcrete. The first involves the mixing of the water at the nozzle. This is called the dry mix method. This method may be used in mining applications where transport of bulk materials underground is limited. This method will not be discussed. The second method of placing shotcrete is called the wet mix method. Wet mix shotcrete is generally batched on surface and delivered to the spraying location using a standard concrete truck. The concrete truck is used to agitate the mix (including the fibres) and prevent segregation during transport. Shotcrete can be placed using a hand sprayer controlled manually or mechanically by a spraying machine. Manually controlled spraying is undertaken only in specialised situations and is not discussed. The mechanised spraying of shotcrete requires a high degree of skill and competence. The operator of the spraying equipment is called the nozzleman. There are several nozzleman certification standards that have been published across the world including ACI 506.3R-91 *“Guide to the certification of shotcrete nozzlemen”* (1991).

The nozzleman must control the air pressure, accelerator dosages and water content. In particular the air pressure must be kept consistent to ensure proper compaction of the final product.

The spraying technique can also have a significant effect on the final product. Layers must be built up slowly and evenly on excavation surfaces. This is generally achieved by moving the nozzle in small circles. The nozzle of the spraying machine must be kept perpendicular to the excavation surface and at an optimum distance of between 1 and 2 metres.

5.7 PREVIOUS SHOTCRETE TESTING

Shotcrete has been very well researched over the decades. Full conferences and magazines have been dedicated to the topic. This thesis has concentrated on the determination of shotcrete mechanical properties through testing, relevant to mining applications. Over 100 papers have been collated within this scope. Many of these papers apply the same test methods. The most common of the test methods are:

- Unconfined compressive strength (UCS) test.
- Third point beam tests
- EFNARC plate test
- Round Determinate panel (RDP) test.

These methods are governed by standards from various countries such as the United States (ASTM) and Europe (DIN, ISO). Some Australian standards exist for shotcrete although the primary references are often the ASTM standards.

There are three principal areas that apply specifically to mining applications. These are:

- Early strength.
- Quality assurance and control (QA/QC).
- Large-scale testing.

Brief outlines of the test methods used in each of these areas are provided in the following sections.

5.7.1 EARLY STRENGTH

The development of the strength of shotcrete over time is critical in the mining environment. Production schedules require excavation availability to be maximised to achieve optimal production levels and equipment utilisation. The mining cycle with shotcrete placement typically involves the following steps:

1. Bore the excavation face ready for charging and firing.
2. Charge and fire and excavation.
3. Remove the fragmented rock.
4. Spray shotcrete over the required excavation surfaces.
5. Install rock reinforcement and mesh.
6. Add additional layers of shotcrete where required.

In this mining cycle, the installation of the rock reinforcement and mesh cannot take place until shotcrete has achieved a minimum strength. The specification of the minimum strength is somewhat contentious. Ideally it should be based on the expected loading rate caused by rock failure at each individual site; realistically it is difficult to characterise the loading rate and often a balance must be achieved between the minimum support requirement and the curing time. This creates a need for curing times to be minimised without compromising performance and safety standards.

Bernard (2005) provides a summary of each of the test methods commonly used in mining operations in Australia. These methods include:

- Penetrometer test (Soil penetrometer).
- Penetrometer test (Needle penetrometer)
- Hilti gun test
- Beam test
- Plate pull test

The soil penetrometer (Figure 114) has a rounded plunger which is pushed against the shotcrete surface. The pressure required to penetrate the plunger to a certain depth is assumed to be a measure of the strength of the shotcrete. Re-entry to the shotcreted areas is usually granted when the soil penetrometer gauge reaches between 1.0 and 1.4MPa, depending on the site specification.

The needle penetrometer test applies the same principle as the soil penetrometer but uses a finer “needle” point (Figure 115).



Figure 114: Soil Penetrometer (Bernard 2005).



Figure 115: Needle Penetrometer (Bernard 2007).

Both penetrometer tests are very dependent upon the material that the point is pressed against. Shotcrete consists of coarse aggregate with a fine grained cement matrix. If the tip of the penetrometer is pushed against a piece of aggregate, false readings may be recorded. For this reason, it is recommended that several tests are conducted in the same area.

The Hilti gun method involves firing a pin into the shotcrete and recording its penetration. As with the penetrometer tests, this method is sensitive to the material that the pin contacts. Several tests are required to determine an average penetration that is then related to the shotcrete strength.

The beam test is conducted on small beams (75mm x 75mm x 400mm) of freshly sprayed shotcrete (Figure 116). The beams are placed within a beam end tester where a compressive stress is applied. Bernard (2005) suggests that the advantage of the beam test is that no conversions are required to obtain the compressive strength value.



Figure 116: Beam test.

None of the methods described above test the shotcrete under realistic loading conditions, nor do they evaluate realistic failure mechanisms; namely, shear strength, flexural strength and adhesion. More recently, plate pull tests have been conducted at several mines in an attempt to account for these mechanisms. The method involves fixing a plate to the wall of the excavation with an attachment point protruding from the wall. The area is sprayed, ensuring that the plate is completely covered. A hydraulic jack is connected to the attachment point. The jack is activated and the plate is pulled off the wall. The force required to remove the plate is recorded. This test method is lengthy and is often only used to characterise the early age strength for design purposes. It is not used in the routine monitoring of shotcrete.

The determination of the minimum required strength of shotcrete and when it is required is contentious. Curing times are often dictated by competing production demands and minimum strength requirements. Currently most sites specify that shotcrete must achieve 1MPa in strength before access is granted. To enable shorter duration production cycles the curing time must be optimised. Often higher accelerators dosages are used to achieve curing times of less than 1 hour. This is known to have a detrimental effect on the long term strength of the shotcrete.

Minimal field monitoring has been undertaken to determine the forces acting on the shotcrete throughout its life span. Realistically, shotcrete is required to perform from the moment it is applied to the excavation. Some mines have reduced re-entry times to shotcrete headings from 4 hours to less than one hour by using increased accelerator dosages.

Further investigation is required into the actual forces that are applied to the shotcrete as a result of ground movement and blasting, and into the development of shotcrete strength within the first hour.

5.7.2 QUALITY CONTROL AND ASSESSMENT

5.7.2.1 Unconfined compressive strength (UCS) test

The UCS test method is specified in ASTM C 39 05 “*Standard Test Method for compressive strength of cylindrical concrete specimens*” and in AS1012.9 “*Method 9: Determination of the compressive strength of concrete specimens*”.

The test method involves the application of axial load to cylinders of specific sizes. The cylinders are typically either 50mm or 100mm in diameter. The height of the sample is 2.5 times the diameter. The test setup is shown in Figure 117. Force and displacement are measured as the cylinder is crushed.

The cylinders may be poured during the batching process, or drilled from sprayed panels or from in-situ layers.



Figure 117: UCS test setup in the WASM test lab.

UCS testing is the most common and cheapest measure of concrete quality. Jastrzebski (1959) states that *“the compressive strength of any concrete material is affected by the water cement ratio, the degree of consolidation, the type and quality of the cement, and its curing length and conditions”*.

The minimum UCS value is often specified in quality control documents and contractors often attract penalties for not adhering to the specifications. Typically 32MPa at 28 days is specified; although, the engineering basis for the minimum UCS is not clear. In most cases a maximum value is not specified. The mix design is tailored to meet the minimum requirements.

The value of determining strength at 28 days is also questionable. The mining cycle is often very rapid with each 3m “cut” taking between 12 and 24 hours. An excavation can extend up to 80 metres beyond the spraying location at 28 days.

Furthermore, poured cylinders are usually formed from the concrete truck just after the batching process has been completed. Consequently, the cylinders do not contain many of the chemical admixtures such as retardants and accelerators that are added during transport and spraying. These admixtures often have a detrimental effect on the quality of the shotcrete which is not evaluated in many cases.

5.7.2.2 Third point beam test

The third point beam test was originally prescribed in ASTM C 1018 *“Standard test method for flexural toughness and first crack strength of fibre reinforce concrete (using beam with third point loading)”* and in the *“European specification for sprayed concrete”* (EFNARC 1996). More recently ASTM C 1018 has been superseded by ASTM C 078 *“Standard test method for flexural strength of concrete (using simple beam with third-point loading)”* and ASTM C 1609 *“Standard Test Method for flexural performance of fiber-reinforced concrete (using beam with third-point loading)”*. The test is also prescribed in AS1012.11-2000 *“Methods of testing concrete: Method 11: Determination of the modulus of Rupture”*.

The test is undertaken on a beam that is either cast or sprayed in formwork or sawn from larger panels. The following specimen dimensions are prescribed (ASTM C 1609 07):

- *“The length of test specimens shall be at least 50 mm greater than three times the depth, and in any case not less than 350 mm. The length of the test specimen shall not be more than two times the depth greater than the span.*
- *The tolerances on the cross-section of the test specimens shall be within +/-2%. The test specimens shall have a square cross-section within these tolerances.*
- *The width and depth of test specimens shall be at least three times the maximum fiber length”.*

Once the samples have been prepared they are cured. ASTM C 031 08 provides the specifications for laboratory curing and field curing. Laboratory curing is undertaken in water baths kept at approximately 23°C. Beams require the addition of calcium hydroxide to the bath.

Field curing is undertaken *“near to the point of deposit of the concrete represented as possible. Protect all surfaces... from the elements in as near as possible the same way as the formed work. Provide the (samples) with the same temperature and moisture environment as the structural work. Test the specimens in the moisture condition resulting from the specified curing treatment”*.

In practice, curing is undertaken in a variety of ways. Some mine sites have been observed to immerse the samples in water baths to prevent drying out and ensure the proper hydration of the cement. The improved hydration often results in better quality samples than would otherwise be achieved.

In the other extreme, some sites leave the sample in the open weather for weeks, exposing the sample to extreme temperature and humidity changes. In typical Western Australian summer conditions these changes can be up to 20 degrees Celsius. Humidity conditions can range from 0% humidity to 100% humidity. Samples exposed to these extremes suffer from evaporation of the water within the concrete resulting in poor hydration of the cement and can also cause the sample to undergo rapid expansion and contraction with consequent cracking.

Neither of these environments represents the temperature and humidity conditions that occur in the underground environment.

Once the sample is cured it is delivered to the test facility. The treatment of the sample during the transport process is often harsh and can result in damage to the sample.

The beam is supported on two rollers, located a minimum distance of 25mm from the ends. The sample is loaded using a bearing plate and rollers, located at the "third" positions between the supports (Figure 118). The test setup is shown in Figure 119.

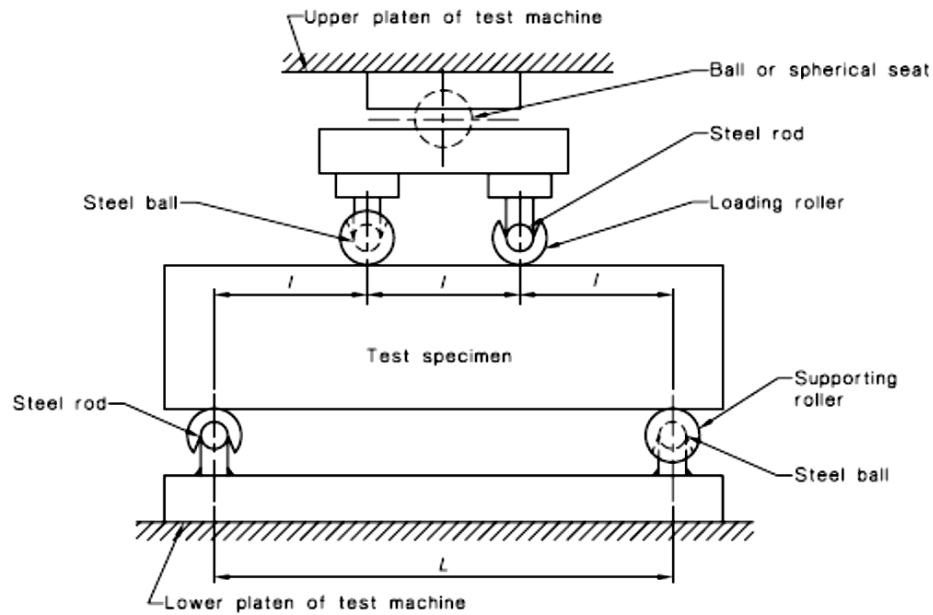


Figure 118: Position of the rollers in the third point loading test setup (ASTM C 07 08).

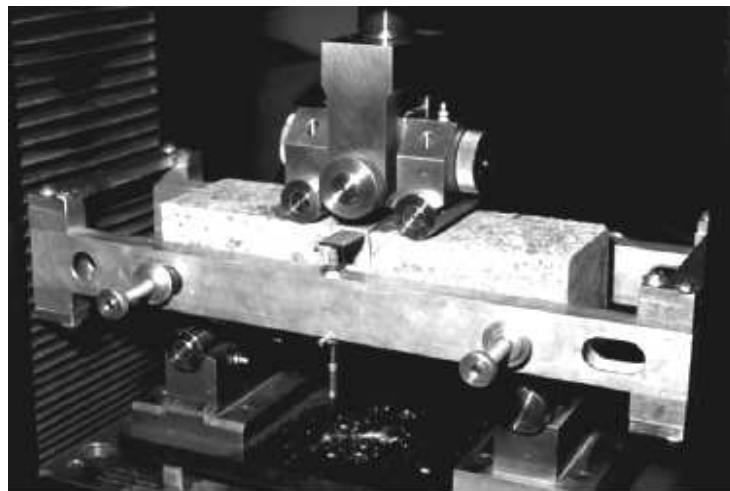


Figure 119: Third point loading test setup (ASTM C 1609 07)

The test is displacement controlled and forces are measured. ASTM C 1609 07 specifies that *“the net deflection of the specimen increases at a constant rate. For a 350 by 100 by 100 mm specimen size, the rate of increase of net deflection shall be within the range 0.05 to 0.10 mm/min until a net deflection of $L/600$ is reached. After that, the rate of increase of net deflection shall be within the range 0.05 to 0.20 mm/min until the specified end-point deflection is reached. For a 500 by 150 by 150 mm specimen size, the rate of increase of net deflection shall be within the range 0.06 to 0.12 mm/min until a net deflection of $L/600$ is reached. After that, the rate of*

increase of net deflection shall be within the range 0.06 to 0.24 mm/min until the specified end-point deflection is reached. The corresponding rate for other sizes and shapes of specimens shall be based on reaching the first-peak deflection 30 to 60 s after the start of the test”.

Force - displacement response curves are used to calculate the following parameters:

- P_p - peak force (N).
- P_1 - first peak force (N).
- δ_p - displacement (mm) at peak force.
- δ_1 - displacement (mm) at first peak force.
- P_{600}^D - residual force (N) at displacement of $L/600$.
- P_{150}^D - residual force (N) at displacement of $L/150$.
- L - span (mm) between the base supports.

These parameters are shown graphically in Figure 120.

Peak force may or may not correspond to the first peak force.

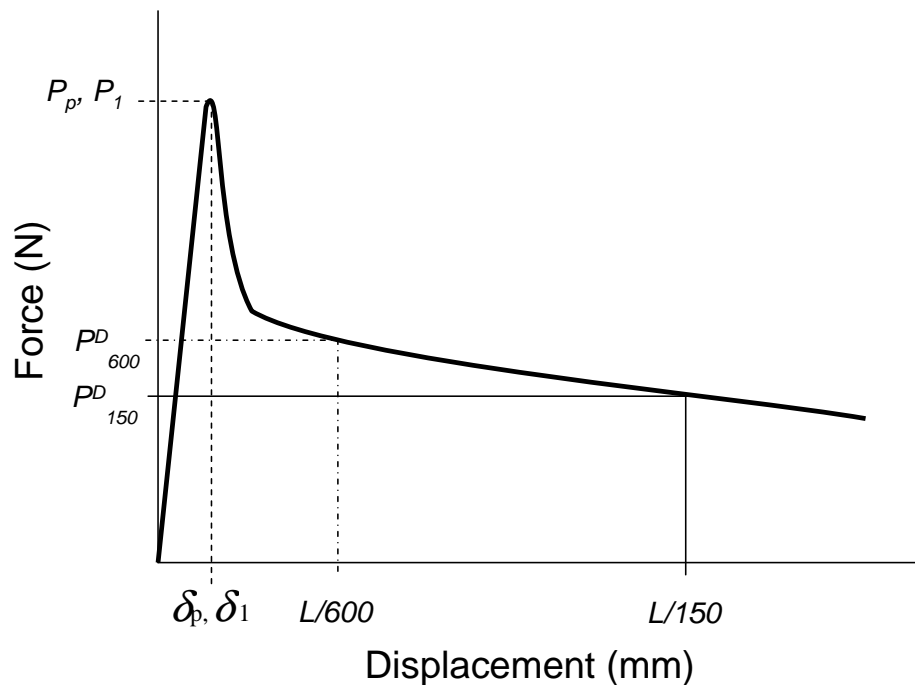


Figure 120: Force displacement parameters calculated for the third point loading test (ASTM C 1609 07).

“Strength” is calculated using the following formula:

$$f = \frac{PL}{bd^2} \quad (5.2)$$

- f = strength (MPa).
- P = force (N).
- L = the span length (mm).
- b = the average width of the specimen at the fracture (mm).
- d = the average depth of the specimen at the fracture (mm).

The strength is calculated at the first peak load, first crack load and at P_{600}^D and P_{150}^D .

Toughness (energy absorption) may also be determined by calculating the area under the force – displacement curve up to $L/150$.

The flexural strength is calculated using the following formula:

$$MoR = \frac{PL}{BD^2} \quad (5.3)$$

where:

- MoR is the modulus of rupture (MPa)
- P equals the load (N)
- L is the span (mm)
- B is the average width of the specimen at the fracture location (mm)
- D equals the depth of the sample at the fracture location (mm)

Ozyildirim and Carino (2006) make a series of comments regarding the flexural strength formula. They state that *“the formulas in ASTM C 078 and ASTM C 293 for computing flexural strength (modulus of rupture) are based on several assumptions that are approximations when testing concrete beams to failure. One assumption is that the concrete behaves as a linear-elastic material throughout the test, which is not true at stresses approaching failure. The flexural stress equations apply to long, shallow beams, whereas the actual test specimens are short and deep. The failure stress calculated using the two test methods is higher than the actual extreme fiber*

stress due to the simplifying assumption that the stress distribution over the depth of the beam is linear. It is likely, however, that compared with the variability inherent to concrete strength, this approximation is not significant. Various other factors have been found to affect flexural strength test results obtained using either third-point or center-point loading". These factors include:

- Sample size
- Aggregate size
- Loading rate
- Loading location relative to the boundaries.

5.7.2.3 EFNARC plate test

The EFNARC plate test is prescribed in "*The European specification of sprayed concrete*" (1996). This test method is also referred to as the EFNARC panel test. The confusion is caused by the specification, which uses the term "panel" to describe the large area slabs from which UCS cylinders and beams for the third point loading test are cut. These panels have a similar dimension sample size specification in the plate test.

The plate test is used to determine the energy absorption capacity (toughness) of shotcrete. The test methods states that "*a test plate of 600 x 600 x 100mm shall be supported on its 4 edges and a centre point load applied through a contact surface of 100 x 100mm*" (EFNARC 1996).

Typically the sample is prepared by spraying into a mould that is slightly larger than the specified dimensions and has sloped edges to prevent rebound build-up. The sample is levelled off to a thickness of 100mm. The plate is cured in a water bath for a minimum of 3 days prior to testing. The sloped edges are "sawn" off prior to testing.

The test is displacement controlled; the displacement rate is specified as 1.5mm per minute.

Little (1985), Ding and Kusterle (1999), and Cengiz and Turanli (2004) all applied the EFNARC panel tests to evaluate various parameters of shotcrete.

5.7.2.4 Round determinate panel (RDP) test

The RDP test method was developed by Bernard (1999) and was developed into ASTM C 1550 (2002). The test is undertaken by centrally loading a circular shotcrete panel supported at 3 discrete points (Figure 121).



Figure 121: Round Determinate Panel (RDP) test setup (Bernard 2005).

ASTM C 1550 08 states that the sample must have the following dimensions:

- The overall diameter of the circular panel must be 800mm with a tolerance of +/- 10mm.
- The sample must be between 70mm and 90mm in thickness and have no greater variation than +/- 3mm.

These dimensions are maintained “*regardless of the size of aggregate or length of fiber used in the concrete or shotcrete*” (ASTM C 1550 08).

The standard also states that the specimens should be prepared *“in such a way as to approximate the mode of placement in-situ. Specimens representing cast concrete shall therefore be cast, while those representing shotcrete shall be sprayed”*.

The spraying techniques used for the placement of shotcrete cannot produce samples within these tolerances and consequently the procedure provides instructions for screeding and floating the sample. The accelerator dosages must be dropped significantly to enable this process; furthermore, the screeding and floating process changes the inherent nature of the product by altering the compaction and the water content.

Curing conditions are specified according to ASTM C 031 08. Descriptions of the curing specification and the actual curing methods used on site have been described in Section 5.7.2.2.

The test facility comprises of three supporting plates and a central loading point. The three flat supports are mounted on pivot points (Figure 122). The sample is loaded using a 50mm spherical point (Figure 123). Load is imparted on the system by displacing the centrally located point at 4mm per minute.

According to the standard *“a successful test involves a failure that includes at least three radial cracks. Specimens occasionally fail in a beam-like mode involving a single crack across the specimen that is characterized by low energy absorption. The result of such a test shall be discarded”*.

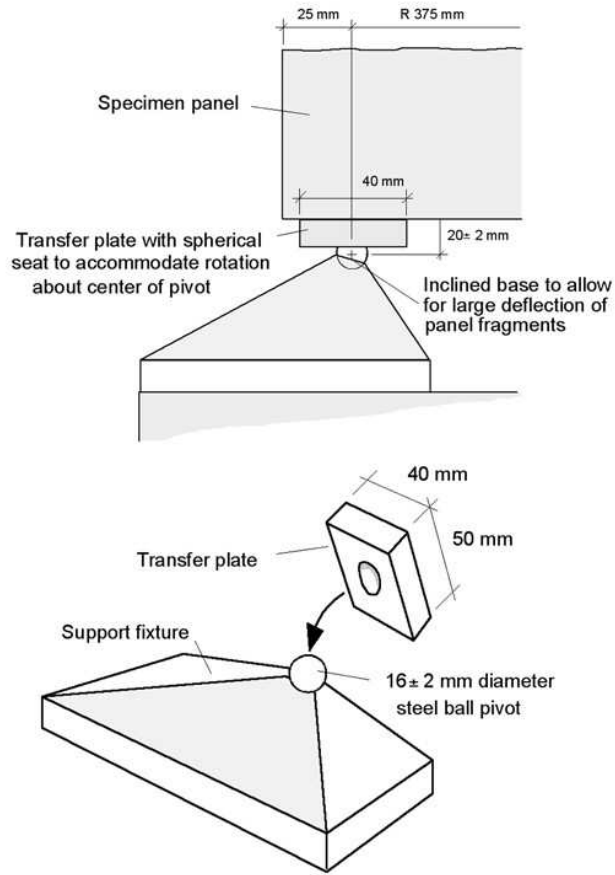


Figure 122: Specification for sample supports used in RDP tests (ASTM C 1550 08).

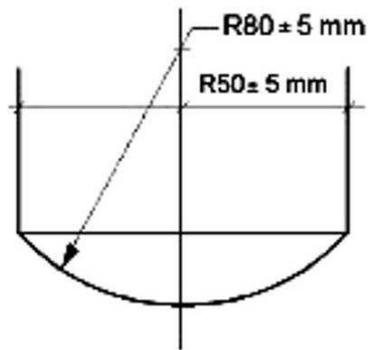


Figure 123: Spherical loading point used in the RDP test (ASTM C 1550 08).

5.7.3 LARGE-SCALE TESTING

There are a small number of papers dedicated to the large-scale testing of shotcrete. These include Fernandez Delgado et al. (1976), Holmgren (1976, 2001), Little (1985), Kirsten and Labrum (1990), Kirsten (1992, 1993), Tannant and Kaiser (1997) and Kaiser and Tannant (2001). A summary is provided below of the test methods applied used by these investigations.

5.7.3.1 *Fernandez-Delgado et al.*

Fernandez Delgado et al. (1976) tested large-scale shotcrete panels using realistic loading conditions. They attempted to replicate the following variables experienced in the underground mining environment:

- Geometrical configuration (planar, arched and irregular surfaces)
- Bond strength (between the shotcrete and the simulated rock surface)
- Boundary conditions
- Thickness of the layer
- Strength of the shotcrete

To enable the testing of these variables a vertical test frame was constructed consisting of the following elements:

1. A reaction abutment
2. A test wall with fixed and movable portions
3. Two hydraulic rams stacked vertically which applied load to the moveable portion of the test wall.

Three test setups were created to simulate the planar, arched and irregular geometrical profiles (Figure 124). The first test setup (Setup 1) consisted of a flat wall 3m long x 2m high made up of three separate panels. The centre panel consisted of two 0.6m² moveable blocks that were located one above the other. The blocks were moved by two hydraulic rams located 0.5m and 1.2m above the floor. The rams were electrically controlled to provide “*either a predetermined rate of loading or rate of displacement*”. It was also possible to stop the displacement or load to any desired level and to maintain that level as long as desired “*to allow for incremental testing*”.

The second test setup (Setup 2) simulated an arched excavation profile. The abutment blocks were changed to triangular shapes whilst the centre blocks remained planar.

The third set setup (Setup 3) simulated an irregular shaped drive similar to blasted rock surfaces. The triangular abutment blocks from test setup 2 were maintained but the flat centre blocks were replaced with triangular blocks.

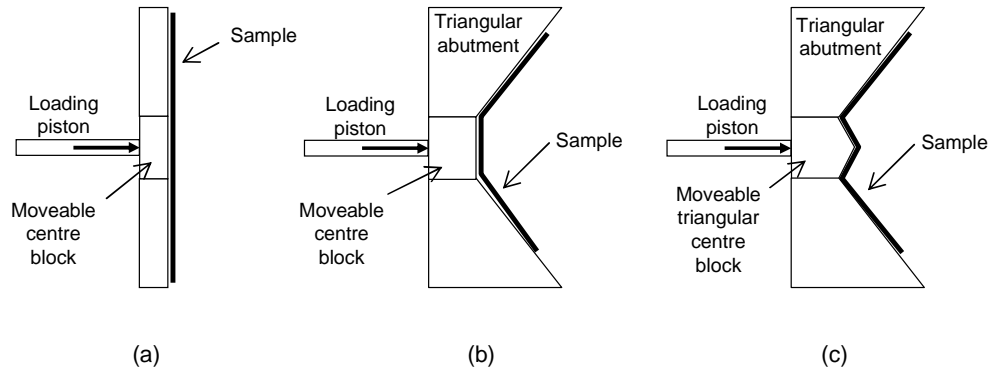


Figure 124: Plan of (a) Setup 1 flat profiles (b) Setup 2 arched profiles and (c) Setup 3 irregular profiles.

Each profile was tested with free boundary conditions and restricted boundary conditions. Restricted boundary conditions were simulated by fixing the sample ends to the abutment walls using a steel plate (600mm x 150mm x 25mm).

Each test setup was used to test varying thicknesses of shotcrete, different mix designs (to determine the properties of different strengths of shotcrete) and simulated adhesion properties.

Samples were sprayed directly onto the test frame. The dry mix placement method was used for all tests. The cement content was fixed at 17.8%. To simulate a low adhesion environment the wall was covered in a plastic filament. To simulate good adhesion properties the roughness of the wall was increased using an abrasive disc. Once sprayed, the wall samples were covered in moistened burlap and left to cure.

The results from Setup 1 (without confinement) showed that *“for good bond layers, the layer capacity can be represented as a function of the thickness, up to a thickness of about (50mm), above which the capacity was independent of thickness”*.

Tests undertaken using Setup 1 exhibited one of 3 failure modes; namely, diagonal shear failure, adhesive failure or bending failure (Figure 125). Both diagonal tensile failure and adhesion loss occurred where the sample was not externally fixed to the wall. Diagonal shear failure was characterised by rapid failure with no residual strength. They found that *“layers thinner than (50mm), regardless of the strength of the shotcrete, always failed by diagonal tension through the shotcrete material”*.

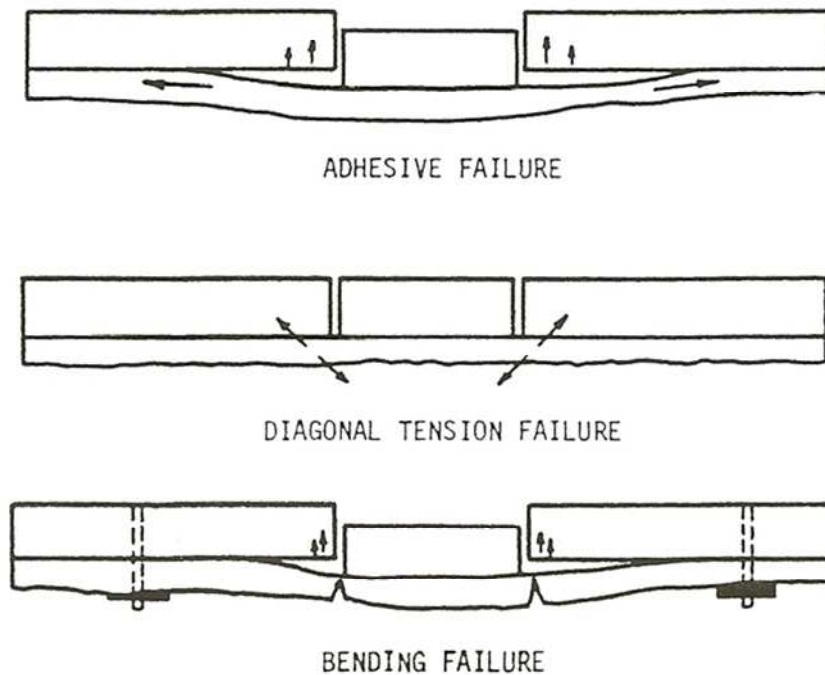


Figure 125: Failure modes described by Fernandez Delgado et al. (1976).

Adhesion failure occurred when the shotcrete was pulled from the wall. They found that *“layers thicker than (50mm) regardless of the shotcrete strength, always failed by separation from the fixed wall”*.

Bending failure only occurred in the restrained tests. The sample initially exhibited adhesion loss but in this case full separation was not achieved due the restraining forces provided by the end plates. Once the separation had reached the plates the sample began to act as a beam with some residual load carrying capacity until bending failure took place.

Test Setup 2 (without confinement) also exhibited diagonal tension failure and adhesion failure. Once again samples less than 50mm in thickness failed through the shotcrete material. The capacity of the material was proportional to the strength of the mix and the thickness of the layer. Samples with thicknesses above 50mm once again exhibited adhesion failure.

The mechanism of failure was once again changed by the addition of the end constraints. Two new failure modes were observed; arching and buckling (Figure 126). Both these modes were similar to the bending failure mode; the samples would partially separate from the wall but were constrained by the plates at the ends of the samples. Instead of the panel acting as a beam, the sample acted as a thin arch. The thin arch either failed by a combined moment thrust mechanism or by the buckling. The failure mode was controlled by the sample thickness. Samples less than 50mm tended to buckle whereas samples with a thickness above 50mm tended to fail under the moment tension mechanism.

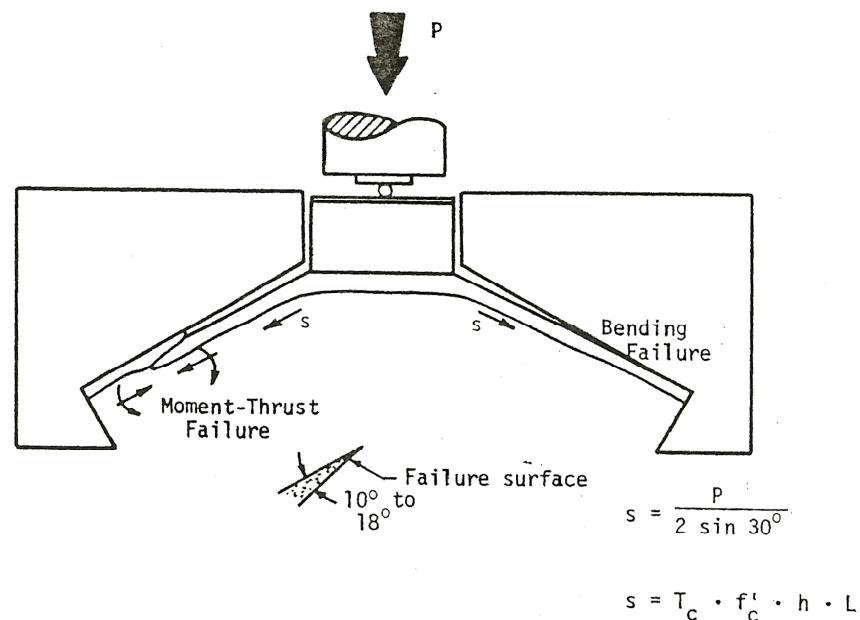


Figure 126: Test Setup 2 failure modes (confined) – Fernandez Delgado et al., 1976.

Test Setup 3 (unconfined) once again displayed very similar failure modes to test Setups 1 and 2. As with the other two setups, the application of the end restraints changed the behaviour of the sample and resulted in three new failure modes. These were:

1. "A shear failure through the shotcrete material in the neighbourhood of the fixed wall – moveable wall contact.
2. Layer separation along the fixed wall contact followed by moment thrust failure in the inclined portion of layer in contact with the fixed wall.
3. Layer separation along the fixed wall contact as well as along the moveable block contact followed by a tension failure along the apex of the triangular moveable block".

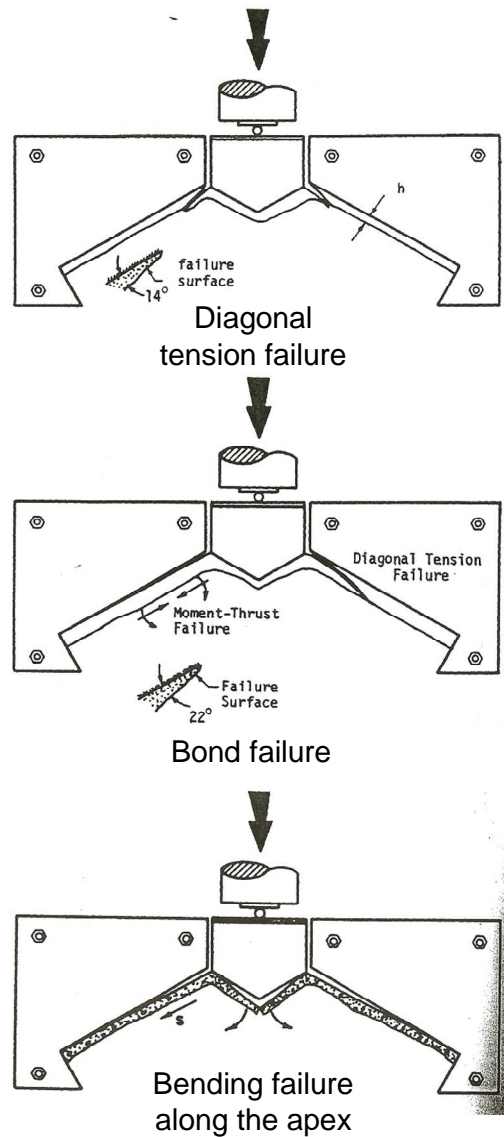


Figure 127: Test Setup 3 failure modes (confined) – Fernandez Delgado et al., 1976.

Fernandez Delgado et al. (1976) also evaluated the effect of reinforcing on the behaviour of the shotcrete. They found that *“the presence of steel fiber reinforcing did not affect the value of the residual capacity. But it significantly increased the ductility of the layer which exhibited an undiminished residual capacity for moveable block displacements 3 times larger than those at which complete collapse of unreinforced planar shotcrete layers took place.*

The presence of a (250mm) square mesh with (1mm) diameter wires placed close to the outside surface of the layer... not only increased the residual strength but also the ductility of the layers. The residual capacity increased from 15% to 95% of the peak load”.

5.7.3.2 Holmgren

Holmgren (1976, 2001) undertook large-scale testing using the same principles as Fernandez Delgado et al (1976). The test arrangement consisted of three flat granite panels mounted on a hinged bed. The overall size was 3.7m x 1.2m. The hinged bed allowed the assembly to be rotated such that spraying could occur in the vertical position. The spraying method and mix design are not provided. The test facility is shown in Figure 128.

The centre rock panel was loaded via a hydraulic jack. Force and displacement were recorded; displacement was only measured at the centre of the middle slab.

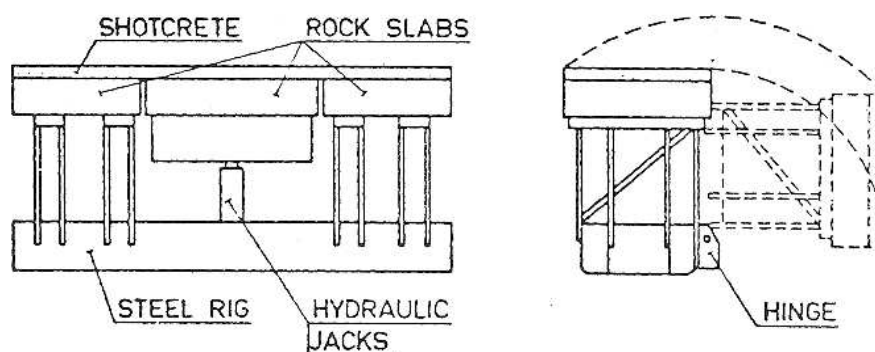


Figure 128: Holmgren (1976) test facility with hinged base for spraying.

Adhesion failure was the primary mode of failure. *“The failure mode was not affected by the layer thickness”* (Holmgren 1976), although this may have been a function of the test arrangement.

Holmgren (2001) used yield line theory and a series of equations in an attempt to develop design guidelines for shotcrete. This method has not been universally adopted by industry.

5.7.3.3 *Kirsten and others*

Kirsten and Labrum (1990) compared the performance of different shotcrete reinforcing systems such as fibres and mesh. The test facility consisted of a 1.6m square panel supported on a steel frame and restrained by bolts located on a 1m square pattern. Bearing plates, attached to the bolts, were used to simulate realistic restraint conditions.

Samples were either uniformly loaded using a hydraulically pressurised bag or point loaded at the centre of the sample using a hand operated hydraulic jack. The pressurised bag *“ensured that the energy in the loading system was limited, and that deflection of the panels could be tracked in a controlled manner beyond peak load”*. Dimensions of the loading systems are not provided.

Displacement was measured at three positions using linear variable displacement transducers (LVDTs); *“one at each of two diametrically opposite bolt positions and one at the centre of the panel”*. The LVDTs had a maximum displacement capacity of 25mm. The displacement capacity of the loading systems was 150mm; consequently the LVDTs were regularly reset to enable continued monitoring.

Eighteen panels of shotcrete containing 15% cement were prepared using the dry mix spraying method. Table 16 provides the various panels configurations and the number of tests conducted on each configuration.

Table 16: Number of tests conducted on each configuration.

Thickness	Reinforcing	
	30mm Steel fibres	3.1mm Ø 75mm aperture diamond Mesh
50mm	3	3
100mm	3	3
150mm	3	3

Some samples were damaged during transport to the laboratory; consequently only 11 successful tests were completed.

The results showed that mesh reinforced shotcrete was much more effective in sustaining large deformations. Further assessment of the results found that *“the superiority of the mesh over the fibre reinforcement was ascribed to the low content and relatively limited length of the fibre used. The mesh reinforcement was located in the middle of the test panels and, as such, was more efficient than the fibre reinforcement of which only a small fraction of total content was available in the tension sides of the panels tested”* (Kirsten 1992).

Kirsten (1992) undertook a second series of testing comprising of a total of 24 panels. The panels were prepared in the same way as the previous test series using the same mix design. Table 17 provides the number of tests and the sample configurations

Table 17: Number of tests conducted on each configuration.

Thickness	Reinforcing				
	30mm steel fibres	25mm melt extract fibres	35mm melt extract fibres	50mm melt extract fibres	3.1mm Ø 75mm aperture diamond mesh
50mm	2	1	1	2	2
100mm	2	1	1	2	2
150mm	2	1	1	2	2

Both series of testing found little difference in the behaviour of the material between uniform loading conditions (using the hydraulically pressurised bag) and point loading conditions. The second series of testing found that the fibre type had very little effect on the behaviour of the samples, despite the steel fibre being applied at higher dosages than the plastic fibres. In essence the second series of testing reaffirmed the results of the first series of testing.

5.7.3.4 Tannant and Kaiser

Tannant and Kaiser (1997) used the same test facility described in Section 4.3.4 to evaluate the force – displacement capacity of mesh reinforced shotcrete. The procurement of the samples is not described. The shotcrete layers were “approximately 60 to 70mm thick and were reinforced with one sheet of #6 gauge mesh”. The exact dimensions of the sample were not provided. The samples were held in position using bolts spaced at 1.2m x 1.2m and located in a diamond configuration.

A plate was pulled upwards through the sample using an overhead winching system.

“The peak load in the shotcrete occurred at displacements in the range of 50 – 100mm. At this stage in the pull tests the shotcrete was extensively fractured but no wires in the mesh reinforcement had failed. Only after displacements of 100 to 150mm did the shotcrete start to become extensively damaged and wires began to fail” (Tannant and Kaiser 1997). Further testing was conducted using an impact test method similar to that used by Stacey and Ortlepp (1997). Dynamic testing of shotcrete will not be discussed.

Tannant and Kaiser conclude that shotcrete behaves stiffer than mesh during the initial stages of deformation and that mesh reinforced shotcrete can deform up to 150 – 200mm.

5.7.4 OTHER TEST METHODS

Large-scale testing has also been undertaken by Little (1985), Ding and Kusterle (1999) and Dufour et al (2003), Cengiz and Turanli (2004) to name but a few.

Dufour et al. (2003) used a large-scale pull plate test method to evaluate the early strength of shotcrete in-situ. The method is similar to that used by Pakalnis and Ames (1983) to evaluate mesh.

Van Sint Jan (2004) tested shotcrete using the same method applied to mesh by Ortlepp and others (Section 4.3.1) to test shotcrete. The sample size was 1.6m square and was restrained using bolts positioned on a 1m square pattern. Eight tests were conducted using this method with the aim of evaluating the performance of synthetic fibres compared with the performance of mesh reinforcing. The samples underwent some warping during transport; consequently, the results are assessed as being unreliable.

There are also several small scales tests that have been applied to shotcrete with limited success. These tests include adhesion tests, shear testing and tensile testing.

5.8 SHOTCRETE TEST METHODOLOGY

The aim of the shotcrete testing was to determine the force – displacement properties of shotcrete and to enable the comparison of shotcrete test results with result from the mesh testing program. The test method was expected to satisfy a number of criteria; namely;

- The test had to be suitable for all sprayed layers (e.g. shotcrete and membranes).
- The sample had to be of suitable size to enable realistic spraying techniques.
- The test had to evaluate realistic shotcrete failure mechanisms such as shear strength, flexural strength and adhesion.
- The results had to enable comparison of variations in mix design, reinforcing, thickness and curing times.

A large – scale punch test method similar to that used by both Holmgren (1976) and Fernandez Delgado et al. (1976) was selected.

The large-scale punch test method involves applying a liner to a thin substrate which has a centrally located loading disc cut into and then separated from the surrounding substrate. After a specified curing period, the sample is placed on the test frame and testing is undertaken.

5.8.1 SUBSTRATE PREPARATION

Several substrate materials were considered; these included foam, glass, concrete and rock. A stiff material was required to ensure the panel was robust enough to withstand the spraying process and to ensure the material did not flex under the weight of the shotcrete. The surface of the panel required a rough texture to simulate underground rock surfaces and had to be readily available.

Concrete was considered as it is relatively inexpensive and the disc could easily be moulded into the centre. After further consideration, it was decided that concrete could not provide a repeatable consistent surface that represented the roughness of a rock surface. Furthermore, the curing concrete would potentially affect the curing of the sprayed product and thus bias the results.

Natural rock was selected as the most appropriate material. Sandstone was selected, after discussions with various quarries. A sandstone slab prepared for spraying is illustrated in Figure 129.

A 500mm diamond drill was used to cut the central loading disc from the slab. The drill assembly is shown in Figure 130.

The drilling process left an 8mm gap between the main slab and the centre disc. This gap was filled with polystyrofoam gap filler (Figure 131) to prevent shotcrete penetrating the gap during spraying.

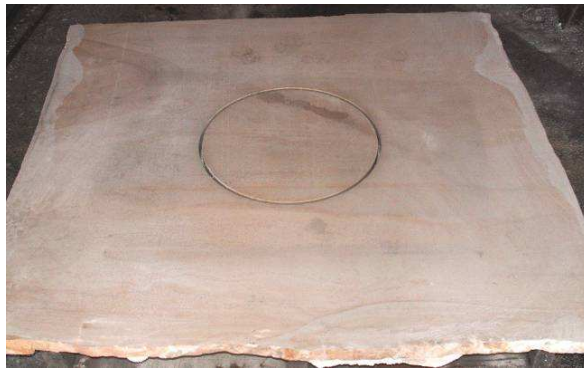


Figure 129: Sandstone substrate prepared for spraying.



Figure 130: Diamond drill assembly for drilling punch plate in the substrate.



Figure 131: Gap filler is used to fill between the punch plate and the main substrate.

5.8.2 SAMPLE PROCUREMENT

The samples were taken to site and sprayed. The samples were placed in an upright position to replicate an excavation wall (Figure 132). Formwork around the outside of the sample was used as a depth guide for the sprayers. The sample was sprayed by an experienced operator.

If the spraying process resulted in a highly irregular profile on the face of the sample, the edges (up to 100mm maximum distance from the edge) were screed to improve the seating of the sample on the test frame. The internal area of 1.3m x 1.3m was left undisturbed, to ensure that the sample remained consistent with the final sprayed product.



Figure 132: Upright substrate ready for spraying.

5.8.3 CURING

Curing is critical to the development of strength of shotcrete particularly in the hours immediately after spraying. Shotcrete curing conditions will vary depending on the conditions at individual sites.

Once the samples have been sprayed they were wrapped in plastic and transported back to the laboratory where they were placed in a sea container specifically modified to enable a temperature and humidity controlled environment for curing.

The samples are specifically not water cured as this may increase the hydration of the cement and result in a strength increase that would not normally be associated with mining applications.

The time period between spraying and storage varied between 2 and 12 hours as a result of transporting samples from site back to the laboratory. This is likely to have an effect on the sprayed product but cannot be avoided.

The temperature and humidity within the sea container are set to reflect conditions at the site where the sample was sprayed. This information is obtained from the site ventilation officer.

The curing time for each sample was set to reflect the requirements of the individual mine sites. Tests were not conducted beyond 7 days as loading of the shotcrete was expected within the first week at all the sites.

5.8.4 TEST METHODOLOGY

The testing facility has been described in Chapter 3. Shotcrete tests are setup using the following process:

1. The sample is removed from the curing chamber.
2. The exterior formwork is removed and the centre is marked up (Figure 133).
3. The sample is rotated using the forklift (Figure 134).
4. The sample is placed on the test frame with the centre of the loading disc located beneath the centre of the loading point (Figure 135).



Figure 133: The formwork is removed and the centre of the sample is marked.



Figure 134: Rotation of the sample.

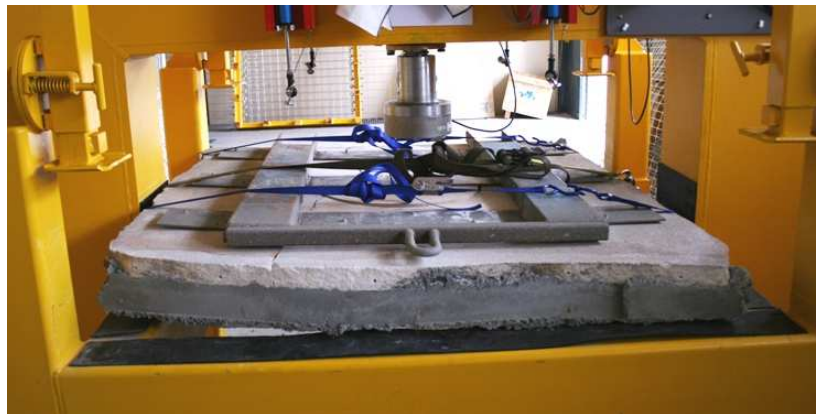


Figure 135: Sample on the test frame ready for the final test setup.

5. The transport frame and bolts are removed.
6. The clamping frame is positioned over the edges of the sample and the corner restraints are lowered to provide confinement.
7. The foam insert between the disc and the outer substrate is removed.

8. The square loading plate is positioned under the jack to provide distributed force over the disc.
9. The jack is lowered into position (Figure 136).
10. The data acquisition and the video recorded are started and the jack is activated.

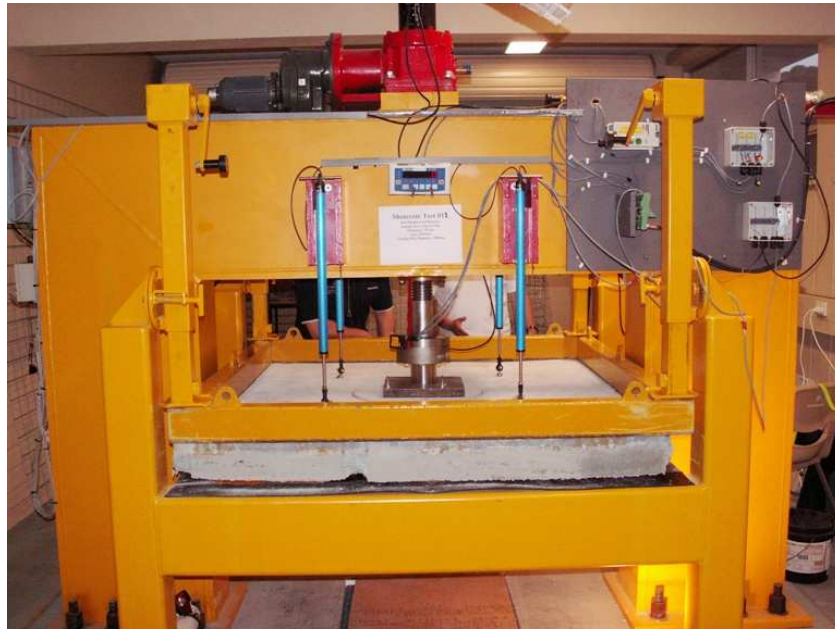


Figure 136: Shotcrete test setup.

5.9 MATERIALS

Testing has been conducted on behalf of three different sites. All three sites used a mix design containing a cement content of approximately 15%. The actual mix designs are provided in Appendix 7.

The mix designs for Sites 1 and 2 were similar: that is, similar water cement ratios were used and both sites applied 6 kilograms of polypropylene fibres per cubic metre; however, slightly different chemical admixtures and aggregates were used by the two sites.

The third site used a significantly different mix design. The sand and gravel ratios varied from the other two sites along with the chemical admixtures. This site applied 30kg of steel fibre per cubic metre.

The standard mix design from Site 3 was used to prepare a mesh reinforced sample. This test was conducted to enable the comparison of the force – displacement properties of standard fibre reinforced shotcrete with mesh reinforced shotcrete. To ensure consistency the same mix was used to spray three samples; consequently the mesh reinforced shotcrete was also reinforced with steel fibres. This replicated the current site practice of spraying over mesh in areas of rehabilitation.

5.10 RESULTS

A total of 15 tests were conducted on shotcrete samples obtained from 3 mine sites. The samples comprised of a variety of mix designs, fibre types, curing times and thicknesses. Individual report sheets for each test are presented in Appendix 8. Three test results have not been presented as part of this thesis (Table 18).

Table 18: Test results excluded from analysis.

Sample number	Reason for exclusion
ST002	Air pressure problems during spraying at a 4 th mine site led to poor compaction of the sample and an extremely uneven surface.
ST006	Sample was damaged during the test setup process. The sample was tested but the results have not been included.
ST011	Data acquisition system failed resulting in no test data.

5.10.1 SITE 1 AND 2 - POLYPROPYLENE FIBRES

The mix designs for sites 1 and 2 were very similar; consequently, these sites have been analysed together.

A total of 8 tests were conducted on samples from Sites 1 and 2. The force – displacement responses for Sites 1 and 2 are shown in Figure 137 and Figure 138, respectively. A summary of the results is provided in Table 19. Figure 139 shows a comparison of results from samples with the same thickness and the same curing time from the two sites.

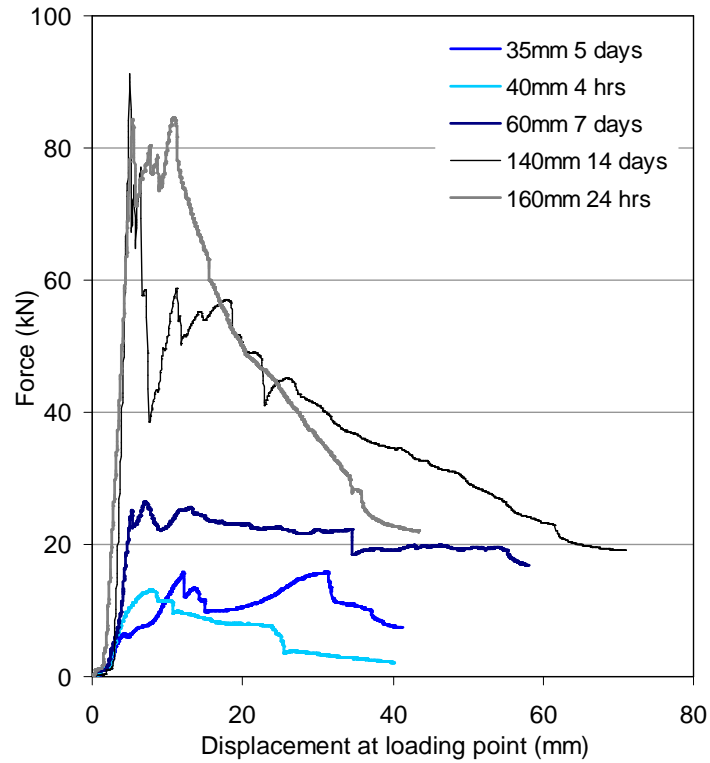


Figure 137: Site 1 force – displacement results.

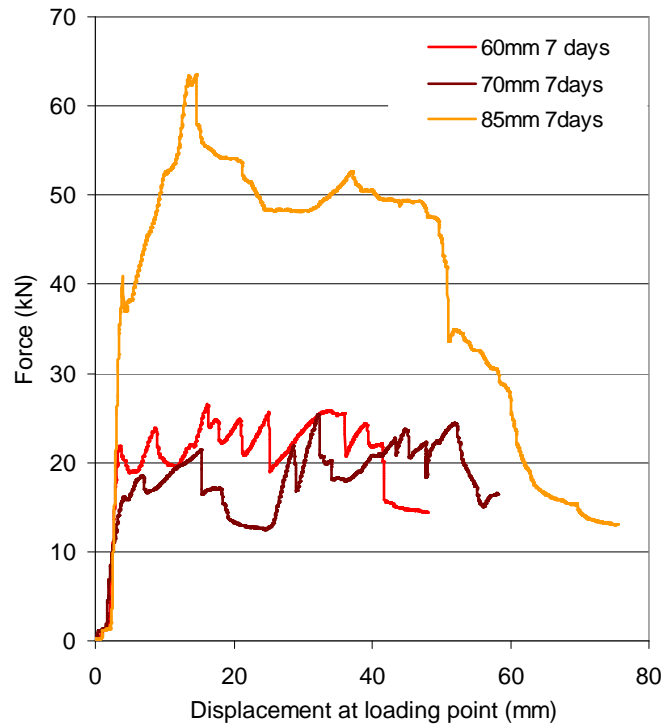
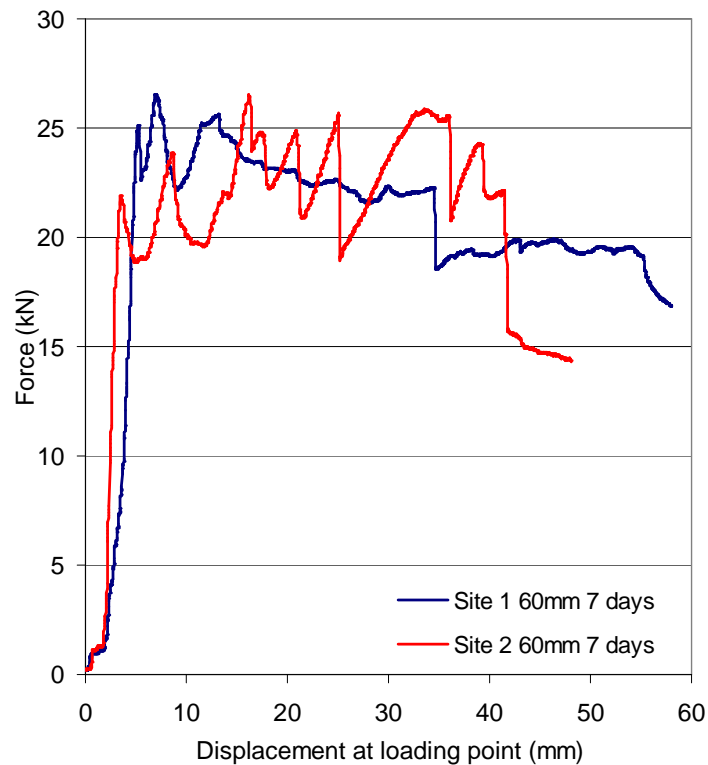


Figure 138: Site 2 force – displacement results.

Table 19: Summary of test results for Sites 1 and 2.

Site	Test number	Average thickness (mm)	Age	Rupture force (kN)	Rupture displacement (mm)
1	001	140	14 days	91.19	5
1	003	160	24 hours	84.30	5
2	004	70	7 days	16.12	4
2	005	60	7 days	21.92	4
2	007	85	7 days	40.89	4
1	008	40	4 hours	13.20	8
1	009	35	5 days	6.52	4
1	010	60	7 days	25.11	5

**Figure 139: Comparison of Site 1 and Site 2 test results using the same thickness and curing time.**

As with the mesh test results, the shotcrete force – displacement results can be divided into a number of phases (Figure 140); namely, the pre-rupture phase, the post rupture phase and the sandstone rupture phase.

The pre-rupture phase is characterised by a rapid load increase at the start of the test. A small step occurred at the start of each test, which is believed to be a function of the test setup. The load increased rapidly up until rupture. This increase can be approximated by a straight line. The rupture point is also known as the first peak force. First peak force is defined by ASTM C 1609 07 as *“the load value at the first point on the load-deflection curve where the slope is zero”*. For consistency and clarity, rupture force and rupture displacement will be used instead of first peak force.

Rupture generally occurred between 4 and 5mm of central displacement. Rupture is believed to correspond to the breaking of the matrix of the shotcrete; cracking sounds could be heard but visible cracks were not discernable on the face of the sample.

The rupture force may or may not correlate to the peak force which is defined as the maximum force recorded during the test.

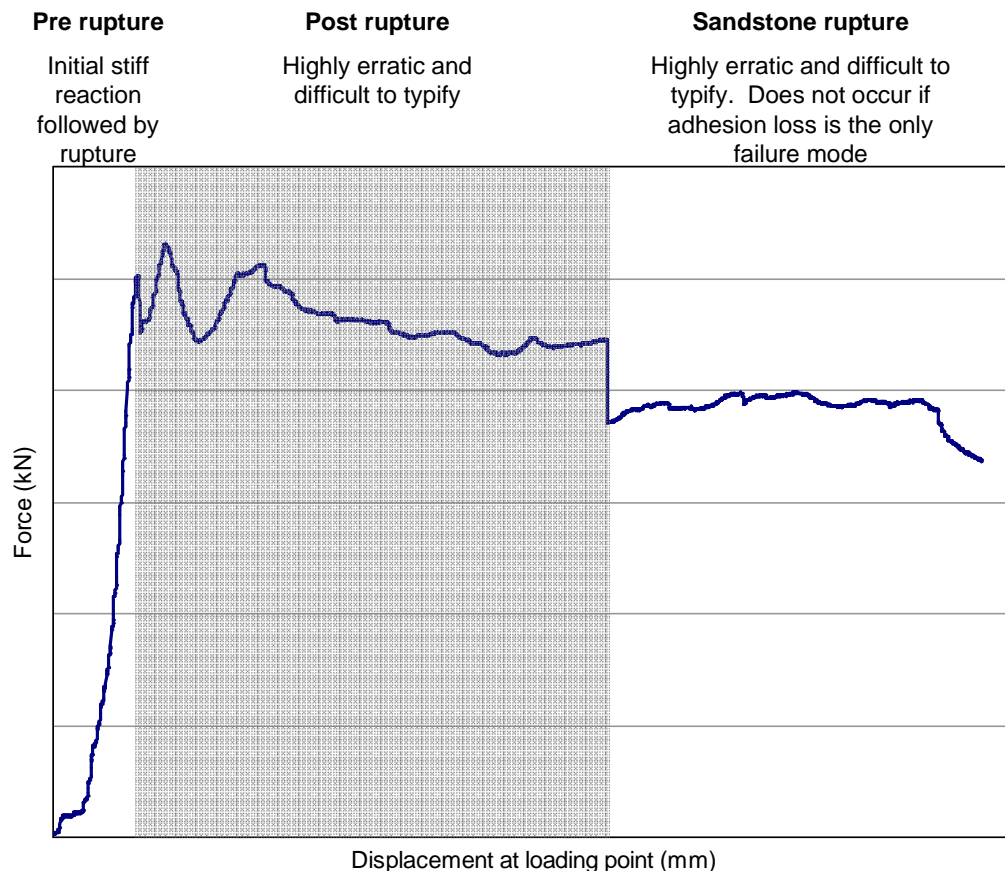


Figure 140: Shotcrete test phases.

The post rupture behaviour was difficult to characterise as each test behaved differently. The post peak behaviour was dependent upon the failure mode, the shotcrete thickness and the type of reinforcing.

The failure mode for all tests was a combination of flexural failure and adhesion loss. With the exception of Test ST001, adhesion loss occurred some time after initial cracking. ST001 exhibited adhesion loss as the primary failure mode, followed by flexural cracking of the layer after adhesion loss had started.

The LVDT results provided information regarding the deformation of the substrate. Significant deflection of the sandstone substrate occurred in all tests except ST001. Generally the sandstone substrate began to crack after 4 to 6mm of deflection of the substrate at the position of the LVDTs. This equated to approximately 10mm to 15mm of central displacement. Figure 141 provides an example of the LVDT results with the corresponding phases indicated. The cracking of the sandstone occurred after rupture and therefore only influenced the post peak results of the sample.

The LVDTs stopped displacing towards the end of the test. This suggests that there was no longer any downward force acting on the sandstone substrate. This is possibly related to adhesion loss or a reduction in the force capacity of the sample indicating failure.

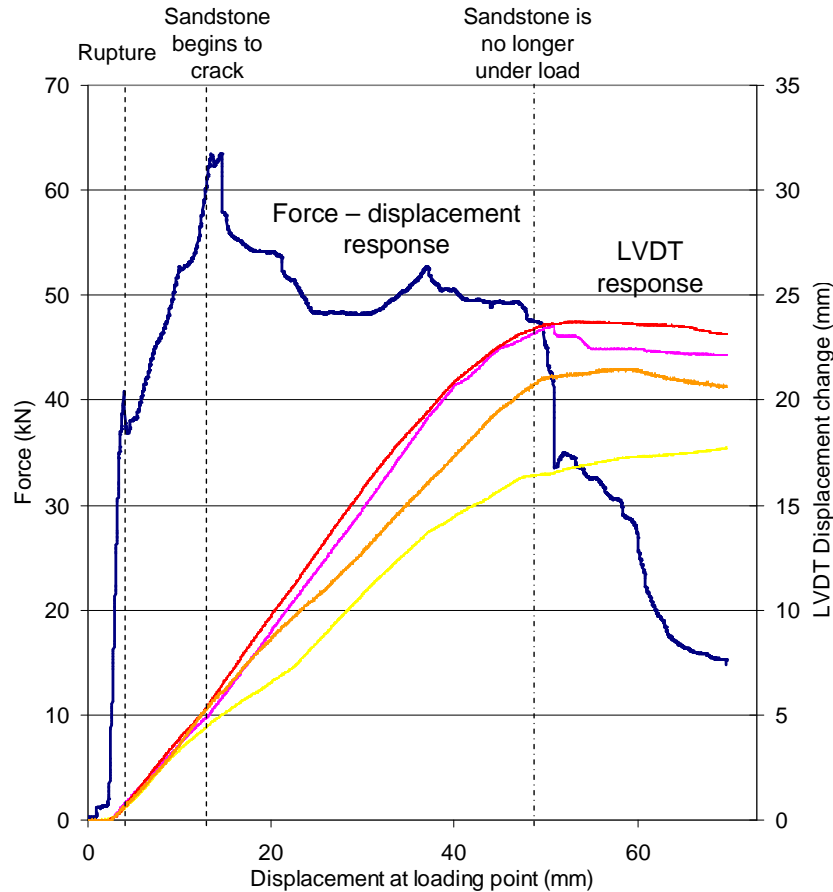


Figure 141: An example indicating how the LVDT results can be used to determine the behaviour of the substrate.

The LVDT results from Test ST001 indicated that the substrate only deformed 2mm and then returned back to zero (Figure 142). The slow rebound suggests that the forces acting to deflect the substrate were reducing as time progressed, indicating adhesion loss.

At the termination of the tests, most samples had cracks between 15 and 20mm wide across the face of the sample. The cracks were randomly oriented but were wider in the centre of the sample. The crack patterns have been included in the individual test report sheets contained in Appendix 8. Two different fibre failure modes were observed within the cracks of the sample. Some fibres appear not to have been loaded indicating that they had not bonded effectively with the shotcrete matrix. Some fibres within the larger cracks were frayed indicating tensile failure of the fibres (Figure 143). Often these two failure modes were observed side by side. This suggests that the fibres that showed no signs of stress may have been oriented parallel to the cracks or had an ineffective embedment length.

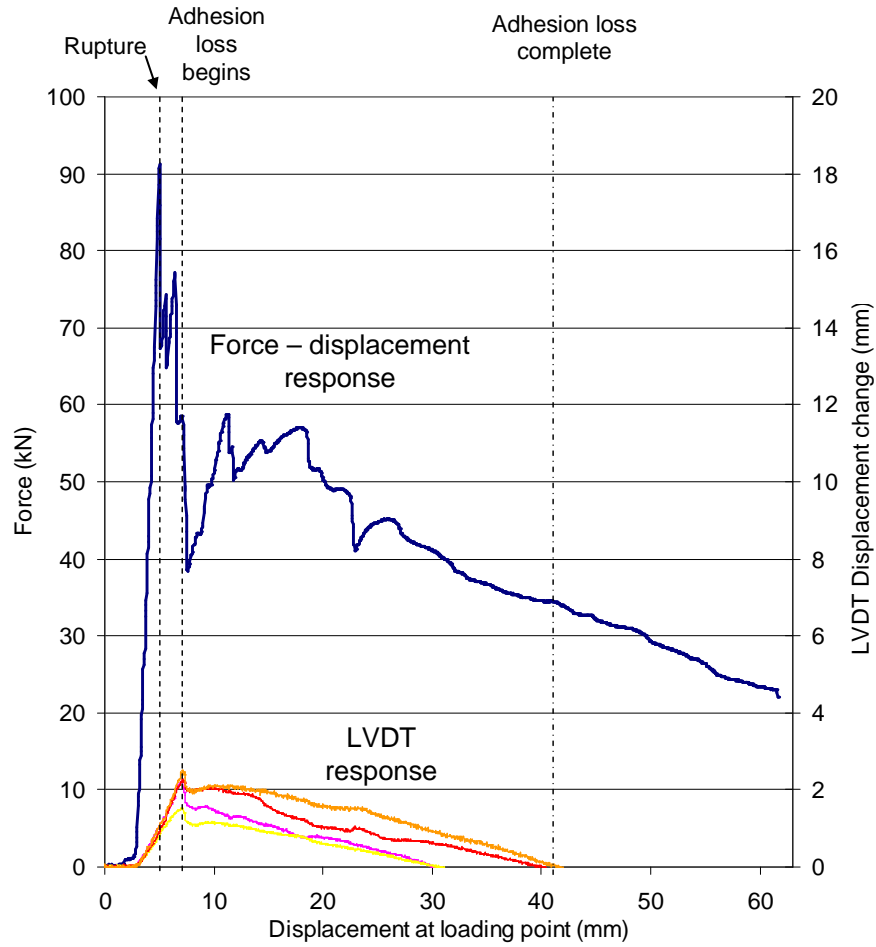


Figure 142: The LVDT results from ST001 indicated where adhesion loss began.

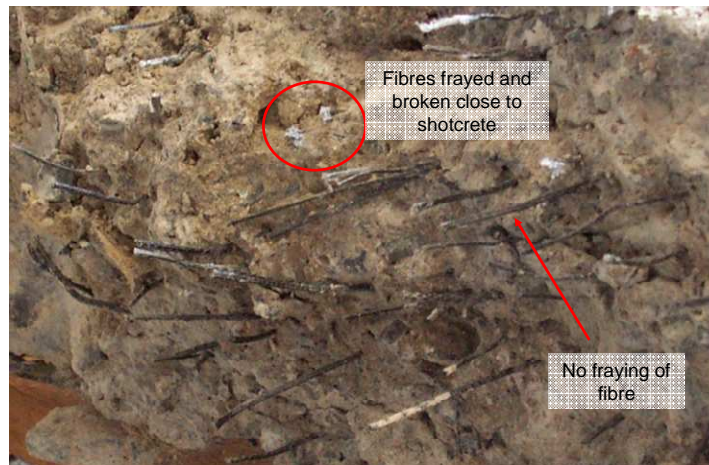


Figure 143: Poly fibres with two different failure modes.

Energy absorption (toughness) was determined by calculating the area under the force – displacement curve. The total displacement was not consistent across all the tests; consequently, total energy cannot be used as a comparative measure. Determining energy at an arbitrary displacement is also not indicative of the energy capacity of shotcrete. In order to effectively assess the energy absorption capabilities of shotcrete, the cumulative energy absorption variation with central displacement should be considered. Figure 145 and Figure 146 provide the cumulative energy absorption for samples from each site.

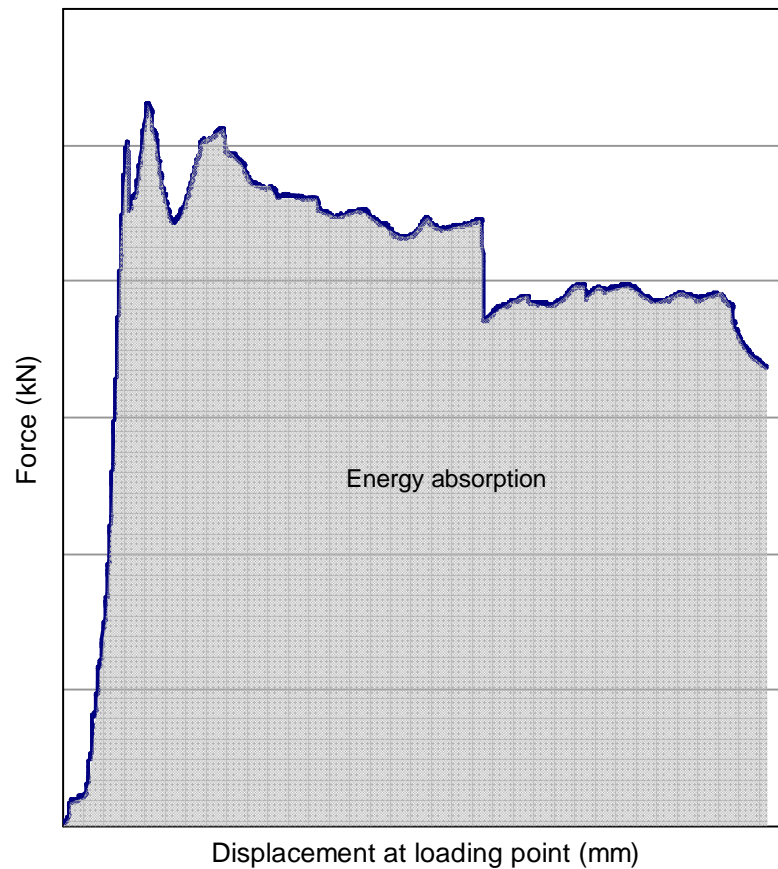


Figure 144: Typical force – displacement curve with energy shown as the shaded area.

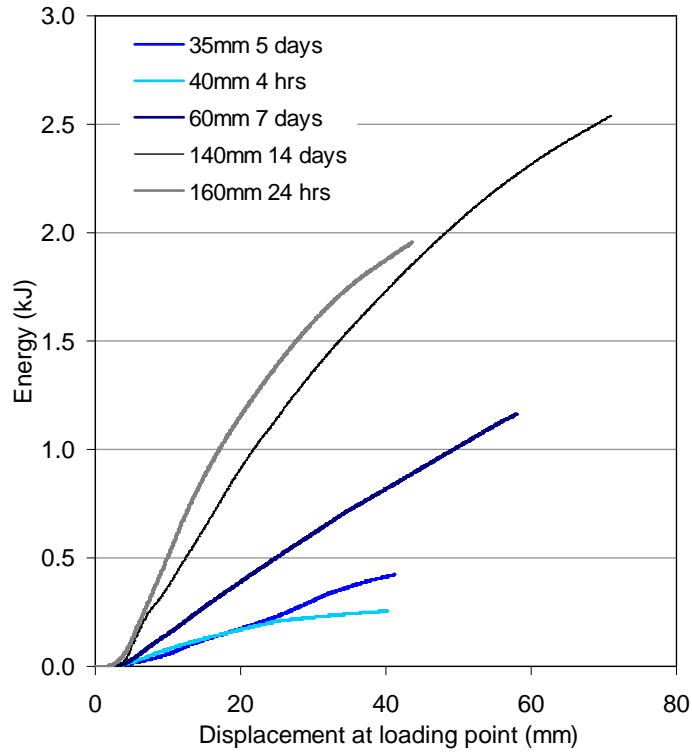


Figure 145: Site 1 cumulative energy results.

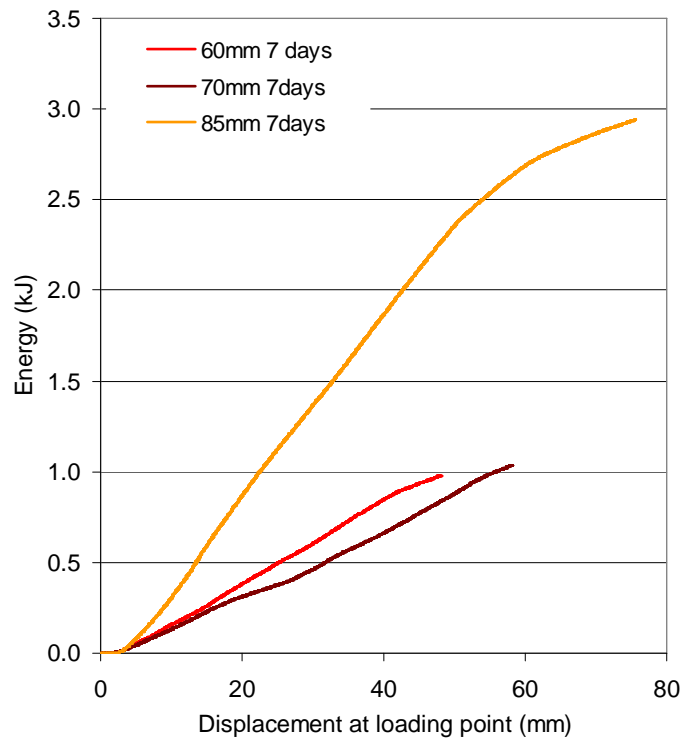


Figure 146: Site 2 cumulative energy results.

5.10.2 SITE 3 - STEEL FIBRES

The force – displacement results for Site 3 are presented in Figure 147. A summary of the test results is presented in Table 20. The failure mode for all tests was the same as for Sites 1 and 2; namely, flexural failure of the layer followed by debonding from the sandstone towards the end of the test. The sandstone flexed in the same manner as the sandstone in the tests conducted for Sites 1 and 2. The crack patterns for Site 3 were also random with the crack in the face also between 15mm and 20mm in width.

The “hook” ends of the fibres within the cracks were straightened, suggesting that they were pulled through the shotcrete matrix (Figure 148). The fibres within the cracks showed no signs of any tensile failure.

The energy absorption results are presented in Figure 149.

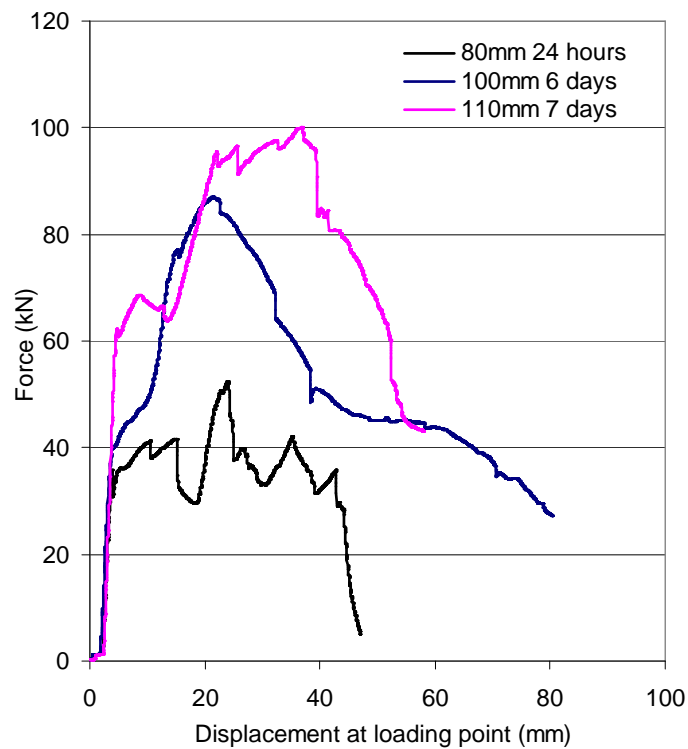


Figure 147: Site 3 force – displacement results.

Table 20: Summary of Site 3 test results.

Site	Test number	Average thickness (mm)	Age	Rupture force (kN)	Rupture displacement (mm)
3	012	80	24 hours	35.70	4
3	013	100	6 days	39.68	4
3	014	115	7 days	62.25	5

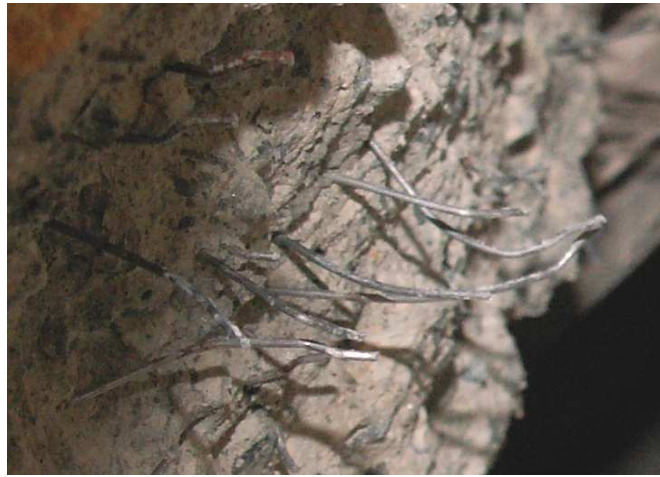


Figure 148: Steel fibres showed no signs of tensile yield.

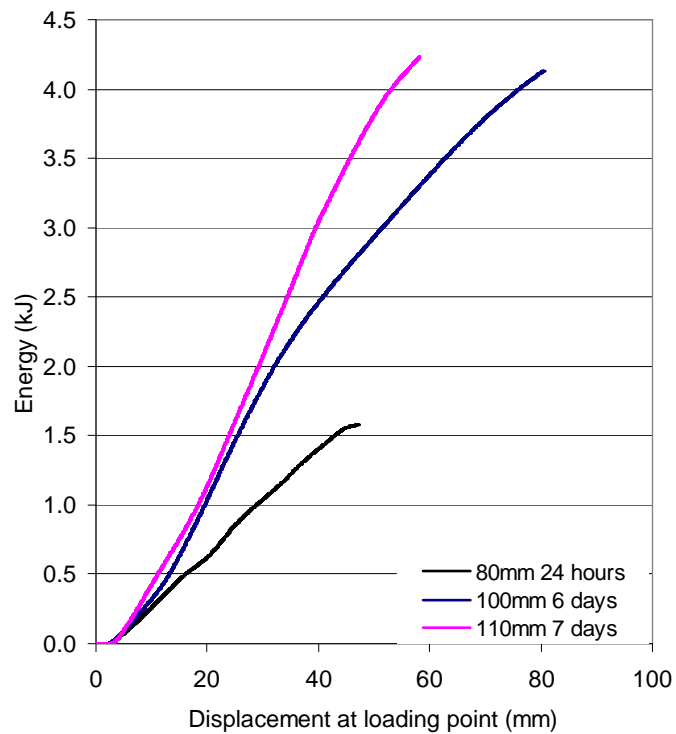


Figure 149: Cumulative energy results for Site 3.

5.10.3 SITE 3 - MESH REINFORCING

Only one test was conducted using mesh reinforcing within a fibre reinforced shotcrete panel. Standard weld mesh (100mm square grid using 5.6mm diameter wires) was used as reinforcing. The results are shown alongside the other results from Site 3 in Figure 150.

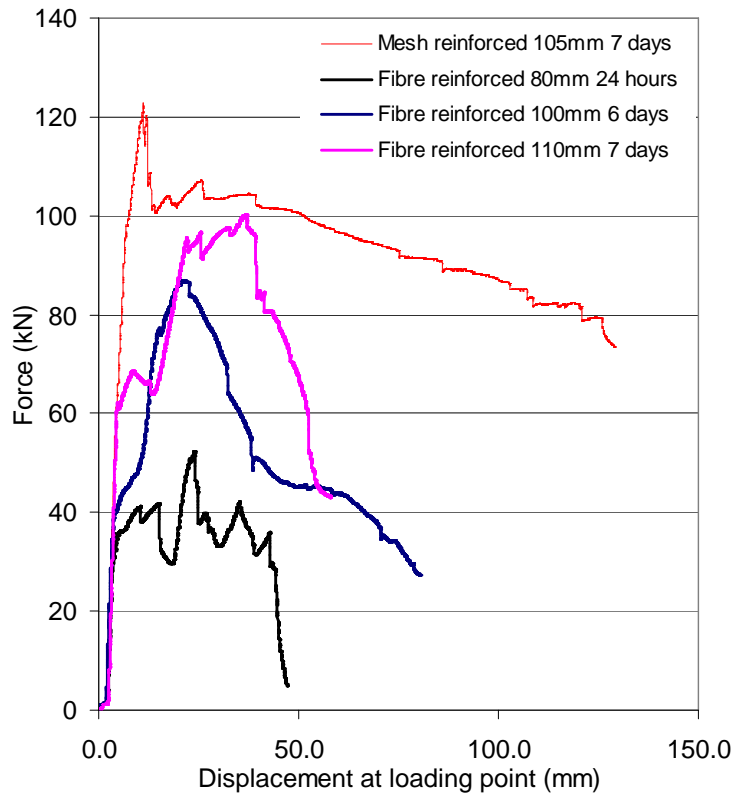


Figure 150: Mesh and fibre reinforced shotcrete force – displacement results alongside fibre reinforced shotcrete results.

The mesh reinforced sample exhibited much higher forces both at rupture and in the post rupture phase. The displacement of the sample was also much greater. Accordingly, the energy absorption capacity is also much greater (Figure 151).

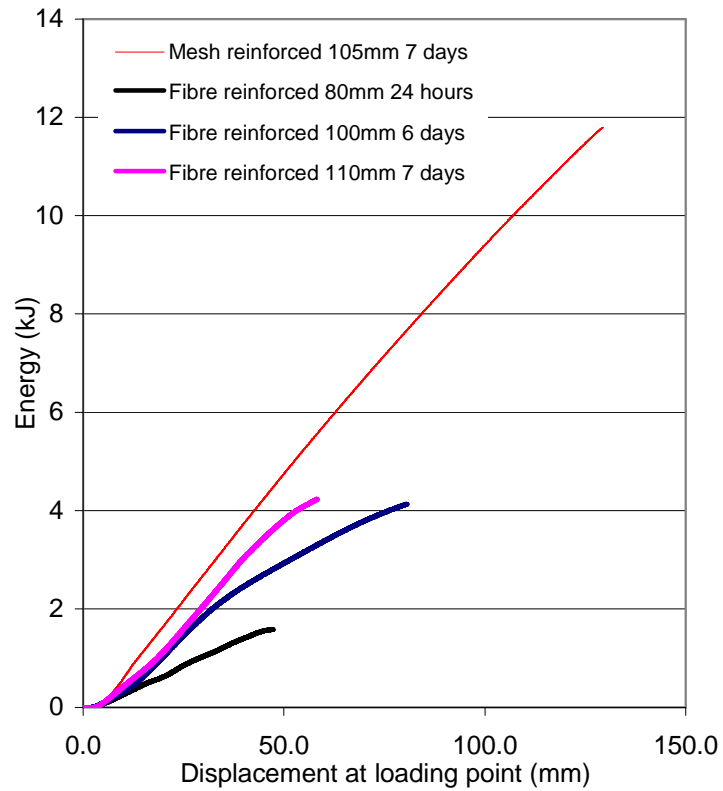


Figure 151: Mesh and fibre reinforced shotcrete energy results alongside fibre reinforced shotcrete results.

The primary failure mode was adhesion loss combined with flexural failure of the sample. The test was stopped due to excessive rotation of the loading plate. Only a small portion of the mesh could be seen at the base of the fracture (Figure 152); consequently, the displacement capacity of the sample was potentially much greater than the results indicated.



Figure 152: Mesh reinforcing within the cracked shotcrete sample.

5.10.4 COMPARISON OF RESULTS

Each test had four main variables:

- Mix design.
- Reinforcing.
- Thickness.
- Curing time.

In addition to these variables, the air pressure, the spraying machines, and the spraying technique all have the potential to affect the results.

Despite the variables, it is clear that fibre reinforced shotcrete has a displacement capacity of less than 80mm regardless of the fibre type. The force and displacement capacities of shotcrete can be enhanced by the use of mesh reinforcing. Further work is required in testing and analysing different mesh reinforcing products to enable the development of improved design parameters.

The post peak results were highly variable; consequently, analysis can only be undertaken on the rupture results. Figure 153 shows the rupture force – displacement results for all sites. The chart does not appear to indicate a relationship between the three sites; although it appears that curing may have an effect on the behaviour of the samples. All samples, except ST008, were cured for longer than 24 hours. ST008 was cured for 4 hours prior to testing. The behaviour of ST008 was less stiff than the behaviour of the other samples; consequently, the rupture displacement was much greater.

Further research is required to determine the behaviour of shotcrete at curing times less than 24 hours.

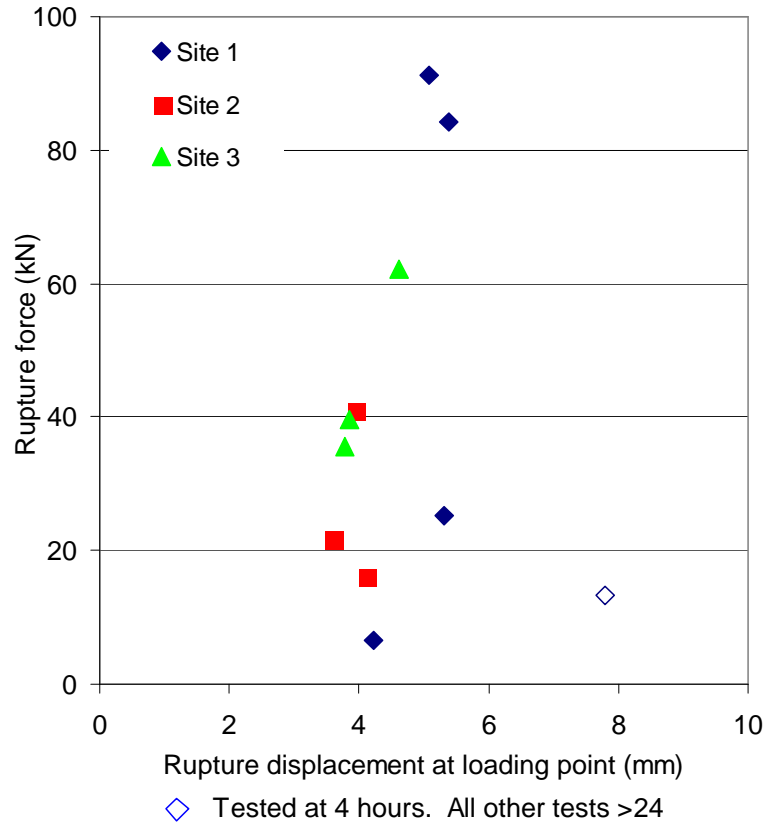


Figure 153: Rupture force – displacement results for all sites.

As there was no discernable relationship in the rupture force – displacement results, the rupture forces were analysed with respect to thickness. The results (Figure 154) indicate a clear relationship between the thickness and the force capacity of the fibre reinforced shotcrete. The relationship is approximately quadratic and has an R^2 value of 1.0. The mesh reinforced shotcrete did not conform to this relationship. The test had a much higher force capacity than the fibre reinforced shotcrete suggesting that mesh is a much better reinforcing material than fibres (at the applied dosages).

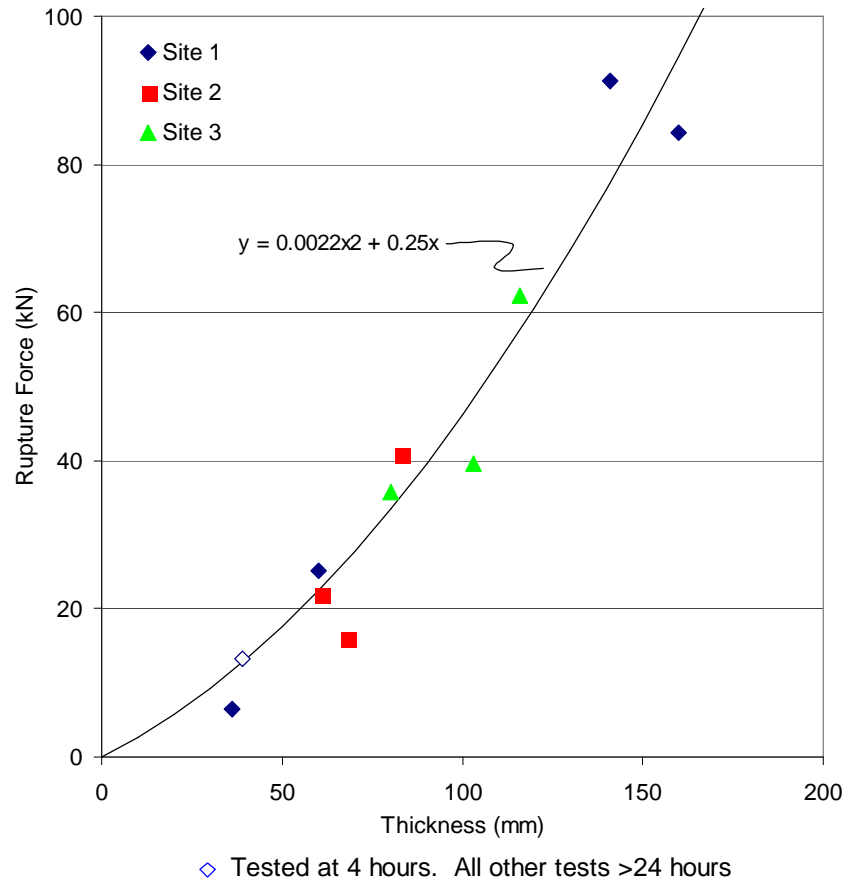


Figure 154: Rupture force – thickness results for all sites.

The rupture force / thickness relationship is likely to be related to the cement content of the samples. All samples contained approximately 15% cement. It is unlikely that samples containing different cement contents will conform to this relationship. However, it is evident that the overall mix design, curing time and fibre material has a limited effect on the rupture force capacity of relatively thin layers.

Due to the brittle nature of shotcrete, the energy required to rupture the shotcrete is less than 0.2kJ; however a quadratic relationship between the thickness and the rupture energy still exists (Figure 155). The overall energy absorption results were dependent on the behaviour of the sample and the length of the test. In particular, the thinner layers tended to have a lower residual force capacity but those forces were maintained for longer periods. The thicker layers typically had higher force capacities but these forces were not maintained over long displacements.

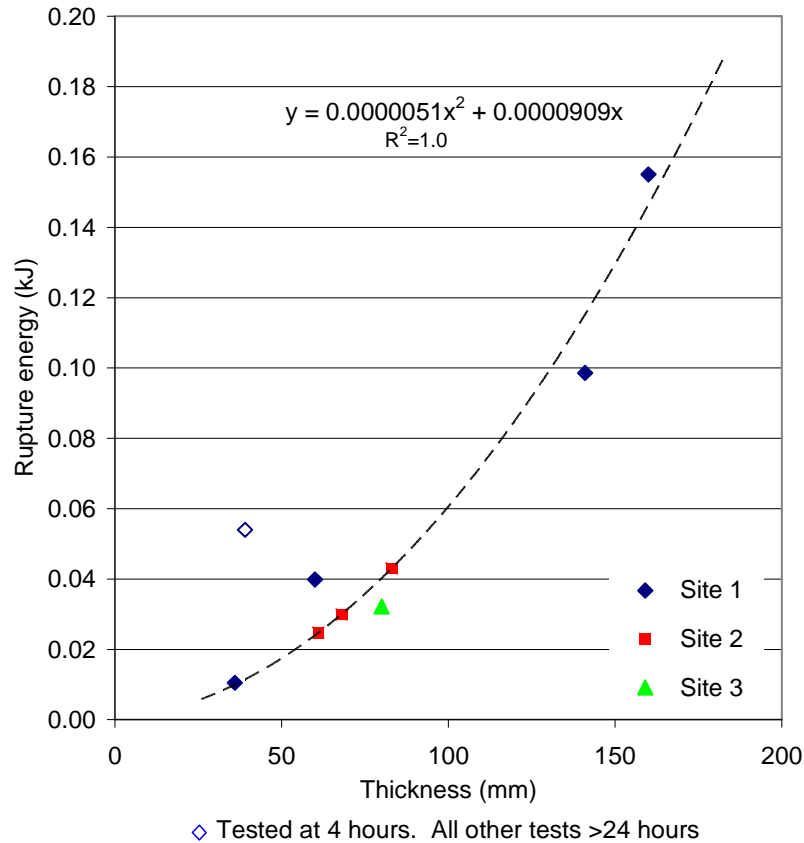


Figure 155: Rupture energy / thickness relationship.

5.11 DISCUSSION

The punch test methodology developed as part of this research program has the flexibility to enable the comparison of each variable listed in Section 5.10.4, providing that only one variable is modified each time. The limited quantity of tests conducted to date and the variability in each test meant detailed conclusions could not be generated from the test results. Notwithstanding, it is clear that rupture force is dependent upon the cement content and the thickness of the shotcrete. The role of the cement content in the formation of this relationship is still to be investigated.

The failure modes generated by this test configuration indicate that the primary mode of failure for shotcrete layers greater than 50mm is a combination of flexural failure and adhesion loss. In reality, it is difficult to determine the true level of adhesion to the rock surface. Many rock types are not conducive to good adhesion. This is further exacerbated by the presence of water, blasting residue and dust on the rock surface. In-situ monitoring is required to determine the level of adhesion in an underground mining environment.

Recently, industry has placed a great emphasis on the measurement of toughness as a quality assurance measure and a design tool. The toughness results were highly dependent on the length of the test. Due to the brittle nature of shotcrete, the energy required to fracture the shotcrete is less than 1kJ. The overall toughness results were dependent on the behaviour of the sample and the length of the test. In particular the thinner layers tended to have a lower residual force capacity than the thicker layers, but those forces were maintained over a much greater displacement; consequently, measuring the toughness at 10mm, 20mm or 40mm is not representative of the behaviour of the material.

It is clear from these results that further evaluation of shotcrete is required. It is recommended that further investigations be conducted in the following areas:

- Investigation of the relationship between cement content, thickness and force capacity that will aid in the development of improved design tools for shotcrete.
- In-situ monitoring to determine the level of adhesion that is achieved in an excavation.
- In-situ monitoring to determine the actual forces that act on shotcrete, particularly during the first 24 hours of curing.
- Laboratory investigations into the development of the shotcrete strength over the first 24 hours.
- Investigation into various types of mesh reinforcing to enable the better design of shotcrete reinforcement elements.
- Field investigation to determine the realistic failure mechanisms of shotcrete.

CHAPTER 6 MEMBRANES

6.1 INTRODUCTION

Membranes are known by several titles including polymer shotcrete, thin spray-on liners (TSLs) and plastic liners. They are most commonly referred to as thin spray on liners however TSL refers to all thin spray on liners including shotcrete and polymer based spray on liners. The author has chosen to refer to polymer based spray on liners as membranes throughout this thesis.

Membranes can generally be described as thin coatings of polymer based material used for areal rock support. The recommended application thickness for most membrane products is between 3 and 6 millimetres.

Anecdotal evidence suggests that membranes were initially developed somewhere between the 1930s and the 1950s to enable the fire proofing of timbers used for support in coal mines. Arnold (1967) quotes Mitchell and Murphy (1966) as stating that *“urethane foam is currently being applied in more than 200 mines... The foam is produced by mixing two liquids (an isocyanate and a resin with additives) which expand within seconds to almost three times their original volume. After expansion the foam fills cracks and crevices of surfaces and produces a virtually air-tight, moisture-proof seal of cellular material which bonds strongly onto most surfaces. The foam sets within five minutes and develops full strength within 30 hours”*. The benefits of using the foam coating were reported to be improved ventilation, reduced spalling in weak strata, reduced maintenance, and decreased operating costs as a result of a reduction in application time compared to that of shotcrete.

More recent research into membranes has been well documented. The first documentary evidence of research into polymer based liners for use as ground support was published in the early 1970s. Research was conducted by the United States Bureau of Mines, (Schwendeman et al., 1972), the Mining Research Centre, (a sub branch of the Department of Energy, Mines and Resources Canada), (Gyenge and Coates, 1973) and the Bureau of Reclamation, (United States), (Graham, 1973).

As stated in Section 5.2, Gyenge and Coates (1973, Department of Energy Mines and Resources Canada) describe the theories of how shotcrete provides support.

They set out to confirm the theories of support using modelling and theoretical analysis and investigate *“the possibility of creating such an air - tight membrane by spraying material onto the rock surface”*. They investigated polyethylene and sprayed araldite as two potential support products.

Graham (1973, Bureau of Reclamation, United States) discussed the development of a polymer shotcrete containing methacrylate. The polymer was used to replace accelerators and cement in standard shotcrete mixes in order to achieve rapid setting times and high early strengths.

In 1973, the United States Bureau of Mines published an open-file report into *“Plastic liners extended with sand and other fillers for use in coal mines”* (Schwendeman et al. 1973). The report documents the outcomes of research conducted between 1971 and 1972 that was *“directed towards determining which state-of-the-art resin systems might have utility as a means of roof support in a coal mine”*. Forty-five different resins were initially evaluated for suitability, with only ten of these products (2 phenolics, 3 epoxies and 5 polyesters) meeting the initial criteria set for support. Further testing determined that the phenolic resins had good adhesion properties but relatively low flexural strength compared with the epoxies and polyesters. More detailed testing was conducted on the best performing epoxy and polyester resin mixes. The outcome of the report states that *“the concept of using a resin liner containing both particulate and fibrous fillers to obtain support in a mine appears to be feasible. Because of the cost these liners should be considered for use in particularly troublesome areas of a mine. Such areas are those where especially bad roof conditions exist that require continuous support over the entire area”*.

No further documentary evidence of membrane research can be found again until the early 1990s. Several companies began developing membrane products with the stated objective to replace mesh and shotcrete as surface support in underground mines. Archibald is credited with undertaking the most extensive research; but research was also conducted in North America (e.g. Archibald et al., 1992, Archibald et al., 1999, Tannant et al., 1999a, Tannant et al., 1999b), Europe (Spearing and Champa, 2001, Spearing et al., 2001, Spearing and Pretorius, 2006), South Africa (Wojno and Toper, 1999, Stacey, 2001, Kuijpers, 2001, Kuijpers et al., 2004) and Australia (Finn et al., 1999).

Between 2001 and 2003 three international workshops were held entitled “*Surface support liners: Thin sprayed Liners, Shotcrete and Mesh*”. One of the aims of these workshops was to “*integrate the knowledge and experience of manufacturers, users and researchers to develop guidelines for testing and evaluating the performance of TSL’s*” (Potvin et al., (ed.) 2004). A considerable number of papers on membrane testing techniques were presented at these workshops, but the proposed guidelines were not established.

Despite extensive research and marketing efforts, membranes have not been accepted as a suitable replacement for conventional surface support elements in the mining industry. The reasons for this are varied, though in general, it has not been proven that membranes are capable of replacing conventional ground support other than in specialised circumstances.

The Western Australian School of Mines was approached by a manufacturing company to provide test data for a commercially available membrane product designated for use as a ground support product. The product data sheet suggests the membrane can be used “*as an alternative to mesh / screen protection, with or without bolts*”. Furthermore, the product data sheet suggests that the membrane can be applied in “*areas where large deformations are expected... for the rehabilitation of collapsed areas... and as prevention against hard rock strain bursting*”.

The company representatives expected the failure mechanism to be a combination of adhesion loss followed by tensile failure of the material.

Membranes have two theoretical support models (Norcroft, 2006); namely, the membrane support model and the beam support model. A total of 6 tests were undertaken to investigate the behaviour of the product under the two theoretical support models. These tests were aimed at determining a suitable test method that could determine the capacity of the membrane and the behaviour of the membrane under realistic loading conditions. The results of the testing are discussed in this chapter.

6.2 PRODUCT TYPES

Broadly speaking there are two main accepted types of membrane products, reactive and non-reactive membranes. Rispin and Garshol (2003) define reactive polymers as those with an *“initial reaction and set time within ten minutes off application, with a gain in tensile strength to a minimum of 75% of the ultimate strength within the first hour after application (at 20°C)”*. Non-reactive polymers have properties that fall well below these parameters.

The most common polymer bases used in ground support applications, along with their classifications, are as follows:

- Polyurethane (Reactive),
- Polyurea (Reactive),
- Methacrylate (Reactive),
- Acrylic (Non-reactive) and
- Vinyl Acetate or Latex (Non-reactive)

Reactive polymers often have adverse occupational health and safety (OHS) characteristics due to the presence of isocyanate. OHS testing and analysis is discussed further in Section 6.5.1.1.

Non – reactive membrane products are typically cementitious based with a polymer added to provide greater elasticity than would otherwise be achieved with a straight concrete mix. Compared with reactive membrane non-reactive membranes generally have low tensile strength but high adhesion strength and high shear strength

Over 20 products have been developed since the 1990s. Table 21 lists the most publicised membrane products together with the base components.

Only three of these products are presently available in Australia; namely Tekflex, Tunnel Guard and Masterseal 845A.

Table 21: Available membrane products with primary polymer base.

Product	Mix base	Mix type
Tekflex®	Latex / Cement	Liquid / Powder
Evermine	Cement / Acrylic	Liquid / Powder
Mineguard™	Polyurethane (Isocyanate)	Liquid
Tunnel Guard	Polymer (unknown) / cement	Liquid / Powder
Masterseal® 840	Methacrylate	Liquid
Masterseal® 845A	Vinyl Acetate (Latex) / Cement	Powder

6.3 THEORY OF MEMBRANE SUPPORT

Several theories have been developed as to the role of membranes in providing areal surface support (e.g. McCreath and Kaiser, 1992 and Espley et al., 1996). One theory is that membranes exhibit similar support functions to shotcrete; for example, the retention of individual blocks, the promotion of block interlock, or the prevention of rock deterioration due to environmental exposure (Stacey, 2001). More recent research tends to refute this theory. Norcroft (2006) suggests that membranes are *“different materials with different functions and different ways of stabilising the rock”* (compared with shotcrete). He also suggests that membranes *“provide area protection and excavation surface strengthening rather than structural support”* and that they *“assist the rock to remain self-supporting”*.

Norcroft clearly states that understanding of the support mechanisms provided by membranes is not well developed, but provides two theoretical models to represent their behaviour.

The first model is called the membrane model which involves discrete blocks being supported by the thin liner (Figure 156).

The second model is called the beam model, whereby the membrane keeps the surface layer of rocks in position to enhance the rock's arching or interlocking capability and to enable the rock to be somewhat self-supporting (Figure 157). Tannant (2001b) provides a description of this mechanism. He states that *“in jointed or fractured rock masses, a thin liner prevents the rock mass from dilating, loosening and unravelling, thus forcing fragments of the rock mass to interact with each other creating a stable beam or arch of rock”*.

Norcroft believes that the beam model is a more realistic mechanism for the performance of membranes but expresses caution in designing liners based on this approach using numerical modelling due to the sensitivity of the model to the thickness of the rock / membrane composite beam.

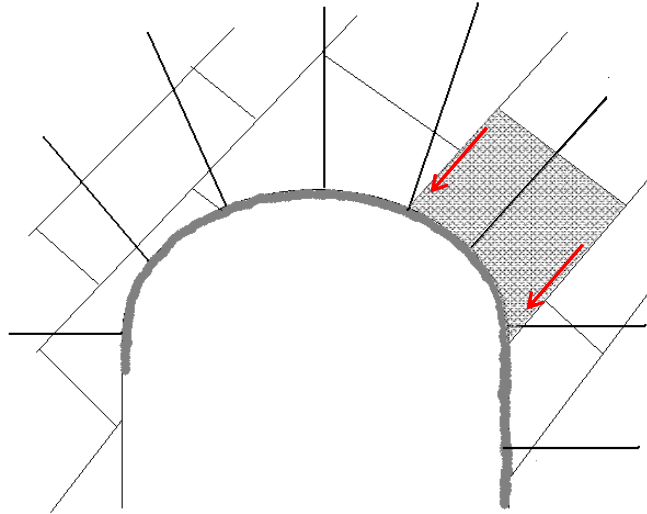


Figure 156: Membrane support model.

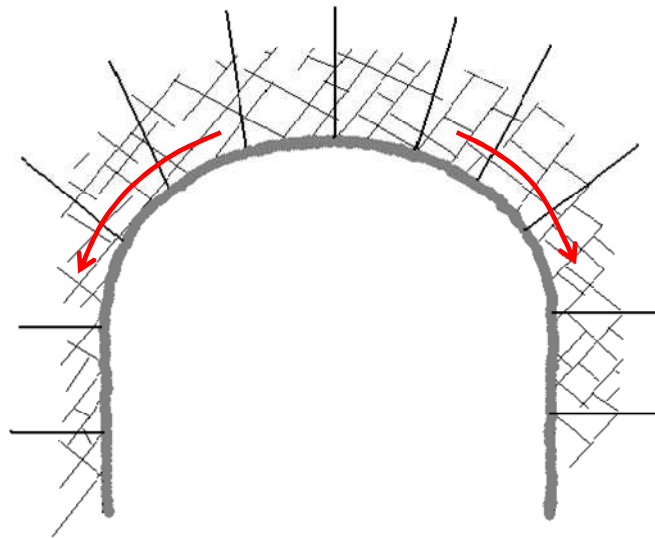


Figure 157: Beam support model.

6.4 MEMBRANE FAILURE MECHANISMS

There are several material properties that control membrane behaviour and, in particular, the failure mechanism of the membrane. The most prevailing properties are adhesion, elongation, tensile strength and shear strength.

In the early literature only one mechanism of failure was used to describe all products. This mechanism (provided in Figure 158) suggests that blocks are retained by relying on partial adhesion loss and the elongation of the polymer material.

Espley and Kaiser (2002) provide a more realistic summary of the likely failure modes of membranes. They describe three modes of membrane failure; direct shear, direct tension and adhesion loss (see Figure 159). They also suggest that these modes are entirely dependent upon the adhesion strength of the material. If adhesion is good no adhesion loss is likely to occur, consequently direct shear is the probable failure mode. If localised adhesion loss occurs, the membrane will be acting in direct tension during loading and tensile failure is likely. If minimal adhesion is achieved then the membrane, in the absence of restraint, can be expected to peel away from the rock resulting in no support.

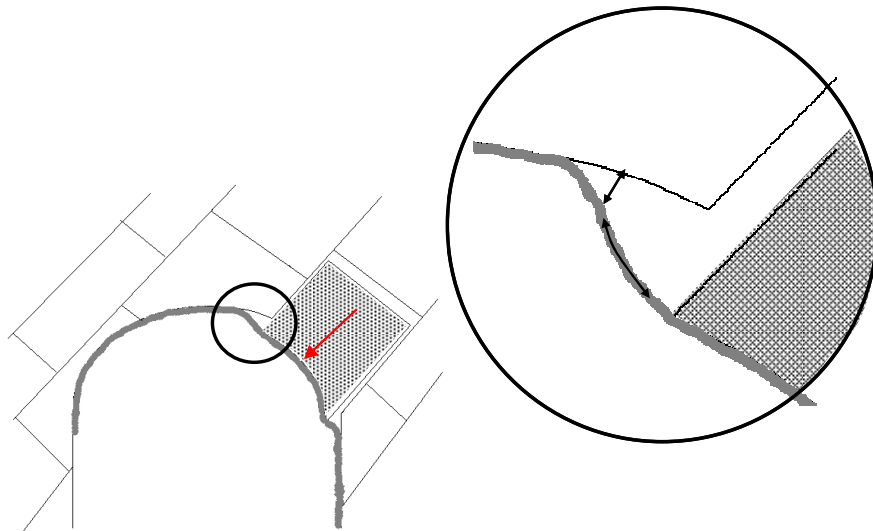


Figure 158: Failure mechanism of membranes.

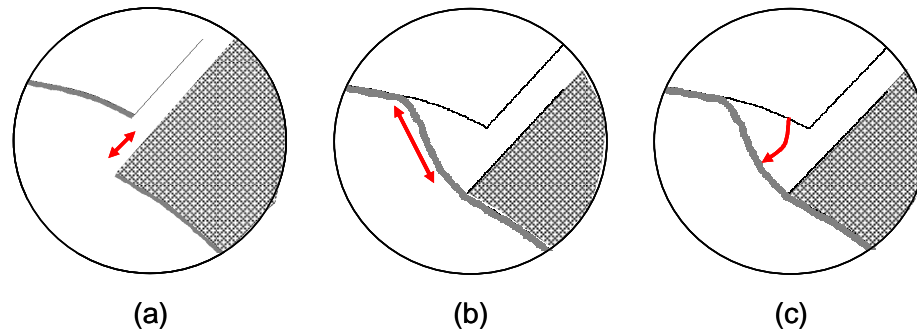


Figure 159: Membrane failure modes; (a) direct shear, (b) direct tension and (c) adhesion loss (after Espley and Kaiser 2002).

All these failure modes assume the membrane support model. The modes do not take into account any penetration of the membrane into the rock discontinuities. Realistically, the failure mechanism will not be based on one property such as adhesion. The failure mechanism will be a function of the mechanical and physical properties of the liner. As described in Section 6.2, a range of polymer products are commercially available. The main constituents of each product have been selected for values of ruling characteristics, e.g. elongation, adhesive strength, tensile strength. Accordingly the behaviour of the material will vary depending on which property has been selected to dominate.

Creep is one failure mechanism that may apply to all membranes. The susceptibility of polymers to creep is well known and well documented in material property handbooks from the 1960s and 70s. Creep is defined by Jastrzebski (1959) as the *“slow and progressive deformation of a material with time under constant stress”*.

He states that polymers *“show high rates of deformation under relatively low stresses and temperatures. This seriously limits the use of plastics for structural purposes, particularly when appreciable stresses may develop or even when there are low stresses at temperatures around 100°C”*.

The polymer industry has undergone rapid development over the last 30 years and it is possible that many of the creep and time dependency issues have been resolved with modern materials. However without testing it is difficult to assess whether this failure mechanism is relevant to membranes.

Tannant (1999b) states that *“one concern with some of the materials currently being evaluated for spray-on support is their long term creep response”*. He suggests using a modified tensile test to evaluate this property, though no actual testing was undertaken.

Kuijpers et al. (2004) suggest that polymer products display a high degree of sensitivity to loading rate data. Testing was conducted at displacement rates between half a millimetre per minute and 10 millimetres per minute to determine the degree of sensitivity.

The cement based products were not expected to be affected by the loading rate and as such were not exposed to the 10mm per minute displacement rate. The polyurethane and acrylic based materials indicated high sensitivity to the rate of loading. Some small-scale creep testing was conducted on the acrylic and polyurethane products and demonstrated a significant decrease in strength over time.

6.5 PREVIOUS TESTING

Many test methods have been established to determine the support capacity of membranes. These tests include small-scale tests and large-scale tests. Small-scale tests (such as adhesion and tensile tests) are used to determine a singular property that is relevant to the product being tested. Large-scale tests (such as the pull plate test and the punch test) attempt to simulate realistic scenarios in order to develop an understanding of the support mechanism or failure mechanisms of the membrane. The large-scale tests often result in multiple interacting mechanisms rather than the single mechanism observed in the small-scale tests.

6.5.1 SMALL-SCALE TESTING

A number of standard material tests have been used to determine the mechanical properties of membranes. Tensile, elongation and adhesion tests are the most common.

Although it is important to determine the mechanical properties of products being used for surface support in mining, for use in confined spaces such as the underground environment, toxicity and flammability also play a major role in product selection. Some plastic materials are known to cause allergic reactions due to exposure (e.g. skin reactions on contact or asthmatic symptoms when inhaled). Some plastic products also have a high flammability rating or release toxic gases as they burn. Due to concerns regarding some of these properties, occupational health and safety (OHS) testing has also been conducted. Due to the high number of non-standard test methods published, it is not possible to discuss all test methods. This thesis will only examine the more common test methods utilised by several authors. This section provides a summary of the more common small-scale test methods.

6.5.1.1 Tensile and elongation testing

Tensile and elongation tests are commonly applied within the materials industry to products such as metals and plastics. ASTM D 638 describes the methodology to be used for testing plastics and has been applied to membranes by Tannant et al. (1999b), Archibald (2001a and 2001b), and Kuijpers et al. (2004).

Sample preparation is undertaken by spreading a thin layer of membrane over a surface and stamping or cutting a dog bone shaped sample using a mould (Figure 160). The length of the sample is dependent upon the thickness e.g. a 4mm thick sample should be between 63 and 115mm long whilst a 14mm sample will be approximately 246mm long. The width is between 19 and 29mm. Table 22 provides sample specifications according to ASTM D 638.

Each end of the sample is clamped grips placed into a displacement controlled test machine as shown in Figure 161.

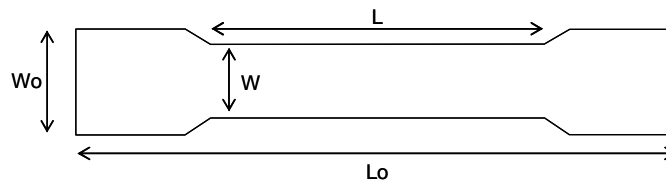


Figure 160: Tensile test sample (dog bone shape).

Table 22: Sample dimensions for various thicknesses. Adapted from ASTM D 638.

Thickness	7mm or under		7 – 14mm	4mm or under	
Sample Type	Type I	Type II	Type III	Type IV	Type V
Lo – Min overall length	165	183	246	115	63.5
Wo – Min overall width	19	19	29	19	9.53
L – Length of test section	57	57	57	33	9.53
W – Width of test section	13	6	19	6	3.8

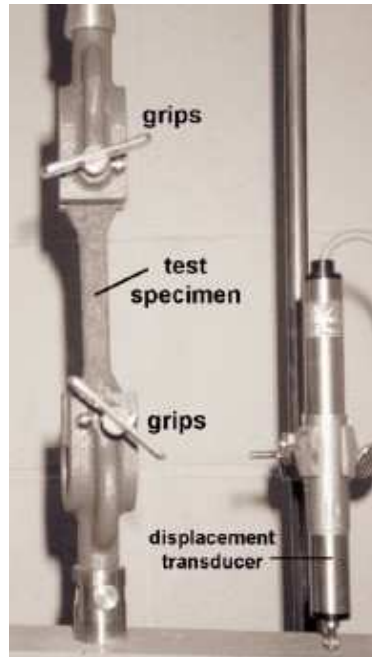


Figure 161: Tensile testing of “dog bone” sample (Tannant et al., 1999b).

The sample grips are pulled apart at a constant rate and the force and displacement are measured. The peak force is used to determine the tensile stress (Equation 8.1) which may be calculated at the yield or break. The displacement is used to determine the elongation as a percentage of the original length (Equation 8.2). The elongation is also calculated at yield or break but is only valid if uniform deformation occurs. If non- uniform deformation such as necking occurs, the results are no longer valid.

$$\sigma_t = \frac{F}{A_o} \quad (6.1)$$

$$\% \text{Elongation} = \frac{L - L_o}{L_o} \times 100 \quad (6.2)$$

The displacement rate is dependent upon the material type. Toper et al. (2003) suggest the loading rates should be varied according to the elongation capacity of the material. Materials with low elongation properties (<10% max elongation) should be displaced at rates between 1 and 6mm per minute. Materials with high elongation properties (>50% max elongation) should be loaded at displacement rates between 6mm/min and 60mm/min.

Kuijpers et al. (2004) also conducted tensile tests on a number of different products using loading rates between 1 and 8mm per second. Two cement based products, two acrylic based products and one polyurethane based product were tested as part of the program. The report shows that performance of the polyurethane based product was highly dependent upon the loading rate whilst the cement and acrylic based products displayed less sensitivity.

6.5.1.2 Adhesion testing

The most common method of testing adhesion involves the pulling of a dolly away from a surface (usually concrete or rock) which has been coated by the test product. The dolly may be glued onto the applied membrane or the membrane may be applied over the dolly and rock surface. The two configurations are given in Figure 162. These methods have been applied by Archibald et al. (1997), Tannant et al. (1999b), Archibald (2001a and 2001b), Ozturk and Tannant (2003), amongst others.

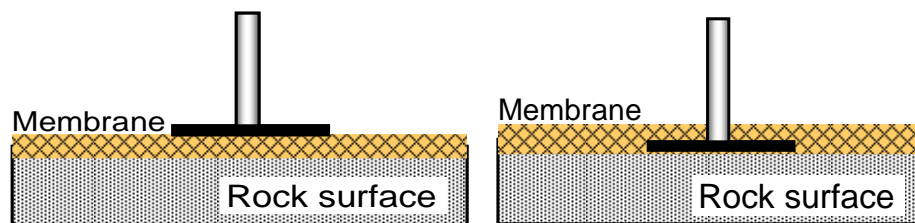


Figure 162: Two variations of the glued dolly adhesion test.

Archibald (2001b) states that *“for most adhesion tests conducted (on membranes), peak bond strengths were generated between 1 and 3mm of displacement”*. He suggests the results may be variable and recommends that a minimum of 10 tests be conducted on each material to overcome the variability. Archibald states that *“the test does not assess typical conditions which may be encountered by spraying onto rock surfaces in-situ”*.

6.5.1.3 Coated cores test

Coated core tests have been used to determine the confining action of membrane products. Tests have been conducted by Finn et al. (1999), Espley et al. (1999) Archibald and Lausch (1999), Archibald and Nichols (2000). The method involves coating a cored rock sample with a membrane layer and subjecting the sample to an unconfined compressive strength (UCS) test. Failed coated and uncoated cores are illustrated in Figure 163. Espley et al. (1999) state that the *“post peak failure response of the coated specimens was non-violent, and the liner was able to absorb some of the stored strain energy”*. Finn et al. (1999) tested coated and uncoated cores of porphyry. The tests demonstrated that *“the uncoated porphyry samples resulted in explosive failure between 300 and 500 kN”*. Mineguard and Everbond were used as coatings on the cores. The coated samples all reached similar peak loads but contained explosive failure of the rock cores. Despite the change in failure mechanism, no change in the ultimate load of the sample was noted by the authors and therefore any confinement benefits cannot be quantified.

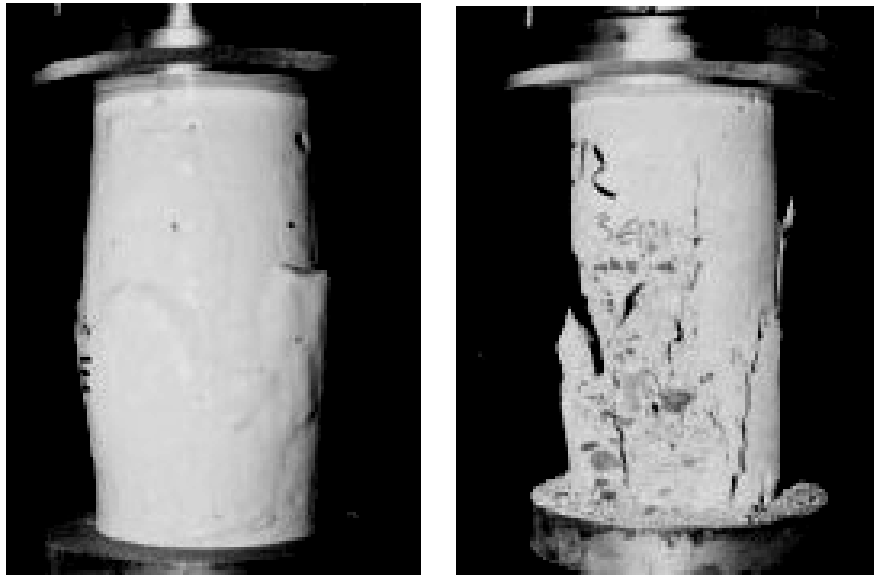


Figure 163: Coated and uncoated cores under compression (Espley et al., 1999).

6.5.1.4 Toxicity tests

The occupational health and safety of operators spraying the products are significant factors in the selection of membrane products. The underground environment is confined and often has low ventilation flows. Schwendeman et al. (1972) suggest that *“the degree of toxic hazard encountered for any system is controlled by the following:*

- *Amount of ventilation at the working space.*
- *Nature of the chemicals used.*
- *Physical form in which the resins are dispensed. A fine spray directed into the air would obviously present more of a problem than a solid stream of liquid or a spray made up of relatively large droplets.*
- *The protective clothing or equipment worn by personnel exposed to the chemical”.*

Schwendeman et al. (1972) summarised the toxicity of the primary polymer candidates identified as being potentially suitable for underground support purposes. This summary is provided in Table 23.

Table 23: Toxicity rating of various polymers (after Schwendeman 1972).

Polymer component	Toxicity	
	Before Cure	After Cure
Epoxy	Slight to high (eye irritant)	Non toxic
Polyester	Moderate (styrene monomer component)	Non toxic
Urethane	Slight to high (isocyanate component)	Non toxic
Phenolic	Slight	Non toxic
Urea – Formaldehyde	Slight to high	Non toxic
Furan	High (eye and skin irritant)	Non toxic
Poly vinyl acetate	Non toxic	Non toxic
Coumarone - Indene	Slight	Non toxic

Research into the toxicity of various products has been conducted by Schwendeman et al. (1972), Archibald et al 1999, Espley – Boudreau (1999) and Finn et al (1999) amongst others.

Some membrane products such as polyurethane contain methylene bisphenyl isocyanate (MDI) which is a known respiratory irritant. Most regulatory bodies specify exposure limits for MDI. The US National Institute for Occupational Health and Safety (NIOSH) specifies a maximum concentration of $75\text{mg}/\text{m}^3$ as being immediately dangerous to life or health. Research conducted by Espley-Boudreau (1999) indicated that MDI were detectable up to 120m away from the spray site, though the highest concentrations were within 20m of the spray site.

In order to reduce exposure to MDI's Finn et al. (1999) proposed the spraying operators (and other personnel entering the area) use full-faced positive pressure breathing apparatus. Water curtains were also used "down wind" of the spraying site to "*neutralise any products in the air stream*" and appeared to be effective in dissipating concentrations of MDI's.

6.5.1.5 Flammability tests

Flammability is also an important consideration in the selection of membrane products. There are a considerable number of fire sources within the confines of the underground environment. Therefore, the susceptibility of the material to ignite, to spread fire and the fumes produced as a result of burning are particularly important. Schwendeman et al. (1972) assessed the flammability of the same polymer candidates tested for toxicity. The results are given in Table 24.

Table 24: Flammability rating of polymer components (after Schwendeman et al., 1972).

Polymer component	Flammability	
	Before Cure	After Cure
Epoxy	Flammable (flash point $>79.4^{\circ}\text{C}$)	Self - extinguishing
Polyester*	Flammable*	Flammable
Urethane	Slow burning	Slow burning, Self extinguishing
Phenolic	Non - flammable	Non - flammable
Urea – Formaldehyde	Non - flammable	Non - flammable
Furan	Flammable	Non - burning
Poly vinyl acetate	Flammable	Flammable
Coumarone - Indene	Flammable	Flammable

*There are also a number of fire resistant grades of polyester

The flammability of four commercial products was tested by Archibald (2001b). He found that three of the four products (Mineguard, Everbond and Rockweb) were self-extinguishing but the fourth product (Masterseal) was able to maintain a flame once the source was removed. Given that the active ingredient for Masterseal is vinyl acetate, the results correspond to the findings produced by Schwendeman et al.

6.5.1.6 Discussion of test methods

Small-scales tests are most beneficial when providing useful data for quality control or product development but do not provide an understanding of the overall support mechanism of membranes. The test methods described above are not performed using realistic loading mechanisms nor do they assess realistic failure mechanisms. Small-scale test results should not be used to justify the support capacity of any product.

As seen from shotcrete testing (Section 5.3), one property is not enough to determine the overall effectiveness of a product in the provision of areal support. Some confusion exists over which property is regarded as the most essential for determining the support capacity of a membrane. Some literature suggests that high tensile strength is critical in membrane products whilst others suggest high shear strength and good adhesion are required. In reality, the support mechanisms are very complex. Often a good rating in one category is counteractive to the performance in another category (e.g. high shear strength is counteractive to high elongation). Therefore, the effectiveness of a membrane product should not be based solely on property alone but rather a combination of properties.

6.5.2 LARGE-SCALE TESTING

As described in Section 6.3 and 6.4, membranes often rely on a number of parameters to provide support and accordingly a number of large-scale test methods have been established to better reflect the action of the membrane in providing support.

As with the small-scale testing, many non-standard large-scale tests have been published. Due to the high number of different test methods, this thesis only describes test methods applied by more than one author.

6.5.2.1 *Pull plate testing*

This method uses the same principles as the adhesion testing described in Section 6.5.1.2. The coating is applied over the enlarged dolly rather than having the dolly glued to the membrane as in the small-scale tests. This method, provided in Figure 164, has been used by Finn et al. (1999), Tannant et al. (1999b) and Archibald (2001a and 2001b).

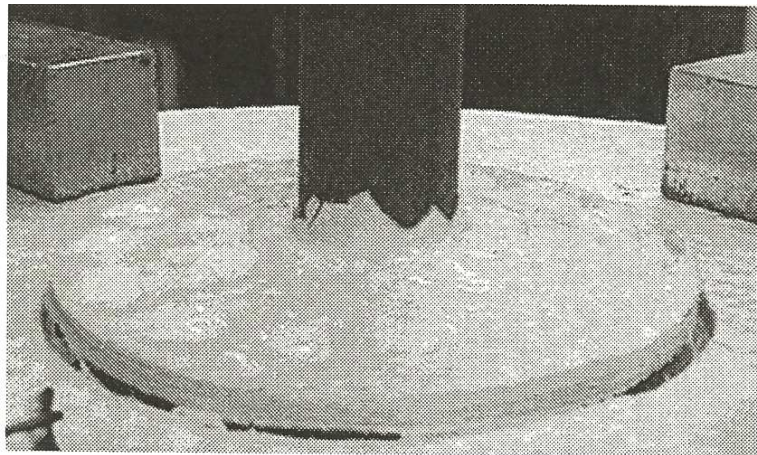


Figure 164: Pull plate test (Archibald 2001a).

The shear strength is determined using the following equation:

$$\tau = \frac{F_p}{A} \quad (6.3)$$

where:

- F_p is the peak force
- A is the area of the shear failure surface calculated by multiplying the circumference of the loading plate (C) by the thickness of the membrane layer (t) ($A = Ct$)

Finn et al. (1999) conducted tests on two types of materials; namely, Mineguard and Everbond. They used various sized, loading plates, between 100mm and 1000mm square, that were pulled through the material as illustrated in Figure 165.

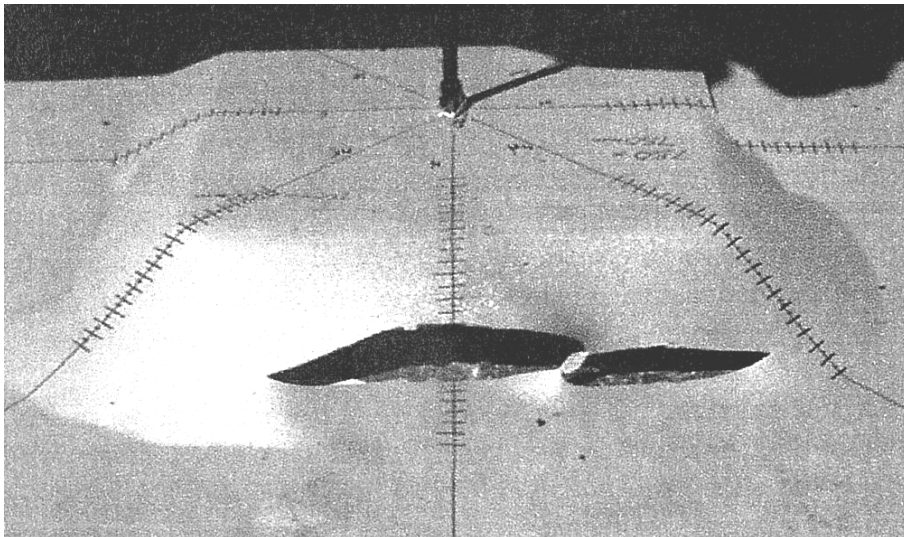


Figure 165: Large-scale pull test (Finn 2001).

The failure mechanism of the Mineguard was characterized by an initial stiff reaction, followed by a period of plastic deformation (with associated adhesion loss). Ultimate failure occurred after complete adhesion loss.

The failure modes for the Everbond tests were similar to those observed in the Mineguard tests but the tensile strength of Everbond was less than Mineguard and the ultimate failure mechanism was tensile failure of the material. Everbond was observed to reach lower peak forces than Mineguard.

6.5.2.2 *Punch testing*

This method involves the spraying of the sample over a concrete slab with a moveable disc cut into the centre of the slab. The basic concept is shown schematically in Figure 166.

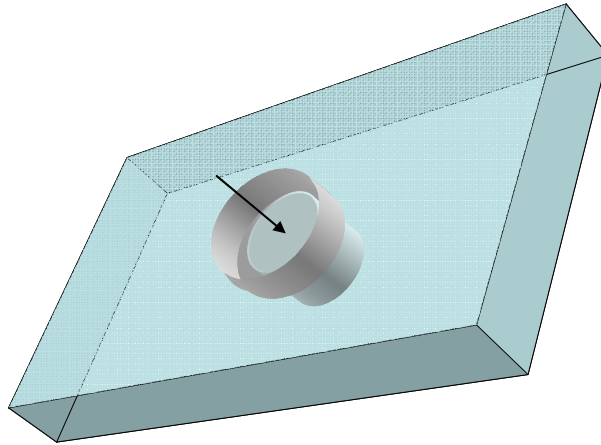


Figure 166: Punch test concept.

This method has been described by Spearing et al. (2001) who used dimensions 610mm x 610mm with a loading area of approximately 100mm in diameter, and Kuijpers (2001) who used natural rock slabs of dimensions of 200mm x 200mm with a 51mm diameter moveable disc.

Kuijpers describes a similar failure mechanism to that described in the previous section by Finn et al. (1999). That is, the reaction could be characterised by an initial stiff reaction followed by elongation and progressive adhesion loss.

Kuijpers also modified the punch plate method to use a completely solid panel rather than having a free moving disc cut into the centre of the panel. The panel was coated over its entire area and loaded over a 100mm square area (Figure 167).

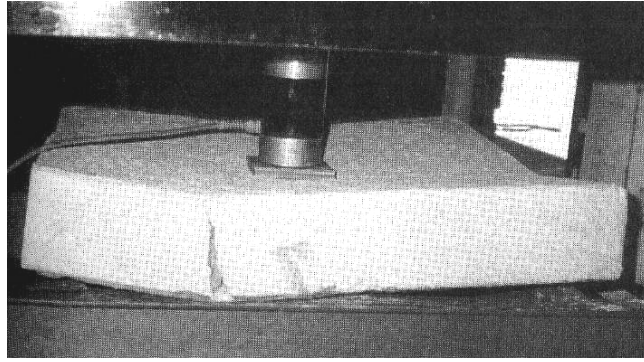


Figure 167: Coated panel test (Kuijpers 2001).

The results showed that blocks coated in membrane had “a three fold increase in energy absorption capability” compared with the uncoated blocks. This leads to the conclusion that the membranes do provide support through an increase in confinement. One of the limitations of this method is that the load capacity of the membrane cannot be separated from the total sample strength.

6.5.2.3 Simulated rock surface testing

This method tries to simulate the beam loading mechanism. It was originally developed by Gyenge and Coates (1972) who used pavers to simulate the rock surface. The membrane is sprayed over the pavers and the centre of the sample is loaded. A test setup is provided in Figure 168. This methodology was also used by Finn et al. (1999), Tannant (described by Espley et al., 1999) and Kuijpers (2001).

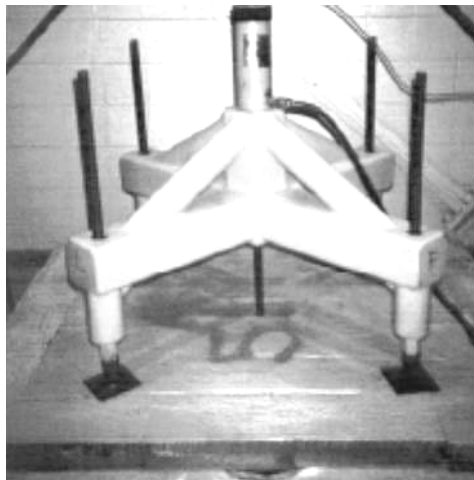


Figure 168: Coated paver test setup (Espley et al., 1999).

Finn's attempts to use this method were largely unsuccessful. Tannant (Espley et al., 1999) concluded that *"polyurethane coatings are capable of supporting the same load as #6 gauge (approx 4.8mm) or even #4 gauge (approx 5.8mm) welded wire mesh as long as a continuous membrane of sufficient thickness is created"*. Further to this, Espley et al. note that *"thin spray-on membranes cannot effectively fill in or bridge across wide open fractures in the rock. Mineguard appears to be limited to bridging gaps less than 5mm wide"*. It is stated that *"the membrane is able to enhance the interaction between the various blocks of coated rock and thus a significant portion of the supporting function arises from the block to block interaction"*. It is difficult to determine quantitative results from this method as a portion of the forces are being absorbed by the blocks rather than being imparted on the membrane. Only qualitative assessments were provided. Tannant observed crushing of the blocks over the central portion of the test indicating that the portion of forces absorbed by the blocks may be significant.

Kuijpers found that *"the coating (Evermine) prevented the dislodgement of blocks under gravitational conditions but the resistance to external loading was limited"*. He suggests the reaction was *"contradictory to theoretical considerations and requires further investigation"*.

A variation on this test was developed by Swan and Henderson (1999), who developed a test utilising the waste rock from the mine site to simulate the underground loading scenario. A steel frame was filled with 100mm rock fragments (Figure 169). The membrane was sprayed over the surface and tested using a large hydraulic jack. The sample size was 1.1m x 1.1m. The capacity of a 6mm liner of Tekflex using this method was 2.4 tonnes after 8 hours. Deformation at rupture was between 35 and 65mm.

This method has also been described by Tarr et al. (2006); however the results appear to be inconclusive.



Figure 169: Box of rocks test set-up (Tarr et al., 2006).

6.5.2.4 Discussion of test methods

Each of the test methods described attempt to replicate the complex loading scenarios experienced in the field. The numerical values of strength achieved from these tests only have relevance to the individual method and therefore the results from different tests cannot be compared.

6.6 ANALYSIS METHODS

There have been limited attempts to determine the support reaction of membranes. Most analysis techniques have relied up modelling to replicate the support reaction (e.g. Kuijpers and Topper (2003), Wang et al. (2004), Mason and Stacey (2008))

Tannant (2001b) uses a complex failure mechanism (Figure 170) to determine the tensile strengths and displacement limits of the membrane. The formulas generated from this diagram are complex and not well define and so have not been reproduced here.

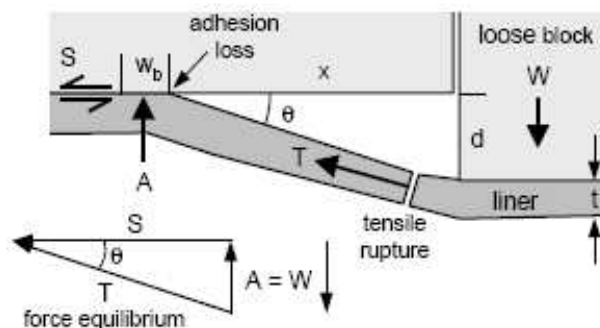


Figure 170: Force diagram explaining failure mechanism of membranes (Tannant 2001b).

As discussed in Section 6.4 the failure mechanisms of membranes are usually very complex and often comprise of more than one mode of failure. The failure mechanism is also dependent upon the properties of the membrane; consequently, the simplified model proposed by Tannant is unlikely to be relevant.

6.7 WASM MEMBRANE TESTING

The purpose of the WASM membrane test program was to develop a test arrangement that would test membranes under realistic loading conditions and determine the capacity of membrane liners. Only one product was used to develop the test methods. The product tested is commercially available within Australia.

Two different test methods were applied to the membrane product. The different tests were used to determine the ability of the product to provide support using the different models described in Section 6.3; namely, the beam model and the membrane model.

The first test method applied the beam principle to the product to determine its performance characteristics. The test method involved spraying the membrane over a bed of interlocked pavers and applying load to determine the force and displacement response characteristics of the product. A review of the ability of the product to bridge cracks, and the penetration of the product into the cracks was completed after the test to determine its potential interlocking abilities.

The second test method used the membrane model. The punch test method used for shotcrete testing was also applied to the membrane to determine the product's ability to resist punching loads. This method involves spraying the product over a simulated rock surface (substrate). The sample was then loaded in the centre of the sample.

Both methods are described in detail below.

6.7.1 PAVER TEST - BEAM MODEL

Pavers were selected as a base for the initial test program as it was thought that they would provide a reasonable representation of highly jointed rock mass conditions. Zigzag edged pavers were selected to prevent a preferential failure plane forming along the interface of the pavers. It was also thought that the shape would allow for more interlock between the pavers to result in a more uniform load transfer over the area of the sample.

Two tests were conducted using the paver test beam model.

The pavers were laid out onto a 1.6m x 1.6m square wooden pallet. The size of the pavers resulted in a sample size of 1.55m x 1.55m (Figure 171). Steel strapping was wrapped around the edge of the pavers and tensioned to provide lateral constraint.

The pavers were sprayed with water to prevent excess water being drawn from the product. The product was prepared by the manufacturer's representative using the manufacturing company's large-scale equipment. The membrane was then sprayed onto the pavers (Figure 172).



Figure 171: Pavers setup ready to be used as a base for the membrane.



Figure 172: Spraying of the pavers.

The samples were left undisturbed for 24 hours and then moved indoors. The samples were cured at room temperature for 7 days.

Testing was undertaken using the following methodology:

1. The sample was attached to the pallet using a face plate and threaded rods (Figure 173).
2. The sample was rotated using a forklift such that the sample was on the base and the pallet was on top (Figure 174).



Figure 173: Face plate and planks on top of sample ready for rotation.



Figure 174: Sample rotation in progress.

3. The sample was placed on the testing frame and the nuts on the threaded bar were undone to allow the face plate to drop to the floor.
4. The wooden pallet was removed from the sample leaving the sample and pavers resting on the main test frame (Figure 175). A clamping frame was placed over the edges of the pavers and clamps were wound down on each corner to provide restraint around the boundary of the sample (Figure 176).



Figure 175: Sample after pallet has been removed.



Figure 176: Sample setup with LVDT's and clamping frame in place.

The instrumentation setup has been described in Section 3.4 and testing was undertaken with the displacement rate set at 4mm per minute.

The test was continued until the sample was considered to have failed. In some cases testing was continued beyond failure of the membrane material in order to assess the reaction of the pavers.

It should be noted that at the time of the first test, the instrumentation for data collection had not been fully commissioned and was not used during the test. Central deformation was recorded by marking the jack extension at the start of the test and measuring the change in extension at regular intervals. The force was recorded from the load cell readout unit attached to the load cell.

6.7.2 PUNCH TEST - MEMBRANE MODEL

The punch test method was also used for the testing of shotcrete and has been described in Section 5.8. The method involved the spraying of the test sample over a rough substrate of dimensions 1.5m x 1.5m. The substrate comprised of a 40mm thick solid sandstone slab with a pre-cut, free moving disc in the centre to allow loading of the sample. The disc was drilled using a 500mm core bit as described in Section 5.8.1.

The substrates were rotated to approximately 60 degrees to allow better compaction and more realistic spraying conditions.

The samples were first sprayed with water and then sprayed with the membrane (Figure 177). Immediately after spraying, the thickness of the membrane was measured using a small probe on the end of digital callipers (Figure 178).



Figure 177: Membrane spraying.



Figure 178: Measurement of sample thickness.

The samples were placed directly into a modified sea container (Figure 179) where humidity and temperature were controlled. The humidity was set at 70% and the temperature was set to 26°C to reflect conditions in an underground environment. Curing was undertaken for 7 to 8 days prior to testing.



Figure 179: Sprayed samples in curing chamber.

The test methodology and the instrumentation setup was the same as for shotcrete testing as detailed in Section 3.4.

6.8 RESULTS

Summary report sheets for each test can be seen in Appendix 9.

The loading rate of 4mm per minute was used for both membrane test methods to enable the comparison of results and to enable the comparison of the test results with the shotcrete test results. Different results may have been achieved if different loading rates were applied; this is beyond the scope of this project.

6.8.1 PAVER TEST RESULTS

During the spraying of the first panel, a consistent surface was not achieved at the design thickness of 3mm. The sample thickness was built up to bridge the gaps between the pavers (which were between 3 and 10mm in width). The final thickness of the sample was 10mm. In order to assess the performance of the membrane at the recommended thickness, the second sample was sprayed to 3mm despite a consistent layer not being achieved. Some of the larger gaps were up to 7mm wide (Figure 180). These were labelled and photographed prior to testing.

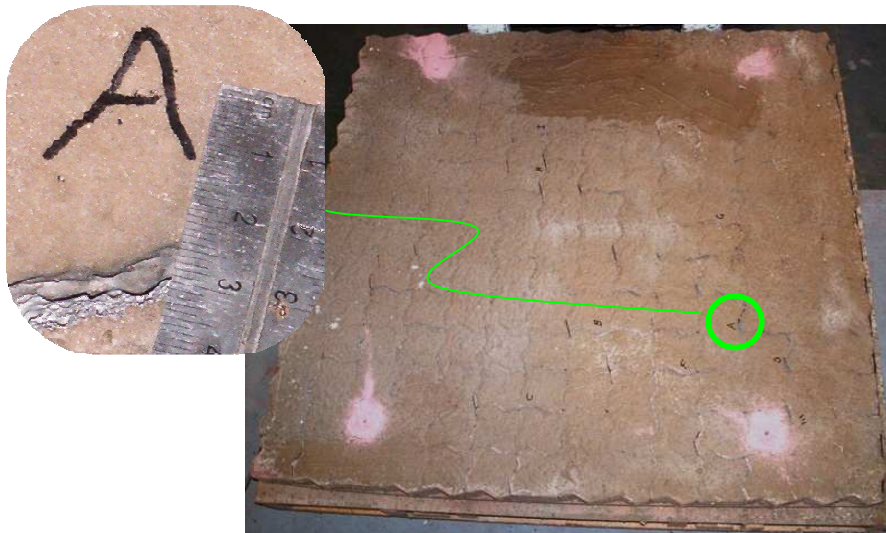


Figure 180: The gaps in the membrane measured up to 7mm.

During the first test (TT001), audible noise attributed to creep of the sample was noted prior to positioning the clamping frame. Once the clamping frame was in place, the audible creep subsided. This audible creep was not observed in the second test.

The force - displacement results for the two tests are given in Figure 181. The difference in peak force between the two tests was 3kN and can be attributed to the differences in thickness of the samples. The total reaction curves for both tests are remarkably similar although it is likely that this can be attributed to the reaction mechanism of the interlocking pavers.

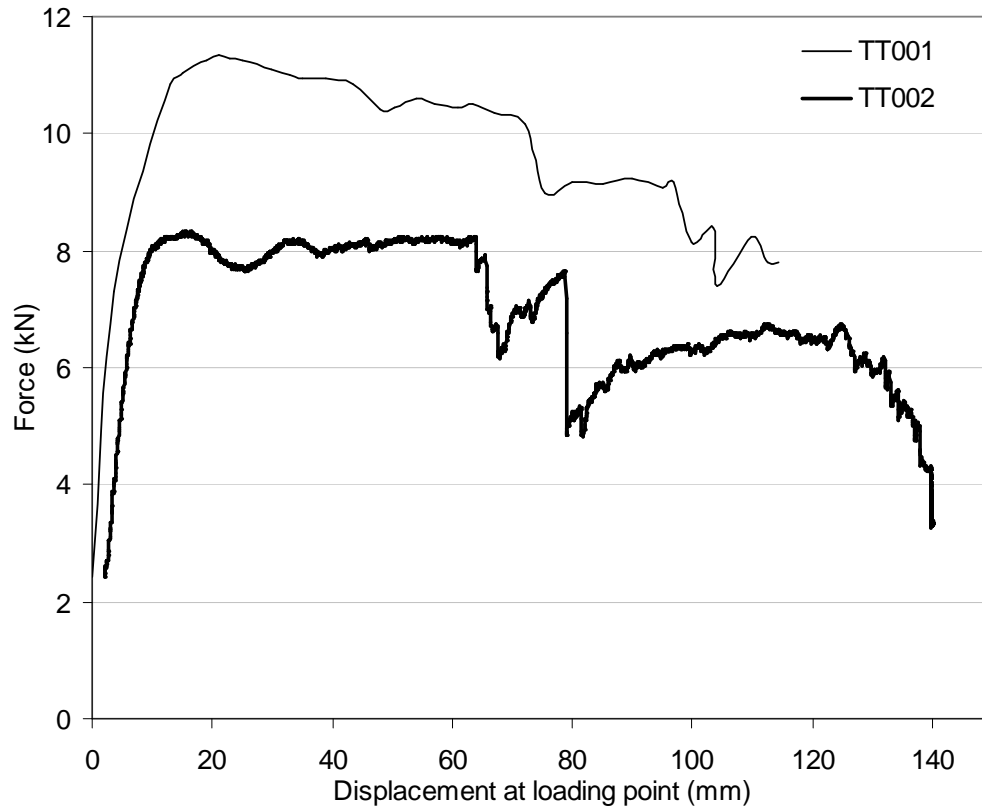


Figure 181: Force – displacement results for the paver test method.

The tests were continued until it was deemed that the membrane was no longer contributing to the reaction to loading. After the first test had been completed, two pavers fell out of the sample. This was attributed to time dependent behaviour. The failure mechanism for both tests was shear failure (Figure 182). No adhesion loss was observed and the elastic deformation of the material appeared to be minimal.

Some penetration of the membrane through the gaps in the pavers was noted. However, during the test, it was established that there was not enough membrane to bond the pavers together and provide any substantial resistance to loading.



Figure 182: Shear failure of the sample.

During the testing it was identified that the interlock of the pavers was contributing to the force - displacement response of the sample. Observations indicated that to allow significant displacements, the pavers needed to rotate and the sharp edges of the pavers interlocked as illustrated in Figure 183. The pavers were observed to crush at the points of compression (Figure 184).

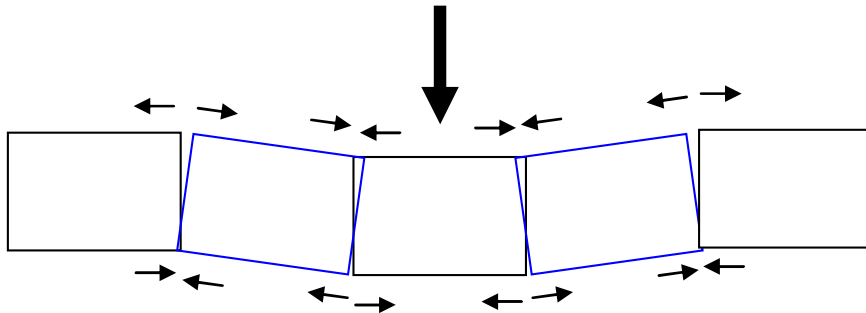


Figure 183: Deformation of the sample results in the pavers going into compression and tension.

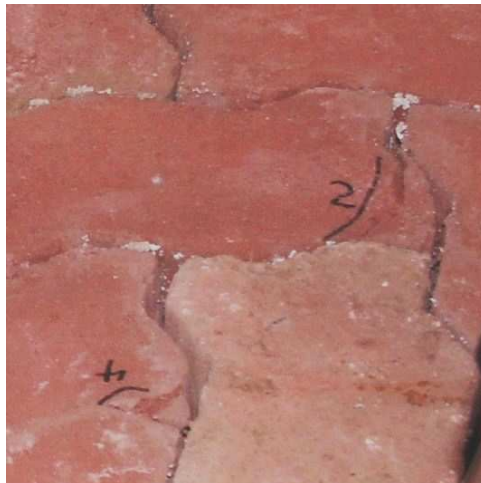


Figure 184: Cracking in pavers.

In an attempt to determine the effect of the pavers on the force - displacement responses, an uncoated paver test was conducted. All steps described in Section 6.7 were followed except Step 2 (the spraying of the membrane). Figure 185 shows the strapping around the edge of the pavers and the faceplate holding the pavers in place during the rotation process (Step 4). It is important to note that even though the face plate did not cover the entire surface area of the pavers, no pavers dislodged during the rotation process (Step 4).



Figure 185: Flipping of paver pallet.

The pavers were placed on the testing frame in the same manner as the coated paver tests (Step 5). As the nuts holding the faceplate in position were loosened, the pavers started to dislodge. As the face plate fell away, 29 pavers also dropped (Figure 186).



Figure 186: Failure of uncoated pavers once face plate had been removed.

This process was repeated to ensure that the failure of the pavers was not related to the test setup process. This second test showed similar results to the first test.

Although some creep was audible in the coated paver tests, no pavers dislodged during the test setup. As the pavers dislodged during the test setup of the uncoated pavers it can be assumed that the membrane was transferring some load prior to test commencement. Figure 186 shows that some pavers remained in place during the uncoated test. Consequently, the load contribution of the pavers prior to the test commencing cannot be determined with any confidence.

For analysis purposes it has been assumed that all the pavers not being supported by the frame are contributing to the load on the membrane. The weight of the pavers not supported by the frame (225kg) has been incorporated into the results provided in Figure 181.

6.8.2 PUNCH TEST RESULTS

The approximate membrane thicknesses for the punch test method are displayed in Table 25.

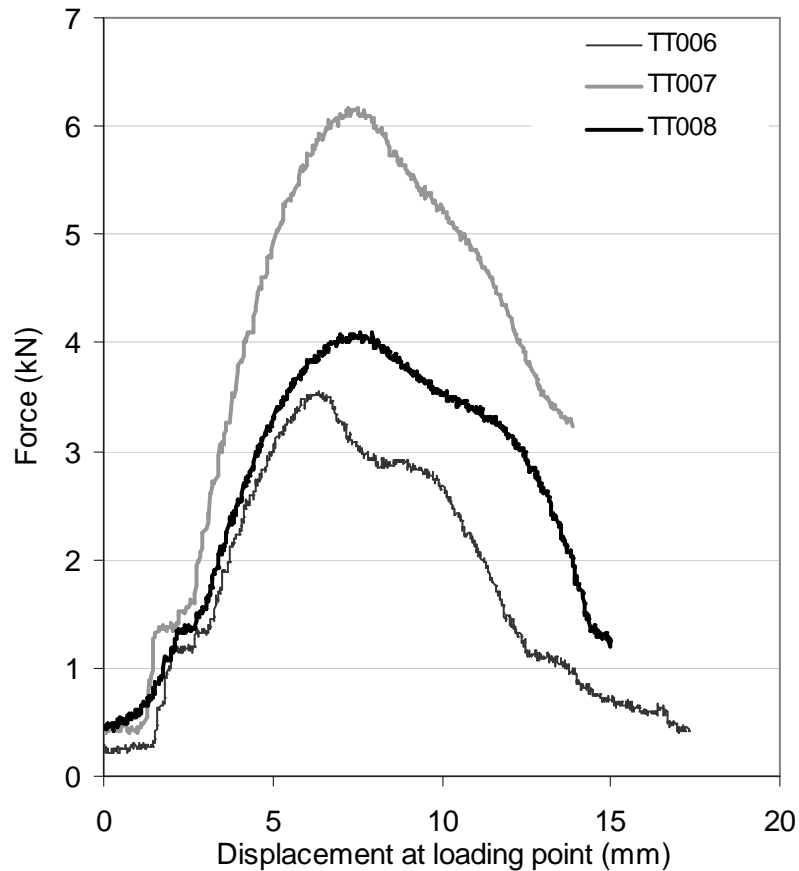
A summary of the force and displacement results is given in Table 26 with the force-displacement curves provided in Figure 187. Visible cracks were observed on the face of the samples very early in the tests. Unlike the shotcrete and mesh, the cracking did not correspond to a clear peak force followed by any significant drop in the force. The force - displacement response was more curved. This is likely to be attributed to a yielding failure mechanism rather than a brittle failure mechanism. As a clear rupture point could not be determined from the force – displacement response, the peak force has been used for analysis purposes.

Table 25: Average thickness of each membrane test.

Test Number	Average Thickness
TT001	6.28mm
TT002	4.45mm
TT003	5.68mm

Table 26: Summary of Punch Test results.

Test Number	Thickness (mm)	Peak force (kN)	Displacement at peak force (mm)
TT006	7	3.6	6
TT007	5	6.2	7
TT008	6	4.1	8

**Figure 187: Force - displacement results.**

The force – displacement results clearly show that the displacement capacity of the membrane is minimal. This is in contradiction to the product data sheet which states that this product can be applied in “*areas where large deformations are expected*”.

The peak force is less than 10kN in all cases, suggesting that this product is only suitable for application as a small block stabiliser in low stress environment where low loading conditions are expected. Figure 188 shows the relationship between peak force and the thickness of the material. It can be clearly seen that there is a reduction in the force capacity of the material as thickness increases. This may be attributed to the characteristics of the material and in particular to its cement content. At thin thicknesses, the polymer material is the dominant material and its flexible properties dominate the product performance. As the thickness of the layer increases the cement becomes the dominant material component; this results in an increase in the stiffness of the material and it cannot sustain the tensile strain.

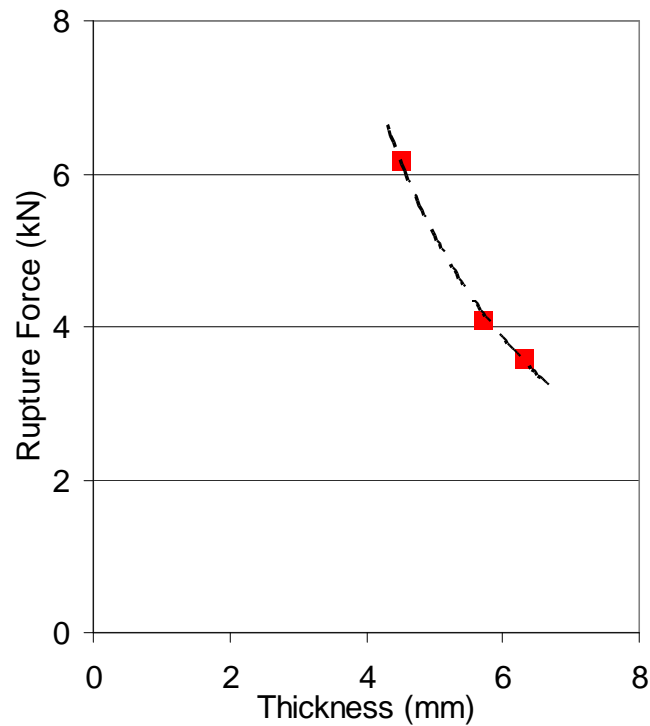


Figure 188: Peak force and thickness relationship for punch test method.

All three tests displayed tensile material failure as the predominant failure mechanism. No adhesion loss and only a small amount of elastic deformation were observed. This was in contradiction to the manufacturers' expected failure mechanism. The sample displayed no obvious signs of load transfer away from the immediate load area (i.e. around the disc) to outer areas of the substrate. Tests were continued until the loading disc had pushed through approximately half the circumference of the disc (Figure 189).

Tests TT006 and TT008 were left on the frame after testing. Although only a partial portion of circumference of the disc had been failed, after a period (1 hour for Test TT006 and approximately 7 days for Test TT008) the discs dislodged from the sample. The load on the membrane at the time of complete failure was approximately 40kg. TT007 was removed from the test frame immediately after testing and therefore its time dependency could not be assessed.



Figure 189: Test TT008 at the completion of the test.



Figure 190: The punch disc after failure.

6.8.3 COMPARISON OF THE TEST METHODS

Figure 191 shows the difference in the force-displacement results between a paver test and a punch test with a similar membrane thickness (3mm). The displacement scale on the chart has been limited for clarity, but still shows the considerable difference in displacement capacity between the two tests. The extended displacement observed within the paver test is believed to be a function of the paver interlock. The load is transferred around the paver base through the pavers allowing for higher deformations of the entire substrate than would otherwise be expected.

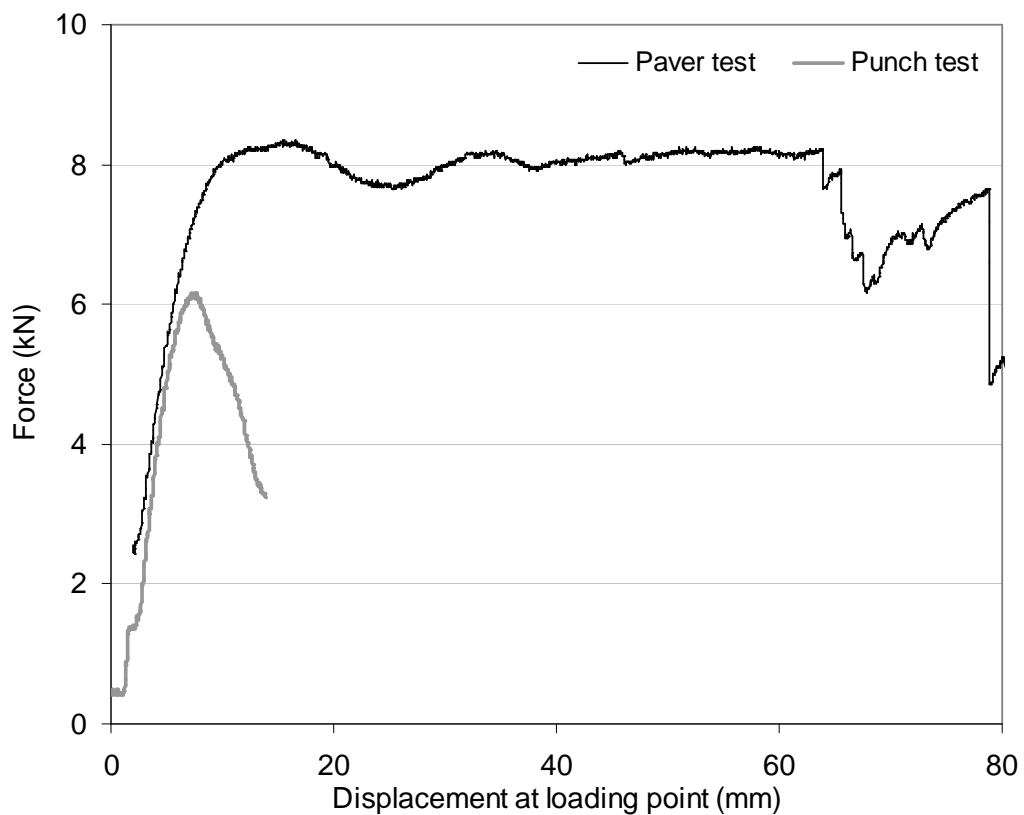


Figure 191: Comparison of Paver test results and Punch test results.

6.9 DISCUSSION

Although only a limited number of tests were conducted, a number of relevant observations were recorded regarding the behaviour of the product being tested.

Neither test method was conclusive in determining the support capacity of the membrane product tested; however the punch test results clearly indicate that the load capacity of the membrane under discrete loading conditions is minimal and it is questionable as to whether there is value in using the product for ground support applications where these conditions occur.

The limited displacement capacity of the membrane also indicates that the product has limited applications. It is not recommended that this product be used in areas of large deformation or in high stress environments as claimed in the product data sheet.

Contrary to the product data sheet claims, the product does not have the capacity to replace mesh or even thin layers of shotcrete. This is discussed further in Chapter 7.

The product did not have the capacity to bridge large cracks nor did it extensively penetrate into the cracks between the pavers. This greatly limits the application of the product in mining applications where the rock mass often has cracks much greater than the 7 – 10mm cracks simulated in the testing.

The contradiction of observed failure mechanisms from our testing and the current generic membrane failure mechanism indicates that further work is required by the manufacturer to assess the failure mechanism.

The time dependent failures observed in the punch test are crucial to the understanding of the product and bring into question the safety of this product as a surface support element. No significant research has been undertaken in this area despite in the opinion of the author; this area poses the greatest risk to the viability of any membrane product as a surface support element.

CHAPTER 7 COMPARISON OF MATERIALS

A comparison of mesh, shotcrete and membrane performance is shown in Figure 192. All samples had an unconfined area of 1.3m x 1.3m.

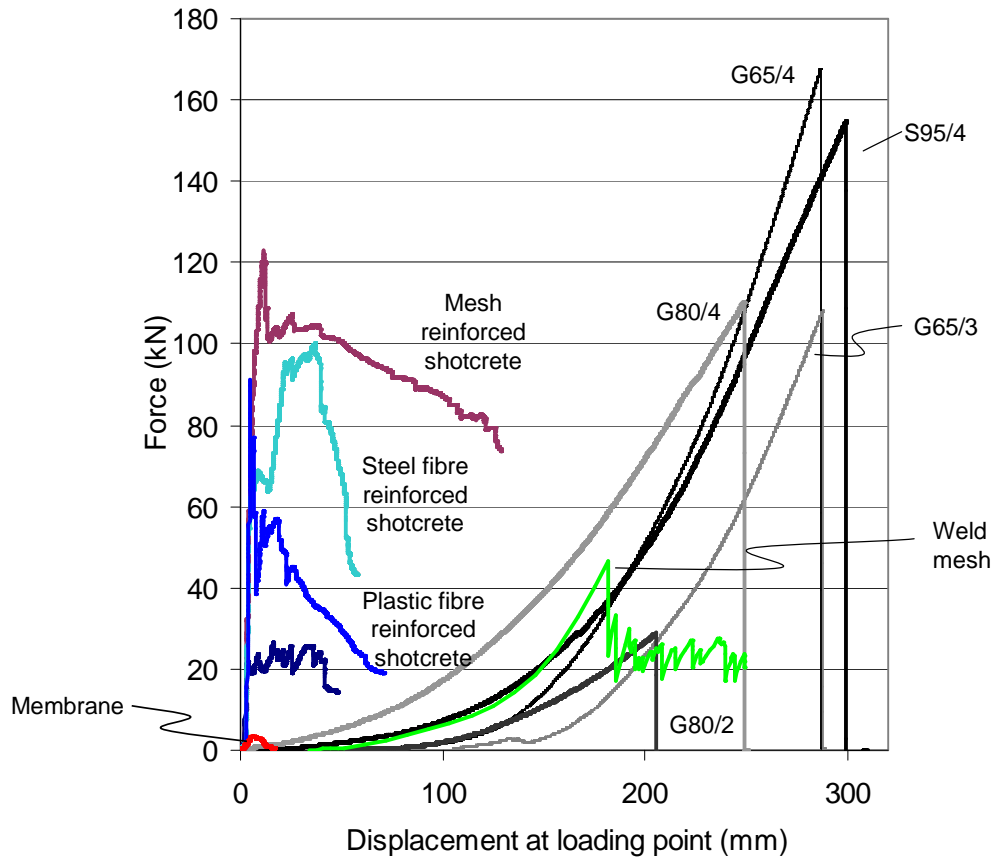


Figure 192: Comparison of surface support elements.

The membrane product tested exhibited significantly less force and displacement capacity than both shotcrete and mesh and as such is not recommended to replace mesh or shotcrete under static loading conditions as suggested in the product data sheet.

Fibre reinforced shotcrete behaves very stiffly; reacting immediately to loading, but its displacement capacity was limited to approximately 80mm.

This is in stark contrast to mesh, whereby the force developed slowly in response to displacement; however, the overall displacement capacity of mesh was significantly higher than that of shotcrete.

Mesh reinforced shotcrete also behaved stiffly, but unlike fibre reinforced shotcrete, the forces were maintained over much greater displacements. The displacement capacity of mesh reinforced shotcrete was almost equivalent to that of mesh; although further testing is required to confirm the results.

Energy absorption capacity is commonly used to evaluate shotcrete. It has been evaluated at rupture and also calculated for the entire test.

Fibre reinforced shotcrete ruptured at less than 0.2kJ, independent of the fibre type. The total capacity of fibre reinforced shotcrete is between 2.5kJ and 4.5kJ, depending on the length of the test and thickness of the layer.

Mesh reinforced shotcrete ruptured at 0.7kJ and the overall energy absorption capacity was 11.9kJ.

Energy absorption capacity can also be calculated for mesh. As with shotcrete, it is determined by calculating the area under the force – displacement curve (Figure 193). Figure 194 provides a summary of the rupture energy capacities of the various mesh types.

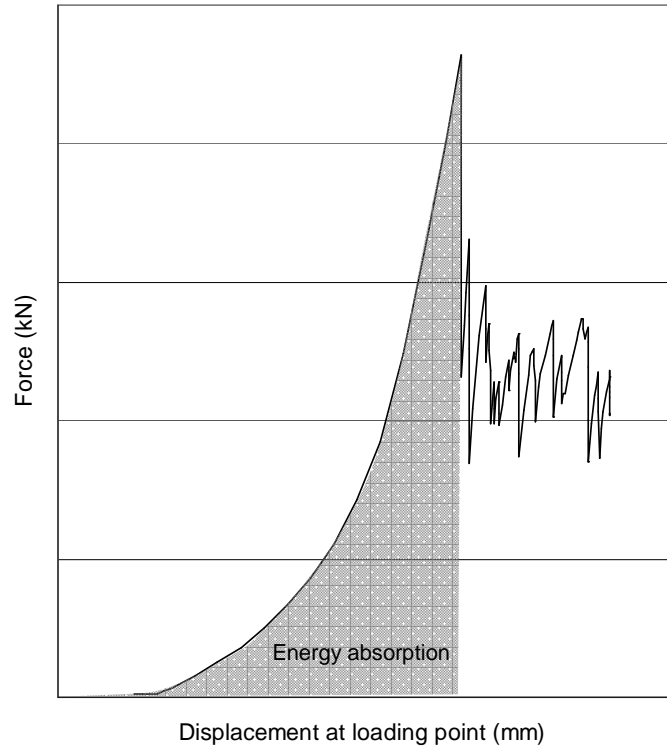


Figure 193: Typical force – displacement curve with energy shown as the shaded area.

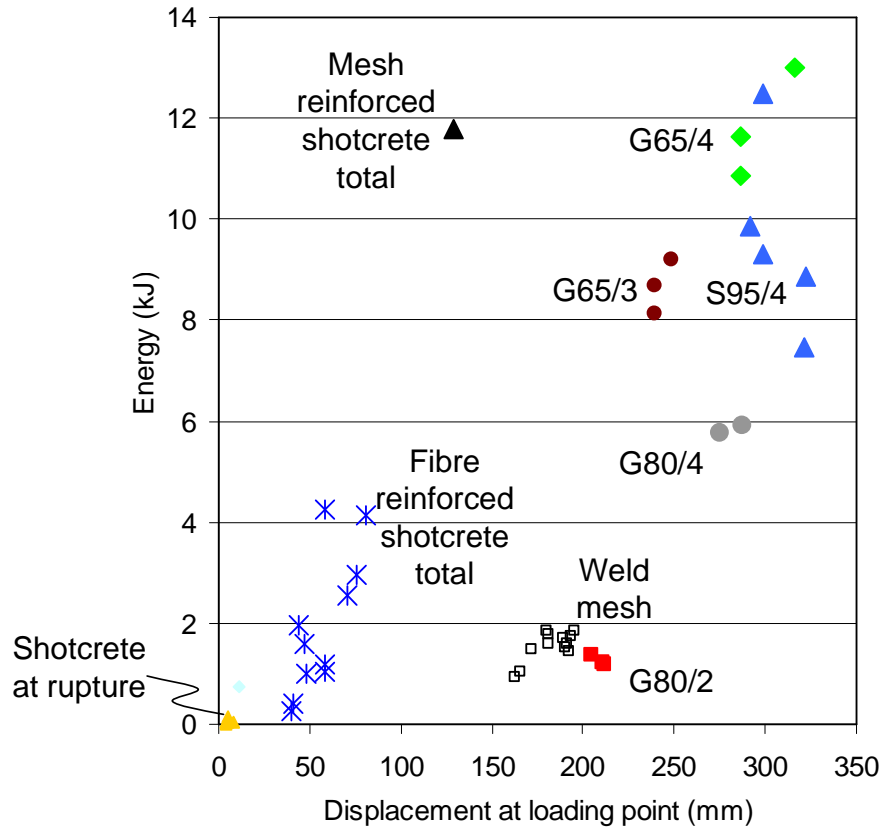


Figure 194: Energy absorption capacities of various mesh types at rupture and shotcrete.

The energy absorption capacity of weld mesh at rupture is 1.5kJ. The total energy absorption capacity for weld mesh is dependent on the test length and is not considered representative.

The energy absorption capacity of high tensile chain link mesh is dependent on the wire diameter and the diamond configuration. Table 27 provides the average rupture energy absorption capacities for each of the chain link mesh types.

Table 27: Average energy absorption capacity of chain link mesh at rupture.

Chain link mesh type	Average energy absorption capacity at rupture (kJ)
S95/4	9.6
G65/4	11.8
G80/4	8.7
G65/3	5.8
G80/2	1.3

Due to the failure mechanism of the high tensile chain link mesh, the tests were stopped immediately after rupture; consequently, the energy absorption capacity at rupture is equal to the total energy absorption capacity.

The results clearly show that the average energy absorption capacity of all mesh types at rupture is much greater than that of fibre reinforced shotcrete at rupture, independent of whether fibres or mesh are used as reinforcing.

The total energy absorption capacity of fibre reinforced shotcrete can be greater than weld mesh depending on the thickness of the layer; however it cannot match the energy absorption capacity of high tensile chain link mesh. Mesh reinforced shotcrete has a high total energy absorption capacity, exceeding the capacity of weld mesh, even though weld mesh was used as the reinforcing material in the shotcrete.

CHAPTER 8 CONCLUDING REMARKS

Detailed discussions of the results of each material tested have been provided in the relevant sections.

The test results demonstrated that the force - displacement response of mesh, shotcrete and the membrane product is different. The force – displacement response of both weld mesh and chain link mesh has been shown to be non-linear and can be approximated using a third order polynomial relationship. The reaction begins with an initial bedding and force redistribution phase which absorbs the lack of tension within the boundary restraints and the mesh wires. Up to 80% of the displacement capacity of mesh occurs within these two phases. Force distribution around a weld mesh sheet begins with the directly loaded wires and continues to the periphery areas as the test progresses. Failure typically occurs on a directly loaded wire. Three failure mechanisms were observed; namely, weld failure, failure through the heat affected zone and wire failure. The failure mechanism and the rupture force are highly dependent on the manufacturing quality. Poor manufacturing standards result in weld failure at low forces.

Testing of various weld mesh configurations demonstrated that the weakest point within a mesh support system is at the over lap between meshing sheets. Force capacity at the overlap was shown to be significantly less than within the internal area of the mesh. The overlap can be improved by using a connection device between the two sheets. Further research is required to identify and adequate restraint system that satisfies industry requirements.

High tensile chain link mesh has a much higher capacity than the equivalent diameter weld mesh. The forces within chain link mesh are transferred diagonally across the wires rather than laterally along the wires as is the case with weld mesh. Chain link mesh typically occurs at a link. The post failure progression was not able to be determined using the WASM test method.

Current analysis techniques for both mesh types assume linear behaviour of the mesh; consequently these methods are unreliable as design tools. Further work is required in developing an appropriate design tool for mesh systems.

Shotcrete is characterised by a high initial stiffness; however, without mesh reinforcing, it has limited displacement capacity.

Rupture of fibre reinforced shotcrete generally occurs at less than 5mm of displacement. The rupture force of fibre reinforced shotcrete is dependent on the mix design and the thickness of the layer. The overall displacement capacity of fibre reinforced shotcrete is generally less than 100mm independent of the fibre type. The failure mechanism is complex and usually comprises a combination of adhesion loss and flexural and shear failure. Thick layers tend to exhibit adhesion loss as the primary mode of failure whereas thinner layers exhibit flexural and shear failure as the primary mode.

The force – displacement response of shotcrete can be greatly increased with the addition of mesh reinforcing. Further test work is required to determine the effect of different mesh configurations on the shotcrete.

Despite claims by the manufacturer, the membrane product tested does not have the ability to replace mesh or shotcrete. The force capacity was shown to be less than 10kN in both test methods. The displacement capacity was also minimal in comparison to shotcrete and mesh. The failure mechanism of the membrane was shear failure with minimal adhesion loss. Failure was observed to continue beyond the end of the test. Further work is required in assessing the response of membranes to sustained loading.

Test programs can only be conducted under specific controlled conditions. In-situ behaviour of surface support elements is affected by many variables such as complex loading conditions and inconsistent installation practices. Accordingly, further research is required to determine the in-situ interaction between the rock mass and the various surface support elements.

CHAPTER 9 REFERENCES

ACI Committee 506 1991. ACI 506.3R-91. Guide to Certification of Shotcrete Nozzlemen. American Concrete institute

Archibald, J 2001a. Canadian field and laboratory testing. Section 23. International seminar on mine surface support liners: Membrane, shotcrete and mesh. August. Perth ACG

Archibald, J 2001b. Assessing acceptance criteria for and capabilities of liners for mitigating ground falls. Mining health and safety conference. April.

Archibald, J, Espley, S, DeGagne, D and Bikis, U 1999. Occupational Hazards of Spray-on Liner Applications in Underground Environments: Truths and Myths. Proceedings of the 101st CIM/ AGM. Calgary. May.

Archibald, J, Espley, S and Lausch, P 1997. Field and laboratory support response of spray on MINEGUARD polyurethane liners. International symposium on rock support. Applied solutions for underground rock structures. Broch, E, Myrvang, A and Stjern, G (ed). Jun. pp. 475-490. Lillehammer Norway.

Archibald, J and Lausch, P 1999. Thin spray on linings for rock failure stabilisation. 37th US rock mechanics symposium. Rock mechanics for industry. June. pp. 617-624.

Archibald, J, Mercer, R and Lausch, P 1992. The evaluation of thin polyurethane surface coatings as an effective means of ground control. Rock support in mining and underground construction. Kaiser, P and McCreath, D (ed). Jun. pp. 105-115. Rotterdam Balkema

Archibald, J and Nicholls, T 2000. Validation of rock reinforcement capacity offered by spray on mine coatings. 102nd Annual general meeting of the CIM. Toronto Ontario. March.

Arnold, A 1967. Water in and around mine openings. Symposium on stress and failure around underground openings. March 1 - 2 1967. Vol.2, University of Sydney (ed). Mar 1 -2.

AS 1012.9 "Method 9: Determination of the compressive strength of concrete specimens".

AS 1012.11-2000 "Methods of testing concrete: Method 11: Determination of the modulus of Rupture".

AS 1304 2001. AS1304 – 1991 Welded wire reinforcing fabric for concrete. Standards Australia, Melbourne

AS 4671 2001. AS4671 – 2001 Steel reinforcing materials. Standards Australia, Melbourne

ASTM A 497 2007. ASTM A 497/A-07 “Standard Specification for Steel Welded Wire Reinforcement, Deformed, for Concrete”

ASTM C 31 2008. ASTM C 31/C 31M – 08a. Standard practice for making and curing concrete specimens in the field. ASTM International

ASTM C 39 2005. ASTM C 39/C 39M - 06. Standard test method for compressive strength of cylindrical concrete specimens. ASTM International

ASTM C 078 2008. ASTM C 078 - 08. Standard test method for flexural strength of concrete (using simple beam with third point loading). ASTM International

ASTM C 1018 1994. ASTM C 1018 – 94b. Standard test method for flexural toughness and first crack strength of fibre reinforced concrete (using beam with third point loading). ASTM International

ASTM C 1550 2005. ASTM C 1550 - 05. Standard test method for flexural toughness of fibre reinforced concrete (using centrally loaded round panel). ASTM International

ASTM C 1609 2006. ASTM C 1609/C 1609M - 06. Standard test method for flexural performance of fibre reinforced concrete (using beam with third point loading). ASTM International

ASTM D 638 2008. ASTM D 638. Standard test method for tensile properties of plastics. ASTM International

Austin, S and Robins, P (ed). 1995. Sprayed concrete. Properties design and applications. pp. 52-86. Whittles Publishing

Bae, G, Chang, S, Lee, S and Park, H 2004. Evaluation of interfacial properties between rock mass and shotcrete. Sinrock 2004 Symposium. Int. J. Rock Mech. Min. Sci., Vol.43, No.1,

Bernard, S 1999. Correlations in the performance of fibre reinforced shotcrete and panels. Part 1. Engineering report no CE9. July. Sydney Australia University of Western Sydney Nepean

Bernard, S 2002. Correlations in the behaviour of fibre reinforced shotcrete beam and panel specimens. Materials and Structures, Vol.35, No.3, April. pp. 156-164. Netherlands Springer

Bernard, S 2003. Release of new ASTM round panel test. Shotcrete. Vol.5, No.2, Spring. American Shotcrete Association

Bernard, S 2005. Early age test methods for fibre reinforced shotcrete. Shotcrete. Vol.7, No.2, Spring. American Shotcrete Association

Bernard, S and Geltinger, C 2007. Determination of early age compressive strength for FRS. Shotcrete. Vol.9, No.4, Fall. American Shotcrete Association

Barrett, S and McCreath, D 1995. Shotcrete support design in blocky ground: Towards a deterministic approach. Tunnelling and Underground Space Technology, Vol.10, No.1, pp. 79-89. Great Britain Elsevier Science

Cengiz, O and Turanli, L 2004. Comparative evaluation of steel mesh, steel fibre and high performance polypropylene fibre reinforced shotcrete in panel tests. Cement and concrete research. Vol.34, Jan. pp. 1357-1364. Elsevier

Coates, D 1965. Rock mechanics principles. Mines branch monograph 874.

Deere, U, Peck, R, Monsees, J and Schmidt, B 1969. Design of tunnel liners and support systems. Final report for office of high speed ground transportation. Washington US department of transportation

Ding, Y and Kusterle, W 1999. Comparative study of steel fibre-reinforced concrete and steel mesh - reinforced concrete at early ages in test panels. Cement and concrete research. Vol.29, July. pp. 1827-1834. Elsevier Science

Dolinar, D 2006. Load capacity and stiffness characteristics of screen materials used for surface control in underground coal mines. 25th International conference on ground control in mining. Morgantown. August.

Dufour, J, Denis, J, O'Donnell, P and Ballou, M 2003. Determination of early age ductility of steel fibre reinforced shotcrete lining system at INCO's Stobie mine. Shotcrete. Vol.5, No.2, Spring. American Shotcrete Association

European federation of national associations of specialist contractors and material suppliers for the construction industry (EFNARC) (ed). 1996. European specification for sprayed concrete. www.efnarc.org

Espley-Boudreau, S 1999. Thin spray-on liner support and implementation in the hard rock mining industry. MSc Thesis. Laurentian University.

Espley S J and Kaiser P K 2002. Design methods for spray - on liners as support in underground hard rock mining. Proceedings of 5th North American Rock Mechanics Symposium. NARMS - TAC. Hammah et al. (ed). pp. 889-897. Toronto University of Toronto

Espley, S, O' Donnell, D, Thibodeau, D and Paradis - Sokoloski, P 1996. Investigation into the replacement of conventional support with spray on liners. CIM Bulletin, Vol.89, No.1001, June. pp. 135-143.

Espley, S, Tannant, D, Baiden, G and Kaiser, P 1999. Design criteria for thin spray on membrane support for underground hard rock mining. Proceedings of the 101st CIM/ AGM. Calgary.

Fernandez-Delgado, G, Mahar, J and Parker, H 1976. Structural behaviour of thin shotcrete liners obtained from large scale tests. Shotcrete for ground support. Proceedings of the engineering foundation conference. Oct 4-8. pp. 399-442. ACI

Finn, D, Teasdale, P and Windsor, C 1999. In-situ trials and field testing of two polymer restraint membranes. Rock support and reinforcement practice in mining. Villaescusa, E, Windsor, C and Thompson, A (ed). pp. 139-153. Rotterdam Balkema

Graham, J 1973. Polymer shotcrete. Use of shotcrete for underground structural support. Proceedings of the engineering foundation conference. July. pp. 418-435. ACI

Grimstad, E., Barton, N., 1993. Updating the Q-system for NMT. Proc. Int. Symp. on Sprayed Concrete, Fagernes, Norway. Norwegian Concrete Association, Oslo.

Gyenge, M and Coates, D 1973. The support mechanism of sprayed thin linings. Proceedings of the 8th Canadian rock mechanics symposium. Toronto 1972. Horn W (ed). pp. 101-117. Ottawa department of energy Mines and resources

Haile, A 1999. Observations of dynamic performance of South African tunnel support systems. Rock support and reinforcement practice in mining. Villaescusa, E, Windsor, C and Thompson, A (ed). pp. 155-159. Rotterdam Balkema

Hoek, E and Brown, T 1982. Underground excavations in rock. Revised first edition. London E & FN SPON

Holmgren, J 1976. Thin shotcrete layers subject to punch loads. Shotcrete for ground support. Proceedings of the engineering foundation conference. Oct. pp. 443-459. ACI

Holmgren, J 2001. Shotcrete linings in hard rock. Underground mining methods. Engineering fundamentals and international case studies. Hustrulid, W and Bullock, R (ed). pp. 569-577. Colorado Society for mining, metallurgy and Exploration

ISO 15630-2:2002(E) 2002. Steel for the reinforcement and prestressing of concrete — Test methods - Part 2: Welded fabric. International standard.

Jastrzebski, Z 1959. The nature and properties of engineering materials. New York John Wiley and Sons Inc

Johnston, C. 1982. Definition and Measurement of Flexural Toughness Parameters for Fiber Reinforced Concrete Cement, Concrete, and Aggregates, CCAGDP, Vol. 4, No. 2, Winter pp. 53-60.

Jolin, M, Beaupre, D, 2003. Understanding Wet-Mix Shotcrete: Mix Design, Specifications, and Placement. Shotcrete. Vol.5, No.3, Summer. American Shotcrete Association

Kaiser, P and Tannant, D 2001. The role of shotcrete in hard rock mines. Underground mining methods. Engineering fundamentals and international case studies. Hustrulid, W and Bullock, R (ed). pp. 579-592. Colorado Society for mining, metallurgy and Exploration

Keeley, D 1934. Guniting the McIntyre Mine. Canadian institute of mining and metallurgy. Annual general meeting.

Kirsten, H 1993. Equivalence of mesh and fibre reinforced shotcrete at large deflections. Can. Geotech. J., Vol.30, pp. 418-440. Ottawa, Canada National Research Council

Kirsten, H 1992. Comparative efficiency and ultimate strength of mesh and fibre - reinforced shotcrete as determined from full scale bending tests. J. S. Afr. Inst. Min. Metall., Vol.92, No.11/12, Nov / Dec. pp. 303-323.

Kirsten, H A D and Labrum, P R 1990. The equivalence of fibre and mesh reinforcement in the shotcrete used in tunnel support systems. J. S. Afr. Inst. Min. Metall., Vol.90, No.7, Jul. pp. 153-171.

Kuchta, M 2002. Quantifying the increase in adhesion strength of shotcrete applied to surfaces treated with high pressure water. SME Annual Meeting. Phoenix Arizona. Feb 35 - 27.

Kuijpers, J 2001. Evaluation of membrane support behaviour. Section 21. International seminar on mine surface support liners: Membrane, shotcrete and mesh. August. Perth ACG

Kuijpers, J, Milev, A, Jager, A and Acheampong, E 2002. Performance of various types of containment support under quasi-static and dynamic loading conditions. Part I. Gap report 810a. May. South Africa SIMRAC

Kuijpers, J, Sellers, E, Toper, A, Rangasamy, T, Ward, T, van Rensburg, A, Yilmaz, H and Stacey, R 2004. Final report: Required technical specifications and testing methodology for thin sprayed linings. SIMRAC 020206. November. CSIR SIMRAC

Kuijpers, J and Topper, A 2003. Model of TSL behaviour under punch through conditions. 3rd international seminar on surface support liners. Section 16. August. Quebec City

Leslie H and Potter R (ed). 2004. Glossary of building terms. 5th Edition. HB50 - 2004. Sydney Australia Standard Australia and National Committee on Rationalised Building (NCRB)

Little, T 1985. An evaluation of steel fibre reinforced shotcrete for underground support. Can. Geotech. J., Vol.22, No.4, pp. 501-507. Ottawa, Canada National research publisher

Maher, J, Parker, H and Wuellner, W 1975. Shotcrete practice in underground construction. US department of transport report FRA-OR&D 75-90. Springfield Virginia

Malmgren, L, Nordlund, E and Rolund, S 2005. Adhesion strength and shrinkage of shotcrete. Tunnelling and underground technology. Vol.20, pp. 33-48. Elsevier

Mason, D and Stacey, T 2008. Support to excavations provided by sprayed liners. Int. J. Rock Mech. Min. Sci., Vol.45, No.5, July. pp. 773-788.

McFarlane, G 1978. Load retention of welded wire fabric mine screening. Steel company of Canada Ltd.

Melbey, T and Garshol, K 1994. Sprayed concrete for rock support. Switzerland MBT international

McCreath D R and Kaiser P K 1992. Evaluation of current support practices in burst prone ground and preliminary guidelines for Canadian hard rock mines. Rock support in mining and underground construction. Kaiser P K and McCreath D R (ed). June 16 - 19. pp. 611-619. Rotterdam Balkema

Mitchell, D and Murphy, E 1966. Role of urethane foam in mines. March. pp. 72 - 74.

Norcroft, I W 2006. Innovative materials and methods for ground support, consolidation and water sealing for the mining industry. SAIMM 2nd Underground Operators Conference. 11 - 12 Sept. SAIMM

Ortlepp, W 1983. Considerations in the design of support for deep hard rock tunnels. 5th international congress on rock mechanics. Vol.2, pp. 179-187. Rotterdam Balkema

Ortlepp, W and Erasmus, P 2002. The performance of yielding straps under dynamic loading. 2nd International seminar on surface support liners. Section 2. July 29-31. Sandton South Africa SAIMM

Ortlepp, W, More O'Ferrall, R and Wilson, J 1975. Support methods in tunnels. Association of mine managers of South Africa. Papers and discussions 1972-1973. pp. 167-198. Cape Town Chamber of Mines South Africa

Ortlepp, W and Stacey, T 1996. The performance of containment rock support such as wire mesh under simulated rock burst conditions. Geomechanics 96. Rakowski (ed). Rotterdam Balkema

Ortlepp, W and Stacey, T 1997. Testing of tunnel support: Dynamic load testing of rock support containment systems (e.g. wire mesh). GAP report 221. August. South Africa SIMRAC

Ozturk, H and Tannant, D 2003. Influence of rock properties and environmental conditions on adhesive bond to a thin liner. 3rd international seminar on surface support liners. August. Quebec City

Ozyildirim, C and Carino, N 2006. Chapter 13 Concrete strength testing. Significance of Tests and Properties of Concrete and Concrete-Making Materials STP 169D. Lamont, J and Pielert, J (ed). Bridgeport NJ ASTM International

Pakalnis, V and Ames, D 1983. Load tests on mine screening. Underground support systems. Udd, J (ed). pp. 79-83. Montreal, Quebec CIMM

Papworth, F 2002. Design guidelines for the use of fibre reinforced shotcrete in ground support. Our world in concrete and structures. Singapore. Aug.

Player J, Morton E, Thompson A and Villaescusa E 2008. Static and dynamic testing of steel wire mesh for mining applications of rock surface support. 6th International conference on ground support. Cape Town. April. SAIMM

Potvin, Y and Giles, G 2008. The Development of a New High-Energy Absorption Mesh. 10th Underground operators conference. Launceston Tasmania. 14 - 16 April. Melbourne AusIMM

Potvin, Y, Stacey, D and Hadjigeorgiou, J (ed). 2004. Surface support in mining. Perth Australian Centre for Geomechanics

Prudencio Jr, LR 1998. Accelerating admixtures for shotcrete. Cement and Concrete Composites, Vol.20, pp. 213-219. Great Britain Elsevier Science

Rispin, M and Garshol, K 2003. Reactive vs. Non-reactive TSL's: A comparison illustrated with two prototype technologies. 3rd international seminar on surface support liners. Section 24. August. Quebec City

Roth, A, Ranta-Korpi, R, Volkwein, A and Wendeler, C 2007. Numerical modelling and dynamic simulation of high tensile steel wire mesh for ground support under rock burst loading. 1st US - Canada rock mechanics symposium. May.

Roth, A, Windsor, C, Coxon, J and de Vries, R 2004. Performance assessment of high tensile wire mesh ground support under seismic conditions. Ground support in mining and underground construction. Villaescusa and Potvin (ed). pp. 589-594. London Taylor and Francis Group

Schwendeman, J, Sun, S and Salyer, I 1972. Plastic liners extended with sand and other fillers for use in coal mines. United States bureau of mines open file report. United States Bureau of Mines

Spearing, A and Champa, J 2001. Superskin - The present and the future. Section 16. International seminar on mine surface support liners: Membrane, shotcrete and mesh. August. Perth ACG

Spearing, A, Ohler, J and Attigobe, E 2001. The effective testing of thin support membranes (superskins) for use in underground mines. Section 26. International seminar on mine surface support liners: Membrane, shotcrete and mesh. August. Perth ACG

Spearing, S and Pretorius, H 2006. The development of a high strength thin support liner and two case studies. Golden Rocks 2006. 41st U.S. symposium on rock mechanics. June 17-21. Golden, Colorado ARMA

Stacey, T 2001. Review of membrane support mechanisms, loading mechanisms, desired membrane performance, and appropriate test methods. J. S. Afr. Inst. Min. Metall., Oct. pp. 343-351.

Stacey, T and Ortlepp, W 2001. The capacities of various types of wires mesh under dynamic loading. Section 2. International seminar on mine surface support liners: Membrane, shotcrete and mesh. ACG

Swan, G and Henderson, A 1999. Water based spray on liner implementation at Falconbridge Limited. Proceedings of the 101st CIM/ AGM. Calgary. CIM

Tannant, D 1994. Pull tests on various types of mesh. Internal report. Geomechanics Research centre.

Tannant, D 1995. Load capacity and stiffness of welded wire mesh. 48th Canadian geotechnical conference. Vancouver

Tannant, D 2001a. Load capacity and stiffness of welded wire, chain link and expanded metal mesh. Section 3. International seminar on mine surface support liners: Membrane, shotcrete and mesh. August. Perth ACG

Tannant, D 2001b. Thin spray on liners for underground rock support - testing and design issues. Section 27. International seminar on mine surface support liners: Membrane, shotcrete and mesh. August. Perth ACG

Tannant, D, Barclay, B, Espley, S and Diederichs, M 1999a. Field trials of thin sprayed-on membranes for drift support. 9th International congress on rock mechanics. Vol.2, Vouille, G and Berest, P (ed). pp. 1471-1474. Rotterdam Balkema

Tannant, D and Kaiser, P 1997. Evaluation of shotcrete and mesh behaviour under large imposed deformations. International symposium on rock support - Applied solutions for underground structures. Lillehammer Norway. Broch, E Myrvang, A Stjern, G (ed). June 22-25. pp. 782-792.

Tannant, D, Kaiser, P and Maloney, S 1997. Load - displacement properties of welded wire, chain link and expanded metal mesh. International symposium on rock support - Applied solutions for underground structures. Lillehammer Norway. Broch, E Myrvang, A Stjern, G (ed). June 22-25. pp. 651-659.

Tannant, D, Swan, G, Espley, S and Graham, C 1999b. Laboratory test procedures for validating the use of thin sprayed on liners for mesh replacement. Proceedings of the 101st CIM/ AGM. Calgary.

Tarr, K, Annor, A and Flynn, D 2006. Laboratory testing procedures for evaluating thin spray on liners. Proceedings of the core project on deep mining. Division report CANMET MMSL 05-032 (TR). June. CANMET

Thompson, A 2001. Rock support action of quantified by testing and analysis. Section 1. International seminar on mine surface support liners: Membrane, shotcrete and mesh. August. Perth ACG

Thompson, A, Windsor, C and Cadby, G 1999. Performance assessment of mesh for ground control applications. Rock support and reinforcement practice in mining. Villaescusa, Windsor, Thompson (ed). pp. 119-130. Rotterdam Balkema

Vandewalle, M 1996. Tunnelling the world. Dramix

Vandewalle, M 2005. Tunnelling is an art. Belgium NV Bekaert SA

Van Sint Jan, M and Cavieres, P 2004. Large scale static laboratory test of different support systems. Ground support in mining and underground construction. Villaescusa and Potvin (ed). pp. 571-577. London Taylor and Francis Group

Villaescusa, E 1999. Laboratory testing of weld mesh for rock support. Rock support and reinforcement practice in mining. Villaescusa, E, Windsor, C and Thompson, A (ed). pp. 155-159. Rotterdam Balkema

Wang, C and Tannant, D 2004. Rock fracture around a highly stressed tunnel and the impact of a thin tunnel liner on ground control. Int. J. Rock Mech. Min. Sci., Vol.41, No.3, May. Elsevier Inc

Windsor, C 2007. Section 4. A Decade in Ground Support. Villaescusa, E Thompson, A and Windsor, C (ed). April. Kalgoorlie Western Australian School of Mines

Wojno, L and Toper, Z 1999. In-situ trials for structural membrane support. Rock support and reinforcement practice in mining. Villaescusa, E, Windsor, C and Thompson, A (ed). pp. 131-138. Rotterdam Balkema

Every reasonable effort has been made to acknowledge the owners of copyright material. I would be pleased to hear from any copyright owner who has been omitted or incorrectly acknowledged.

CHAPTER 10 FURTHER READING

10.1 MESH

Ortlepp, W and Swart, A 2002. Performance of various types of containment support under quasi-static and dynamic loading. Part II. GAP 810b. Oct. South Africa SIMRAC

Robertson, S, Molinda, G, Dolinar, D, Pappas, D and Hinshaw, G 2003. Best practices and bolting machine innovations for roof screening. SME annual meeting. Cincinnati, Ohio. February 24-26. SME

Villaescusa, E 2001. Weld mesh for rock support in Australia. Section 4. International seminar on mine surface support liners: Membrane, shotcrete and mesh. August. Perth ACG

10.2 SHOTCRETE

Anderson, G and Poad, M 1973. Early age strength properties of shotcrete. Use of shotcrete for underground structural support. Proceedings of the engineering foundation conference. July 16-20. pp. 277-296. ACI

Banthia, N 2001. Fracture toughness of fibre reinforced shotcrete: Issues and challenges. Shotcrete: Engineering developments. Bernard, S (ed). pp. 3-5. Lisse Swets& Zeitlinger

Bernard, E S 2007. Early-age load resistance of fibre reinforced shotcrete linings. pp. In print. Elsevier Science

Bernard, S 1998. Measurement of post cracking performance in fibre reinforced shotcrete. Australian shotcrete conference. Session 4. Bernard, S (ed). London IBC

Bernard, S 1999. Correlations in the performance of fibre reinforced shotcrete and panels. Part 1. Engineering report no CE9. July. Sydney Australia University of Western Sydney Nepean

Bernard, S 2000. Correlations in the performance of fibre reinforced shotcrete and panels. Part 2. Engineering report no CE15. June. University of Western Sydney Nepean

Bernard, S 2000. Correlations in the performance of fibre reinforced shotcrete and panels. Part 3. Engineering report no CE19. December. Sydney, Australia University of Western Sydney Nepean

Bernard, E S (ed). 2004. Shotcrete. More engineering developments. London Balkema

Bernard, S (ed). 2001. Application of yield line theory to round determinate panels. Shotcrete: Engineering developments. 90 5809 176 7 pp. 245-254. Lisse swets & Zeitlinger

Bernard, S, Fagerberg, K and Overmo, E 2000. Moment - crack rotation relationships for fibre reinforced shotcrete beams and panels. Engineering report no CE13. January. 1326-0693 Sydney UWS Nepean

Celestino, T, Castro, G, Vessaro, P, Bortolucci, A and Santos, O 2006. Strength and deformability anisotropy of fibre reinforced shotcrete. Shotcrete for ground support X. Proceedings 10th international conference Whistler, British Columbia, Canada. 12-16 September. American Society of Civil Engineers

Clements, M 1999. The use of shotcrete in Australian underground mining - A contractors perspective. Rock support and reinforcement practice in mining. Villaescusa, E, Windsor, C and Thompson, A (ed). pp. 199-208. Rotterdam Balkema

Clements, M 2004. Comparison of methods for early age strength testing of shotcrete. Shotcrete: More engineering developments. Bernard (ed). Oct. 04 1535 898 1 London Taylor and Francis Group

DiNoia, T and Rieder, K 2004. Toughness of fibre reinforced shotcrete as a function of time, strength development and fibre type according to ASTM C1550-02. Shotcrete: More engineering developments. Bernard, S (ed). Oct. pp. 127-135. London Taylor and Francis

Garshol, K 1997. Single shell sprayed concrete linings, why and how. International symposium on rock support - Applied solutions for underground structures. Lillehammer Norway. Broch, E Myrvang, A Stjern, G (ed). June 22-25. pp. 491-503.

Grov, E and Blindheim, O 1997. Selecting properties of sprayed concrete for different rock support applications. International symposium on rock support - Applied solutions for underground structures. Lillehammer Norway. Broch, E Myrvang, A Stjern, G (ed). June 22-25. pp. 68-82.

Holmgren, J 1998. Shotcrete linings in hard rock. Australian shotcrete conference. Session 6. Bernard, S (ed). London IBC

Holmgren, J and Ansell, A 2006. Design of bolt anchored reinforced shotcrete linings subject to impact loadings. Shotcrete for ground support X. Proceedings 10th international conference Whistler, British Columbia, Canada. 12-16 September. American Society of Civil Engineers

Jolin, M, Gagon, F and Beaupre, D 2004. Determination of criteria for the acceptance of shotcrete for certification. Shotcrete: More engineering developments. Bernard, S (ed). Oct. pp. 175-181. London Taylor and Francis group

MacKay, J and Trottier, J-F 2004. Post crack behaviour of steel and synthetic FRC under flexural loading. Shotcrete: More engineering developments. Bernard, S (ed). Oct. pp. 183-192. London Taylor and Francis

Malmgren, L, Nordlund, E and Rolund, S 2005. Adhesion strength and shrinkage of shotcrete. Tunnelling and underground technology. Vol.20, pp. 33-48. Elsevier

Morton E C, Thompson A G and Villaescusa E 2008. Static testing of shotcrete and membranes for mining applications. 6th International conference on ground support. Cape Town. April. SAIMM

Morton E C, Thompson A G, Villaescusa E and Howard D 2008. Static testing of shotcrete. 13th Australian tunnelling conference. Melbourne. May. AusIMM

Oliveira de Barros, J 2001. Experimental behaviour of mesh reinforced shotcrete and steel fibre reinforced panels. Mechanics of composite materials and structures. Vol.8, No.1, Jan. pp. 29-45. Taylor and Francis

Rock Technology 1997. Shotcrete, mesh and bolts. AMIRA project 489. Newsletter 1. March. Rock Technology

Rutenbeck, T 1976. Shotcrete strength testing - comparing results of various specimens. Shotcrete for ground support. Proceedings of the engineering foundation conference. Oct 4-8. pp. 97-105. ACI

Saiang, D, Malmgren, L and Nordlund, E 2004. Strength and stiffness of shotcrete - rock interface - A laboratory study. Ground support in mining and underground construction. Villaescusa, E and Potvin, Y (ed). pp. 555-564. London Taylor & Francis group

Seabrook, P 1976. Properties of shotcrete on construction projects. Shotcrete for ground support. Proceedings of the engineering foundation conference. Oct. pp. 29-45. ACI

Spearing, S 1995. The potential for shotcrete as a tunnel support system in gold and platinum mines. Colloquium. Innovative mining and support systems for safety and productivity. May 24. Mintek, Randburg SA IMM

Stacey, T 2001. Shotcrete in mines - state of the art in South Africa. Section 6. International seminar on mine surface support liners: Membrane, shotcrete and mesh. August. Perth ACG

Tatnall, P 2006. Standards, test methods and guides for shotcrete ground support. Shotcrete for ground support X. Proceedings 10th international conference Whistler, British Columbia, Canada. 12-16 September. American Society of Civil Engineers

Tatnall, P 2003. Update on standards for shotcrete. Shotcrete. Vol.5, No.3, Summer. pp. 32-33.

Tran, V, Bernard, S and Beasley, A 2005. Constitutive modelling of fibre reinforced shotcrete panels. May. pp. 512-521.

Windsor, C 2001. Shotcrete in mines - state of the art in Australia. Section 5. International seminar on mine surface support liners: Membrane, shotcrete and mesh. August. Perth ACG

Windsor, C 1998. Structural design of shotcrete linings. Australian shotcrete conference. Session 3. Bernard, S (ed). London IBC

Windsor, C and Thompson, A 1999. The design of shotcrete linings for excavations created by drill and blast. Rock support and reinforcement practice in mining. Villaescusa, E, Windsor, C and Thompson, A (ed). pp. 231-242. Rotterdam Balkema

Xu, H and Mindess, S 2006. Behaviour of concrete panels reinforced with welded wire mesh and fibres under impact loading. Shotcrete for ground support X. Proceedings 10th international conference Whistler, British Columbia, Canada. 12-16 September. American Society of Civil Engineers

Xu, H, Gu, Q and Mindess, S 2006. Deformation of round panels containing fibres. Shotcrete for ground support X. Proceedings 10th international conference Whistler, British Columbia, Canada. 12-16 September. American Society of Civil Engineers

10.3 MEMBRANES

Archibald, J and DeGagne, D 2000. Recent Canadian advances in the application of spray-on polymeric linings. Mining health and safety conference. Sudbury Ontario. April 13.

Archibald, J and Katsabanis, P 2004. Evaluation of liner capacity for blast damage mitigation. C.I.M. Bulletin, Vol.97, No.1079, April. pp. 47-51.

Archibald, J, Baidoe, J and Katsabanis, P 2003a. Rock burst damage mitigation benefits deriving from use of spray-on rock linings. 3rd international seminar on surface support liners. Section 19. August. Quebec City

Archibald, J, Baidoe, J and Katsabanis, P 2003b. Comparative assessment of conventional support systems and spray-on rock linings in a rock burst prone environment. 3rd international seminar on surface support liners. Section 20. August. Quebec City

Archibald, J, Pelley, C, Espley, S and DeGagne, D 2000. Economic and productivity comparison of bolt and screen, shotcrete and polymer rock support methods. Proceedings of the 102nd CIM/ AGM. Toronto, Ontario. March.

Espley-Boudrea, S 1999. Thin spray-on liner support and implementation in the hardrock mining industry. MSc Thesis. Laurentian Univeristy.

Espley, S, Gustas, R, Heilig, J and Moreau, L 2001. Thin spray on liner research and field trials at INCO. Section 25. International seminar on mine surface support liners: Membrane, shotcrete and mesh. August. Perth ACG

Finn, D 2001. Polymer membrane tests at WMC St Ives. Section 20. International seminar on mine surface support liners: Membrane, shotcrete and mesh. August. Perth ACG

Kuijpers, J, Rangasamy, T and Sellers, E 2005. Performance and design of thin sprayed liners as rock support in mine tunnels. SAIMM Colloquium. A new era of tunnelling. February. SAIMM

Langlois, R, Conlon ,B, Anderson, T and Labrie, D 2006. Effect of polyurethane coatings on strain energy absorption capacity of rock specimens in compression. Proceedings of the core project on deep mining. Division report CANMET MMSL 05-032 (TR). June. CANMET

Pappas, D, Barton, T and Weiss, E 2003. The long term performance of surface support liners for ground control in an underground limestone mine. 3rd international seminar on surface support liners. Section 22. August. Quebec City

Pritchard, C, Swan, G, Henderson, A, Tannant, D and Degville, D 1999. TekFlex as a spray on screen replacement in an underground hard rock mine. Proceedings of the 101st CIM/AGM. Calgary.

Robert, R 2001a. Locals weigh up support for thin liners. Australia's mining monthly magazine. September. pp. 70-73. AusIMM

Roberts, R 2001b. Time to look below the surface of membranes. Australia's mining monthly magazine. August. pp. 62-63. AusIMM

Scott, J (ed). 1967. New materials for underground support. Chapter 56. Mining. pp. 187. Moscow MIR Publishers

Spearing, A and Champa, J 2000. The design, testing and application of ground support membranes for use in underground mines. MASSMIN. Chitombo, G (ed). Oct/ Nov. pp. 199-208. AusIMM

Spearing, S 2003. Proposed thin support liner definitions, performance categories and test methods. 3rd international seminar on surface support liners. Section 11. August. Quebec City

Stacey, T and Yu, X 2004. Investigations into mechanisms of rock support provided by sprayed on liners. Ground support in mining and underground construction. Villaescusa, E and Potvin, Y (ed). pp. 565-569. London Taylor & Francis group

Swan, G and Henderson, A 2001. Water based spray on liner implementation at Falconbridge. Section 24. International seminar on mine surface support liners: Membrane, shotcrete and mesh. August. Perth ACG

Swan, G, Fantin, P, Doyle, G, Mikalachki, S, Martin, B and Brummer, R 2003. Technical and business case arguments supporting the development of a TSL mining system. 3rd international seminar on surface support liners. Section 23. August. Quebec City

Tooper, A, Kuijpers, J, Stacey, T, Yilmaz, H and Saydam, S 2003. Proposed procedure for the testing of TSL properties. 3rd international seminar on surface support liners. Section 14. August. Quebec City

Windsor, C 2001. Sprayed plastic linings or ground support membranes. Section 19. International seminar on mine surface support liners: Membrane, shotcrete and mesh. August. Perth ACG

Wojno, L and Tooper, Z 1999. In-situ trials for structural membrane support. Rock support and reinforcement practice in mining. Villaescusa, E, Windsor, C and Thompson, A (ed). pp. 131-138. Rotterdam Balkema

**Appendix 1: Ground support design tables provided by
Ortlepp et al. (1975).**

TABLE IV. GUIDE FOR SELECTION OF SUPPORT FOR TUNNELS AND LARGER CHAMBERS

1. Hard Rock—U.C.S. greater than $\bar{1}75$ MN/m² (25 000 p.s.i.) (e.g. quartzite, lava, dolerite, dolomite)(A) Low Stress (vertical component less than 30 MN/m² or 4 000 p.s.i.)

	(a) Massive (spacing between joints etc. > width of excavation)	(b) Jointed, Laminated, Blocky (spacing between joints etc. < 1/10 width of excavation)
(i) Increasing	<p><i>Tunnels:</i> Failure of corners and sides possible if tunnel is badly shaped, therefore if increase is considerable:—</p> <p>* Rockbolting—types 1, 3 or 4</p> <p>** Fabric—types (a) or (b) on sidewalls only.</p> <p><i>Larger chambers:</i> Any form of concrete walls suspect unless independent of rock sidewall.</p> <p>Roof—widely spaced rope anchors of length not less than diagonal of excavation cross-section, spaced $\frac{1}{2}$ length apart, interspersed with shorter rockbolts type 1 or 4.</p> <p>Sidewalls—rockbolts 1 or 4 of length = $\frac{1}{2}$ sidewall height (max. 4m) spaced $\frac{1}{2}$ length apart. Fabric (c) or (d) for permanence.</p>	<p><i>Tunnels:</i> Rockbolting—closely spaced small diameter bolting of types 1 or 4² throughout</p> <p>Fabric—on sidewalls only, type (b) or (c), or (d) for very closely jointed rock.</p> <p><i>Larger chambers:</i> Roof—Rope anchors of length not less than one-half minimum span, interspersed with rockbolting types 1, 3 or 4 spaced $\frac{1}{2}$ length apart.</p> <p>Sidewalls—as for massive rock 1Aa(i). Fabric (c) or (d). Mass concrete suspect.</p>
(ii) Static	<p><i>Tunnels:</i> No support.</p> <p><i>Larger chambers:</i> No support necessary if smooth-blasted and properly shaped. Concrete lining acceptable.</p> <p>Shotcrete by itself may be useful for surface finish and sealing of permanent chambers.</p>	<p><i>Tunnels:</i> Shotcrete alone should provide adequate support.</p> <p>Alternatively, rockbolting of small diameter type 1 or 4 closely spaced in roof only.</p> <p>“Rams-horn” caps, closely cribbed to roof also acceptable.</p> <p><i>Larger chambers:</i> Properly shaped, orientated with respect to bedding and smooth blasted.</p> <p>Rockbolting not less than $\frac{1}{2}$ min. span in length with 10cm of shotcrete to provide support and final finish.</p> <p>Traditional concrete lining methods acceptable.</p>
(iii) Decreasing	<p><i>Tunnels:</i> No support.</p> <p><i>Larger chambers:</i> As in the static case 1Aa(ii) above.</p>	<p><i>Tunnels:</i> Shaped with respect to prominent bedding planes.</p> <p>Shotcrete alone should be quite adequate. Alternatives as in static case 1Ab(ii) above.</p> <p><i>Larger chambers:</i> Rockbolting as in static case 1Ab(ii), with shotcrete to provide permanent finish.</p> <p>Traditional concrete lining methods acceptable.</p>

* Type of “reinforcing”

- (1) conventional rockbolts (low yieldability)
- (2) yielding rockstuds
- (3) fully grouted rods or tubes (considerable yieldability claimed)
- (4) fully grouted ropes or re-bar (yieldability as yet undetermined)

** “Fabric” between reinforcing elements:

- (a) steel strapping
- (b) rope lacing
- (c) wire mesh
- (d) wire mesh and shotcrete
- (e) wire mesh plus lacing

Appendix 1

(B) High Stress (vertical component greater than 60 MN/m² or 9 000 p.s.i.)

	(a) Massive (spacing between joints etc. > width of excavation)	(b) Jointed, Laminated, Blocky (spacing between joints etc. < 1/10 width of excavation)
(i) Increasing	<p><i>Tunnels:</i> Shaped and smooth-blasted if possible. Moderate stress increase—rock reinforcement of type 4 with fabric (b) or (c). Considerable increase—intensive bolting of type 2 or possibly type 3 with fabric (d) or (e). Conventional bolts (1) should not be used. Mass concrete, in any form, is to be avoided. <i>Larger chambers:</i> Roof—rope anchors with bolts 1, 3 or 4. Sidewalls—intensive bolting of type 2 or 3. Fabric type (d) or (e). Length and spacing as in 1Aa(i) above.</p>	<p><i>Tunnels:</i> Smooth-blasted and shaped w.r.t. bedding planes with radiused sidewalls and arched roof in crosscuts. Support as for massive rock 1Ba(i) with increased density of possibly smaller diameter bolts, and fabric (c), (d) or (e) throughout. <i>Larger chambers:</i> Orientate with respect to bedding planes. Support as in massive rock case 1Ba(i) with increased density of bolts to suit joint spacing. Type (d) fabric preferred to (c) or (e). Sidewalls bounded near roof and floor by "lubricated" bedding planes may require extra long bolts or rope anchors longer than $\frac{1}{4}$ sidewall height. Max. length probably 5m.</p>
(ii) Static	<p><i>Tunnels:</i> Shaped and smooth-blasted. Rockbolting—types 1, 3 or 4. Fabric—types (a), (b) or (c) on sidewalls only. Alternatively shotcrete without mesh is adequate. Concrete—monolithic lining acceptable if required for other purposes. <i>Larger chambers:</i> Concrete, masonry or well-blocked steelwork acceptable, but rope-anchors, and rockbolts preferred as in case 1Aa(i) above.</p>	<p><i>Tunnels:</i> Shaped w.r.t. bedding planes and smooth-blasted as in 1Bb(i) above. Bolting of types 1, 3 or 4 more closely spaced depending on joint spacing. Fabric (b) or preferably (c) on sidewalls only. Shotcrete by itself, 8cm thick, should be adequate. <i>Larger chambers:</i> As for massive rock case 1Ba(ii) with increased density of short, smaller diameter bolts to suit joint spacing when rope-anchor system is used. Shotcrete recommended for permanence. Orientate w.r.t. bedding planes.</p>
(iii) Decreasing	<p><i>Tunnels:</i> Same as for static case 1Ba(ii) except concrete lining not recommended whether reinforced or monolithic. <i>Larger chambers:</i> Rope anchors in roof. Bolting 1 or 4 and fabric (c) or (d) in roof and sidewall. Dimensions of bolts and anchors as in case 1Aa(i) above.</p>	<p><i>Tunnels:</i> Same as in massive case 1Ba(iii) except increased spacing of smaller diameter bolts may be necessary to suit jointing. Shotcrete applied over mesh may crack in roof but should be unaffected in sidewalls. Traditional forms of concrete liable to serious roof failure. <i>Larger chambers:</i> As in massive rock 1Ba(iii) with suitably increased frequency of interspersed bolts. Possibility of shotcrete cracking in roof is not serious as mesh will prevent any fragments from falling. Orientate w.r.t. bedding.</p>

Appendix 1

2. Soft Rock—U.C.S. less than 100 MN/m² (15 000 p.s.i.) (e.g. shale, tuff, running dykes, etc.)

(A) Low Stress (vertical component less than 30 MN/m² or 4 000 p.s.i.)

	(a) Massive (definition as for hard rock)	(b) Jointed, Laminated, crumbling, friable (definition as for hard rock)
(i) Increasing	<i>Tunnels:</i> Anticipate failure of sidewalls even if tunnel is well shaped. Rockbolting of types 1, 3 or 4 in roof and 2, 3 or 4 fabric (a) or (b) in sidewalls. <i>Larger chambers:</i> As with hard rock case 1Aa(i) except that likelihood of serious sidewall failure demands more intensive bolting of types 2, 3 or 4 and fabric (c) or (d) in sidewalls. Conventional concrete acceptable if properly designed with gap to permit possible movement of sidewall, and is well anchored to roof.	<i>Tunnels:</i> Mass concrete—G. R. Jones, A.M.M., 1960 p. 343. Colgrouted sidewalls—D. W. Webster, A.M.M. 1960, p. 477 and reinforced roof. <i>Larger chambers:</i> As with massive rock case 2Aa(j). Immediate application of shotcrete should be sufficient to provide temporary support during excavation.
(ii) Static	<i>Tunnels:</i> No support required if machine cut or smooth-blasted to appropriate shape. Shotcrete to prevent weathering if necessary. <i>Larger chambers:</i> Distributed loading is desirable and weather-sealing probably necessary hence shotcreting or complete concrete lining is indicated. Any of the traditional forms of concrete quite acceptable.	<i>Tunnels:</i> Rockbolting of roof with small dia. bolts of type 1 or reinforcement of type 3, if possible. Alternatively, 8cm thick shotcrete by itself might be adequate. <i>Larger chambers:</i> As with massive rock 2Aa(ii).
(iii) Decreasing	<i>Tunnels:</i> As with static case 2Aa(ii) above. <i>Larger chambers:</i> As in static case 2Aa(ii) above.	<i>Tunnels:</i> As in static case 2Ab(ii) above. <i>Larger chambers:</i> As in hard rock 1Ab(iii).

(B) High Stress (vertical component greater than 60 MN/m² or 9 000 p.s.i.)

	(a) Massive (spacing between joints etc. width of excavation)	(b) Jointed, Laminated, Blocky (spacing between joints etc. 1/10 width of excavation)
(i) Increasing	<i>Tunnels:</i> Conventional arches, even when lagged and waste-packed, are completely inadequate. Shotcrete applied immediately behind advancing face may delay sidewall fracture sufficiently to permit effective, intensive bolting of type 2 or 3 and fabric (d) or (e). Bolts of types 1, 3 or 4 and fabric (b) or (c) for roof. <i>Larger chambers:</i> Intensive rock reinforcement as for tunnel, together with rope anchors as in case 1Ba(i). Excavation sequence planned to permit early installation of support. Mass of cast concrete in any form, is to be avoided.	<i>Tunnels:</i> Spiling, steel sets—H. Arndt, A.M.M. 1939, p. 578 and concrete. Alternate suggestion: Temporary support during development as for static case 2Bb(ii) below, followed by close-spaced bolting of type 2, 3 or 4 and fabric (d). Alternatively, yielding arch or circular arch well-studded, lagged and waste-packed. <i>Larger chambers:</i> Avoid location in this environment if at all possible.
(ii) Static	<i>Tunnels:</i> As in case 2Ba(i) above except that type 2 bolts not necessary and 3 or 4 quite acceptable. Fabric of type (c) adequate for sides. <i>Larger Chambers:</i> As for case 2Ba(i) above except that type 2 bolts are not necessary. Type 3 or 4 quite adequate for sidewall and type 1 for roof. Traditional forms of concrete lining acceptable.	<i>Tunnels:</i> Pre-cementation and circular steel arches with concrete—A. Knight A.M.M. 1948, p. 175. Re-inforcing cage of grouted rods, followed by pipe and rail sets—R. K. Briggs, A.M.M. 1970, p. 73. Alternate suggestion—immediate application of shotcrete as in 2Ba(i) with rockbolting 1, 3 or 4 and fabric (d). <i>Larger chambers:</i> As with massive rock 2Ba(ii).
(iii) Decreasing	<i>Tunnels:</i> As in static case 2Ba(ii) above. <i>Larger chambers:</i> As in static case 2Ba(ii) except that concrete lining of roof is not recommended.	<i>Tunnels:</i> As in static case 2Bb(ii) above. <i>Larger chambers:</i> As with massive rock 2Ba(iii).

Appendix 2: Summary of weld mesh testing results.

Appendix 2

Test Number	Boundary Restraint Method	Mesh Type	Description of Test	Rupture Force (kN)	Rupture Displacement (mm)	Peak Force (kN)
MT001	Clamping	Weld Mesh	1.6m x 1.6m sample	NA	NA	10.010
MT002	Lacing	Weld Mesh	Standard test setup with 3mm clothes line wire	NA	NA	26.476
MT005	Lacing	Weld Mesh	Standard test setup	46.171	253	46.171
MT006	Clamping	Weld Mesh	1m x 1.6m sample	NA	NA	19.791
MT007	Lacing	Weld Mesh	Standard test setup	46.681	260	46.681
MT008	Lacing	Weld Mesh	Sample orientation modified	35.884	232	38.860
MT009	Lacing	Weld Mesh	Standard test setup	34.089	218	38.381
MT010	Lacing	Weld Mesh	Standard test setup	28.137	225	41.447
MT011	Lacing	Weld Mesh	Standard test setup	44.049	238	44.094
MT013	Lacing	Weld Mesh	Standard test setup	45.440	250	45.440
MT014	Lacing	Weld Mesh	Standard test setup	33.416	232	35.420
MT015	Fixed	Weld Mesh	Hooks used as boundary condition 5 per side	23.305	224	29.227
MT016	Fixed	Weld Mesh	5 restraints per side	18.895	193	32.997
MT017	Fixed	Weld Mesh	Standard test setup	45.036	180	45.036
MT020	Fixed	Weld Mesh	Standard test setup	44.139	192	44.139
MT021	Fixed	Weld Mesh	Sample orientation modified	37.858	151	37.858
MT022	Fixed	Weld Mesh	Standard test setup	40.939	182	43.406
MT024	Fixed	Weld Mesh	Sample orientation modified	38.516	150	38.516
MT025	Fixed	Weld Mesh	Standard test setup	46.382	181	46.382
MT026	Fixed	Weld Mesh	Sample orientation modified	44.917	188	44.917
MT027	Fixed	Weld Mesh	Hole cut in mesh	40.744	195	40.744
MT028	Fixed	Weld Mesh	Overlap of two sheets	29.738	209	29.738
MT029	Fixed	Weld Mesh	Standard test setup	41.265	181	41.265
MT030A	Fixed	Weld Mesh	1.3m x 0.4m sample size	13.660	203	13.660

Appendix 2

Test Number	Boundary Restraint Method	Mesh Type	Description of Test	Rupture Force (kN)	Rupture Displacement (mm)	Peak Force (kN)
MT030B	Fixed	Weld Mesh	1.3m x 0.4m sample size	12.282	151	12.282
MT030C	Fixed	Weld Mesh	1.3m x 0.4m sample size	13.375	205	13.375
MT030D	Fixed	Weld Mesh	1.3m x 0.4m sample size	8.899	142	8.899
MT030E	Fixed	Weld Mesh	1.3m x 0.4m sample size	11.459	150	11.459
MT030F	Fixed	Weld Mesh	1.3m x 0.4m sample size	10.770	194	10.770
MT030G	Fixed	Weld Mesh	1.3m x 0.4m sample size	11.743	150	11.743
MT033	Fixed	Weld Mesh	Standard test setup	43.420	188	44.169
MT034	Fixed	Weld Mesh	Standard test setup	43.001	191	47.238
MT036	Fixed	Weld Mesh	Standard test setup	46.190	193	46.190
MT037 – MT055 Confidential						
MT056	Fixed	Weld Mesh	Standard test setup	44.20	176	41
MT057	Fixed	Weld Mesh	Standard test setup	45.40	183	55
MT058 – MT060 Confidential						
MT061	Fixed	Weld Mesh	Standard test setup	28.330	166	46.0
MT062	Fixed	Weld Mesh	Standard test setup	25.875	163	46.0
MT063 – MT075 Confidential						
MT076	Fixed	Weld Mesh	Standard test setup	40.651	190	57
MT077	Fixed	Weld Mesh	Standard test setup	41.699	172	49
MT0778	Fixed	Weld Mesh	Standard test setup	34.38	221	80
MT079	Fixed	Weld Mesh	Standard test setup	57.103	245	63
MT080 – MT084 Confidential						

Appendix 3: Individual mesh test report sheets – weld mesh



WASM Static Test Report

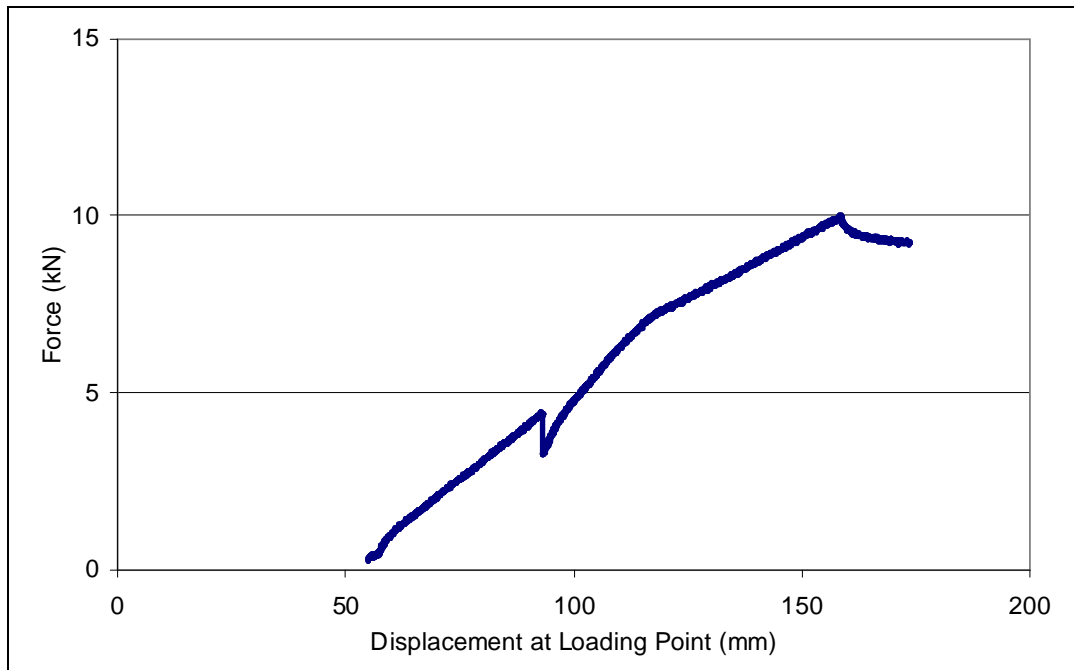


Test Date	17/03/2006	Person testing	Ellen Morton
Test Number: MT001 Type: Weld Mesh			

Sample Specifications			
Length	Width	Grid Size	Wire Diameter
1.6m	1.6m	100mm x 100mm	5.6mm

Boundary Condition	Clamped	Loading Condition	Square Flat Plate 300mm x 300mm
---------------------------	---------	--------------------------	------------------------------------

No of Restraints per side	NA
Sample Configuration	Cross wires in contact with load plate and parallel to load bearing beam



Rupture Load	NA	kN	Peak Load	10.01	kN
---------------------	----	----	------------------	-------	----

Rupture Displacement	NA	mm	Displacement prior to active response	55	mm
-----------------------------	----	----	--	----	----

Rupture Mechanism	No failure	Position of Rupture	NA
--------------------------	------------	----------------------------	----

Comments: The mesh slipped from under the clamping failure and so failure was not achieved.



WASM Static Test Report

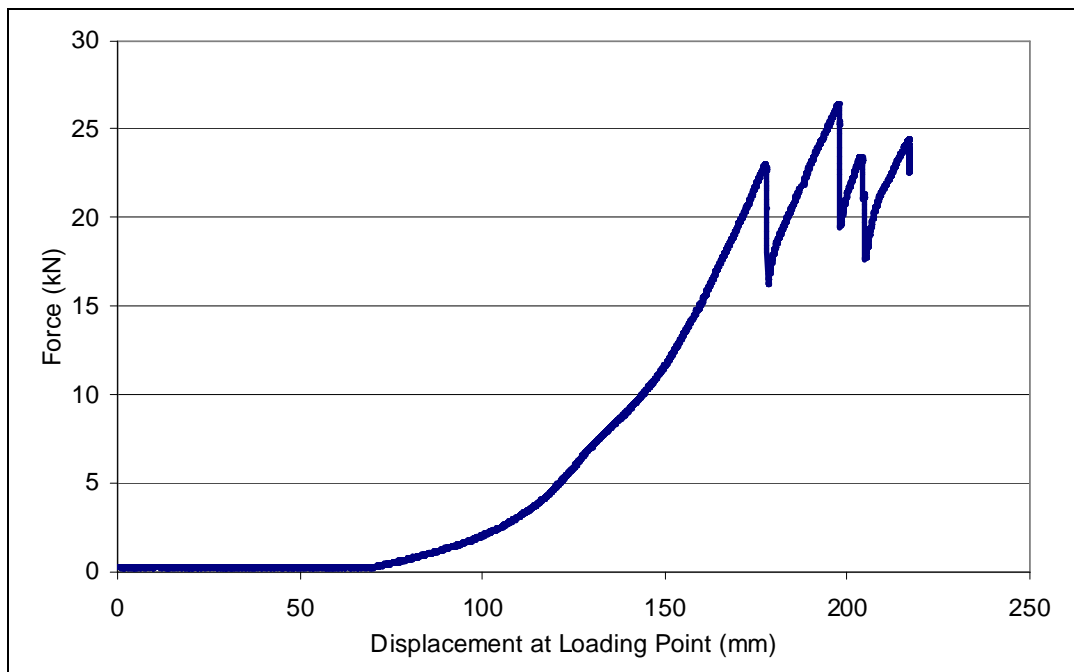


Test Date	23/03/2006	Person testing	Ellen Morton
Test Number: MT002 Type: Weld Mesh			

Sample Specifications			
Length	Width	Grid Size	Wire Diameter
1.3m	1.3m	100mm x 100mm	5.6mm

Boundary Condition	Lacing (3mm)	Loading Condition	Square Flat Plate 300mm x 300mm
			

No of Restraints per side	13
Sample Configuration	Cross wires in contact with load plate and parallel to load bearing beam



Rupture Load	NA	kN	Peak Load	26.48	kN
---------------------	----	----	------------------	-------	----

Rupture Displacement	Na	mm	Displacement prior to active response	73	mm
-----------------------------	----	----	--	----	----

Rupture Mechanism	No failure	Position of Rupture	NA
--------------------------	------------	----------------------------	----

Comments: The 3mm mild steel wire rope ruptured at 22.8 kN. Subsequent steps in the force displacement chart are related to the wire rope slippage and failure. No mesh rupture was observed.



WASM Static Test Report

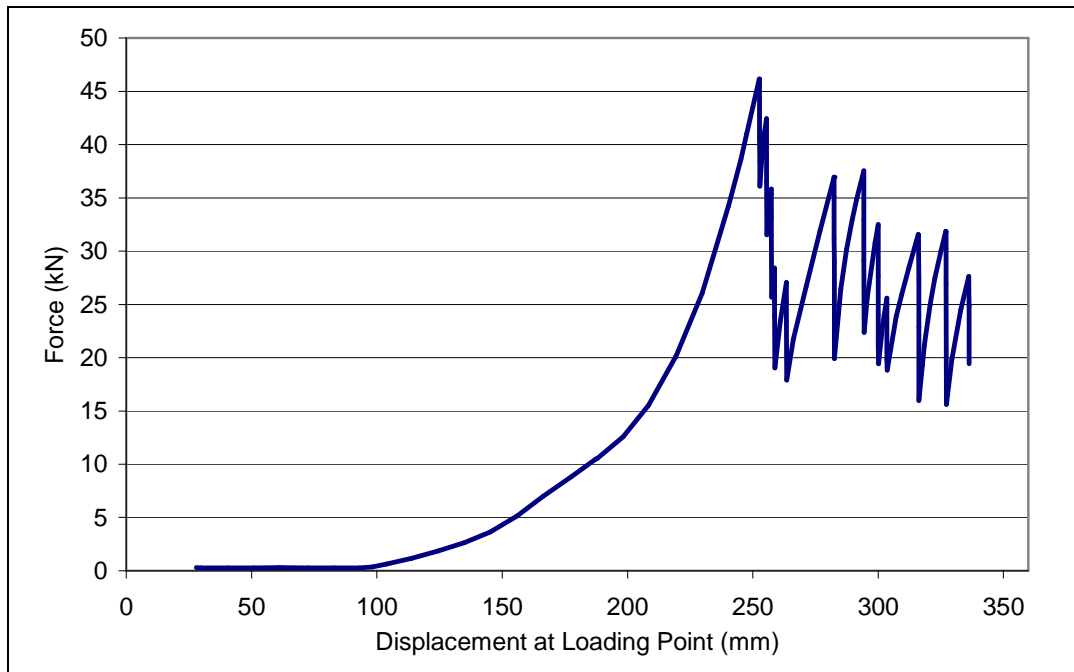


Test Date	11/04/2006	Person testing	Ellen Morton
Test Number: MT005 Type: Weld Mesh			

Sample Specifications			
Length	Width	Grid Size	Wire Diameter
1.3m	1.3m	100mm x 100mm	5.6mm

Boundary Condition	Lacing 	Loading Condition	Square Flat Plate 300mm x 300mm
---------------------------	---	--------------------------	------------------------------------

No of Restraints per side	13
Sample Configuration	Cross wires in contact with load plate and parallel to load bearing beam



Rupture Load	46.2	kN	Peak Load	46.2	kN
---------------------	------	----	------------------	------	----

Rupture Displacement	253	mm	Displacement prior to active response	96	mm
-----------------------------	-----	----	--	----	----

Rupture Mechanism	Weld Failure	Position of Rupture	Loaded wire on manufacturers boundary
--------------------------	--------------	----------------------------	---------------------------------------

Comments:



WASM Static Test Report

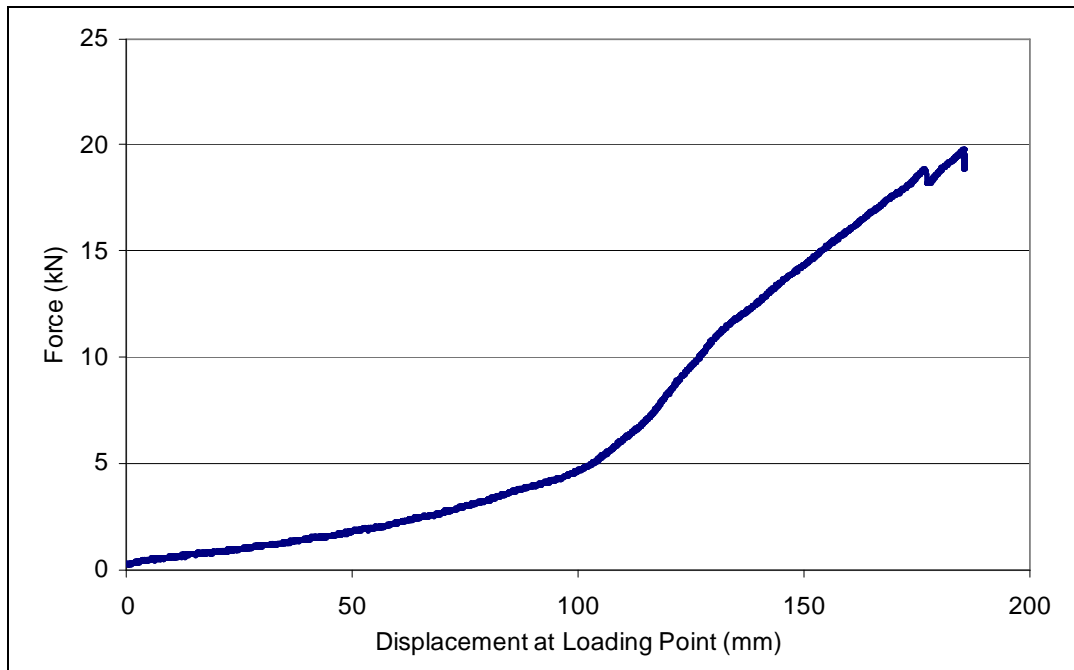


Test Date	27/04/2006	Person testing	Ellen Morton
Test Number: MT006 Type: Weld Mesh			

Sample Specifications			
Length	Width	Grid Size	Wire Diameter
1.6m	0.9m	100mm x 100mm	5.6mm

Boundary Condition	Clamped	Loading Condition	Square Flat Plate 300mm x 300mm
---------------------------	---------	--------------------------	------------------------------------

No of Restraints per side	NA
Sample Configuration	Cross wires in contact with load plate and parallel to load bearing beam



Rupture Load	NA	kN	Peak Load	19.79	kN
---------------------	----	----	------------------	-------	----

Rupture Displacement	NA	mm	Displacement prior to active response	2	mm
-----------------------------	----	----	--	---	----

Rupture Mechanism	No failure	Position of Rupture	NA
--------------------------	------------	----------------------------	----

Comments: The mesh slipped from under the clamping failure and so failure was not achieved.



WASM Static Test Report

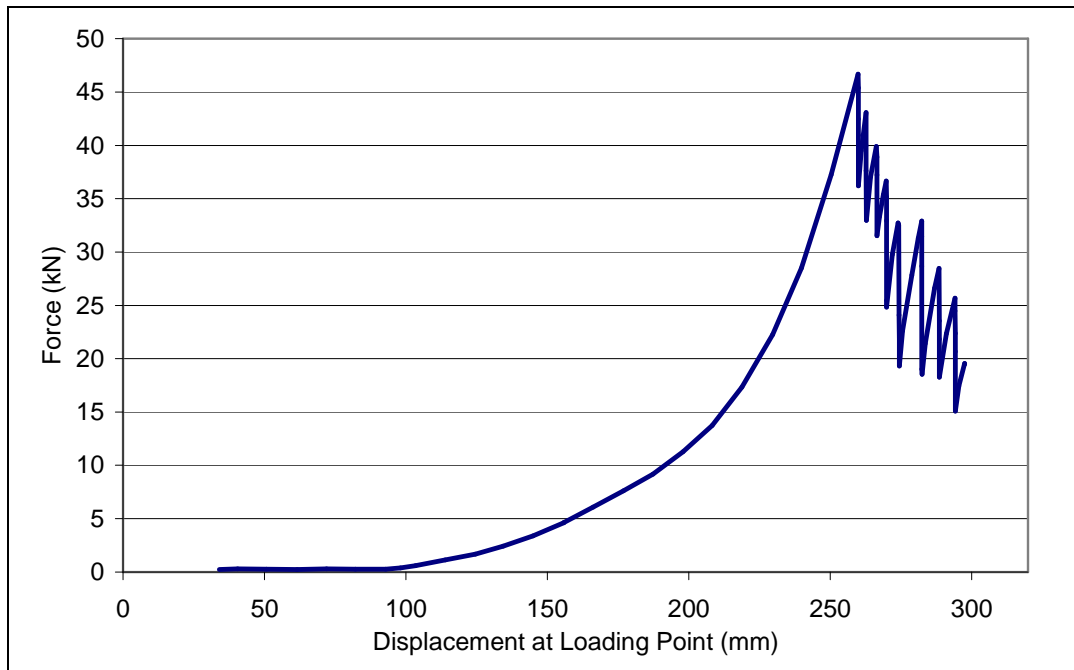


Test Date	03/05/2006	Person testing	Ellen Morton
Test Number: MT007 Type: Weld Mesh			

Sample Specifications			
Length	Width	Grid Size	Wire Diameter
1.3m	1.3m	100mm x 100mm	5.6mm

Boundary Condition	Lacing 	Loading Condition	Square Flat Plate 300mm x 300mm
---------------------------	---	--------------------------	------------------------------------

No of Restraints per side	13
Sample Configuration	Cross wires in contact with load plate and parallel to load bearing beam



Rupture Load	46.68	kN	Peak Load	46.68	kN
---------------------	-------	----	------------------	-------	----

Rupture Displacement	260	mm	Displacement prior to active response	96	mm
-----------------------------	-----	----	--	----	----

Rupture Mechanism	Weld Failure	Position of Rupture	Loaded wire on manufacturers boundary
--------------------------	--------------	----------------------------	---------------------------------------

Comments:



WASM Static Test Report

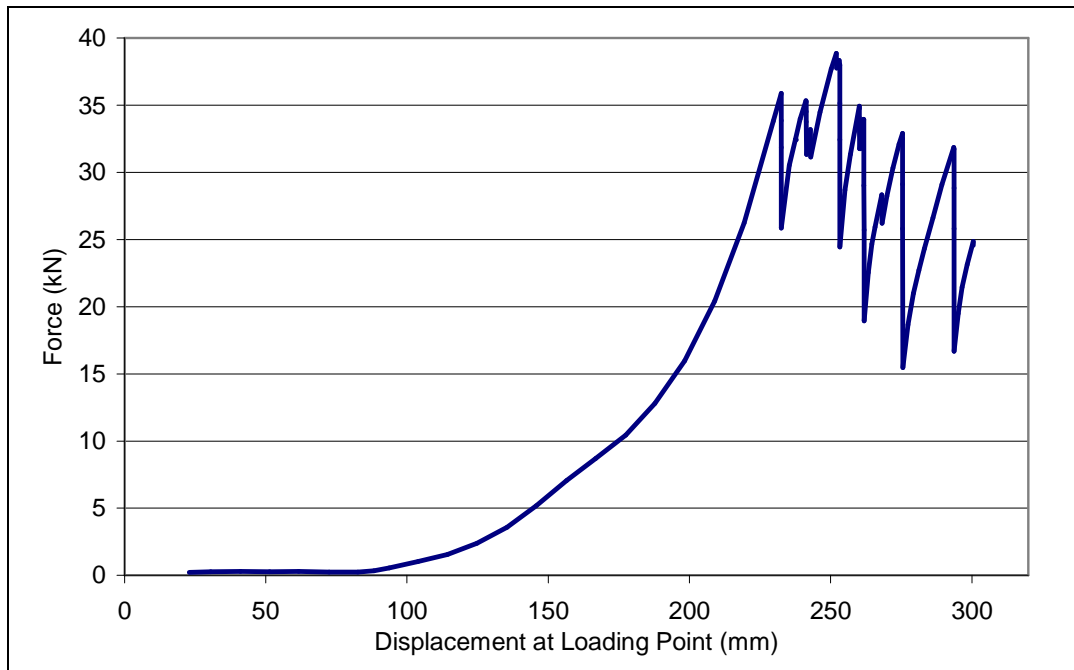


Test Date	11/05/2006	Person testing	Ellen Morton
Test Number: MT008 Type: Weld Mesh			

Sample Specifications			
Length	Width	Grid Size	Wire Diameter
1.3m	1.3m	100mm x 100mm	5.6mm

Boundary Condition	Lacing 	Loading Condition	Square Flat Plate 300mm x 300mm
---------------------------	---	--------------------------	------------------------------------

No of Restraints per side	13
Sample Configuration	Long wires in contact with load plate and parallel to load bearing beam



Rupture Load	35.88	kN	Peak Load	38.86	kN
---------------------	-------	----	------------------	-------	----

Rupture Displacement	232	mm	Displacement prior to active response	87	mm
-----------------------------	-----	----	--	----	----

Rupture Mechanism	Wire failure through HAZ	Position of Rupture	Loaded wire on manufacturers boundary
--------------------------	--------------------------	----------------------------	---------------------------------------

Comments:

HAZ – Heat Affected Zone on wire as a result of welding process



WASM Static Test Report

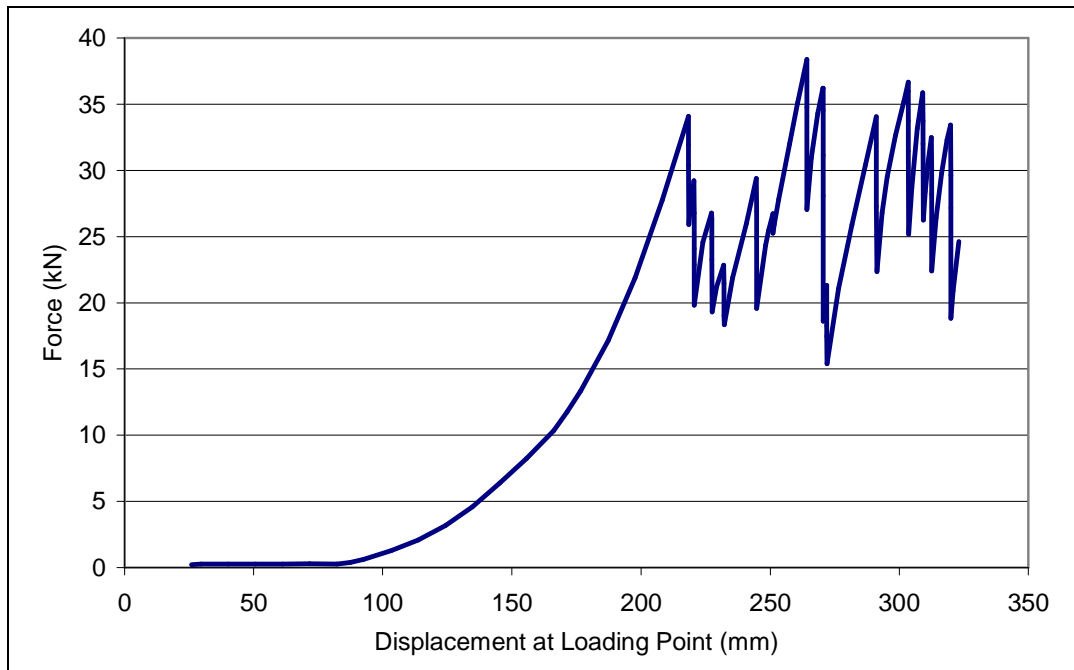


Test Date	16/05/2006	Person testing	Ellen Morton
Test Number: MT009 Type: Weld Mesh			

Sample Specifications			
Length	Width	Grid Size	Wire Diameter
1.3m	1.3m	100mm x 100mm	5.6mm

Boundary Condition	Lacing 	Loading Condition	Square Flat Plate 300mm x 300mm
---------------------------	---	--------------------------	------------------------------------

No of Restraints per side	13
Sample Configuration	Cross wires in contact with load plate and parallel to load bearing beam



Rupture Load	34.089	kN	Peak Load	38.381	kN
---------------------	--------	----	------------------	--------	----

Rupture Displacement	218	mm	Displacement prior to active response	86	mm
-----------------------------	-----	----	--	----	----

Rupture Mechanism	Weld Failure	Position of Rupture	Loaded wire on manufacturers boundary
--------------------------	--------------	----------------------------	---------------------------------------

Comments:



WASM Static Test Report

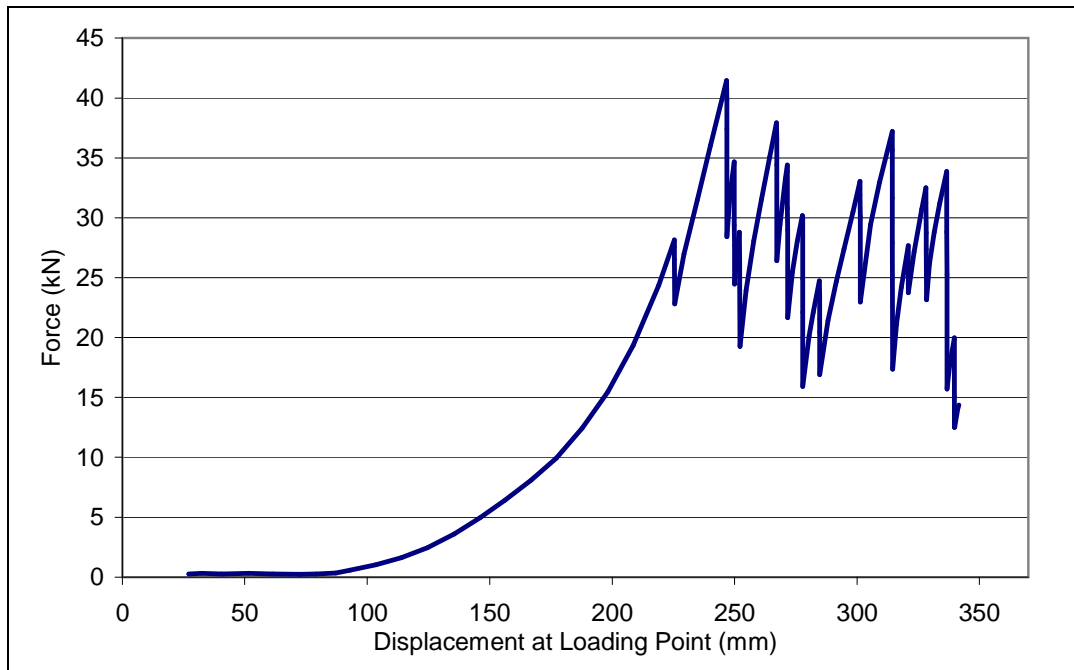


Test Date	19/05/2006	Person testing	Ellen Morton
Test Number: MT010 Type: Weld Mesh			

Sample Specifications			
Length	Width	Grid Size	Wire Diameter
1.3m	1.3m	100mm x 100mm	5.6mm

Boundary Condition	Lacing 	Loading Condition	Square Flat Plate 300mm x 300mm
---------------------------	---	--------------------------	------------------------------------

No of Restraints per side	13
Sample Configuration	Cross wires in contact with load plate and parallel to load bearing beam



Rupture Load	28.14	kN	Peak Load	41.45	kN
---------------------	-------	----	------------------	-------	----

Rupture Displacement	225	mm	Displacement prior to active response	87	mm
-----------------------------	-----	----	--	----	----

Rupture Mechanism	Weld Failure	Position of Rupture	Loaded wire on manufacturers boundary
--------------------------	--------------	----------------------------	---------------------------------------

Comments: Poor weld quality resulted in low level rupture.



WASM Static Test Report

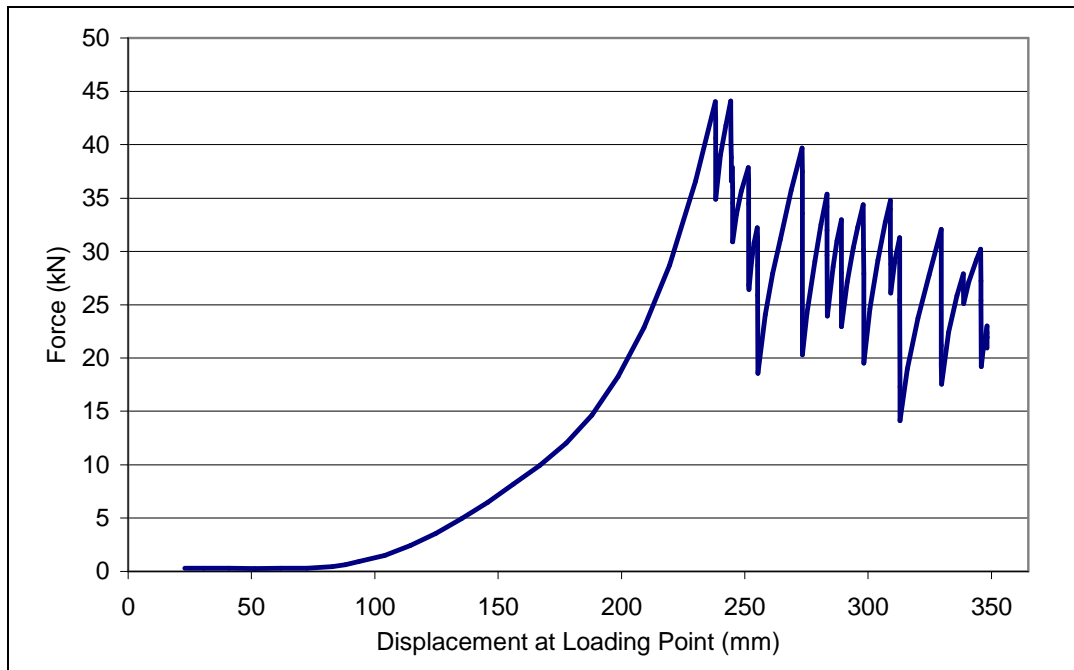


Test Date	02/06/2006	Person testing	Ellen Morton
Test Number: MT011 Type: Weld Mesh			

Sample Specifications			
Length	Width	Grid Size	Wire Diameter
1.3m	1.3m	100mm x 100mm	5.6mm

Boundary Condition	Lacing 	Loading Condition	Square Flat Plate 300mm x 300mm
---------------------------	---	--------------------------	------------------------------------

No of Restraints per side	13
Sample Configuration	Cross wires in contact with load plate and parallel to load bearing beam



Rupture Load	44.05	kN	Peak Load	44.09	kN
---------------------	-------	----	------------------	-------	----

Rupture Displacement	238	mm	Displacement prior to active response	79	mm
-----------------------------	-----	----	--	----	----

Rupture Mechanism	Weld Failure	Position of Rupture	Loaded wire on manufacturers boundary
--------------------------	--------------	----------------------------	---------------------------------------

Comments:



WASM Static Test Report

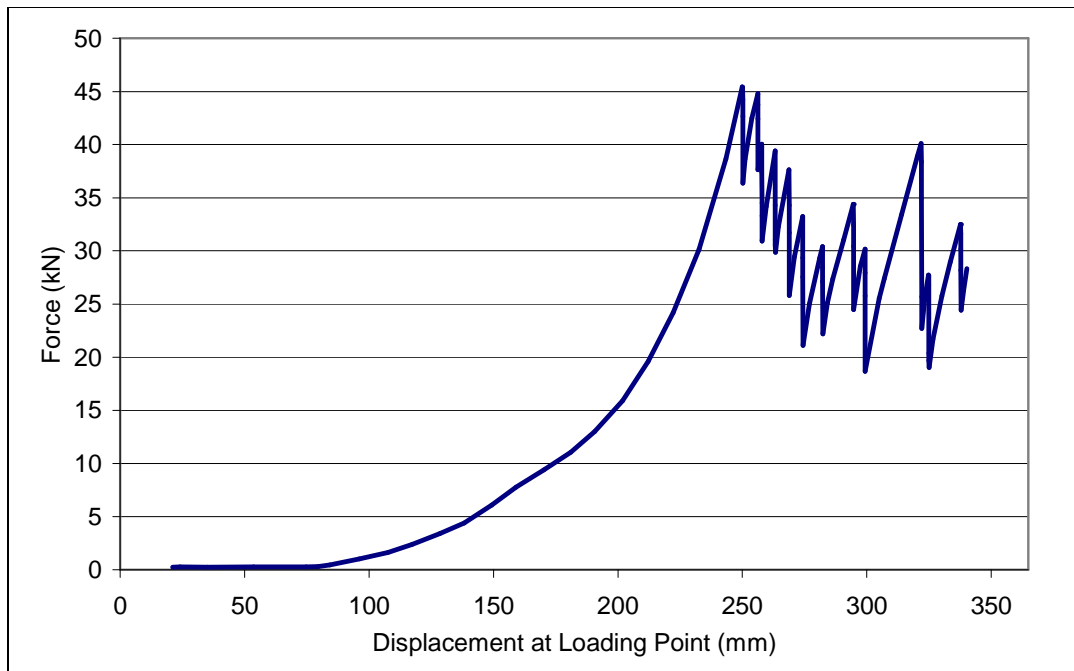


Test Date	16/06/2006	Person testing	Ellen Morton
Test Number: MT013 Type: Weld Mesh			

Sample Specifications			
Length	Width	Grid Size	Wire Diameter
1.3m	1.3m	100mm x 100mm	5.6mm

Boundary Condition	Lacing	Loading Condition	Square Flat Plate 300mm x 300mm + Flat Rubber plate 500mm x 500mm
			

No of Restraints per side	13
Sample Configuration	Cross wires in contact with load plate and parallel to load bearing beam



Rupture Load	45.44	kN	Peak Load	45.44	kN
---------------------	-------	----	------------------	-------	----

Rupture Displacement	250	mm	Displacement prior to active response	80	mm
-----------------------------	-----	----	--	----	----

Rupture Mechanism	Weld Failure	Position of Rupture	Loaded wire on manufacturers boundary
--------------------------	--------------	----------------------------	---------------------------------------

Comments: Rubber plate trying to soften sharp edge of load plate. Steel plate cut into rubber plate but otherwise successful.



WASM Static Test Report

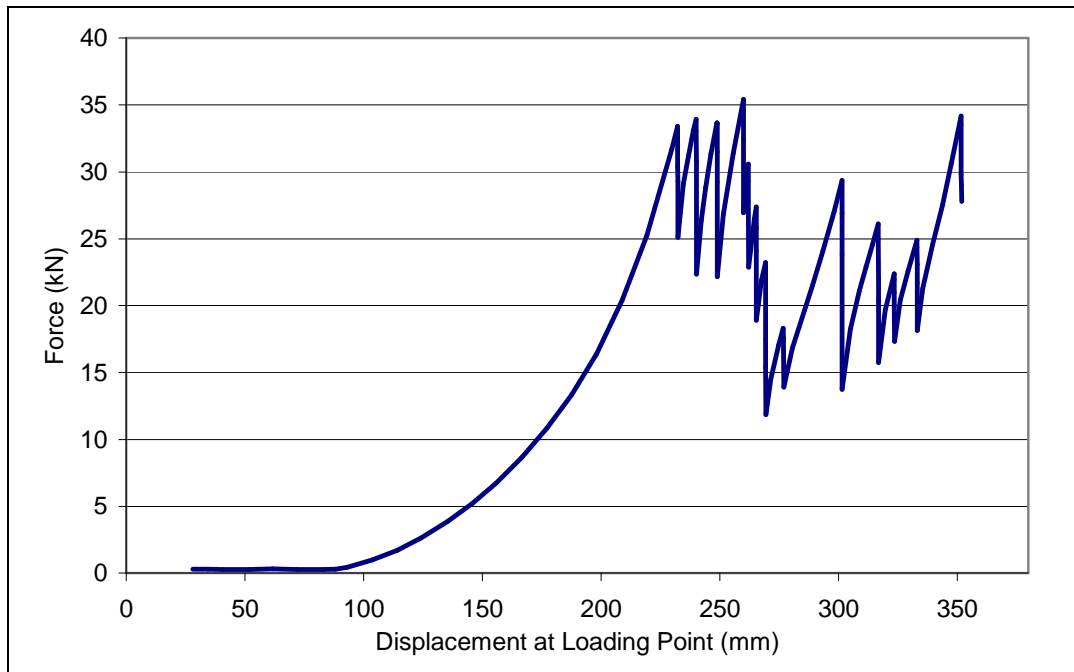


Test Date	12/07/2006	Person testing	Ellen Morton
Test Number: MT014 Type: Weld Mesh			

Sample Specifications			
Length	Width	Grid Size	Wire Diameter
1.3m	1.3m	100mm x 100mm	5.6mm

Boundary Condition	Lacing 	Loading Condition	Square Flat Plate 300mm x 300mm
---------------------------	---	--------------------------	------------------------------------

No of Restraints per side	13
Sample Configuration	Cross wires in contact with load plate and parallel to load bearing beam



Rupture Load	33.42	kN	Peak Load	35.42	kN
---------------------	-------	----	------------------	-------	----

Rupture Displacement	232	mm	Displacement prior to active response	91	mm
-----------------------------	-----	----	--	----	----

Rupture Mechanism	Weld Failure	Position of Rupture	Loaded wire on manufacturers boundary
--------------------------	--------------	----------------------------	---------------------------------------

Comments:



WASM Static Test Report

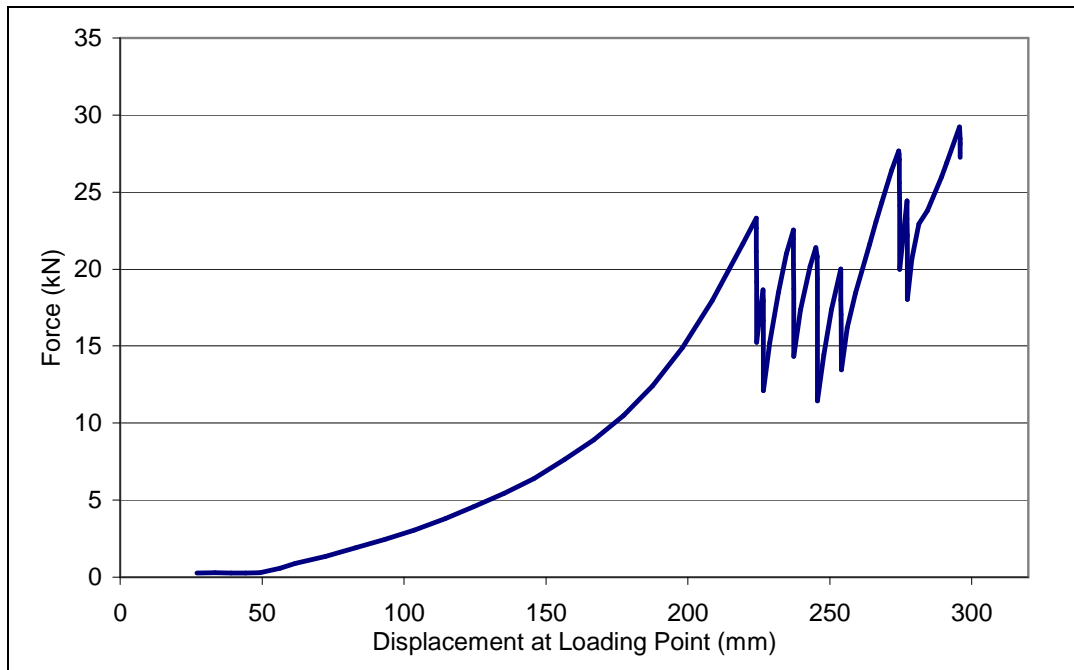


Test Date	09/08/2006	Person testing	Ellen Morton
Test Number: MT015 Type: Weld Mesh			

Sample Specifications			
Length	Width	Grid Size	Wire Diameter
1.3m	1.3m	100mm x 100mm	5.6mm

Boundary Condition	Hooks 	Loading Condition	Square Flat Plate 300mm x 300mm
---------------------------	--	--------------------------	------------------------------------

No of Restraints per side	5
Sample Configuration	Cross wires in contact with load plate and parallel to load bearing beam



Rupture Load	23.31	kN	Peak Load	29.23	kN
---------------------	-------	----	------------------	-------	----

Rupture Displacement	224	mm	Displacement prior to active response	50	mm
-----------------------------	-----	----	--	----	----

Rupture Mechanism	Weld Failure	Position of Rupture	Loaded wire on cut edge of sample
--------------------------	--------------	----------------------------	-----------------------------------

Comments: Commissioning test for new test frame. Trial of new fixtures. Hooks had too much moment and bent during testing. Test results not valid.



WASM Static Test Report

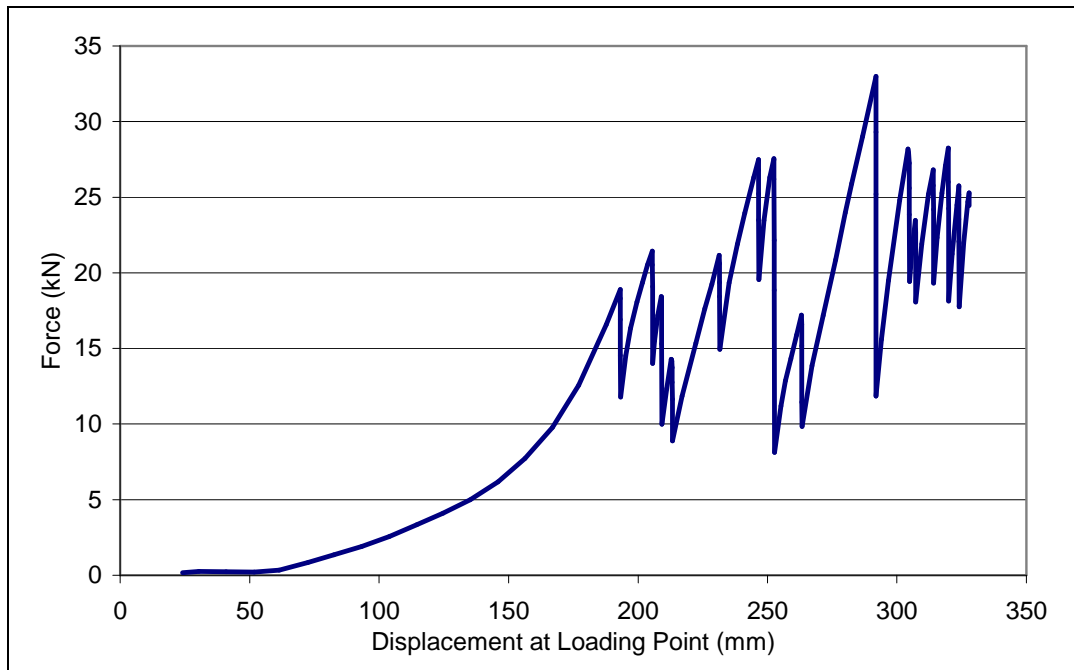


Test Date	16/08/2006	Person testing	Ellen Morton
Test Number: MT016 Type: Weld Mesh			

Sample Specifications			
Length	Width	Grid Size	Wire Diameter
1.3m	1.3m	100mm x 100mm	5.6mm

Boundary Condition	Fixed 	Loading Condition	Square Flat Plate 300mm x 300mm
---------------------------	-----------	--------------------------	------------------------------------

No of Restraints per side	5
Sample Configuration	Cross wires in contact with load plate and parallel to load bearing beam



Rupture Load	18.90	kN	Peak Load	33.00	kN
---------------------	-------	----	------------------	-------	----

Rupture Displacement	193	mm	Displacement prior to active response	61	mm
-----------------------------	-----	----	--	----	----

Rupture Mechanism	Weld Failure	Position of Rupture	Loaded wire on manufacturers boundary
--------------------------	--------------	----------------------------	---------------------------------------

Comments: Commissioning test for new test frame. First test using shackles and eye nuts. Method considered successful and adopted as standard.



WASM Static Test Report

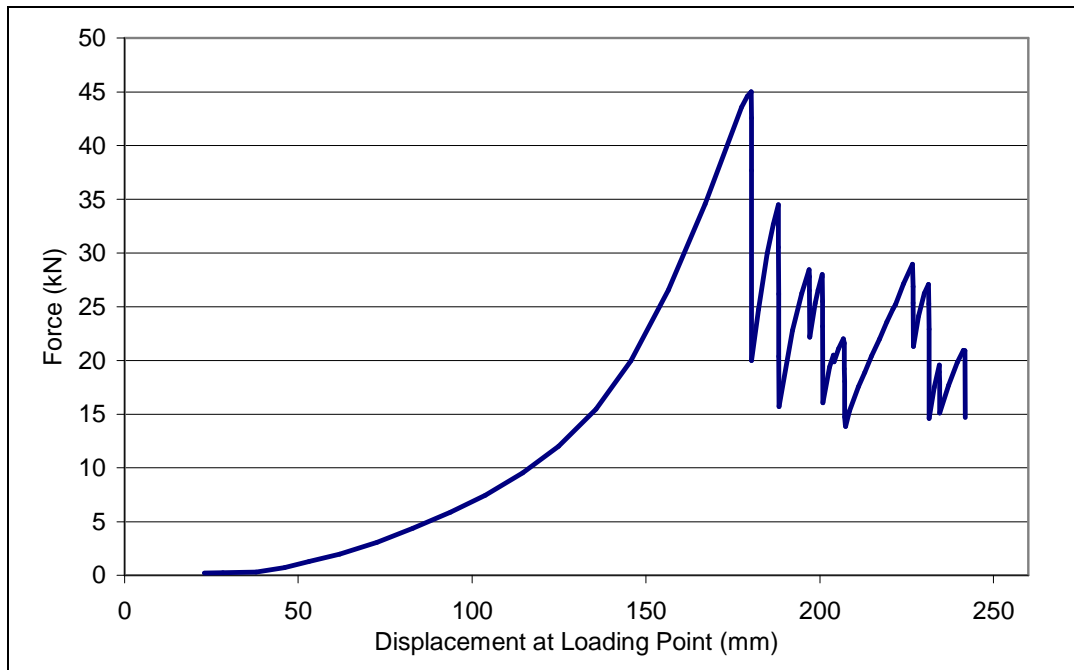


Test Date	25/08/2006	Person testing	Ellen Morton
Test Number: MT017 Type: Weld Mesh			

Sample Specifications			
Length	Width	Grid Size	Wire Diameter
1.3m	1.3m	100mm x 100mm	5.6mm

Boundary Condition	Fixed 	Loading Condition	Square Flat Plate 300mm x 300mm
---------------------------	--	--------------------------	------------------------------------

No of Restraints per side	13
Sample Configuration	Cross wires in contact with load plate and parallel to load bearing beam



Rupture Load	45.04	kN	Peak Load	45.036	kN
---------------------	-------	----	------------------	--------	----

Rupture Displacement	180	mm	Displacement prior to active response	38	mm
-----------------------------	-----	----	--	----	----

Rupture Mechanism	Combination weld failure and tensile wire failure	Position of Rupture	Loaded wire on cut edge of sample
--------------------------	---	----------------------------	-----------------------------------

Comments:

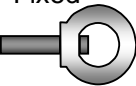


WASM Static Test Report

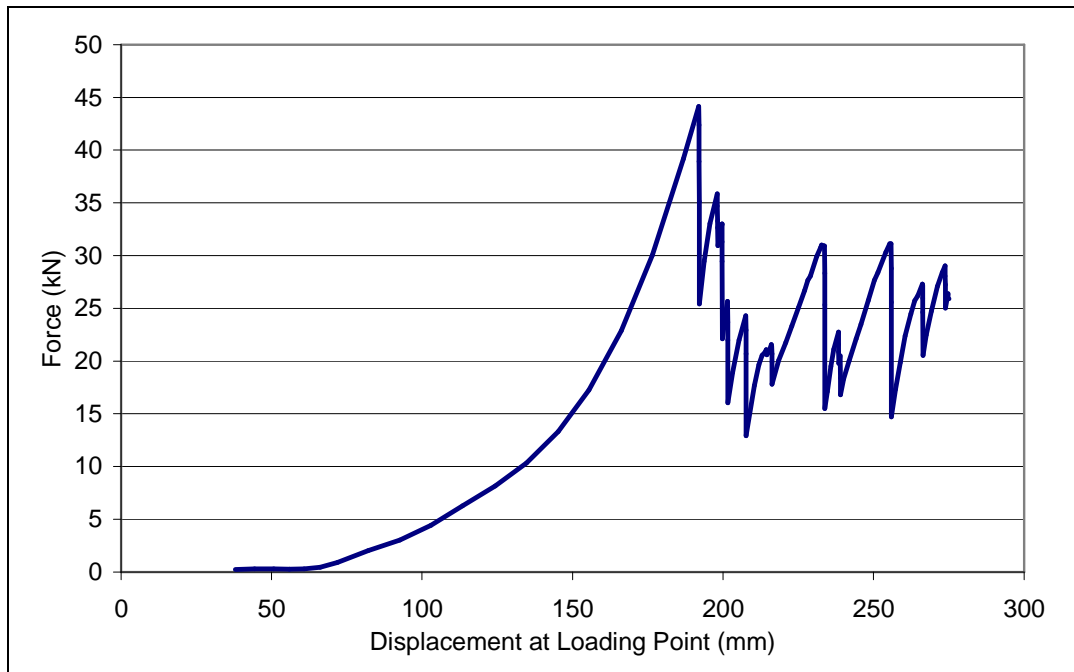


Test Date	15/09/2006	Person testing	Ellen Morton
Test Number: MT020 Type: Weld Mesh			

Sample Specifications			
Length	Width	Grid Size	Wire Diameter
1.3m	1.3m	100mm x 100mm	5.6mm

Boundary Condition	Fixed 	Loading Condition	Square Flat Plate 300mm x 300mm
---------------------------	--	--------------------------	------------------------------------

No of Restraints per side	13
Sample Configuration	Cross wires in contact with load plate and parallel to load bearing beam



Rupture Load	44.139	kN	Peak Load	44.139	kN
---------------------	--------	----	------------------	--------	----

Rupture Displacement	192	mm	Displacement prior to active response	65	mm
-----------------------------	-----	----	--	----	----

Rupture Mechanism	Wire failure through HAZ	Position of Rupture	Loaded wire on manufacturers boundary
--------------------------	--------------------------	----------------------------	---------------------------------------

Comments:

HAZ – Heat Affected Zone on wire as a result of welding process

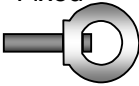


WASM Static Test Report

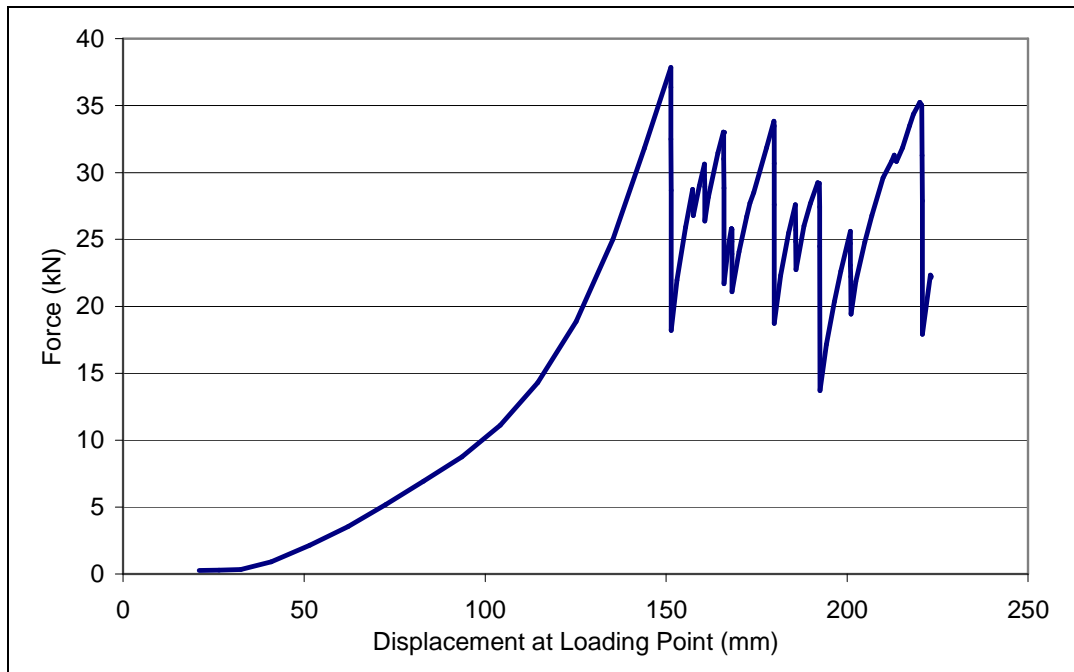


Test Date	03/10/2006	Person testing	Ellen Morton
Test Number: MT021 Type: Weld Mesh			

Sample Specifications			
Length	Width	Grid Size	Wire Diameter
1.3m	1.3m	100mm x 100mm	5.6mm

Boundary Condition	Fixed 	Loading Condition	Square Flat Plate 300mm x 300mm
---------------------------	--	--------------------------	------------------------------------

No of Restraints per side	13
Sample Configuration	Long wires in contact with load plate and parallel to load bearing beam



Rupture Load	37.86	kN	Peak Load	37.86	kN
---------------------	-------	----	------------------	-------	----

Rupture Displacement	151	mm	Displacement prior to active response	32	mm
-----------------------------	-----	----	--	----	----

Rupture Mechanism	Wire failure through HAZ	Position of Rupture	Loaded wire on manufacturers boundary
--------------------------	--------------------------	----------------------------	---------------------------------------

Comments: Sample flipped and rotated from standard setup.

HAZ – Heat Affected Zone on wire as a result of welding process



WASM Static Test Report

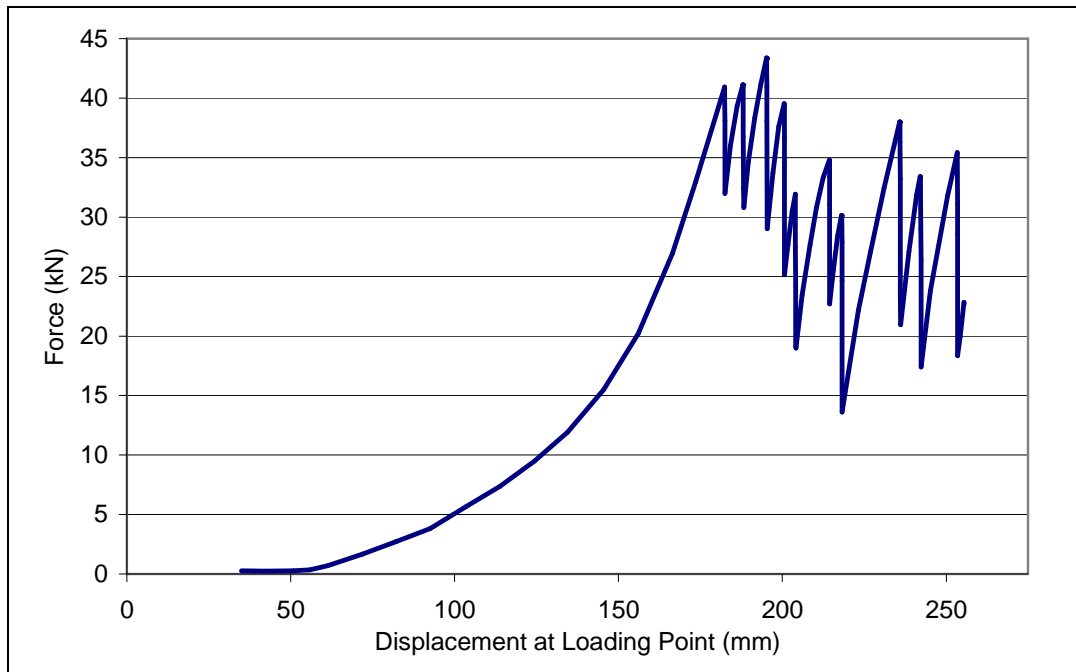


Test Date	09/10/2006	Person testing	Ellen Morton
Test Number: MT022 Type: Weld Mesh			

Sample Specifications			
Length	Width	Grid Size	Wire Diameter
1.3m	1.3m	100mm x 100mm	5.6mm

Boundary Condition	Fixed 	Loading Condition	Square Flat Plate 300mm x 300mm
---------------------------	--	--------------------------	------------------------------------

No of Restraints per side	13
Sample Configuration	Cross wires in contact with load plate and parallel to load bearing beam



Rupture Load	40.94	kN	Peak Load	43.41	kN
---------------------	-------	----	------------------	-------	----

Rupture Displacement	182	mm	Displacement prior to active response	56	mm
-----------------------------	-----	----	--	----	----

Rupture Mechanism	Weld Failure	Position of Rupture	Loaded wire on cut edge of sample
--------------------------	--------------	----------------------------	-----------------------------------

Comments:

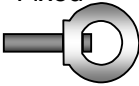


WASM Static Test Report

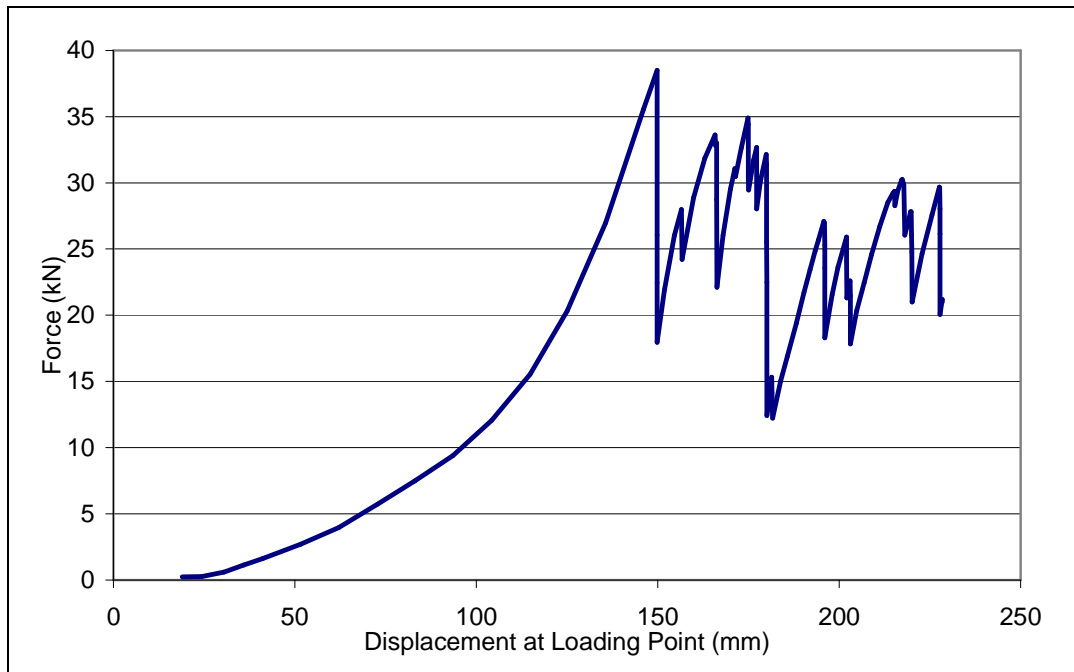


Test Date	11/10/2006	Person testing	Ellen Morton
Test Number: MT024 Type: Weld Mesh			

Sample Specifications			
Length	Width	Grid Size	Wire Diameter
1.3m	1.3m	100mm x 100mm	5.6mm

Boundary Condition	Fixed 	Loading Condition	Square Flat Plate 300mm x 300mm
---------------------------	--	--------------------------	------------------------------------

No of Restraints per side	13
Sample Configuration	Long wires in contact with load plate and parallel to load bearing beam



Rupture Load	38.52	kN	Peak Load	38.52	kN
---------------------	-------	----	------------------	-------	----

Rupture Displacement	150	mm	Displacement prior to active response	25	mm
-----------------------------	-----	----	--	----	----

Rupture Mechanism	Wire failure through HAZ	Position of Rupture	Loaded wire on manufacturers boundary
--------------------------	--------------------------	----------------------------	---------------------------------------

Comments: Sample rotated and flipped from standard setup.

HAZ – Heat Affected Zone on wire as a result of welding process

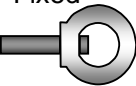


WASM Static Test Report

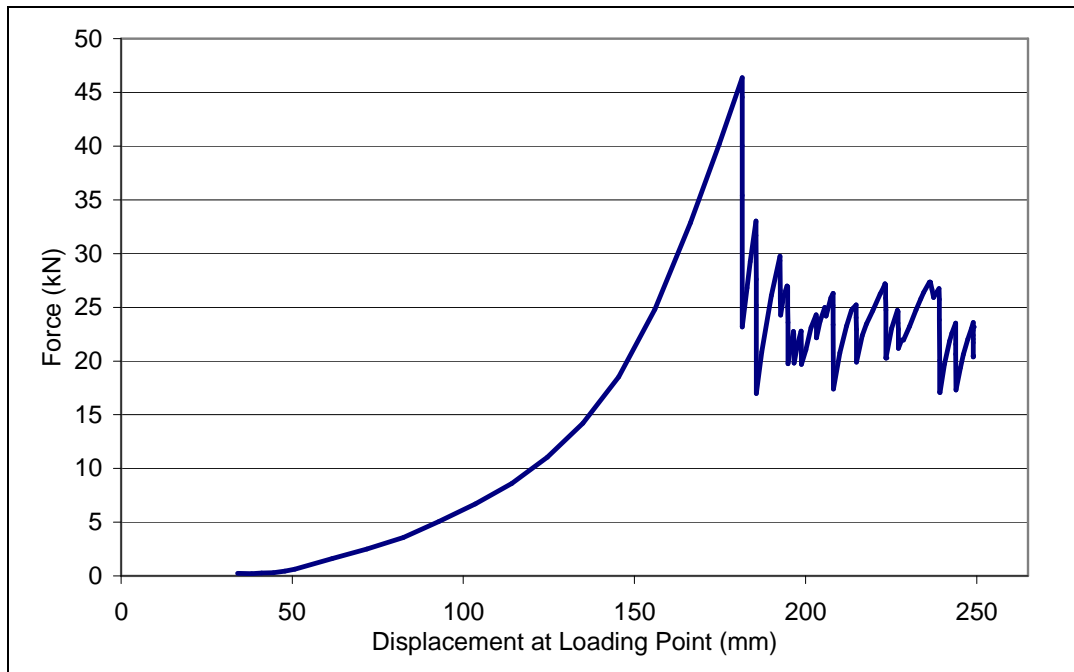


Test Date	13/10/2006	Person testing	Ellen Morton
Test Number: MT025 Type: Weld Mesh			

Sample Specifications			
Length	Width	Grid Size	Wire Diameter
1.3m	1.3m	100mm x 100mm	5.6mm

Boundary Condition	Fixed 	Loading Condition	Square Flat Plate 300mm x 300mm
---------------------------	--	--------------------------	------------------------------------

No of Restraints per side	13
Sample Configuration	Cross wires in contact with load plate and parallel to load bearing beam



Rupture Load	46.38	kN	Peak Load	46.38	kN
---------------------	-------	----	------------------	-------	----

Rupture Displacement	181	mm	Displacement prior to active response	45	mm
-----------------------------	-----	----	--	----	----

Rupture Mechanism	Tensile failure of wire	Position of Rupture	Loaded wire on manufacturers boundary
--------------------------	-------------------------	----------------------------	---------------------------------------

Comments:

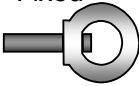


WASM Static Test Report

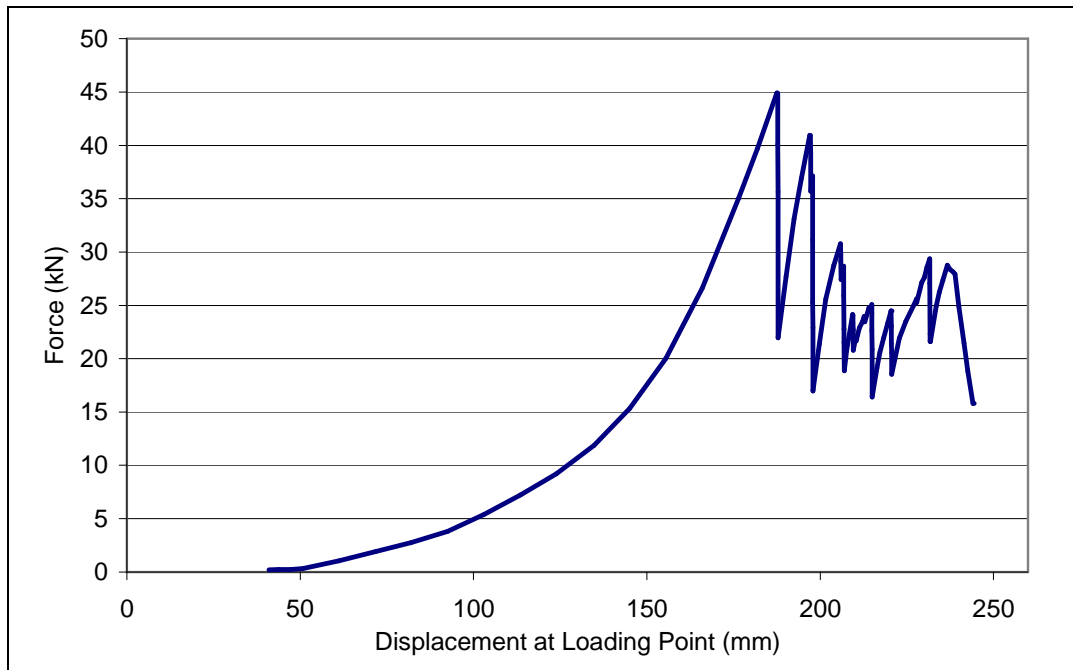


Test Date	26/10/2006	Person testing	Ellen Morton
Test Number: MT026 Type: Weld Mesh			

Sample Specifications			
Length	Width	Grid Size	Wire Diameter
1.3m	1.3m	100mm x 100mm	5.6mm

Boundary Condition	Fixed 	Loading Condition	Square Flat Plate 300mm x 300mm
---------------------------	--	--------------------------	------------------------------------

No of Restraints per side	13
Sample Configuration	Long wires in contact with load plate and parallel to load bearing beam



Rupture Load	44.92	kN	Peak Load	44.92	kN
---------------------	-------	----	------------------	-------	----

Rupture Displacement	188	mm	Displacement prior to active response	49	mm
-----------------------------	-----	----	--	----	----

Rupture Mechanism	Tensile failure of wire	Position of Rupture	Loaded wire on cut edge of sample
--------------------------	-------------------------	----------------------------	-----------------------------------

Comments: Sample rotated and flipped from base case



WASM Static Test Report

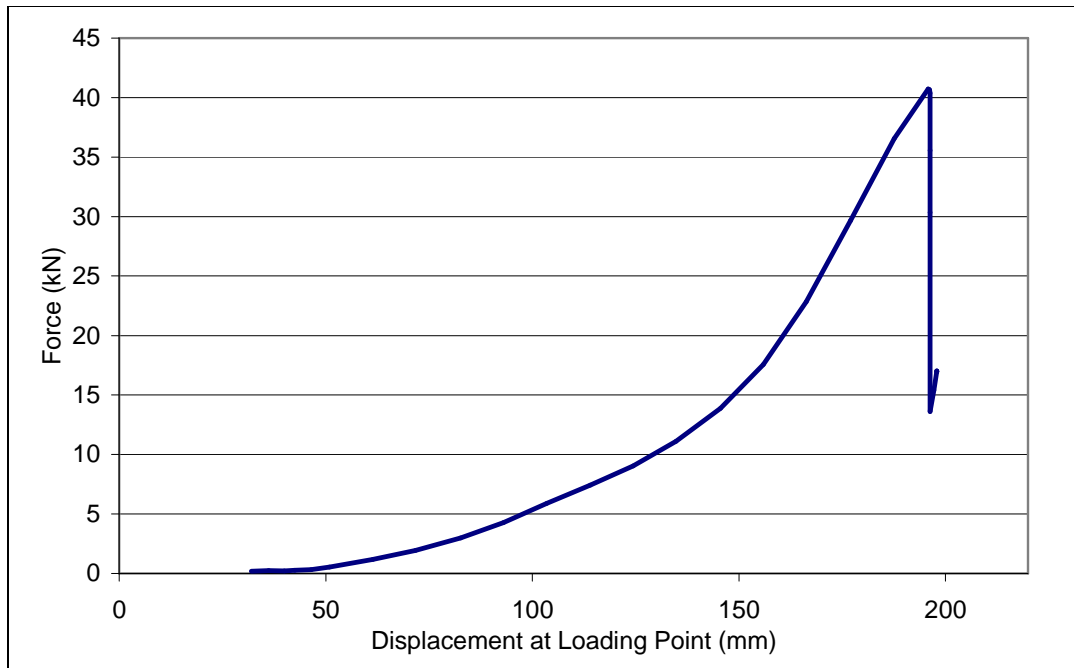


Test Date	31/10/2006	Person testing	Ellen Morton
Test Number: MT027 Type: Weld Mesh			

Sample Specifications			
Length	Width	Grid Size	Wire Diameter
1.3m	1.3m	100mm x 100mm	5.6mm

Boundary Condition	Fixed 	Loading Condition	Square Flat Plate 300mm x 300mm
---------------------------	--	--------------------------	------------------------------------

No of Restraints per side	13
Sample Configuration	Cross wires in contact with load plate and parallel to load bearing beam. Hole (150mm x 150mm) cut in mesh under load plate



Rupture Load	40.74	kN	Peak Load	40.74	kN
---------------------	-------	----	------------------	-------	----

Rupture Displacement	195	mm	Displacement prior to active response	46	mm
-----------------------------	-----	----	--	----	----

Rupture Mechanism	Wire failure through HAZ	Position of Rupture	Under load plate
--------------------------	--------------------------	----------------------------	------------------

Comments: Flat square plate hooked around corners of cut hole leading to unrealistic results. If hooking had not occurred plate would have pushed through. Test to be repeated using curved plate.

HAZ – Heat Affected Zone on wire as a result of welding process



WASM Static Test Report

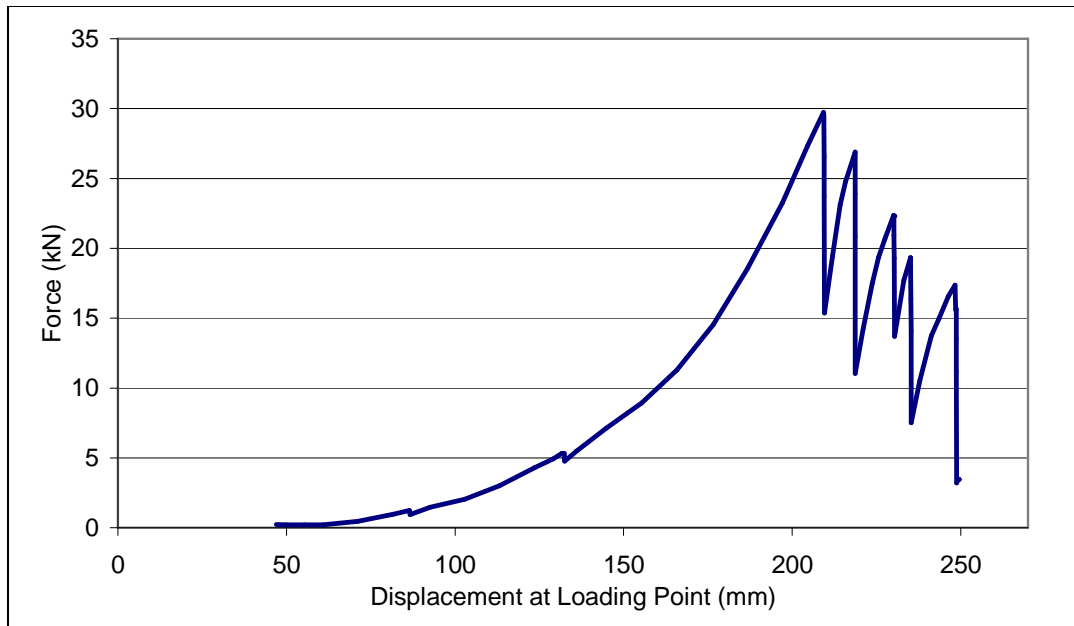


Test Date	01/11/2006	Person testing	Ellen Morton
Test Number: MT028 Type: Weld Mesh			

Sample Specifications			
Length	Width	Grid Size	Wire Diameter
0.8m	1.3m	100mm x 100mm	5.6mm
0.7m	1.3m	100mm x 100mm	5.6mm

Boundary Condition	Fixed 	Loading Condition	Square Flat Plate 300mm x 300mm
---------------------------	--	--------------------------	------------------------------------

No of Restraints per side	13
Sample Configuration	Cross wires in contact with load plate and parallel to load bearing beam. 2 samples overlapped by 200mm in centre of frame. Overlap direction parallel to load bearing beam



Rupture Load	29.74	kN	Peak Load	29.74	kN
---------------------	-------	----	------------------	-------	----

Rupture Displacement	209	mm	Displacement prior to active response	66	mm
-----------------------------	-----	----	--	----	----

Rupture Mechanism	Weld Failure	Position of Rupture	Loaded wire on manufacturers boundary
--------------------------	--------------	----------------------------	---------------------------------------

Comments: During the initial stages of the test the plate pushed the mesh samples apart (shown by the two slips at less than 5kN force). At around 20kN, the flat square plate hooked around the wires making the results unrealistic. Observations indicate load transfer around the mesh when loading occurs on the overlap is significantly different from when loading occurs in the centre of a sheet. Test to be repeated using curved plate.

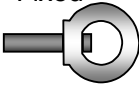


WASM Static Test Report

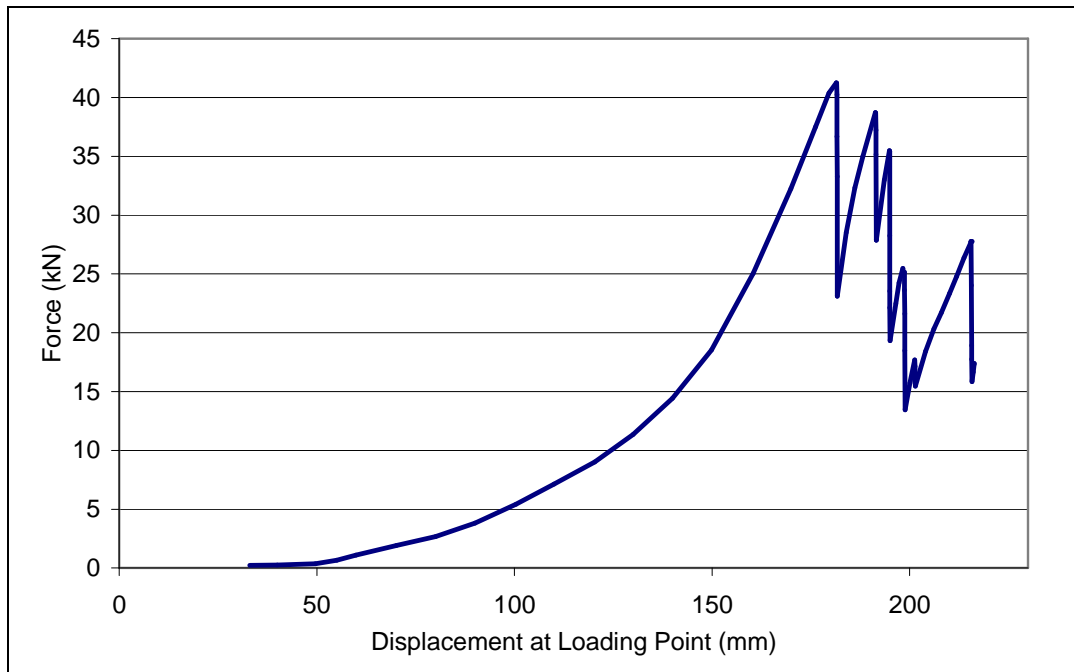


Test Date	03/11/2006	Tester Name	Ellen Morton
Test Number: MT029 Type: Weld Mesh			

Sample Specifications			
Length	Width	Grid Size	Wire Diameter
1.3m	1.3m	100mm x 100mm	5.6mm

Boundary Condition	Fixed 	Loading Condition	Square Flat Plate 300mm x 300mm
---------------------------	--	--------------------------	------------------------------------

No of Restraints per side	13
Sample Configuration	Cross wires in contact with load plate and parallel to load bearing beam



Rupture Load	41.27	kN	Peak Load	41.27	kN
---------------------	-------	----	------------------	-------	----

Rupture Displacement	181	mm	Displacement prior to active response	49	mm
-----------------------------	-----	----	--	----	----

Rupture Mechanism	Weld Failure	Position of Rupture	Loaded wire on manufacturers boundary
--------------------------	--------------	----------------------------	---------------------------------------

Comments:

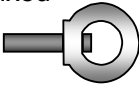


WASM Static Test Report

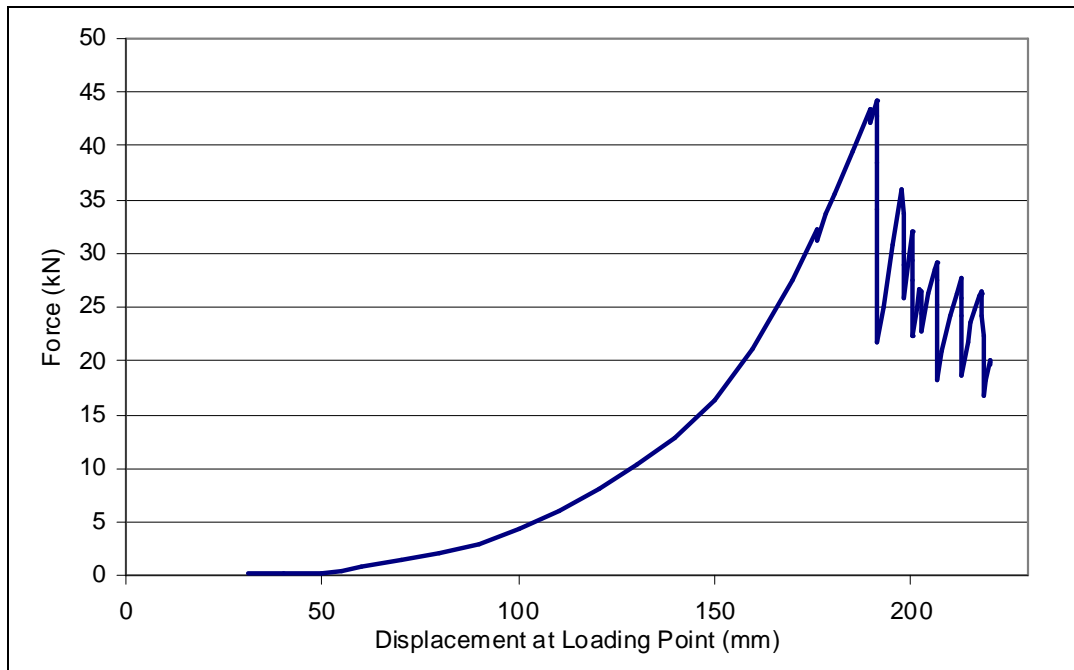


Test Date	12/02/2007	Person Testing	Ellen Morton
Test Number: MT033 Type: Weld Mesh			

Sample Specifications			
Length	Width	Grid Size	Wire Diameter
1.3m	1.3m	100mm x 100mm	5.6mm

Boundary Condition	Fixed 	Loading Condition	Square Curved Plate 300mm x 300mm
---------------------------	--	--------------------------	--------------------------------------

No of Restraints per side	13
Sample Configuration	Cross wires in contact with load plate and parallel to load bearing beam



Rupture Load	43.42	kN	Peak Load	44.17	kN
---------------------	-------	----	------------------	-------	----

Rupture Displacement	189	mm	Displacement prior to active response	52	mm
-----------------------------	-----	----	--	----	----

Rupture Mechanism	Weld Failure	Position of Rupture	Corner weld on manufacturers boundary
--------------------------	--------------	----------------------------	---------------------------------------

Comments:

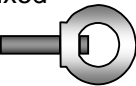


WASM Static Test Report

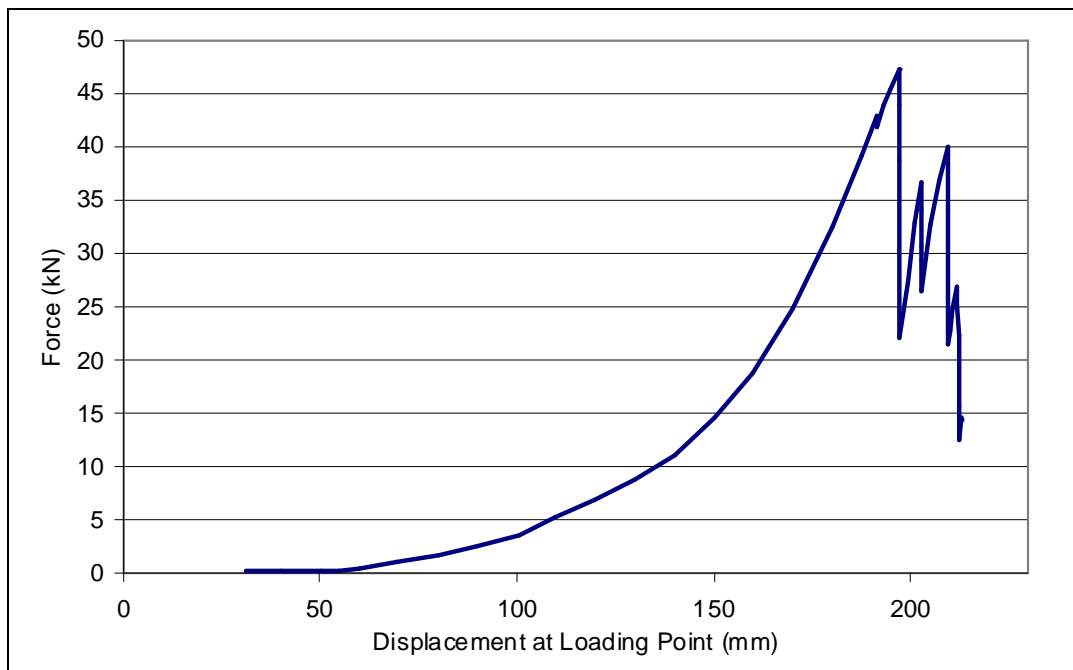


Test Date	17/02/2002	Person Testing	Ellen Morton
Test Number: MT034 Type: Weld Mesh			

Sample Specifications			
Length	Width	Grid Size	Wire Diameter
1.3m	1.3m	100mm x 100mm	5.6mm

Boundary Condition	Fixed 	Loading Condition	Square Curved Plate 300mm x 300mm
---------------------------	--	--------------------------	--------------------------------------

No of Restraints per side	13
Sample Configuration	Cross wires in contact with load plate and parallel to load bearing beam



Rupture Load	43.00	kN	Peak Load	47.24	kN
---------------------	-------	----	------------------	-------	----

Rupture Displacement	191	mm	Displacement prior to active response	57	mm
-----------------------------	-----	----	--	----	----

Rupture Mechanism	Weld Failure	Position of Rupture	Corner weld on manufacturers boundary
--------------------------	--------------	----------------------------	---------------------------------------

Comments:

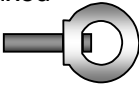


WASM Static Test Report

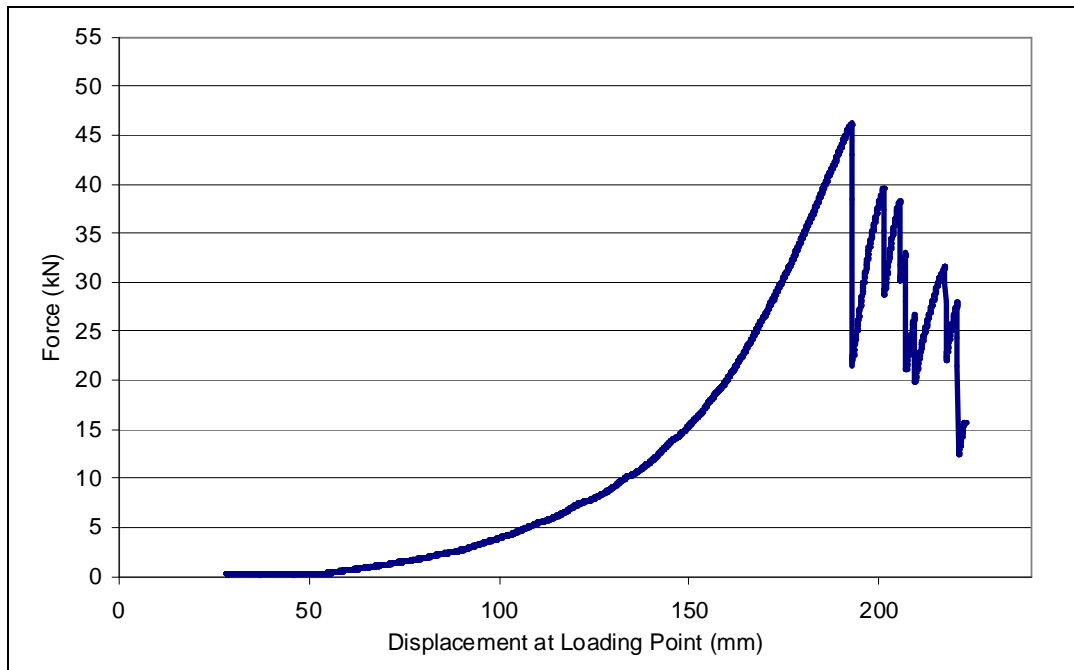


Test Date	21/03/2007	Person Testing	Ellen Morton
Test Number: MT036 Type: Weld Mesh			

Sample Specifications			
Length	Width	Grid Size	Wire Diameter
1.3m	1.3m	100mm x 100mm	5.6mm

Boundary Condition	Fixed 	Loading Condition	Square Curved Plate 300mm x 300mm
---------------------------	--	--------------------------	--------------------------------------

No of Restraints per side	13
Sample Configuration	Cross wires in contact with load plate and parallel to load bearing beam



Rupture Load	46.19	kN	Peak Load	46.19	kN
---------------------	-------	----	------------------	-------	----

Rupture Displacement	193	mm	Displacement prior to active response	54	mm
-----------------------------	-----	----	--	----	----

Rupture Mechanism	Weld Failure	Position of Rupture	Loaded edge on the manufactured boundary
--------------------------	--------------	----------------------------	--

Comments:

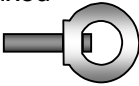


WASM Static Test Report

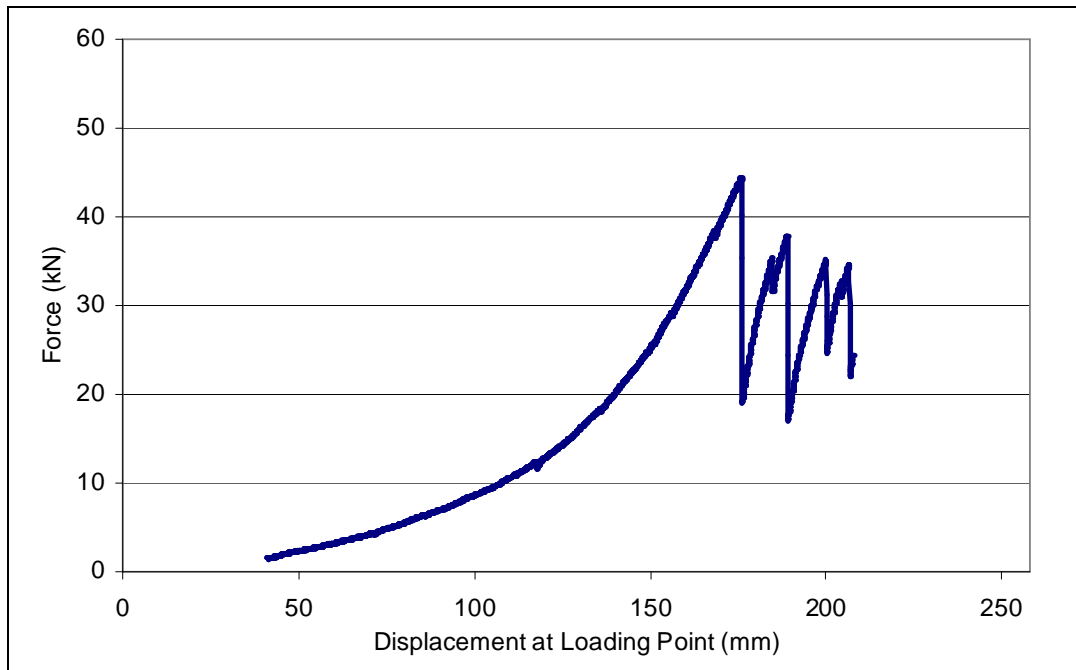


Test Date	12/11/2007	Person Testing	Ellen Morton
Test Number: MT056 Type: Weld Mesh			

Sample Specifications			
Length	Width	Grid Size	Wire Diameter
1.3m	1.3m	100mm x 100mm	5.6mm

Boundary Condition	Fixed 	Loading Condition	Dynamic loading bag 650mm x 650mm with 300kg of steel balls
---------------------------	--	--------------------------	---

No of Restraints per side	13
Sample Configuration	Cross wires in contact with load plate and parallel to load bearing beam



Rupture Load	44.20	kN	Peak Load	44.20	kN
---------------------	-------	----	------------------	-------	----

Rupture Displacement	176	mm	Displacement prior to active response	NA	mm
-----------------------------	-----	----	--	----	----

Rupture Mechanism	Failure of the wire through HAZ	Position of Rupture	Loaded wire on cut edge of sheet
--------------------------	---------------------------------	----------------------------	----------------------------------

Comments:

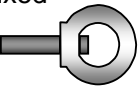


WASM Static Test Report

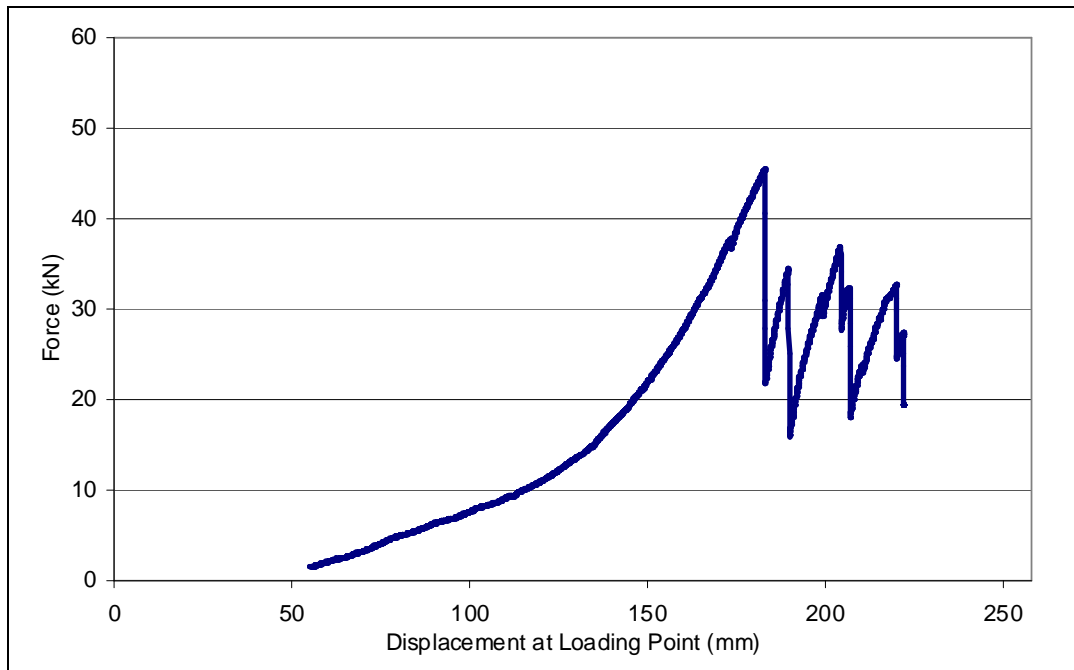


Test Date	13/11/2007	Person Testing	Ellen Morton
Test Number: MT057 Type: Weld Mesh			

Sample Specifications			
Length	Width	Grid Size	Wire Diameter
1.3m	1.3m	100mm x 100mm	5.6mm

Boundary Condition	Fixed 	Loading Condition	Dynamic loading bag 650mm x 650mm with 300kg of steel balls
---------------------------	--	--------------------------	---

No of Restraints per side	13
Sample Configuration	Cross wires in contact with load plate and parallel to load bearing beam



Rupture Load	45.40	kN	Peak Load	45.4	kN
---------------------	-------	----	------------------	------	----

Rupture Displacement	183	mm	Displacement prior to active response	NA	mm
-----------------------------	-----	----	--	----	----

Rupture Mechanism	Failure of the wire through HAZ	Position of Rupture	Loaded wire on cut edge of sheet
--------------------------	---------------------------------	----------------------------	----------------------------------

Comments:

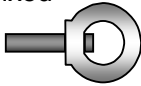


WASM Static Test Report

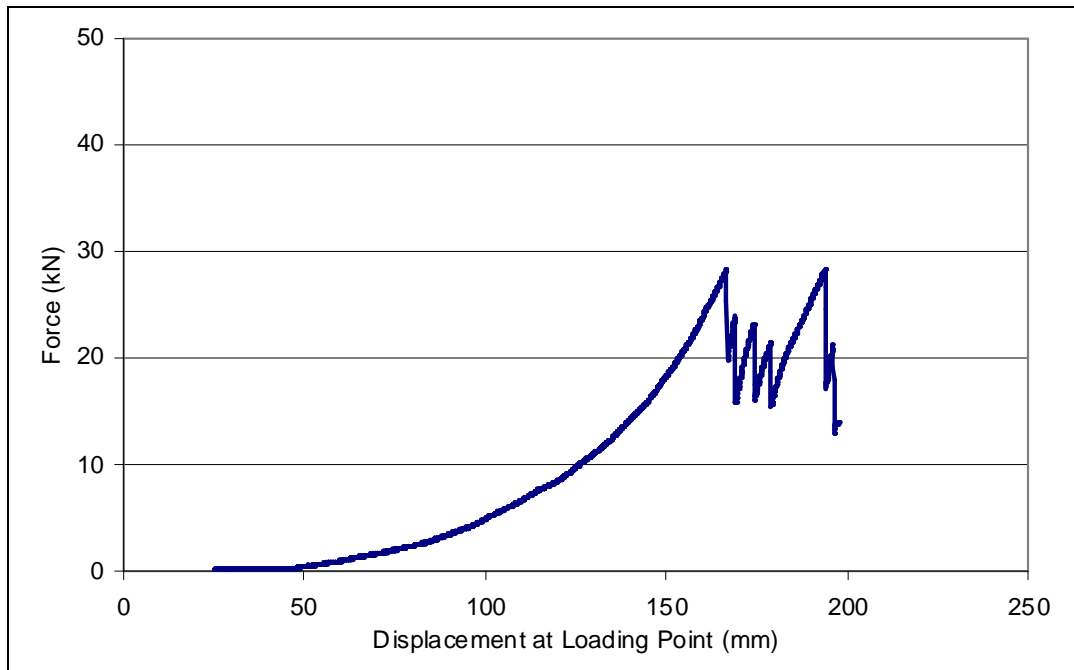


Test Date	03/12/2007	Person Testing	Ellen Morton
Test Number: MT061 Type: Weld Mesh			

Sample Specifications			
Length	Width	Grid Size	Wire Diameter
1.3m	1.3m	100mm x 100mm	5.6mm

Boundary Condition	Fixed 	Loading Condition	Square Curved Plate 300mm x 300mm
---------------------------	--	--------------------------	--------------------------------------

No of Restraints per side	13
Sample Configuration	Cross wires in contact with load plate and parallel to load bearing beam*



Rupture Load	28.33	kN	Peak Load	28.38	kN
---------------------	-------	----	------------------	-------	----

Rupture Displacement	166	mm	Displacement prior to active response	46	mm
-----------------------------	-----	----	--	----	----

Rupture Mechanism	Weld failure	Position of Rupture	Loaded wire on cut edge of sheet
--------------------------	--------------	----------------------------	----------------------------------

Comments: Sample taken from interior of sheet.

* Sample was cut down to smaller size to enable delivery. Long wires and cross wires were marked prior to delivery. Long wires and cross wires may have been confused during this process. The test setup was used according to the marked wires but may be incorrect. This can affect the result by up to 10%.

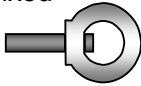


WASM Static Test Report

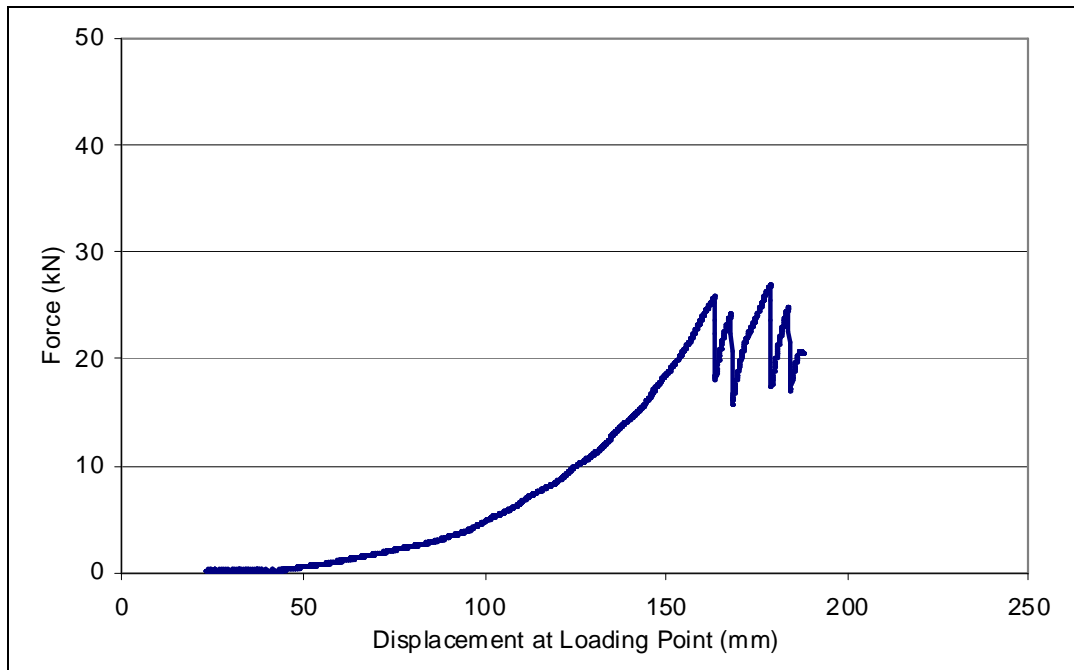


Test Date	05/12/2007	Person Testing	Ellen Morton
Test Number: MT062 Type: Weld Mesh			

Sample Specifications			
Length	Width	Grid Size	Wire Diameter
1.3m	1.3m	100mm x 100mm	5.6mm

Boundary Condition	Fixed 	Loading Condition	Square Curved Plate 300mm x 300mm
---------------------------	--	--------------------------	--------------------------------------

No of Restraints per side	13
Sample Configuration	Cross wires in contact with load plate and parallel to load bearing beam*



Rupture Load	25.88	kN	Peak Load	27.04	kN
---------------------	-------	----	------------------	-------	----

Rupture Displacement	163	mm	Displacement prior to active response	46	mm
-----------------------------	-----	----	--	----	----

Rupture Mechanism	Weld failure	Position of Rupture	Loaded wire on cut edge of sheet
--------------------------	--------------	----------------------------	----------------------------------

Comments: Sample taken from interior of sheet.

* Sample was cut down to smaller size to enable delivery. Long wires and cross wires were marked prior to delivery. Long wires and cross wires may have been confused during this process. The test setup was used according to the marked wires but may be incorrect. This can affect the result by up to 10%.

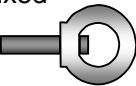


WASM Static Test Report

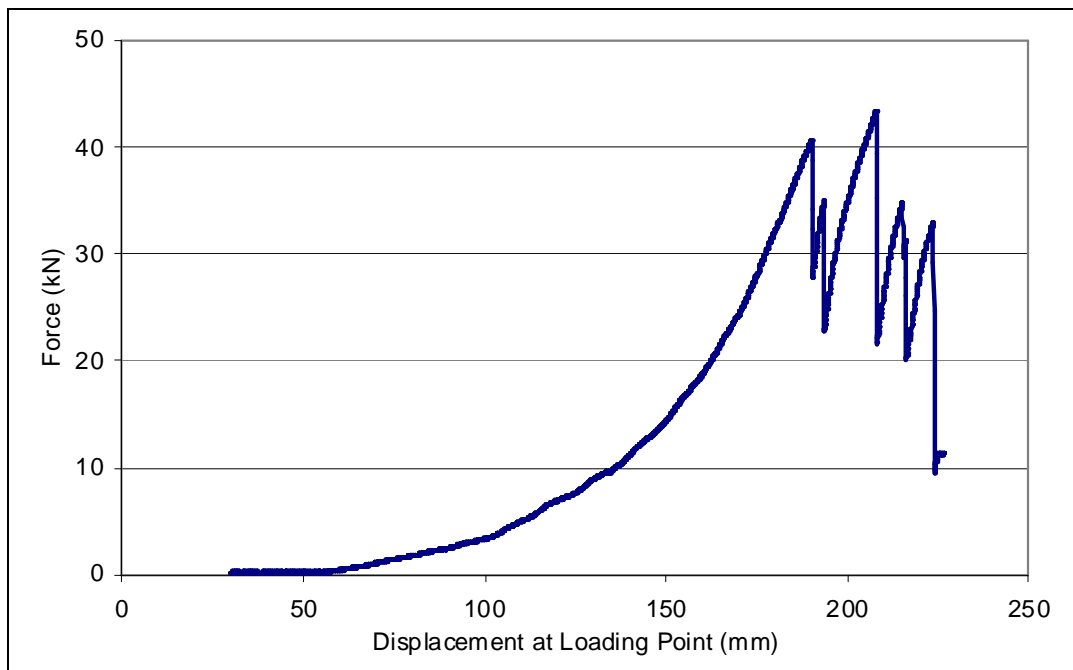


Test Date	18/7/2008	Person Testing	Ellen Morton
Test Number: MT076 Type: Weld Mesh			

Sample Specifications			
Length	Width	Grid Size	Wire Diameter
1.3m	1.3m	100mm x 100mm	5.6mm

Boundary Condition	Fixed 	Loading Condition	Square Curved Plate 300mm x 300mm
---------------------------	--	--------------------------	--------------------------------------

No of Restraints per side	13
Sample Configuration	Cross wires in contact with load plate and parallel to load bearing beam



Rupture Load	40.65	kN	Peak Load	43.42	kN
---------------------	-------	----	------------------	-------	----

Rupture Displacement	190	mm	Displacement prior to active response	57	mm
-----------------------------	-----	----	--	----	----

Rupture Mechanism	Weld Failure	Position of Rupture	Loaded wire on cut edge
--------------------------	--------------	----------------------------	-------------------------

Comments:

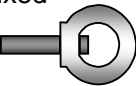


WASM Static Test Report

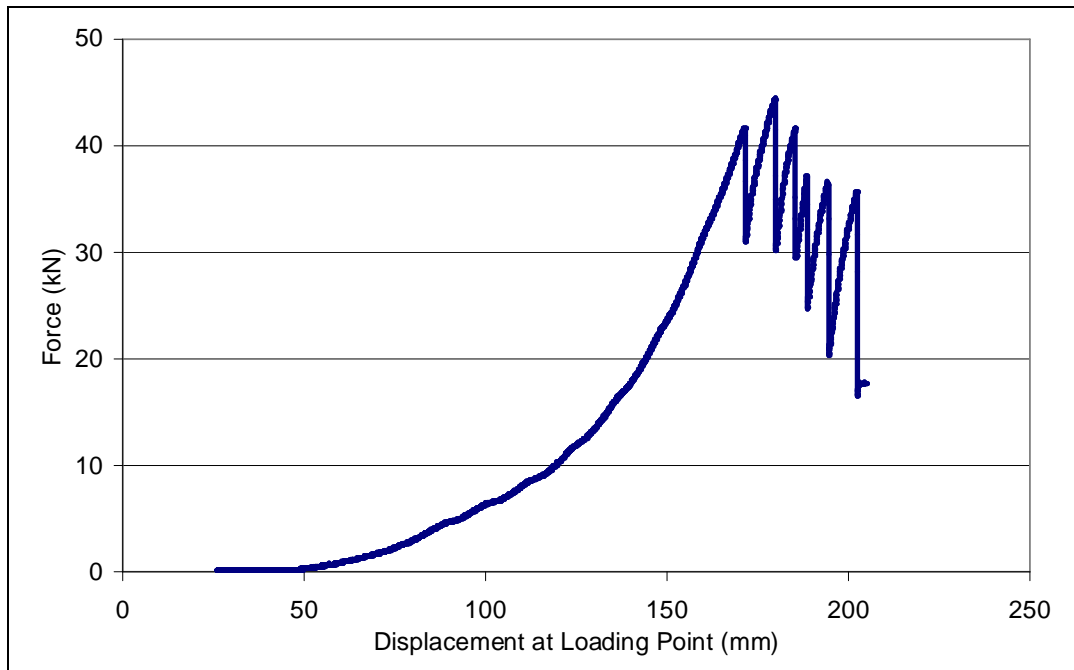


Test Date	18/7/2008	Person Testing	Ellen Morton
Test Number: MT077 Type: Weld Mesh			

Sample Specifications			
Length	Width	Grid Size	Wire Diameter
1.3m	1.3m	100mm x 100mm	5.6mm

Boundary Condition	Fixed 	Loading Condition	Square Curved Plate 300mm x 300mm
---------------------------	--	--------------------------	--------------------------------------

No of Restraints per side	13
Sample Configuration	Cross wires in contact with load plate and parallel to load bearing beam



Rupture Load	41.70	kN	Peak Load	44.39	kN
---------------------	-------	----	------------------	-------	----

Rupture Displacement	172	mm	Displacement prior to active response	49	mm
-----------------------------	-----	----	--	----	----

Rupture Mechanism	Weld Failure	Position of Rupture	Loaded wire on cut edge
--------------------------	--------------	----------------------------	-------------------------

Comments:



WASM Static Test Report

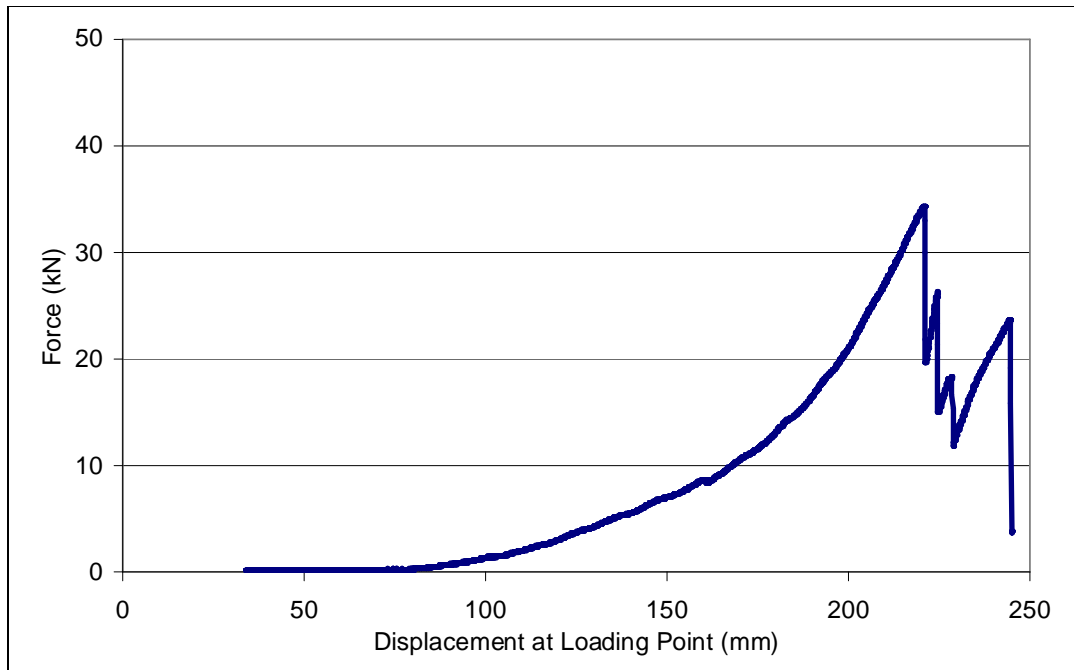


Test Date	12/08/2008	Person testing	Ellen Morton
Test Number: MT078 Type: Weld Mesh			

Sample Specifications			
Length	Width	Grid Size	Wire Diameter
0.8m	1.3m	100mm x 100mm	5.6mm
0.7m	1.3m	100mm x 100mm	5.6mm

Boundary Condition	Fixed 	Loading Condition	Square Curved Plate 300mm x 300mm
---------------------------	-----------	--------------------------	--------------------------------------

No of Restraints per side	13
Sample Configuration	Cross wires in contact with load plate and parallel to load bearing beam. 2 samples overlapped by 200mm in centre of frame. Overlap direction parallel to load bearing beam



Rupture Load	34.38	kN	Peak Load	34.38	kN
---------------------	-------	----	------------------	-------	----

Rupture Displacement	221	mm	Displacement prior to active response	80	mm
-----------------------------	-----	----	--	----	----

Rupture Mechanism	Weld Failure	Position of Rupture	Loaded wire on the overlapped cut boundary
--------------------------	--------------	----------------------------	--

Comments: Observations indicate load transfer around the mesh when loading occurs on the overlap is significantly different from when loading occurs in the centre of a sheet.



WASM Static Test Report

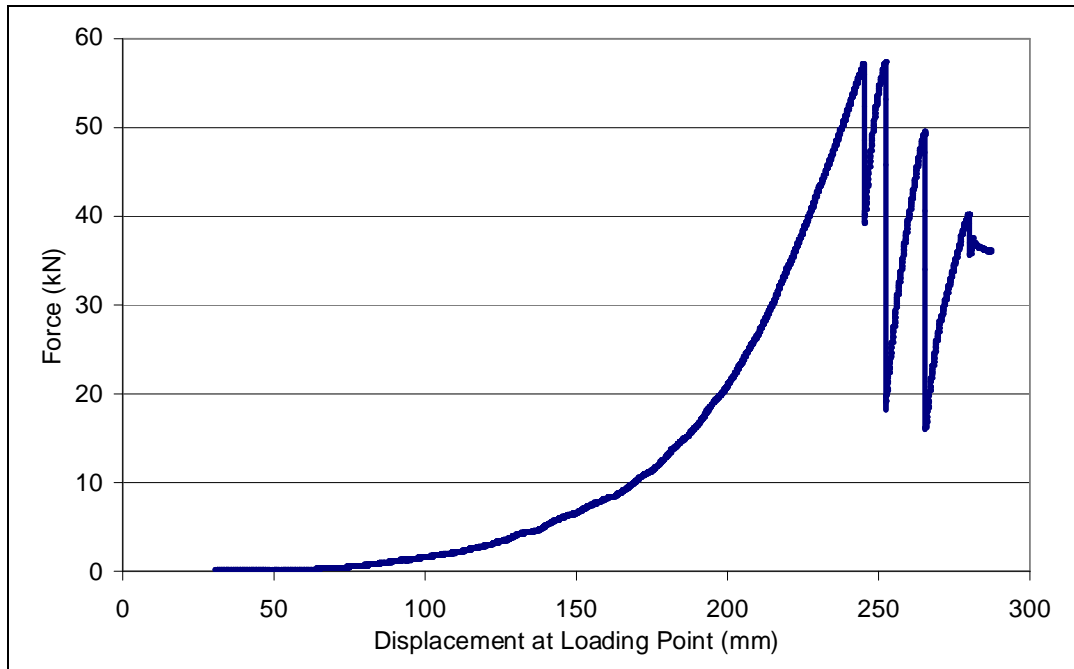


Test Date	13/08/2008	Person testing	Ellen Morton
Test Number: MT079 Type: Weld Mesh			

Sample Specifications			
Length	Width	Grid Size	Wire Diameter
0.8m	1.3m	100mm x 100mm	5.6mm
0.7m	1.3m	100mm x 100mm	5.6mm

Boundary Condition	Fixed 	Loading Condition	Square Curved Plate 300mm x 300mm
---------------------------	--	--------------------------	--------------------------------------

No of Restraints per side	13
Sample Configuration	Cross wires in contact with load plate and parallel to load bearing beam. 2 samples overlapped by 200mm in centre of frame. Overlap direction parallel to load bearing beam. Overlap laced using 6mm steel wire rope. Wire rope grips restrain lacing one square in from the edge of the sample.



Rupture Load	57.10	kN	Peak Load	57.28	kN
---------------------	-------	----	------------------	-------	----

Rupture Displacement	245	mm	Displacement prior to active response	63	mm
-----------------------------	-----	----	--	----	----

Rupture Mechanism	Failure of the wire through HAZ	Position of Rupture	Loaded wire on the overlapped cut boundary
--------------------------	---------------------------------	----------------------------	--

Comments: